

2

TECHNICAL REPORT GL-87-14

SEISMIC STABILITY EVALUATION OF FOLSOM DAM AND RESERVOIR PROJECT

Report 6

RIGHT AND LEFT WING DAMS

by

Ronald E. Wahl, Mary E. Hynes
Donald E. Yule, David J. Elton

Geotechnical Laboratory

DEPARTMENT OF THE ARMY
Waterways Experiment Station, Corps of Engineers
PO Box 631, Vicksburg, Mississippi 39181-0631

DTIC
ELECTE
APR 17 1989
S D & D



April 1989

Report 6 of a Series

Approved For Public Release: Distribution Unlimited

Prepared for US Army Engineer District, Sacramento
Sacramento, California 95814-4794



US Army Corps
of Engineers



AD-A206 660



GEOTECHNICAL
LABORATORY

When this report is no longer needed return it to
the originator.

The findings in this report are not to be construed as an
official Department of the Army position unless so
designated by other authorized documents.

The contents of this report are not to be used for
advertising, publication, or promotional purposes.
Citation of trade names does not constitute an
official endorsement or approval of the use of such
commercial products.

REPORT DOCUMENTATION PAGE

1a. REPORT SECURITY CLASSIFICATION Unclassified		1b. RESTRICTIVE MARKINGS	
2a. SECURITY CLASSIFICATION AUTHORITY		3. DISTRIBUTION / AVAILABILITY OF REPORT Approved for public release; distribution unlimited.	
2b. DECLASSIFICATION / DOWNGRADING SCHEDULE			
4. PERFORMING ORGANIZATION REPORT NUMBER(S) Technical Report GL-87-14		5. MONITORING ORGANIZATION REPORT NUMBER(S)	
6a. NAME OF PERFORMING ORGANIZATION USAEWES Geotechnical Laboratory	6b. OFFICE SYMBOL (if applicable) CEWESGH	7a. NAME OF MONITORING ORGANIZATION	
6c. ADDRESS (City, State, and ZIP Code) PO Box 631 Vicksburg, MS 39180-0631		7b. ADDRESS (City, State, and ZIP Code)	
8a. NAME OF FUNDING / SPONSORING ORGANIZATION US Army Engineer District, Sacramento	8b. OFFICE SYMBOL (if applicable) SPKED	9. PROCUREMENT INSTRUMENT IDENTIFICATION NUMBER	
8c. ADDRESS (City, State, and ZIP Code) 650 Capital Mall Sacramento, CA 95814-4794		10. SOURCE OF FUNDING NUMBERS	
		PROGRAM ELEMENT NO.	PROJECT NO.
		TASK NO.	WORK UNIT ACCESSION NO.
11. TITLE (Include Security Classification) Seismic Stability Evaluation of Folsom Dam and Reservoir Project; Report 6: Right and Left Wing Dams			
12. PERSONAL AUTHOR(S) Wahl, Ronald E., Hynes, Mary E., Yule, Donald E., and Elton, David J.			
13a. TYPE OF REPORT Report 6 of a series	13b. TIME COVERED FROM 1982 TO 1988	14. DATE OF REPORT (Year, Month, Day) April 1989	15. PAGE COUNT 189
16. SUPPLEMENTARY NOTATION Available from National Technical Information Service, 5285 Port Royal Road, Springfield, VA 22161.			
17. COSATI CODES		18. SUBJECT TERMS (Continue on reverse if necessary and identify by block number)	
FIELD	GROUP	SUB-GROUP	
			Dam safety
			Earthquakes and hydraulic structures
			Folsom Dam (California)
19. ABSTRACT (Continue on reverse if necessary and identify by block number)			
<p>The man-made water retaining structures at the Folsom Dam and Reservoir Project, located on the American River about 20 miles upstream of the city of Sacramento, California, have been evaluated for their seismic safety in the event of a Magnitude 6.5 earthquake occurring on the East Branch of the Bear Mountains fault zone at a distance of about 15 km. This report documents the study of the Right and Left Wing Dams, two of the zoned embankment dams at the Folsom Project. The evaluation process involved extensive review of construction records, field and laboratory investigations, and analytical studies. It has been determined that the Right and Left Wing Dams will perform satisfactorily during the design earthquake.</p>			
20. DISTRIBUTION / AVAILABILITY OF ABSTRACT <input checked="" type="checkbox"/> UNCLASSIFIED/UNLIMITED <input type="checkbox"/> SAME AS RPT <input type="checkbox"/> DTIC USERS		21. ABSTRACT SECURITY CLASSIFICATION Unclassified	
22a. NAME OF RESPONSIBLE INDIVIDUAL		22b. TELEPHONE (Include Area Code)	22c. OFFICE SYMBOL

PREFACE

The US Army Engineer Waterways Experiment Station (WES) was authorized to conduct this study by the US Army Engineer District, Sacramento (SPK), by Intra-Army Order for Reimbursable Services Nos. SPKED-F-82-2, SPKED-F-82-11, SPKED-F-82-34, SPKED-F-83-15, SPKED-F-83-17, SPKED-F-84-14, and SPKED-D-85-12. This report is one in a series of reports which document the seismic stability evaluations of the man-made water retaining structures of the Folsom Dam and Reservoir Project, located on the American River in California. The Reports in this series are as follows:

Report 1: Summary

Report 2: Interface Zone

Report 3: Concrete Gravity Dam

Report 4: Mormon Island Auxiliary Dam - Phase I

Report 5: Dike 5

Report 6: Right and Left Wing Dams

Report 7: Upstream Retaining Wall

Report 8: Mormon Island Auxiliary Dam - Phase II

The work on these reports is a joint endeavor between SPK and WES. Messrs. John W. White and John S. Nickell, of Civil Design Section 'A,' Civil Design Branch, Engineering Division at SPK were the overall SPK project coordinators. Messrs. Gil Avila and Matthew G. Allen, of the Soil Design Section, Geotechnical Branch, Engineering Division at SPK, made critical geotechnical contributions to field and laboratory investigations. Support was also provided by the South Pacific Division Laboratory. The WES Principal Investigator and Research Team Leader was Dr. Mary Ellen Hynes, of the Earthquake Engineering and Geophysics Division (EEGD), Geotechnical Laboratory (GL), WES. Primary Engineers on the WES team for the portion of the study documented in this report were Mr. Ronald E. Wahl, EEGD, Mr. Donald E. Yule, EEGD, and Dr. David J. Elton, on temporary assignment to WES from Auburn University. Geophysical support was provided by Mr. Jose Llopis, EEGD. Additional engineering support was provided by Mr. Richard S. Olsen, EEGD. Large-scale laboratory investigations were conducted by Mr. Robert T. Donaghe of the Soil Mechanics Division (SMD), GL, WES. Laboratory instrumentation services were provided by Mr. Thomas V. McEwen, of the Data Acquisition Section, Instrumentation Services Division.

Mr. W. L. Hanks, SMD, Mr. C. Schneider, SMD, Mr. B. L. Washington of the Engineering Geology and Rock Mechanics Division (EGRMD), GL, WES, Mr. M. H. Seid, EEGD, Mr. H. Alderson, EEGD, and Mr. T. Cho, EEGD, assisted in preparation of figures. Key contributions were also made by Dr. Leslie F. Harder, Jr., of Sacramento, California; and Professor Shobha Bhatia, Syracuse University.

Professors H. Bolton Seed, Anil K. Chopra, and Bruce A. Bolt of the University of California, Berkeley; Professor Clarence R. Allen of the California Institute of Technology; and Professor Ralph B. Peck, Professor Emeritus of the University of Illinois, Urbana, served as Technical Specialists and provided valuable guidance during the course of the investigation.

Overall direction at WES was provided by Dr. A. G. Franklin, Chief, EEGD, and Dr. W. F. Marcuson III, Chief, GL.

COL Dwayne G. Lee, CE, is Commander and Director of WES. Dr. Robert W. Whalin is Technical Director.



Accession For	
NTIS CRA&I	<input checked="" type="checkbox"/>
DTIC TAB	<input type="checkbox"/>
Unannounced	<input type="checkbox"/>
Justification	
By	
Distribution/	
Availability Codes	
Dist	Avail and/or Special
A-1	

CONTENTS

	<u>Page</u>
PREFACE.....	1
PART I: INTRODUCTION.....	5
General.....	5
Project History.....	6
Hydrology and Pool Levels.....	6
Description of Wing Dams, Interface Zone and Concrete Gravity Dam.....	7
Site Geology.....	8
Seismic Hazard Assessment.....	9
Seismological and geological investigations.....	9
Selection of design ground motions.....	12
PART II: REVIEW OF CONSTRUCTION RECORDS.....	14
General.....	14
Foundation Preparation at Right and Left Wing Dams.....	14
Embankment Materials.....	15
PART III: FIELD INVESTIGATIONS PERFORMED FOR THIS STUDY.....	17
General.....	17
Geophysical Tests.....	17
Surface vibratory tests.....	17
Crosshole tests.....	18
Undisturbed Samples.....	22
Standard Penetration Tests.....	22
Test Pits.....	23
Comparison of the Characteristics of the Wing Dam Gravels with Mormon Island Auxiliary Dam Gravels.....	25
Becker Hammer Tests Performed at Mormon Island Auxiliary Dam.....	28
Becker Hammer Tests Performed in the Embankment Gravels at the Right and Left Wing Dams.....	28
Results of tests performed at the Right Wing Dam.....	29
Results of tests performed at the Left Wing Dam.....	30
Comparison of the Becker Hammer Tests performed at the Mormon Island Auxiliary Dam with the Becker Hammer Tests performed at the Wing Dams.....	31
PART IV: ESTIMATES OF CYCLIC STRENGTH.....	33
General.....	33
Estimates of Cyclic Strength from In Situ Tests.....	33
Empirical procedure to estimate cyclic strength.....	33
Cyclic strength estimate for shell materials, Zones A, B, E, and F.....	34
Cyclic strength of preexisting embankment and Zone C and Zone G core materials.....	35
Relative Cyclic Strength Behavior of Embankment Gravels.....	35
PART V: STATIC FINITE ELEMENT ANALYSIS.....	38
General.....	38
Section Idealization and Static Finite Element Inputs.....	38

	<u>Page</u>
Results of Static Analysis.....	40
PART VI: DYNAMIC FINITE ELEMENT ANALYSIS.....	42
General.....	42
Description of FLUSH.....	42
Inputs to FLUSH.....	42
Dynamic Response Results.....	44
PART VII: EVALUATION OF LIQUEFACTION POTENTIAL.....	47
General.....	47
Safety Factors Against Liquefaction in Embankment Shell.....	47
Residual Excess Pore Pressures.....	48
Liquefaction Potential Evaluation of Central Impervious Core.....	48
Summary.....	49
PART VIII: STABILITY EVALUATION.....	50
General.....	50
Post-Earthquake Slope Stability Analysis.....	50
Permanent Displacement Analysis.....	51
Computation of yield accelerations.....	51
Makdisi-Seed method.....	52
Sarma-Ambraseys method.....	54
Stability Evaluation.....	55
PART IX: SUMMARY AND CONCLUSIONS.....	56
REFERENCES.....	58
TABLES 1-21	
FIGURES 1-83	
APPENDIX A: EVALUATION OF BECKER PENETRATION TESTS PERFORMED IN 1988 AT RIGHT AND LEFT WING DAMS.....	A1

SEISMIC STABILITY EVALUATION OF FOLSOM DAM AND RESERVOIR PROJECT

Report 6: Right and Left Wing Dams

PART I: INTRODUCTION

General

1. This report is one in a series of reports that document the investigations and results of a seismic stability evaluation of the man-made water retaining structures at the Folsom Dam and Reservoir Project, located on the American River in Sacramento, Placer and El Dorado Counties, California, about 20 airline miles northeast of the City of Sacramento. This seismic safety evaluation was performed as a cooperative effort between the US Army Engineer Waterways Experiment Station (WES) and the US Army Engineer District, Sacramento (SPK). Professors H. Bolton Seed, Anil K. Chopra, and Bruce A. Bolt of the University of California, Berkeley, Professor Clarence R. Allen of the California Institute of Technology, and Professor Ralph B. Peck, Professor Emeritus of the University of Illinois, Urbana, served as Technical Specialists for the study.

2. The man-made water retaining structures at the Folsom Project consist of the Concrete Gravity Dam constructed in the American River channel, the Right and Left Wing Dams which flank the concrete structure, Mormon Island Auxiliary Dam which was constructed in the Blue Ravine (an ancient channel of the American River), and 8 saddle dikes which complete the reservoir rim. This report documents the seismic stability studies of the Right and Left Wing Dams. A location map and plan of the project are shown in Figures 1 and 2.

3. The seismic stability study consisted of a detailed review of construction records, field and laboratory investigations, and analytical studies to estimate the response of the embankment dams to earthquake shaking, to determine the susceptibility of the embankment materials to liquefaction, to assess the stability of the dam slopes during and immediately after the design seismic event, and to estimate the earthquake-induced permanent displacement the slopes might experience. These studies and the conclusions drawn concerning the seismic stability of the Wing Dams are documented in this report.

From these studies, it has been concluded that the Wing Dams will perform satisfactorily during and after the design earthquake event.

Project History

4. The Folsom project was designed and built by the Corps of Engineers in the period 1948 to 1956, as authorized by the Flood Control Act of 1944 and the American River Basin Development Act of 1949. Upon completion of the project in May 1956, ownership of the Folsom Dam and Reservoir was transferred to the US Bureau of Reclamation for operation and maintenance. As an integral part of the Central Valley Project, the Folsom Project provides water supplies for irrigation, domestic, municipal, industrial and power production purposes. It also provides flood protection for the Sacramento Metropolitan area and extensive water-related recreational facilities. Releases from the Folsom Reservoir are used to provide water quality control for project diversions from the Sacramento-San Joaquin Delta, to maintain fish-runs in the American River below the dam, and to help maintain navigation along the lower reaches of the Sacramento River.

Hydrology and Pool Levels

5. Folsom Lake impounds the runoff from 1,875 square miles of rugged mountainous terrain. The reservoir has a storage capacity of 1 million acre-ft at gross pool and is contained by approximately 4.8 miles of man-made water retaining structures that have a crest elevation of 480.5 ft above sea level. At gross pool, elevation 466 ft, there are 14.5 ft of freeboard. This pool level was selected for the safety evaluation on the basis of a review of current operational procedures and hydrologic records (obtained for a 29-year period, from 1956 to 1984) for the reservoir which shows that the pool typically reaches elevation 466 ft about 10 percent of the time during the month of June, and considerably less than 10 percent of the time during the other months of the year. Under normal operating conditions, the pool is not allowed to exceed elevation 466 ft. Hydrologic records show that emergency situations which would cause the pool to exceed elevation 466 ft are extremely rare events.

Description of Wing Dams, Interface Zone and
Concrete Gravity Dam

6. The Wing Dams are zoned embankment dams founded on weathered quartz diorite granite. A plan of the Wing Dams is shown in Figure 3. The Right Wing Dam has a crest length of approximately 6,700 ft, and has a maximum height of approximately 195 ft. The core consists of well-compacted decomposed granite and suitable fine-grained materials from the American River channel. Gravels excavated from the American River channel are used as upstream and downstream transition zones. An uncompacted rock-fill shell was constructed on the upstream and downstream slopes over most of the length of the dam. The upstream slopes are 2.25 horizontal to 1 vertical, and the downstream slopes are 2 horizontal to 1 vertical. Typical sections are shown in Figures 4 and 5.

7. A test fill section was constructed from Station 218+50 to Station 238+55 to determine placement specifications for the core materials. Grouting of the foundation rock was accomplished through this fill, and then the embankment zones were constructed to incorporate the test fill. A typical section in this area is shown in Figure 4. The limits of the test fill in plan are indicated in Figure 3.

8. The Left Wing Dam is approximately 2,100 ft long and 167 ft high. The core consist of well compacted decomposed granite and is flanked upstream and downstream by 12-ft wide filters. The upstream and downstream shells are constructed of gravels, which come from dredged tailings in the Blue Ravine. The filters are the -2 in. fraction of the Blue Ravine gravels. The slopes are the same as the Right Wing Dam. A plan of the Left Wing Dam is shown in Figure 3 and a typical section is shown in Figure 6.

9. The Right and Left Wing Dams flank the Concrete Gravity Dam. The Concrete Gravity Dam consists of 28 50-ft-wide monoliths founded on hard granodiorite rock. The overall length of the concrete structure is 1,400 ft, the maximum height is 340 ft measured from the foundation to the crown of the roadway, elevation 480.5 ft (3.5 ft below the top of parapet, elevation 484.0 ft), and the crest width is about 32 ft. Monoliths are numbered consecutively (1 through 28) beginning at the right abutment. Plans, elevations and sections are shown in Figures 7 through 10.

10. A gated central overflow spillway section with a crest elevation of 418.0 ft was constructed in the Concrete Gravity Dam. This section consists of eight gated sluice outlets, 5 ft-by-9 ft. Three 15 ft-6 in. diameter penstocks are located through the right nonoverflow section of the Concrete Gravity Dam. An 84-in. intake conduit was constructed through the right abutment nonoverflow section to furnish water to the Folsom Power Plant, located immediately downstream of the Right Wing Dam envelopment area on the north side of the river.

11. Concrete Dam Monoliths 1 through 6 interface with the Right Wing Dam and are fully to partially embedded in the Right Wing envelopment fill. Monoliths 22 through 28 interface with the Left Wing Dam and are partially to fully embedded in the Left Wing envelopment fill. Typical envelopment sections are shown in Figures 11 and 12. Three retaining walls were constructed in the vicinity of the Concrete Gravity Dam in the wrap-around area parallel to the river. Downstream retaining walls were constructed on both the Right and Left wrap-around areas. Upstream, only the Right wrap-around area required a retaining wall, denoted Retaining Wall B in Figure 3.

Site Geology

12. At the time of construction, the geology and engineering geology concerns at the site were carefully detailed in the foundation report by US Army Engineer District, Sacramento (1953). This foundation report from construction records and a later paper by Kiersch and Treasher (1955) are the sources for the summary of site geology provided in this section.

13. The Folsom Dam and Reservoir Project is located in the low, westernmost foothills of the Sierra Nevada in central California, at the confluence of the North and South Forks of the American River. Relief ranges from a maximum elevation of 1,242 ft near Flagstaff Hill located between the upper arms of the reservoir, to 150 ft near the town of Folsom just downstream of the Concrete Gravity Dam. The North and South Forks once entered the confluence in mature valleys up to 3 miles wide, but further downcutting resulted in a V-shaped inner valley 30 to 185 ft deep. Below the confluence, the inner canyon was flanked by a gently sloping mature valley approximately 1.5 miles wide bounded on the west and southeast by a series of low hills. The upper

arms of the reservoir, the North and South Forks, are bounded on the north and east by low foothills.

14. A late Pliocene-Pleistocene course of the American River flowed through the Blue Ravine and joined the present American River channel downstream of the town of Folsom. The Blue Ravine was filled with late Pliocene-Pleistocene gravels, but with subsequent downcutting and headward erosion, the Blue Ravine was eventually isolated and drainage was diverted to the present American River Channel.

15. The important formations at the dam site are: a quartz diorite granite which forms the foundation at the Concrete Gravity Dam, Wing Dams, and Saddle Dikes 1 through 7; metamorphic rocks of the Copper Hill Volcanics (formerly included within the Amador Group) which underlie Saddle Dike 8 and the foundation at Mormon Island Auxiliary Dam; the Mehrten formation, a deposit of cobbles and gravels in a somewhat cemented clay matrix which caps the low hills that separate the saddle dikes and is part of the foundation at Dike 5; and the alluvium that fills the Blue Ravine at Mormon Island Auxiliary Dam.

16. Weathered granitic or metamorphic rock is present throughout the area. Figure 13 shows a geologic map of the project area. The Concrete Gravity Dam, the Wing Dams, and Dikes 1 through 7 are founded on the weathered quartz diorite granite. Between Dikes 7 and 8 there is a change in the bedrock. Dike 8 and Mormon Island Auxiliary Dam are underlain by metamorphic rock of the Copper Hill Volcanics. The Copper Hill Volcanics consist of predominantly schists with numerous dioritic and diobasic dikes.

Seismic Hazard Assessment

Seismological and geological investigations

17. Detailed geological and seismological investigations in the immediate vicinity of Folsom Reservoir were performed by Tierra Engineering, Incorporated to assess the potential for earthquakes in the vicinity, to estimate the magnitudes these earthquakes might have, and to assess the potential for ground rupture at any of the water-retaining structures (see Tierra Engineering Consultants, Inc. 1983, for comprehensive report). The 12-mile wide by 35-mile long study area centered on the Folsom Reservoir was extensively

investigated using techniques such as aerial imagery analysis, ground reconnaissance, geologic mapping, and detailed fault capability assessment. In addition, studies by others relevant to the geology and seismicity of the area around Folsom were also compiled. These additional literature sources include numerous geologic and seismologic studies published through the years, beginning with the "Gold Folios" published by the US Geological Survey in the 1890's, the engineering geology investigations for New Melones and the proposed Marysville and Auburn Dams, studies performed for the Rancho Seco Nuclear Power Plant as well as unpublished student theses and county planning studies. As described in this section, the East Branch of the Bear Mountains fault zone is the seismic source of concern.

18. Figure 14 shows a generalized geologic map of north central California and identifies the location of the 12-mile by 35-mile study area. Figure 15 shows a close-up of the study area as it surrounds the Folsom Project. Figure 16 shows the regional geology and highlights the basement rocks in the study zone. The western edge of the study zone contains Quaternary and Tertiary deposits of the Great Valley. The central and eastern portion of the study zone contain primarily metamorphic rock with granitic, gabbroic and ultramafic intrusives.

19. Figure 16 also shows the major faults in the area. In the investigation of faults, shears, and lineaments, five features within the study area were selected for more detailed study. These were: (a) the West Branch of the Bear Mountains fault zone, (b) the Bass Lake fault, (c) the Linda Creek lineament, (d) the Mormon Island fault, and (e) the Scott Road lineament. The East Branch of the Bear Mountains fault zone is located near the boundary of the study area. The characteristics of this fault zone were fully examined and reported in the above mentioned references. This fault zone was not investigated further as part of this study by Tierra Engineering Consultants. Characteristics of this fault zone are discussed later in this section. The five features that were selected for further study are identified on the regional lineament map in Figure 17. On the basis of review of available data, geologic mapping, and imagery analysis, it was determined that the Bass Lake fault is more than 168 million years old and shows no evidence of movement in recent geologic time. Consequently, the fault is not considered capable. Based on the seismological studies for Auburn Dam, it was determined that the Linda Creek lineament also does not represent a capable fault (by

Corps criteria). The Scott Road lineament was determined to be of erosional origin and is not considered to be a fault. The remaining two faults, the West Branch of the Bear Mountains fault zone and the Mormon Island fault, required additional studies.

20. The detailed lineament analyses, geomorphic analyses, geologic mapping and trenching at selected locations indicated that the West Branch of the Bear Mountains fault zone is overlain by undisplaced soils more than 60 to 70 thousand years old. There were no geomorphic indications of Holocene faulting along the zone; so it was concluded that the West Branch of the Bear Mountains fault zone is not a capable fault. Studies of the Mormon Island fault showed that the lineament zone associated with the fault dies out before reaching Mormon Island Auxiliary Dam. A review of the dam construction reports and trenching of the Mormon Island fault south of Mormon Island Auxiliary Dam revealed no evidence of faulting of quaternary alluvium in this ancestral channel of the American River. Based on the observation of undisplaced colluvium and weathering profiles more than 65,000 years old that overlie the sheared bedrock, as well as the lack of geomorphic indicators of Holocene faulting in this zone, it was concluded that the Mormon Island fault is not a capable fault, nor does it pass through the foundation of Mormon Island Auxiliary Dam (Tierra Engineering Consultants, Inc. 1983).

21. Tectonic studies of the Folsom Project show it is located in the Sierran block. Within the Sierran block there is a very low level of seismicity. The more seismically active areas are located along the eastern and southern edges of the block. Figure 18 shows epicentral locations for the western United States. On this map the Sierra Nevada and Great Basin areas are identified. Tectonic studies of the Sierran block indicate an extensional stress regime which suggests that major stress buildup and release sequence associated with large earthquakes is unlikely in the central or northern Sierran block.

22. Figure 19 shows epicentral locations in north central California from data accumulated between 1910 and 1981. As indicated in the previous discussion, a low level of seismicity can be observed in the vicinity of the Folsom Project. The nearest highly active areas are the Calaveras Hayward-San Andreas System located 70 to 100 miles to the west of the study area, or the Genoa Jack Valley zone located more than 70 miles to the east. Table 1 summarizes the characteristics of the capable fault zones near the Folsom Project.

Although these 2 highly active zones are capable of generating maximum earthquake magnitudes in excess of Magnitude $M = 7$, the ground motions generated by such earthquakes would be significantly attenuated by the time the motions arrived at the Folsom Reservoir.

23. The closest capable fault is the East Branch of the Bear Mountains fault zone which has been found to be capable of generating a maximum magnitude $M = 6.5$ earthquake. The return period for this maximum earthquake is estimated to exceed 400 years (Tierra Engineering, Inc. 1983). The tectonic and seismicity studies also indicated that it is unlikely that Folsom Lake can induce major macroseismicity. Faults that underlie the water retaining structures at the Folsom Project were found to be noncapable, so seismic fault displacement in the foundations of the water retaining structures is judged to be highly unlikely.

24. Determination that the East Branch of the Bear Mountains fault zone is a capable fault came from the Auburn Dam earthquake evaluation studies in which it was concluded that this fault was capable of generating a maximum magnitude earthquake of 6 to 6.5. The minimum distance between the East Branch of the Bear Mountains fault zone and Mormon Island Auxiliary Dam is 8 miles, and the minimum distance between this fault zone and the Concrete Gravity Dam is 9.5 miles. The focal depth of the earthquake is estimated to be 6 miles. This hypothetical maximum magnitude earthquake would cause more severe shaking at the project than earthquakes originating from other known potential sources.

Selection of design ground motions

25. The seismological and geological investigations summarized in the Tierra report were provided to Professors Bruce A. Bolt and H. B. Seed to determine appropriate ground motions for the seismic safety evaluation of the Folsom Dam Project. The fault zone of concern is the East Branch of the Bear Mountains fault zone located at a distance of about 15 kilometers from the site. This fault zone has an extensional tectonic setting and a seismic source mechanism that is normal dip-slip. The slip rate from historic geomorphic and geological evidence is very small, less than 10^{-3} centimeters per year with the most recent known displacement occurring between 10,000 and 500,000 years ago in the latter half of the Pleistocene Epoch.

26. On the basis of their studies of the horizontal ground accelerations recorded on an array of accelerometers normal to the Imperial Valley

fault during the Imperial Valley earthquake of 1979, as well as recent studies of a large body of additional strong ground motion recordings, Bolt and Seed (1983) recommend the following design ground motions:

Peak horizontal ground acceleration = 0.35 g

Peak horizontal ground velocity = 20 cm/sec

Bracketed Duration (≥ 0.05 g) ≈ 16 sec

Because of the presence of granitic plutons at the site, it is expected that the earthquake accelerations might be relatively rich in high frequencies. Bolt and Seed (1983) provided 2 accelerograms that are representative of the design ground motions expected at the site as a result of a maximum magnitude M equal to 6.5 occurring on the East Branch of the Bear Mountains fault zone. The accelerograms are designated as follows (Bolt and Seed 1983):

M6.5 - 15K - 83A. This accelerogram is representative of the 84-percentile level of ground motions that could be expected to occur at a rock outcrop as a result of a Magnitude 6-1/2 earthquake occurring 15 kms from the site. It has the following characteristics:

Peak acceleration = 0.35 g

Peak velocity ≈ 25 cm/sec

Duration ≈ 16 sec

M6.5 - 15K - 83B. This accelerogram is also representative of the 84-percentile level of ground motions that could be expected to occur at a rock outcrop as a result of a Magnitude 6-1/2 earthquake occurring 15 kms from the site. It has the following characteristics:

Peak acceleration = 0.35 g

Peak velocity ≈ 19.5 cm/sec

Duration ≈ 15 sec

Figure 20 shows plots of acceleration as a function of time for the two design accelerograms and Figure 21 shows response spectra of the motions for damping ratios of 0, 2, 5, 10, and 20 percent damping.

PART II: REVIEW OF CONSTRUCTION RECORDS

General

27. Detailed construction records were kept to document the initial site reconnaissance, selection of borrow areas, foundation preparation and construction sequence for the dam. Pertinent information from these construction records is summarized in this chapter. This information provides: (a) key background data used in development of an idealized section for analysis, (b) detailed descriptions of embankment materials important to the planning of field investigations and interpretation of results, and (c) initial values for material properties of embankment materials.

Foundation Preparation at Right and Left Wing Dams

28. The foundation rock beneath the Right and Left Wing Dams is a weathered granite. The degree of weathering decreases with depth and in directions away from the joint planes. The primary joint set strikes generally N 45° E and dips NW 40° - 45°. Stripping removed organic material, and loose, wet soils to expose firm decomposed granite. At the Right Wing Dam, the depth of stripping ranged from 0.5 ft where hard rock was close to the original ground surface, to as much as 18 ft in soft, mucky areas. The average depth of core trench excavation at the Right Wing Dam ranged from about 2 to 3 ft near the right abutment to about 10 ft near the envelopment area. No major faults were encountered in the foundation rock during stripping and excavation of the core trench of the Right Wing Dam. At the Left Wing Dam, stripping depths ranged from 1 to 5 ft, and the depth of excavation for the core trench reached a maximum of 20 ft. A fault striking N 88° E and dipping steeply SE was encountered in the core trench near Station 303+00. No special treatment of this zone was considered necessary. The foundation rock in the core trench was slush grouted as necessary, and outside the core trench the decomposed granite was scarified (where possible) to a depth of about 6 in. and compacted with either sheepsfoot or pneumatic rollers. Areas immediately adjacent to hard, bouldery masses were hand-tamped. The foundation rock was grouted with a single line of grout holes along the entire length of both Wing Dams. Staged-grouting methods were used. The grout curtain at the Right Wing

Dam extended to a depth of about 60 ft, and at the Left Wing Dam, the grout curtain extended to a depth of about 75 ft. The grout curtain beneath the Wing Dams was tied-in with the grout curtain beneath the Concrete Gravity Dam at the envelopment areas. Identification and treatment of faults encountered in the envelopment areas are described in Reports 2, 3, and 7 of this series.

Embankment Materials

29. The Right Wing Dam consists of 3 zones, as shown in Figures 4 and 5. Zone A is constructed of a fairly dirty rockfill and forms the upstream and downstream shells over most of the length of the dam. Zone B is a transition zone constructed of gravel from the American River. Zone C is the impervious core constructed of compacted decomposed granite from Borrow Area No. 2. The Left Wing Dam also consists of 3 zones, as shown in Figure 6. Zone E consists of compacted gravel dredged tailings from the Blue Ravine and forms the upstream and downstream shells. Zone F is the -2-in. fraction of the Zone E gravel and was used as a filter zone between the impervious core and the gravel shells. Zone G, the impervious core, is constructed of compacted decomposed granite from Borrow Area No. 1. The embankment zones, their use in the dams, and the borrow sources are listed in Table 2. The specifications for placement of these materials are listed in Table 3. Gradations for the embankment materials are shown in Figures 22-25. Material properties used in initial design, based on laboratory tests performed prior to construction, are listed in Table 4.

30. The Zone A rockfill was originally planned to contain less than 10 percent sand sizes or smaller (passing No. 4 sieve) and to be placed in the same manner as the Zone B gravels. The source materials for Zone A were found to typically contain about 30 percent passing the No. 4 sieve. The construction records indicate that an effort was made to place the cleaner materials in the upstream shell. The decision was made to place the Zone A material in 12-ft dumped lifts. No additional compaction was applied to this material. In the design of the Right Wing Dam, the Zone A rockfill was assumed to have the same properties as the Zone B gravel.

31. A test fill section was constructed from Station 218+50 to Station 238+55 to determine placement specifications for the core materials. Grouting of the foundation rock was accomplished through this fill, and then

the embankment zones were constructed to incorporate the test fill. A typical section in this area is shown in Figure 4. The limits of the test fill in plan are indicated in Figure 3.

PART III: FIELD INVESTIGATIONS PERFORMED FOR THIS STUDY

General

32. Field investigations were conducted at both the Right and Left Wing Dams in the embankment and foundation to acquire information about the cyclic strength and other input parameters required in the seismic stability evaluation. All testing was confined to the downstream side of the centerline. This information is assumed to be representative of the materials on the upstream side, due to symmetry of the embankment zones.

33. The field investigations consisted of Standard Penetration Testing (SPT), disturbed and undisturbed soil sampling, test pits (to obtain disturbed and undisturbed samples and determine the in-situ densities), and a geophysical investigation. The results of Becker Hammer Tests performed in the downstream shell of Mormon Island Auxiliary Dam were used to represent the Wing Dam gravels due to similarity of their gradations and placement specifications. A limited program of Becker Hammer soundings was performed to confirm the penetration resistance of the embankment gravels of the Wing Dams estimated from the Mormon Island Auxiliary Dam results. The Becker Hammer data are presented in Appendix A.

34. A layout of the testing program is shown in Figure 3. The layout shows that the field investigations concentrated on three locations: Stations 235 and 270 at the Right Wing Dam and Station 303 at the Left Wing Dam.

Geophysical Tests

35. The geophysical program consisted of surface vibratory, surface seismic refraction, crosshole, and uphole tests (see Llopis 1983 and 1984). The objective of these tests was to measure in-situ shear-wave (V_s) and compression wave (V_p) velocities as functions of depth within the embankment and underlying foundation materials.

Surface vibratory tests

36. The surface vibratory test is used to measure the surface Rayleigh-wave velocity which is typically about 10 percent (or less) slower than the shear-wave velocity. Rayleigh waves are generated by a surface vibrator which is swept through a range of discrete frequencies and arrival times are

measured by geophones placed at selected intervals along a straight line on the surface of the ground. Rayleigh wave velocities are approximately average values for an effective depth of one-half wave length corresponding to the vibrator frequency (Ballard 1964). The locations of the surface vibratory lines are given in Figure 26. Six surface vibratory lines were performed along the downstream toe of the Wing Dams. The data obtained from these lines are not reported here since the shear wave velocity of the weathered granite foundation was determined from the cross-hole testing.

37. Vibratory lines V-3 and V-4, V-2 and V-1, and V-25 and V-26 were each 200 ft in length and located at Stations 235 and 270 of the Right Wing Dam and at Station 303 on the Left Wing Dam, respectively. Each line was performed on the crest at the centerline and positioned to obtain the velocity-depth distribution of the central impervious core (compacted decomposed granite) for both embankments. The locations of the surface vibratory lines are shown in Figure 26.

38. The results of each of the R-wave velocity tests are presented in the form of R-wave velocity versus depth (half-wavelength) plots. The R-wave velocity data for lines V-3 and V-4 run with the vibrator positioned at Station 235 of the Right Wing Dam are given in Figure 27. The data on this plot show that the R-wave velocity increases slightly with depth and ranges between about 900 and 1,000 fps. The depth range of the testing was between approximately 5 and 60 ft and was limited by the frequency range of the vibrator. Figure 28 shows the results obtained from lines V-1 and V-2 located at Station 270 of the Right Wing Dam. The velocity profile is very similar to that of lines V-1 and V-2. These data show that the velocities increase slightly with depth and range between 900 and 1,000 fps over the 5 ft to 60 ft depth range. The results obtained from lines V-25 and V-26 at Station 303 of the Left Wing Dam are shown in Figure 29. The velocity measured from these lines was about 900 fps and was constant with depth over the 5 to 60 ft depth interval. The data obtained from the six lines are in good agreement and indicate that over the depth interval cited the compacted decomposed granite has a fairly uniform and consistent velocity profile and shows no anomalous zones over the areas tested.

Crosshole tests

39. The crosshole tests were conducted with a downhole vibrator which was swept through a range of frequencies to find one that propagated well

through the soil and transmitted a high amplitude signal to the receiver geophone lowered to the same depth as the downhole vibrator in another hole. Borehole deviation surveys were conducted to eliminate source-to-receiver distance errors in the reduction of the data. Exploding bridge-wire detonators were used as the P-wave source for P-wave crosshole test. Measurements for S-wave and P-wave velocities were made at 5-ft depth intervals. The range of frequencies in the shear wave velocity measurements was 50 to 500 hz.

40. A total of nine sets of crosshole tests were performed at Stations 235 and 270 of the Right Wing Dam, and at Station 303 of the Left Wing Dam. At each location, tests were conducted in sets of borings on the embankment's centerline, downstream shoulder, and downstream slope. The location of each test is shown in Figure 3. The crosshole tests on the centerline provided P- and S-wave velocities as functions of depth in the compacted decomposed granite cores of the Left and Right Wing Dams. The tests on the downstream shoulder were designed to provide velocities of both the impervious core and the embankment gravels. The tests conducted on the downstream slope provided information about the seismic velocities of the embankment gravels (Zone B at the Right Wing Dam and Zone E at the Left Wing Dam), the impervious core, and the Zone A rockfill at the Right Wing Dam.

41. The tests on the centerline and at the downstream shoulder in the impervious core were performed in boreholes which were cased with 4-in. I. D. PVC pipe which was grouted in place with a special grout that sets up to a consistency compatible with that of soil. These borings were the same as those in which SPT's were performed and undisturbed samples were recovered as will be discussed later. Due to the gravelly nature of the shell, the boreholes on the downstream slope were steel-cased holes drilled with Odex equipment. The Odex system consists of a downhole pneumatic hammer with an expanding bit that pulls a steel casing behind the bit. When the casing is in place, the bit can be retracted and withdrawn through the casing. The Odex system was selected for installation of cased holes for subsurface geophysical testing because it did not require grouting of the gravels, the disturbance to the gravels when drilling these holes is felt to be relatively minor, and several holes could be installed in a single day. However, the Odex system does not provide a means of satisfactorily sampling the subsurface.

42. Crosshole P-wave tests performed at Station 235 of Right Wing Dam.
The interpreted P-wave zones resulting from the three crosshole tests

performed at Station 235 are shown in Figure 30. Station 235 is a section in the portion of the Right Wing Dam constructed over the already existing test embankment (constructed of compacted decomposed granite). Borings US-2 and SS-2 used for the crosshole tests on the centerline are 96 ft deep. The P-wave velocities measured in compacted decomposed granite of Zone C and the underlying preexisting embankment generally increased with depth and ranged from 1,600 fps to 3,600 fps. The velocity in the weathered granite foundation was 9,700 fps. Borings US-9 and SS-9 on the downstream shoulder were 31 ft deep. Velocities measured in the upper 18 ft averaged 1,925 fps and are representative of the Zone A rockfill material of the shell. Below 18 ft, the tests were performed in Zone C where a velocity zone of 2,875 fps was measured which extended to a depth of at least 31 ft (limited by the depth of the boreholes). The tests on the downstream slope were performed in steel-cased borings SCB-2 (ABC) which were about 40 ft deep and had a top-of-hole elevation of 433 ft. The upper zone, 20 ft thick, correlated with the Zone A rockfill and had a velocity of about 1,200 ft. This was underlain by the Zone B gravels which had a velocity of about 4,800 fps. A P-wave velocity approaching 4,800 fps is indicative of a soil having a high degree of saturation.

43. Crosshole P-wave tests at Station 269 of Right Wing Dam. Interpreted P-wave velocity zones for Station 269 are shown in Figure 31. The tests at the centerline extended to a depth of about 90 ft. The velocity zones interpreted in Zone C generally increased with depth and ranged from 1,650 to 3,900 fps. This crosshole set did not extend into the foundation rock. The crosshole borings on the downstream shoulder were 31 ft deep. The velocity zone detected for the upper 12 ft correlates with Zones A and B and had a velocity of 1,300 fps. The velocity of the underlying Zone C material was 2,875 fps. The crosshole tests on the downstream slope extended to a depth of about 85 ft and showed the P-wave velocities of the Zone A and Zone B materials tend to increase from 1,500 fps to 1,800 fps with depth. The measured velocity of the underlying Zone C material was 3,600 fps in this location. The weathered granite in the foundation had a measured velocity of 8,975 fps.

44. Crosshole P-wave tests at Station 303 of Left Wing Dam. The P-wave velocity zones interpreted from the crosshole tests performed at Station 303 of the Left Wing Dam are shown in Figure 32. The crosshole tests at the centerline were performed to a depth of 163 ft. The data show the velocities of

the Zone G compacted decomposed granite core generally increase with depth, with the exception of two velocity inversions at 88 ft and 18 ft in depth. The data show that the velocities in the impervious core range from 1,600 to 6,100 fps. The data indicate that at the time of testing the core had a high degree of saturation at depths greater than 62 ft. The water level at the time of testing was at elevation 435 ft. The weathered granite beneath the core had a velocity of 10,000 fps. The measurements obtained from the 31-ft deep crosshole set on the downstream shoulder indicated the velocity of the Zone E gravels is 1,100 fps. The measurements performed in the underlying Zone G core indicated the velocity was about 2,100 fps. The crosshole tests performed on the downstream slope began at elevation 423 ft and extended to a depth of 63 ft. The velocities of the Zone B gravels increased with depth and ranged from 1,150 fps to 2,200 fps. The downstream filter blanket was probably saturated since it had a velocity of 4,800 fps. The weathered granite foundation had a velocity of 8,900 fps at this location.

45. Crosshole S-wave tests performed at Station 235 of the Right Wing Dam. The interpreted S-wave zones for Station 235 are shown in Figure 33. The tests performed on the centerline and at the downstream shoulder show that the velocities of the compacted decomposed granite in Zone C and the preexisting embankment ranged between 975 fps and 1,325 fps. The velocities tended to increase with depth. The measured velocity of the Zone A rockfill was about 800 fps as determined from data gathered between the depths of 0 and 20 ft from the crosshole set on the downstream slope. The velocity of the Zone B gravels was determined to be 1,500 fps as determined from measurements made between 18 and 44 ft in depth from the downstream slope crosshole set. The measured velocity of the weathered granite rock foundation was 2,000 fps beneath the impervious core.

46. Crosshole S-wave tests performed at Station 269 of the Right Wing Dam. Interpreted S-wave velocity zones determined from the crosshole test at Station 235 are shown in Figure 34. Based on data acquired from all three crosshole sets, the velocity zones of the Zone C material in the impervious core tended to increase with depth and ranged from 900 to 1,700 fps. Data acquired from the tests at the downstream shoulder and slope indicated that at depths shallower than 15 ft the shear-wave velocity of the Zone A rockfill ranged from 850 to 950 fps. Data acquired from the downstream slope showed that the velocity of the Zone B gravel ranged from 850 to 1,050 fps at depths

between 10 and 44 ft. The measured shear-wave velocity of the underlying foundation was 1,925 fps in the downstream slope crosshole set.

47. Crosshole tests performed at Station 303 of the Left Wing Dam. Interpreted S-wave zones for Station 303 of the Left Wing Dam are shown in Figure 35. The velocities of the impervious core (Zone G) increased with depth and ranged between 1,000 and 1,600 fps as observed in the crosshole tests conducted at the centerline location. The velocities of the Zone E gravels, measured in the downstream shoulder and downstream slope borings, ranged between 900 and 1,250 fps and also tended to increase with depth. The velocity of the weathered granite varied between 1,925 fps and 2,450 fps.

48. Summary of crosshole test results. The results of all the S-wave velocity tests performed at the Left and Right Wing Dam were analyzed and compiled. The final interpreted form shows the shear wave velocity distribution in a section representative of either the Left or Right Wing Dam. These interpreted S-wave velocity zones for the idealized section are shown in Figure 36. The data on this figure were subsequently used in the dynamic finite element analyses which will be discussed in a later chapter.

Undisturbed Samples

49. Undisturbed samples were recovered from the impervious core from centerline and downstream shoulder locations in borings US-2 and US-9 (Station 235), US-3 and US-8 (Station 270) of the Right Wing Dam, and US-4 and US-5 (Station 303) of the Left Wing Dam. The samples were recovered using a modified Denison sampler. The weathered granite underlying the impervious core was sampled using a rock core barrel. After drilling, the holes were cased with 4-in. polyvinyl-chloride (PVC) pipe and subsequently used for crosshole testing. Undisturbed samples recovered from the boreholes were subsequently used in laboratory testing.

Standard Penetration Tests

50. Standard Penetration Tests (SPT) were performed to estimate the cyclic strength of the central impervious cores in the Left and Right Wing Dams. The SPT soundings were performed along the centerline in borings SS-2 (Station 235) and SS-8 (Station 270) of the Right Wing Dam and in SS-4

(Station 303) of the Left Wing Dam. The SPT measurements were performed using a WES trip hammer and a 2-in. split spoon sampler. The SPT measurements were taken at 5-ft depth intervals in holes stabilized with drilling mud. Jar samples retrieved from the SPT holes were saved for laboratory classification tests performed by the South Pacific Division Laboratory (SPD). The weathered granite foundation underlying the impervious core was sampled with a rock core barrel. After drilling was completed the holes were cased with 4-in. PVC pipe grouted in place and used for geophysical testing.

51. Energy-corrected blowcounts, N_{60} , were determined from the blowcounts measured in borings SS-2, SS-8, and SS-4. Experience with the WES trip hammer shows that it provides 1.3 times more energy than the recommended standard energy level of 60 percent of the theoretical free fall (Seed 1986). Therefore, all field blowcounts were multiplied by 1.3 to adjust the trip hammer blowcounts to their standard energy level equivalent, N_{60} .

52. A second adjustment was made to correct the N_{60} blowcounts to their equivalent at an overburden pressure of 1 tsf. The resulting energy and overburden corrected blowcount is designated $(N_1)_{60}$. The $(N_1)_{60}$ blowcount was computed using Equation 1:

$$(N_1)_{60} = C_n \times N_{60} \quad (1)$$

where C_n is the overburden correction factor. The relationship between C_n and effective overburden stress used in the analysis is shown in Figure 37. Figures 38 through 40 show plots of N_{60} and $(N_1)_{60}$ versus depth for soundings SS-2, SS-8, and SS-4, respectively. The mean $(N_1)_{60}$ values of the compacted core material as determined from SS-2, SS-8, and SS-4 were 45.9, 67.7, and 72 blows/ft, respectively. The combined average $(N_1)_{60}$ was 63 blows/ft.

Test Pits

53. Test pits were excavated at the Wing Dams to determine in situ densities and gradations and obtain disturbed samples of the embankment gravels for laboratory testing. Density measurements were made with four-foot diameter water ring density tests. Approximate locations of the test pits are shown in Figure 3. Test pits TP-1 and TP-2, excavated to depths of 11.0 and 5.5 ft on the downstream slope of the Right Wing Dam near Station 235, were

planned to sample the Zone B shell gravels. Test pit TP-3 was excavated to a depth of 10.5 ft near Station 270 of the Right Wing Dam. Test pit TP-4 was excavated to a depth of 20 ft near Station 303 of the Left Wing Dam and was designed to sample the Zone E gravels.

54. The range of observed in situ gradations obtained from a mechanical sieve analysis of the disturbed samples recovered from the three test pits at the Right Wing Dam is shown in Figure 41. The range of observed gradations from the gravel shell of the Left Wing Dam is shown in Figure 42. The average mean grain size was 22 mm for the Right Wing Dam samples and 24 mm for the Left Wing Dam samples. The fines content (percent passing No. 200 sieve) of the gravel at the Right Wing Dam averaged 4 percent, and at the Left Wing Dam the average was 6 percent. The fines in the Left Wing Dam samples were slightly more plastic than those of the Right Wing Dam. The samples from both embankments classified as GP, GW, GW-GM, GP-GM, GW-GC, GP-GC or GW according to the Unified Soil Classification System (USCS). Comparison of the data on the two figures indicates that the Right Wing gravels have essentially the same gradation as the Left Wing gravels though Right Wing gravels have a slightly higher percentage passing the No. 4 sieve than the Left Wing gravels.

55. The observed field density values from TP-1, TP-2, and TP-3 are listed in Table 5. The dry densities ranged from 122.0 pcf to 152.9 pcf and averaged 136.1 pcf. The in situ dry densities observed in TP-4 at the Left Wing Dam (listed in Table 6) were slightly lower: they ranged from 124.9 pcf to 138.7 pcf, and averaged 132.8 pcf. Relative densities of the Right and Left Wing Dams were estimated from maximum and minimum relative density tests performed on the gravels in the laboratory and from high density values measured in situ. The results of these tests for Right and Left Wing Dam samples are shown in Figures 43 and 44. The laboratory study indicated that the maximum and minimum dry densities are a function of the sample gradation which is indexed according to its uniformity coefficient, C_u . The uniformity coefficient is the ratio of D_{60} to D_{10} . Contours of equal relative density are also plotted on the chart. The in situ relative densities and C_u values of samples from the Right Wing Dam were plotted on the chart in Figure 43 to determine their relative densities. Based on the plotted points the average relative density of the Right Wing Dam samples was 63 percent. The process was repeated for samples recovered from the Left Wing Dam. The results are shown in Figure 44. The average relative density of the Left Wing Dam samples

was determined to be about 60 percent. A great deal of scatter is noted in the observed densities and relative densities plotted in Figures 43 and 44; however the scatter is the same for both the Left and Right Wing Dam gravels and the average densities and relative densities are in good agreement. This result is not surprising since the gravels of both the Left and Right Wing Dam were compacted according to the same specifications as shown in Table 3.

Comparison of the Characteristics of the Wing Dam Gravels
with Mormon Island Auxiliary Dam Gravels

56. Penetration resistance (Becker Hammer) tests were performed in the Wing Dam gravels in the final stages of this study, and the results are given in Appendix A. A knowledge of the penetration resistance of these gravels is necessary to estimate their cyclic strength. In the earlier stages of this study, an extensive program of penetration resistance tests was performed to estimate the penetration resistance of foundation and embankment gravels at Mormon Island Auxiliary Dam to determine their cyclic strength. Since the characteristics of the Wing Dam gravels, especially relative density, are similar to those of the embankment gravels at Mormon Island Auxiliary Dam, their penetration resistances should be about the same. It was considered that the penetration resistances measured at Mormon Island Auxiliary Dam would apply to the gravels in the Wing Dams. In the following discussion, sample gradations, borrow sources, shear wave velocities, and compaction requirements are compared to show that the Wing Dam gravels have essentially the same relative density as the Mormon Island Auxiliary Dam gravels.

57. For reference, plan and cross-sectional views of Mormon Island Auxiliary Dam are shown in Figures 45 and 46. The cross-sectional view shows that both the upstream and downstream shells are labeled as Zone 1 material, which is a compacted gravel. Ring density samples were excavated from the Zone 1 gravels from a test shaft on the downstream slope of the dam (see Report 4 of this series). This test shaft sampled the embankment gravels to a depth of 19 ft. The plan view also shows the location of Becker Hammer soundings, labeled BH, at points along the downstream toe and on the downstream slope of the dam.

58. Laboratory gradations and index tests were performed on the Mormon Island gravels. The gradation range of the Mormon Island embankment gravels

is compared with that of the Right Wing Dam samples in Figure 47. The gradation ranges of both gravels are similar. The Right Wing Dam gravels shows a slightly higher percentage of material passing the No. 4 sieve, 15 percent compared to 10 percent. The gradation ranges of the Mormon Island gravels and the Left Wing Dam gravels are compared in Figure 48. This plot shows that the gradations of the Left Wing and Mormon Island gravels are essentially the same. The Mormon Island gravels classified the same as the Wing Dam gravels, GP, GW-GC, or GW. Also, the Mormon Island gravels have a low fines content of about 5 percent which is approximately the same as the fines contents of the Wing Dam gravels.

59. Tables 2 and 7 list the borrow sources for the gravel materials used in the construction of the Wing Dams and Mormon Island Auxiliary Dam. The Right Wing Dam gravel, Zone B was obtained from Borrow Areas 7 and 8 and Stockpile 7. The Left Wing Dam gravel, Zone E in Table 4, and the Mormon Island gravel, Zone 1 in Table 5, were obtained from the same source area, Borrow Area No. 5, the Blue Ravine. Therefore, it is not surprising that the gradation ranges of these two gravels match.

60. The in situ densities observed from the ring density tests at Mormon Island are listed in Table 8. The dry densities ranged from 130.4 to 148.9 pcf and averaged 137.7 pcf. The average values were slightly higher than those observed in the Wing Dams. The relative density of the Mormon Island gravels was obtained using the in situ densities and the maximum minimum density curves shown in Figure 48. The relative density of Mormon Island gravels was estimated to be 71 percent which is somewhat higher than the 63 and 61 percent relative densities observed in the Right and Left Wing Dam gravels. However, it must be noted that as was the case with the Wing Dams there is a significant amount of scatter in the data pertaining to in situ densities and relative densities.

61. Table 9 shows a list of the compaction requirements for the gravels of the Wing Dams and Mormon Island Auxiliary Dam. The compaction procedure was the same for Zone B in the Right Wing Dam, Zone E in the Left Wing Dam, and Zone 1 in the Mormon Island Auxiliary Dam shell. The specified compaction of these materials required one complete coverage with a D-8 Caterpillar Tractor over a 24-in. lift thickness.*

* It was estimated that one complete coverage corresponds to 3 or 4 passes of the compaction equipment.

62. The shear wave velocities and corresponding $K_{2\max}$ values measured over various depth intervals from the crosshole tests at each of the three embankments are listed in Table 10. The term $K_{2\max}$ is defined in Table 10. Comparisons are made over two depth intervals, 0 to 10 ft and 20 to 60 ft. Between the depths of 0 to 10 ft, the interval sampled by the test pits, the embankments gravels rank (highest to lowest) according to shear wave velocity as Left Wing Dam (900 fps, $K_{2\max}$ of 126), Right Wing Dam (850 fps, $K_{2\max}$ of 112), and Mormon Island Auxiliary Dam (825 fps, $K_{2\max}$ of 106). This is not consistent with the rank according to test pit relative density in which the Mormon Island gravel had a relative density of 71 percent, followed by the Right Wing gravel with 63 percent, and the Left Wing gravel with 60 percent. At greater depths, between 20 and 60 ft, the rank according to shear wave velocity changes to Mormon Island and Left Wing Dam (both with velocities of 1,200 fps and $K_{2\max}$ of 115) followed by the Right Wing Dam gravel (1,050 fps, $K_{2\max}$ of 90).

63. Thus, since the gradations of the three gravels are similar and since the compaction procedures for each are the same it was expected that the relative densities observed at Mormon Island would be about the same as those observed in the Wing Dam gravels. However, as pointed out earlier, the data obtained from the test pits showed that, even from samples taken in the same shaft, the in situ densities and relative densities of each of the three embankment gravel zones show a great deal of scatter and variability. Also the inconsistencies between the rank in relative density and shear wave velocity suggest a degree of variability in the embankment gravels. It was concluded that due to in situ variability, the sample mean relative density of the Mormon Island gravels overestimated and the Wing Dam samples underestimated the true relative density of the entire population which includes the gravels at all three embankments. The gravel zones in the Wing Dams are considered to have about the same relative density as at the Mormon Island Auxiliary Dam because the compaction requirements and gradations were similar, and because the in situ variability can readily account for the differences in mean relative density and shear wave velocity values. Consequently, the Becker Hammer results (discussed in the next section) performed at Mormon Island Auxiliary Dam should be directly applicable to the Wing Dam gravels.

Becker Hammer Tests Performed at Mormon Island Auxiliary Dam

64. A histogram of results of Becker Hammer Tests performed in the Zone 1 embankment gravels at Mormon Island Auxiliary Dam are presented in Figure 50. Becker Hammer blowcounts used in this summary were obtained from soundings BH 15 through 21 and BH 25 and BH 26 whose locations are shown in Figure 45a. The field Becker blowcounts were converted to their equivalent SPT $(N_1)_{60}$ values using a data reduction procedure described in Reports 4 and 8 of this series. Figure 50 shows the distribution for 516 values of $(N_1)_{60}$ obtained in the Mormon Island downstream shells. The mean $(N_1)_{60}$ value from these blowcounts was 24.6 blows/ft. The standard deviation was 8.8 blows/ft. Like the in situ densities, relative densities, and shear wave velocities, the $(N_1)_{60}$ values of the Mormon Island gravels also show a great deal of scatter and lend additional evidence to the hypothesis that the characteristics of the shell gravels are highly variable. Thus, for reasons discussed earlier, the mean value was considered to be applicable to the Wing Dam gravels.

Becker Hammer Tests Performed in the Embankment Gravels at the Right and Left Wing Dams

65. A limited number of Becker Hammer penetration soundings were performed in the downstream shells at the Right and Left Wing Dams to confirm that the Mormon Island Becker data was similar. A total of six closed bit soundings (four at the Right Wing Dam and two at the Left Wing Dam) were performed at the locations shown in Figures 51 and 52. These tests, performed late in the study, were conducted to confirm that the penetration resistance of the embankment gravels in the Wing Dams (Zone B in the Right Wing Dam and Zone E in the Left Wing Dam) was about the same as that of the Mormon Island Auxiliary Dam.

66. The tests were performed between 12 October and 25 October 1988 by Becker Drills, Inc. of Commerce City, Colorado. The drilling was accomplished using a truck mounted B-180 Link-Belt pile driver. Becker Drills, Inc. identifies this rig as No. 011. The soundings were made using an 8-tooth crowd-out bit with a 6-5/8-in. O.D. casing. All tests were performed without a blower or supercharger.

67. For each sounding, Becker blowcounts, N_B , and bounce chamber pressure readings were recorded at 1 ft intervals. Each N_B blowcount was converted to its equivalent SPT $(N_1)_{60}$ blowcount using the data reduction procedures discussed in Appendix A. This conversion process is the result of research performed by Harder (1986) on the Becker Hammer Drill. The basic data acquired during the 1988 field investigations is also presented in Appendix A.

Results of tests performed at the Right Wing Dam

68. The four Becker Hammer soundings performed on the downstream slope of the Right Wing Dam, designated as BH-14-88 through BH-17-88, are shown on the plan of Figure 51. This view shows that a road is routed on the downstream slope between Station 265 and Station 280. Each sounding was situated on the side of the road nearer the centerline. The station, top of hole elevation, and depth of each hole are listed in Table 11.

69. The results of the penetration tests are presented in terms of their equivalent $(N_1)_{60}$ SPT blowcounts. The $(N_1)_{60}$ values for each of the four soundings are plotted on the downstream cross sectional view of the Right Wing Dam so that the blowcounts can be sorted for each material type. This cross sectional view is shown in Figure 53. The figure indicates that blowcount data was obtained in Zones A and B from each of the four soundings. As discussed in Part II, Zone A consists of a dumped rockfill and Zone B is a compacted gravel similar to the gravels found in the shell at the Mormon Island Auxiliary Dam. The $(N_1)_{60}$ blowcounts obtained in Zone A from BH 14-88, BH 15-88, and BH 16-88 are highly variable and show no consistent trends with depth. The Zone A $(N_1)_{60}$ values from these three soundings range between approximately 10 to 60 blows/ft. In contrast to this the Zone A $(N_1)_{60}$ values from BH 17-88 are consistently below 15 blows/ft. These low values are considered locally anomalous and are not considered to involve a large continuous volume of material. Although the difficulties in interpretation of blowcounts in a rockfill were considered, the Zone A data was interpreted as if Zone A were composed of gravel rather than rockfill. A statistical analysis was performed on the $(N_1)_{60}$ data obtained from Zone A. The results are listed in Table 12. Only blowcounts deeper than 5 ft were considered in this analysis. For the 29 penetration tests considered the global average was about 22 blows/ft and the standard deviation was about 8.6 blows/ft for the Zone A material.

70. A similar analysis was performed for the Zone B penetration tests. Figure 53 shows that the $(N_1)_{60}$ values in Zone B are also variable. The blowcounts are relatively low for the first 5 to 8 ft of sounding into Zone B and then increase to about 30+ blows/ft. The plots show that $(N_1)_{60}$ blowcounts in Zone B range from 10 to 60 blows/ft and are typically greater than 30 blows/ft. Between depths of 6 and 12 ft in BH 14-88 and 15 and 18 ft in BH 15-88 the $(N_1)_{60}$ blowcounts were about 10 blows/ft. The low $(N_1)_{60}$ values in these areas were considered to be part of the normal statistical variation. It is noted that similar pockets of low blowcounts were also detected in the similar Zone 1 embankment gravels at the Mormon Island Auxiliary Dam where much more data was acquired (see Reports 4 and 8 of this series). The results of the statistical analysis of the $(N_1)_{60}$ blowcounts in Zone B are listed in Table 13. Based on 84 points, the global mean value for $(N_1)_{60}$ was 35.3 blows/ft. The standard deviation was 13.4 blows/ft.

Results of tests performed at the Left Wing Dam

71. Two Becker Hammer soundings designated BH 18-88 and BH 19-88 were performed at midslope on the downstream side of the Left Wing Dam near Station 304+50 as shown in Figure 52. Table 14 contains information concerning the station, top of hole elevation, and depth for each sounding. The two holes were spaced only 35 ft apart. The foundation report for the Left Wing Dam (US Army Engineer District, Sacramento 1953) shows that bedrock should be encountered at about elevation 360 ft in this vicinity. Thus, both soundings were deep enough to terminate at the rock foundation beneath the shells.

72. Figure 54 shows a transverse cross-sectional view of the downstream portion of the Left Wing Dam in the vicinity of Station 304+50. The location of the two Becker holes is indicated in this figure. The figure shows that all but the bottom 5 ft or so of each sounding penetrated Zone E and Zone F. Zone E is a compacted embankment gravel which is similar to the Zone B gravels of the Right Wing Dam and the Zone 2 gravels of the Mormon Island Auxiliary Dam. Zone F (which underlies Zone E as shown in Figure 54) is a filter blanket composed of the -2 in. fraction of the Zone E materials and compacted according to similar specifications as the Zone E materials (see Table 3 for specification details). The equivalent $(N_1)_{60}$ blowcounts are plotted versus depth in the mid-slope profile shown in Figure 55. Like the data presented earlier for the Right Wing Dam and the Mormon Island Auxiliary Dam, the $(N_1)_{60}$

blowcounts from these two soundings are highly variable (see Reports 4 and 8 of this series). The data from both soundings are remarkably similar showing comparable $(N_1)_{60}$ blowcounts at corresponding depths. It is noted that two zones having $(N_1)_{60}$ blowcounts of less than 10 blows/ft were detected by each soundings between depths of 36 and 41 ft and 54 and 58 ft. These zones are considered to be part of the normal statistical variation since similar zones of low penetration resistance were also observed in the Becker Hammer Tests performed on similar materials at the Right Wing and Mormon Island Auxiliary Dam.

73. The results of a statistical analysis performed on the equivalent $(N_1)_{60}$ values of the Left Wing Dam embankment gravels (including both Zones E and F) are listed in Table 15. Equivalent $(N_1)_{60}$ values from depths less than 5 ft or at elevations less than 360 ft were excluded from the analysis. The global mean $(N_1)_{60}$ from 117 tests was 22.4 blows/ft and the standard deviation was 10.1 blows/ft.

Comparison of the Becker Hammer
Tests performed at the Mormon
Island Auxiliary Dam with the Becker
Hammer Tests performed at the Wing Dams

74. As stated previously, the cyclic strengths of the embankment gravels in the Wing Dams were determined from the Becker Hammer Penetration Tests performed in the similar Zone 1 embankment gravels at the Mormon Island Auxiliary Dam. The Becker Hammer Tests at the Wing Dams were used to validate that the equivalent $(N_1)_{60}$ blowcounts at the Wing Dams were approximately equal to or greater than those at the Mormon Island Auxiliary Dam. Summary statistics of Becker Hammer blowcounts from soundings BH 15 through BH 21 and BH 25 and BH 26 were computed. (The locations of these soundings are shown in Figure 45a. A cross sectional view of the Mormon Island Auxiliary Dam is shown in Figure 46.) The results of this statistical analysis performed on 516 $(N_1)_{60}$ values obtained in Zone 1 show that the mean $(N_1)_{60}$ value was 24.6 blows/ft. The standard deviation was 8.8 blows/ft indicating that these blowcounts have a fairly high degree of variability.

75. As discussed previously the mean $(N_1)_{60}$ value obtained from four soundings (84 tests) in Zone B of the Right Wing Dam was 35.3 blows/ft with a standard deviation of 13.4 blows/ft. This statistical analysis indicates the true mean $(N_1)_{60}$ blowcount for Zone B at the Right Wing Dam is probably at

least as high as that at the Mormon Island Auxiliary Dam and validates the use of the Mormon Island mean for the determination of the cyclic strengths at the Right Wing Dam. Analysis of the data obtained in Zone A showed that the equivalent mean $(N_1)_{60}$ blowcount for Zone A was determined to be 22 blows/ft with a standard deviation of 8.6 blows/ft. Statistical testing indicates the mean $(N_1)_{60}$ of Zone A is not significantly different than that of Zone 1 at the Mormon Island Auxiliary Dam at the 5 percent level of significance even though the materials are dissimilar. Thus, the foregoing analysis which compares Zones A and B with Zone 1 confirms that the mean $(N_1)_{60}$ blowcount are in good agreement with those obtained from Zone 1 at Mormon Island Auxiliary Dam.

76. The mean equivalent $(N_1)_{60}$ from two closely spaced soundings performed at the Left Wing Dam (117 tests) was 22.4 blows/ft with a standard deviation of 10.1 blows/ft. The mean value of this data is only about 2 blows/ft lower than that determined from the Mormon Island Dam samples. On a hole by hole basis statistical testing indicates that the mean $(N_1)_{60}$ blowcounts computed for the Zone E materials of both soundings individually are not significantly different than the mean $(N_1)_{60}$ value for the Mormon Island Auxiliary Dam at the 5 percent level of confidence. This justifies the use of the mean $(N_1)_{60}$ from the Mormon Island Auxiliary Dam tests for determining the cyclic strengths of the embankment gravels at the Left Wing Dam.

PART IV: ESTIMATES OF CYCLIC STRENGTH

General

77. The cyclic strength and pore pressure generation characteristics of the embankment materials were estimated from a combination of in-situ and laboratory test results. This chapter contains descriptions of the procedures used for estimating the cyclic strength from the in-situ SPT tests performed in the core of the Right and Left Wing Dams and Becker Hammer test soundings performed in the downstream shell of Mormon Island Auxiliary Dam. A comprehensive laboratory investigation was performed to determine the relative strength and pore pressure behavior of gravels subjected to cyclic loads. These tests were designed to determine the relative changes in cyclic strength with confining stress (K_{σ}) and consolidation stress anisotropy (K_{α}). The results of these tests are reported in the following pages. A detailed discussion of the laboratory program is included in Report 4 of this series. Tests performed on undisturbed specimens of compacted decomposed granite and index tests of all materials are reported in a report prepared by the US Army Engineer Laboratory, South Pacific Division (1986).

Estimates of Cyclic Strength from In-Situ Tests

Empirical procedure to estimate cyclic strength

78. The cyclic strengths of the shell and dredged and undredged foundation gravels were determined using Seed's empirical procedure (Seed et al. 1983, and Seed et al. 1984a). The chart used for determining cyclic strength based on Seed's work is shown in Figure 56. This chart relates measured $(N_1)_{60}$ values to estimated cyclic stress ratios at a number of sites which have been subjected to earthquake shaking from a $M = 7.5$ seismic event. The lines on the chart distinguish safe combinations of $(N_1)_{60}$ and cyclic stress ratios from unsafe combinations based on whether or not surface evidence of liquefaction was observed in the field. This chart is interpreted to relate $(N_1)_{60}$ to the cyclic stress ratio required to generate 100 percent residual excess pore pressure. Figure 56 provides data for clean and silty sands with different fines contents, and expresses the cyclic stress ratio causing

liquefaction, for a confining pressure of about 1 tsf and level ground conditions and for earthquakes with $M = 7.5$, as a function of the N_1 -value of a soil corrected to a 60 percent energy level, $(N_1)_{60}$. Seed's work (Seed et al. 1983, and Seed et al. 1984) shows that for $M = 6.5$ events, the cyclic loading resistance is about 20 percent higher, for any value of $(N_1)_{60}$, than for $M = 7.5$ earthquakes.

Cyclic strength estimate for
shell materials, Zones A, B, E, and F

79. The representative $(N_1)_{60}$ values used to enter the cyclic strength chart shown in Figure 56 were determined from the field investigations discussed in Part III of this report. The representative $(N_1)_{60}$ value for the shell gravels was 25 blows per foot which is the average $(N_1)_{60}$ for all blow-counts in the shell from Becker closed-bit soundings performed in the downstream shell at Mormon Island Auxiliary Dam. As discussed in Part III, the fines content of the embankment gravel was estimated to be about 5 percent. Thus, entering the chart at an $(N_1)_{60}$ of 25 blows per foot and using the curve for 5 percent or less fines content yields a cyclic stress ratio of 0.29 for a Magnitude 7.5 event. This value was increased by 20 percent to account for the lower Magnitude 6.5 event. This resulted in a cyclic stress ratio of 0.35 required to generate 100 percent excess pore pressure in 8 equivalent cycles (representative for a $M = 6.5$ event) under level ground at a vertical effective stress of 1 tsf.

80. Due to the similarity of the Zone B transition gravel in the Right Wing Dam to the Zone E shell gravel in the Left Wing Dam, in terms of gradation, fines content, and method of placement, it was concluded that the Zone B gravel could reasonably be assumed to have the same cyclic strength as the Zone E embankment shell. The Zone A rockfill was treated as part of Zone B in this analysis as it was in the original design of the dam. The Zone F filter material is the minus 2-in. fraction of the Zone E shell gravel, and was placed in 12-in. layers rather than the 24-in. layers used in Zones B and E. For simplicity, this thin filter zone was assumed to have the same cyclic strength as the shell gravels. The cyclic strength value of 0.35 for Zones A, B, E and F was appropriately corrected to allow for overburden pressures greater than 1 tsf and to allow for the anisotropic confining stresses occurring under sloping ground conditions. These corrections are based on laboratory test results. Figure 57 is a schematic description of the

procedures used for determining the cyclic strengths for any finite element in the idealized embankment cross-section used in the analysis.

Cyclic strength of pre-existing embankment and
Zone C and Zone G core materials

81. The cyclic strength of the compacted decomposed granite filter (Zone 3) was similarly determined from blowcounts. Based on construction records and sieve analysis of disturbed and undisturbed samples obtained during this study, the fines content of the compacted decomposed granite core averaged about 30 percent in the pre-existing embankment and about 20 percent in Zone C of the Right Wing Dam, and about 30 percent in the Zone G core of the Left Wing Dam. At depths greater than 30 ft (where the material is saturated) the $(N_1)_{60}$ values are typically well in excess of 30 blows per foot. Therefore, based on Seed's correlations in Figure 56, the high Standard Penetration Test blowcount resistance, the high fines content, the nature of saprolite, and the method of placement, the compacted decomposed granite in the core zones is not considered susceptible to liquefaction and high pore pressure buildup during the design earthquake.

Relative Cyclic Strength Behavior
of Embankment Gravels

82. A series of cyclic triaxial shear tests was performed in the laboratory to measure the effect of confining pressure and stress anisotropy on the cyclic loading resistance of the embankment gravels. The relationship between residual excess pore pressure and safety factor against liquefaction was also determined from analysis of the laboratory data. A detailed discussion of the analysis of the laboratory data is included in Report 4 of this series and will not be repeated here.

83. The procedure for computing the cyclic strength for a location in the embankment is outlined in Figure 57. The cyclic strength of a soil depends on the states of stress existing in the soil prior to the earthquake, i.e., the static stresses. The cyclic stress ratios (τ_c/σ'_0) determined from Seed's charts using the Becker Penetration Test results for the embankment gravels apply only to level ground conditions where a vertical effective stress of 1 tsf exists. Therefore, adjustments must be made to the chart cyclic stress ratio to take into account sloping ground conditions and

locations where the vertical effective stress is not equal to 1 tsf. The adjusted cyclic stress ratio is calculated with a knowledge of the states of stress using the following equation:

$$\frac{\tau_c}{\sigma'_v} (\alpha \neq 0, \sigma'_v \neq 1 \text{ tsf}) = K_\sigma \times K_\alpha \times \frac{\tau_c}{\sigma'_v} (\alpha = 0, \sigma'_v = 1 \text{ tsf}) \quad (2)$$

For the embankment gravel where the chart cyclic stress ratio equals 0.35, Equation 2 can be rewritten as follows:

$$\frac{\tau_c}{\sigma'_v} (\alpha \neq 0, \sigma'_v \neq 1 \text{ tsf}) = K_\sigma \times K_\alpha \times 0.35 \quad (3)$$

The cyclic strength can be determined by multiplying the adjusted stress ratio in Equation 2 by the vertical effective stress.

84. In Equation 2, K_σ is an adjustment factor which accounts for the nonlinear increase in cyclic strength with increasing confining stress. A chart of K_σ determined in the laboratory for the embankment gravels is shown in Figure 58. This chart shows that K_σ is a function of the vertical effective stress. K_σ is less than 1 for vertical stresses less than 1 tsf and is greater than 1 for vertical stresses greater than 1 tsf.

85. In Equation 2, the adjustment factor K_α accounts for the increase in cyclic strength due to the presence of shear stresses on horizontal planes. Non-zero shear stress on horizontal planes is characteristic of sloping ground conditions. A chart of K_α determined in the laboratory for the embankment gravels is shown in Figure 59. K_α is a function of α which is the ratio between shear stresses on horizontal planes and the vertical effective stress. K_α has a value of one for level ground conditions where α is equal to zero. The chart shows that K_α increases with increasing values of α , however, α is limited by the shear strength of the soil deposit in question. K_α is equal to 1.0 for level ground conditions where α is equal to zero.

86. Pore pressures induced in the embankment gravels are estimated using a relationship between safety factor against liquefaction and R_u which was developed from laboratory test data for Folsom shell gravels. The safety

factor against liquefaction, FS_L , is defined as the ratio of cyclic strength to dynamic shear stress. R_u , the excess pore pressure ratio, is the ratio of residual excess pore pressure to normal effective consolidation stress on the failure plane. A plot showing the relationship between FS_L and R_u is shown in Figure 60. As values of FS_L increase, the corresponding values of R_u decrease.

87. The adjustment factors, K_α and K_σ , are used later to determine the cyclic strengths in the embankment for the seismic stability analysis. The dynamic stresses computed in the dynamic response computations are then compared with the cyclic strengths to obtain the FS_L for each element in the embankment shell. An excess pore pressure field is then computed for the embankment shell by translating FS_L into R_u for each element in the mesh. Post-earthquake stability and permanent displacement calculations are then made with the excess pore pressures in the shell.

PART V: STATIC FINITE ELEMENT ANALYSIS

General

88. A static finite element analysis was performed to determine the pre-earthquake vertical effective stresses and the initial static shear stresses on horizontal planes throughout the dam and foundation. This information was used to calculate values of α , the ratio of initial horizontal shear-stress to initial vertical effective stress, so that the appropriate cyclic strength could be associated with each element. The idealized section that was developed for the finite element analysis is representative of both the Right and Left Wing Dams.

89. The computer program FEADAM84 developed by Duncan, Seed, Wong, and Ozawa was used to calculate the initial effective stresses in the shells of the dam. This program is a two-dimensional, plane strain, finite element solution for determining static stresses, strains, and displacements in earth and rockfill dams and their foundations. The program uses a hyperbolic constitutive model developed by Duncan et al. (1984) to estimate the nonlinear, stress history dependent, stress-strain behavior of the soils. The hyperbolic constitutive model requires 9 parameters. The program performs incremental calculations to simulate the addition of layers of fill during construction of an embankment. A description of the constitutive model, procedures for evaluating the parameters, and a data base for typical parameter values are described by Duncan et al. (1980).

Section Idealization and Static Finite Element Inputs

90. The finite element mesh was developed from a composite of several cross sections along the axes of the Right and Left Wing Dams. The tallest upstream slope occurs near Station 283 near the wrap-around of the Right Wing Dam with the Concrete Gravity Dam. This section was selected for analysis. The field section and the idealized analysis section are shown in Figure 61. Shorter sections of the Wing Dams are similar to the segment of Mormon Island Auxiliary Dam that is founded on rock. A complete analysis appropriate to this shorter section is presented in Report 8 of this series. (This section

was also found to perform satisfactorily during and after the design earthquake.)

91. Table 16 contains a summary of the hyperbolic constitutive model parameter values for each of the materials in the idealized Wing Dam cross section. The parameter values listed in Table 16 were determined from consideration of several different sources of information: drained and undrained triaxial shear tests on Folsom embankment gravels, comparison with soils of similar characteristics from a database of over 150 soils, and geophysical test results.

92. The finite element mesh used to represent the dam cross section is shown in Figure 62. This mesh was used for both the static and dynamic finite element analyses. It contains 325 elements and 343 nodal points. The mesh was constructed giving consideration to the distribution of materials in the cross section, the shear wave velocities measured in the field, and specific criteria for dynamic finite element meshes (Lysmer 1983). Consequently, the mesh is a compromise between the needs of the dynamic and the static finite element computations. Element heights were varied throughout the mesh to meet the Lysmer criteria, as described in the next chapter. The resulting mesh had a maximum element height of 20 ft, and the aspect ratio (length/height) did not exceed 4 for any element.

93. Five material types are represented in the finite element mesh. The properties and hyperbolic parameters for each of these material types are listed in Table 16. The embankment was represented by four materials: (a) submerged shell gravel, (b) moist shell gravel, (c) moist impervious core, and (d) submerged impervious core. The foundation material was rock. Submerged embankment material zones (those below the phreatic surface) had the same properties as their non-submerged counterparts except that buoyant unit weights rather than total unit weights were used in the static stress calculations. The rockfill shell, Zone A, was assumed to have the same properties as the gravel transition, Zone B.

94. The construction sequence of the dam was modeled by building the dam in lifts. A construction increment was typically 1 element high. In the analysis it was assumed that the entire differential head imposed by the reservoir was lost across the core material and that no head was lost in the pervious embankment shells. This situation imposes unbalanced hydrostatic pressures on the upstream face of the core. The unbalanced hydrostatic

pressure distribution acting on the upstream side of the impervious core was simulated in FEADAM84 by an equivalent system of forces applied to the nodes on the upstream face of the core and acting in the downstream direction. These forces were applied after the dam was "numerically" constructed. FEADAM84 was then used to compute the states of stress occurring in the embankment under these conditions.

Results of Static Analysis

95. Contours of vertical effective stress, horizontal effective stress, shear stresses on horizontal planes and α developed from the FEADAM84 static stress computations are shown in Figures 63 through 66. The contours of vertical effective stress shown in Figure 63 reflect the effect of submergence since the vertical effective stresses in the upstream portion of the dam and foundation are lower than those at corresponding points on the downstream portion of the dam. This plot also shows almost no evidence of arching across the impervious core, since the vertical stresses in the impervious core are about the same as vertical stresses at corresponding elevations in the shell just outside the core. Little or no arching is expected since the core is fairly wide. Figure 64 shows that the contours of horizontal effective stress generally follow the surface geometry of the embankment, with the exception that the stresses in the impervious core are slightly lower than at corresponding depths in the shells.

96. Contours of static shear stresses on horizontal planes are shown in Figure 65. Due to the sign convention of the program and coordinate systems used, the shear stresses on the downstream side of the centerline have the opposite sign of those of the upstream side. Near the surface of both the upstream and downstream slopes, the contours run parallel to the slopes. Submergence causes the magnitude of the shear stresses on the downstream side to be higher than the values for corresponding points on the upstream side, and shifts the zero contour slightly to the downstream side of the centerline.

97. Figure 66 shows contours of α values. The α values shown in this figure are the ratios of initial static shear stress acting on horizontal planes to vertical effective stress. The contours show that α ranges from a value of zero near the centerline to maximum of 0.4 near both the upstream and downstream slopes. The contours show that the magnitude of α is slightly

higher in the downstream shell than at corresponding points in the upstream shell.

98. The effective mean normal pressure was computed for each element in the mesh from the FEADAM84 results. The effective mean normal stress was computed using the following equation formulated from theory of elasticity for plane strain conditions:

$$\sigma'_m = (\sigma_x + \sigma_y)(1 + \mu) \quad (4)$$

where

σ'_m = effective mean normal pressure

σ_y = vertical effective stress

σ_x = horizontal effective stress

μ = Poisson's ratio

Each of the parameters on the right hand side of the equation was evaluated with FEADAM84 for each element in the mesh. As with the vertical effective and horizontal effective stresses, the effective mean normal pressure contours generally follow the geometric shape of the embankment. Due to submergence, the values of effective mean normal pressures are lower in the upstream shell than at corresponding points in the downstream shell.

99. These static stress results are used in subsequent portions of the seismic stability study. They are used to estimate overburden correction factors for interpretation of the equivalent SPT blowcounts from Becker Hammer soundings, extrapolation of in situ measurements to other portions of the cross section (such as geophysical results and blowcounts results), and to determine the appropriate cyclic strength for each portion of the embankment, since cyclic strength varies with vertical effective stress and α .

PART VI: DYNAMIC FINITE ELEMENT ANALYSIS

General

100. A two-dimensional dynamic finite element analysis was performed with the computer program FLUSH (Lysmer et al. 1973) to calculate the dynamic response of the idealized cross section to the specified motions. The objectives of this analysis were to determine dynamic shear stresses, maximum accelerations at selected points in the cross section, earthquake-induced strain levels, and the fundamental period of the idealized cross section at both low strain levels and higher earthquake-induced strain levels.

Description of FLUSH

101. FLUSH is a finite element computer program developed at the University of California Berkeley by Lysmer, Udaka, Tsai, and Seed (1973). The program solves the equations of motion using the complex response technique under the assumption of total stress conditions. Non-linear soil behavior is approximated with an equivalent linear constitutive model which relates shear modulus and damping ratio to the dynamic strain level developed in the material. In this approach FLUSH solves the wave equation in the frequency domain and uses an iterative procedure to determine the appropriate modulus and damping values to be compatible with the developed level of strain. FLUSH assumes plane strain conditions. As a two-dimensional, total stress, equivalent linear solution, FLUSH does not take into account the effect of possible pore water pressure dissipation during the earthquake. For most earth dams this introduces an element of conservatism into the results. Each element in the mesh is assigned properties of unit weight, shear modulus, and strain-dependent modulus degradation and damping ratio curves. FLUSH input parameters for the various zones in the cross section are described in the next section.

Inputs to FLUSH

102. The same mesh as that used in the static analysis was used in the dynamic analysis. From the static finite element solution the vertical effective, horizontal effective, initial static shear, and effective mean normal

stresses were computed at the centroid of each element. In the dynamic analysis the dynamic shear stress history is calculated at the centroid of each element. The same mesh is used in both the static and dynamic finite element analyses so that the centroid locations of the computed stresses from each match exactly. This makes the data processing and post processing calculations much simpler.

103. The elements were designed to insure that motions in the frequency range of interest propagated through the mesh without being filtered by the mesh. The maximum element height was determined with Equation 5:

$$h_{\max} = \frac{1}{5} \times v_e \times \frac{1}{f_c} \quad (5)$$

where

h_{\max} = maximum element height

v_e = lowest shear wave velocity compatible with earthquake strain levels in zone of interest

f_c = highest frequency in the range of interest

In the design of this mesh, f_c was limited to 10 Hz. The low strain amplitude shear wave velocity distribution of the cross section determined from geophysical testing and consideration of static stress analysis results is shown in Figure 36. In the upper portion of the embankment the low strain amplitude shear wave velocity is about 800 fps. It was estimated that the earthquake would induce strain levels in the embankment which would degrade the velocity to fifty percent of its low strain value. The value of h_{\max} in the upper section was calculated with Equation 5 as follows:

$$h_{\max} = \frac{1}{5} \times \frac{800}{2} \times \frac{1}{10} = 8 \text{ ft}$$

According to Lysmer's criteria, the height of any element in the upper zone should not exceed 8 ft. Elements throughout the remainder of the cross section were similarly sized in accordance with the measured shear wave velocities. Calculations performed for materials at lower elevations in the embankment indicated that the element heights should not exceed 20 ft. In the final mesh all elements had heights between 8 and 20 ft with the tallest elements located at lower elevations in the embankment.

104. The earthquake-induced dynamic shear stresses were computed with Accelerogram B since preliminary SHAKE (a one-dimensional dynamic response code, Schnabel et al. 1972) analyses of columns through the shells indicated that Accelerogram B resulted in about the same to slightly higher dynamic stresses than Accelerogram A. The ground motions represent rock outcrop motions, and were input to the rock surface at an outcropping baserock layer.

105. The key material properties for each element were unit weight and shear wave velocity. The unit weights required are total unit weight. Total unit weights were distributed throughout the cross section as defined in the static finite element analyses. The shear wave velocity results were estimated to be distributed throughout the cross section as shown in Figure 36. The in situ geophysical measurements were made in the downstream area. In the extrapolation of these results to the upstream shell and foundation, the reduced confining stress due to the presence of the reservoir was considered.

106. The modulus degradation and damping curves used in the FLUSH computations were the average curves for sand from Seed and Idriss (1970). Seed et al (1984) recently published a curve for gravelly soils which shows lower shear moduli for a given shear stress than those for sand. The degradation curves observed in the laboratory tests on Folsom gravels fell within the range of gravel data reported by Seed et al (1984). This comparison is shown in Figures 67 and 68. The consequence of using the sand curve rather than the lower gravel curve is that the computed dynamic shear stresses are generally slightly higher. The difference is most significant when the shear strains equal 10^{-2} percent and less significant when the shear strains exceed the 10^{-1} percent level.

Dynamic Response Results

107. The FLUSH program is used to compute the dynamic shear stress history for the centroid of each element in the finite element mesh and the acceleration history for each nodal point in the mesh. From these calculations, the maximum earthquake-induced horizontal cyclic shear stress computed for each element over the entire time period of shaking was determined from the finite element results and this value was then multiplied by 0.65 to determine the average cyclic load imposed by the earthquake. Contours of average earthquake-induced dynamic shear stresses are plotted on

the cross section shown in Figure 69. These average dynamic shear stresses ranged from approximately 0.5 ksf in the near surface layer in the upper portion of the embankment to 2.5 ksf in the lower portion of the core trench. Safety factors against liquefaction in the embankment shell and foundation are calculated with these dynamic shear stresses, as shown in Part VII.

108. The program FLUSH was used to compute accelerations for each of the nodal points in the finite element mesh. Figure 70 shows accelerations computed for several nodal points in the dam cross section. The rock outcrop record had a peak acceleration of 0.35 g. When these motions are propagated through the dam, the peak acceleration underneath the centerline of the dam at the contact of the bedrock and the core is 0.29 g. When these motions are propagated up through the core of the dam the computed crest acceleration is 0.54 g. In general the finite element analysis results indicate that the incoming earthquake ground motions will be amplified as they propagate through the foundation and embankment materials.

109. During earthquake shaking the embankment undergoes shear straining. Consequently, the shear modulus is reduced in the manner indicated in Figure 67. Figure 71 shows typical effective shear strain (single amplitude) levels computed for various zones of the cross section. The strain levels shown in Figure 71 are effective cyclic strain levels determined with FLUSH, and are equal to 65 percent of the maximum cyclic shear strains. The effective cyclic shear strain levels were typically 0.1 to 0.2 percent. These shear strain levels are quite low. In this shear strain region, the use of the gravel rather than the sand modulus degradation curve for the shell gravels had a conservative effect on the computed dynamic shear stresses. From the modulus degradation curves of Figure 67, at this strain level the shear moduli for elements in these zones have degraded to about 25 percent of their maximum value. This level of degradation is consistent with that estimated in the mesh design and corresponds to a cut off frequency of 10 Hz.

110. At low strain levels (no earthquake shaking), the fundamental period T_o of this section, estimated by Sarma's technique (Sarma 1979) for an idealized two-dimensional section founded on rock was computed with Equation 6:

$$T_o = \frac{2.61 \times H}{v_s} \quad (6)$$

where H is the embankment height and V_g is the average shear wave velocity. From Equation 6, the low-strain level value of T_0 was estimated to equal 0.28 seconds.

111. As the shear modulus reduces due to earthquake-induced straining, the fundamental period of the dam increases. The fundamental period of the idealized two-dimensional section at the strain levels induced by the seismic safety evaluation earthquake was 0.83 seconds, determined from the Fourier amplification function for the nodal point at the crest of the section, shown in Figure 72. The initial fundamental period of 0.28 seconds and the fundamental period of 0.83 seconds effective at the strain levels induced during the earthquake are compared with the response spectra for Accelerogram B in Figure 73. This figure shows that the initial fundamental period of the dam falls well within the high energy portion of the response spectrum of Accelerogram B and that response values are still high at the strain-compatible fundamental period of 0.88 sec. This means that the section selected for analysis will undergo significant earthquake loading in the numerical dynamic response analysis with Accelerogram B as the input ground motion. Hence, the analysis section and Accelerogram B are well suited for the seismic safety evaluation of the Left and Right Wing Dams.

PART VII: EVALUATION OF LIQUEFACTION POTENTIAL

General

112. The cyclic strengths estimated from the in situ Becker Hammer tests and laboratory studies were compared with the average earthquake-induced shear stresses to compute safety factors against liquefaction throughout the upstream submerged embankment shell. A relationship between safety factor against liquefaction and residual excess pore pressure was developed in Part IV from laboratory data and was used to estimate the residual excess pore pressure field in the shell and foundation as a result of the earthquake shaking. These computations and their results are described in this chapter. The residual excess pore pressure fields predicted for the embankment shell in this chapter are later used to compute the post earthquake stability. As discussed later in this chapter, the compacted decomposed granite core is not considered susceptible to liquefaction and no significant excess pore pressures are expected to occur in this zone as a result of earthquake shaking.

Safety Factors Against Liquefaction in Embankment Shell

113. As described in Part IV, the available cyclic strength (expressed as a cyclic stress ratio) of the embankment shells is 0.35. This value was obtained from Seed's field performance correlations, an $(N_1)_{60}$ of 25 and a fines content of 5 percent. This cyclic shear strength ratio is defined as the cyclic shear stress ratio required to develop 100 percent residual excess pore pressure in eight equivalent cycles at a confining stress of 1 tsf for a Magnitude 6.5 event. The cyclic strength ratios for each element were determined with the appropriate values of vertical effective stress, α , K_σ , K_α , and the cyclic strength ratio value of 0.35. Figure 57, presented previously, illustrates the procedure for computing the cyclic strength of an element. The K_σ and K_α curves used in the procedure were presented in Part IV and are shown in Figures 58 and 59, respectively. The safety factor against liquefaction is computed as the ratio of the available cyclic shear strength to the average earthquake-induced cyclic shear stress.

114. Contours of safety factors against liquefaction for the upstream shell of the cross section are shown in Figure 74. The safety factors range

from 1.5 to 2.5. The zone of lowest safety factors occur at the center of the upstream shell and trend parallel to the upstream slope.

Residual Excess Pore Pressures

115. Figure 60 was used to associate residual excess pore pressures with the computed safety factors against liquefaction. The residual excess pore pressures are expressed in terms of the pore pressure ratio R_u , defined as the ratio of residual excess pore water pressure to vertical effective stress. Contours of R_u in the upstream shell are plotted on the cross section shown in Figure 75.

116. The contours show that the maximum predicted R_u in the shell is about 25 percent. This pore pressure zone is located approximately coincident with the zone at lowest factors of safety mentioned above. Throughout the upstream shell the R_u value is typically 20 percent. Figure 75 also shows that the contours are generally oriented parallel to the slope of the dam. Along the surface of the slope R_u will be zero because this surface is a drainage boundary. The residual excess pore pressures in the shell were used to compute the safety factor against sliding in an effective stress post-earthquake stability calculation discussed in a subsequent chapter.

Liquefaction Potential Evaluation of Central Impervious Core

117. The core consisting of decomposed granite is well compacted, has a high fines content (typically 20 to 25 percent), and has high $(N_1)_{60}$ values (average was 63 blows/ft). The relationship between cyclic strength and $(N_1)_{60}$ shown in Figure 56 indicates that threshold values of $(N_1)_{60}$ exist for various fines contents. Materials with values of $(N_1)_{60}$ at or above the threshold will not develop significant residual excess pore pressures regardless of the severity of induced cyclic shear stresses. For a fines content of about 20 percent, the threshold value of $(N_1)_{60}$ is about 24 blows/ft. The average $(N_1)_{60}$ for the core materials at the Wing Dams was about 63 blows/ft. Clearly, the penetration resistance of the core materials in the Wing Dams is much higher than the threshold value for these materials. It was determined that safety factors against liquefaction in this material would be so high that no significant excess pore pressures are expected to develop.

Summary

118. The safety factors against liquefaction in the upstream shell were computed by comparing the cyclic strengths of the gravels with the dynamic stresses induced by the earthquake. The safety factors obtained ranged from 1.5 to 2.5. The computed safety factors against liquefaction were then associated with corresponding residual excess pore pressures to determine the post-earthquake R_u distribution in the shell. The maximum excess pore pressure ratio is expected to be 25 percent and in a significant portion of the shell the excess pore pressure ratio should not exceed about 20 percent.

PART VIII: STABILITY EVALUATION

General

119. The computer program UTEXAS2 was used to evaluate post-earthquake slope stability of the idealized cross section. UTEXAS2 was written and developed by Dr. Stephen Wright at the University of Texas, Austin. It was improved for Corps of Engineers use under the auspices of the Computer Applications of Geotechnical Engineering (CAGE) and Geotechnical Aspects of the Computer-Aided Structural Engineering (G-CASE) programs of the WES (Edris and Wright 1987). UTEXAS2 uses Spencer's method to compute the factor of safety against sliding. Two approaches were used to evaluate the stability of the slope. In the first, the safety factor against sliding was calculated with the assumption that the excess pore pressure fields shown in Figure 75 existed in the shells. In the second approach, a permanent deformation analysis was performed to estimate the amount of Newmark-type movement which might occur along potential failure surfaces in the embankment. The permanent displacement analysis was also performed using the excess pore pressure fields shown in Figure 75.

Post-Earthquake Slope Stability Analysis

120. The post-earthquake safety factor against sliding was calculated using effective stress analysis incorporating the residual excess pore pressure fields shown in Figure 75. In this type of analysis it is assumed that these pore pressures will be developed during the earthquake and they will be present in the shell immediately after the shaking stops. The shear strength parameters and unit weights used for each zone in the embankment are listed in Table 17. As a conservative measure, the tangent of the friction angle of the impervious core was reduced by 20 percent to account for any minor strength loss or pore pressure buildup which might occur as a result of the earthquake.

121. Only upstream circles were investigated in the stability analysis. The investigation involved a thorough search to find the critical circle. The circle judged to be most critical is that which had the lowest safety factor among the set of circles which encompass a significant amount of material in the failure mass. Thus, very shallow circles involving only surficial sliding

were not considered to be among circles considered most critical in this analysis. The critical circle for this analysis is shown in Figure 76. The failure surface of this circle passes through the zone of highest pore pressure where R_u is 25 percent. Although this circle is contained within the upstream shell it involves a significant amount of material. The post-earthquake safety factor against sliding computed for this circle was 1.54. The safety factor against sliding for this same circle before the earthquake shaking was 2.2. The excess pore pressure field used in the analysis reduces the safety factor against sliding for the critical circle by 30 percent. It was concluded that the upstream and downstream slopes of this portion of the dam will be stable immediately following the design earthquake.

Permanent Displacement Analysis

122. A permanent displacement analysis was performed to estimate the amount of displacement which might accumulate along potential failure surfaces during the earthquake. These deformations are determined from yield accelerations and dynamic response accelerations at various embankment levels in a sliding block analysis. The yield acceleration is the pseudo-static acceleration applied at the center of gravity of a sliding mass which will reduce the safety factor against sliding to one. Two methods were used to estimate permanent deformations, namely the Makdisi-Seed and the Sarma-Ambraseys approaches. The yield accelerations were computed using the excess pore pressures in the upstream shell shown in Figure 75. The use of these excess pore pressures in the analysis follows from the conservative assumption that the pore pressures in the shell will build up to their maximum values during the onset of shaking and will be maintained throughout the duration of shaking. Displacements were computed for potential sliding masses which involved material upstream of the centerline, and also for deeper sliding masses which involving materials downstream of the dam centerline.

Computation of yield accelerations

123. The yield acceleration for various elevations in the embankment were calculated with the seismic coefficient option in UTEXAS2. The critical yield accelerations were determined for failure circles tangent to elevations of 442, 404, 366, 328, and 290 ft which correspond to dimensionless depth ratios, y/h , of 20, 40, 60, 80, and 100 percent, respectively. Critical

yield accelerations were computed at these elevation levels for potential sliding masses contained mostly in the upstream shell and for the deeper sliding masses involving materials downstream of the centerline.

124. Figure 77 shows the critical yield accelerations and the slip surfaces for sliding masses which involve material upstream of the dam centerline. The circles tangent to elevations 290, 328, and 366 ft have yield accelerations which range between 0.10 g and 0.11 g and pass through the R_u zones of 20-25 percent which are the zones with the highest amount of residual excess pore pressure. The circles tangent to elevations 404 and 442 have yield accelerations of 0.17 g and 0.23 g, respectively. The slip surfaces of these circles are largely located above the elevations where the high pore pressure zones occur.

125. Figure 78 shows the yield accelerations for potential slip circles which emerge from the embankment downstream of the dam centerline. These yield accelerations range between 0.14 g and 0.28 g and are higher than those at corresponding elevations from the previous case. The requirement that the slip circles emerge in the downstream slope forces the circles to be deeper in the embankment. The yield accelerations computed for the upstream shell circles and the deeper circles are compared in Figure 79.

Makdisi-Seed method

126. The Makdisi-Seed technique (1979) was used to estimate the amount of Newmark-type sliding that might occur along potential slip surfaces in the embankment. The Makdisi-Seed technique was developed for dams founded on rock and is based on the analysis of many dynamic finite element solutions. Permanent displacements are estimated from charts and a knowledge of the embankment crest acceleration, fundamental period at earthquake-induced strain levels, and yield accelerations.

127. Permanent displacements were determined for the failure masses identified in the yield acceleration analyses. These circles were tangent to elevations 442, 404, 366, 328, and 290 ft which correspond to y/h values of 20, 40, 60, 80, and 100 percent, respectively. The charts used in the analysis are shown in Figure 80. Figure 80a shows a range of normalized maximum accelerations, k_{\max}/\ddot{u}_{\max} , versus normalized depth, y/h . In this study the average curve was used to determine the variation of the maximum acceleration ratio, k_{\max}/\ddot{u}_{\max} , with depth. At each of the depths investigated, the earthquake-induced acceleration of the sliding mass, k_{\max} , was determined by

multiplying the maximum acceleration ratio obtained from the chart by the peak crest acceleration, \ddot{u}_{\max} . The peak crest acceleration is 0.54 g as shown in Figure 70. This was determined from the FLUSH dynamic response computations using Accelerogram B. The permanent displacements for each slip circle investigated were determined from Figure 83b. This chart displays the variation of displacement, U , (divided by k_{\max} , the acceleration of gravity, g , and fundamental period, T_o) versus yield acceleration, k_y (normalized by k_{\max}). The ratio k_y/k_{\max} was computed for each sliding mass, and the chart was entered on the abscissa at that point. The corresponding displacement term was obtained from the ordinate axis using the curve for Magnitude 6.5 events. The displacement, U in ft, was calculated by multiplying the chart displacement term by k_{\max} , g in ft/sec², and T_o in seconds. This displacement in turn was multiplied by a factor, α , of 1.3 which accounts for the direction of the resultant shearing resistance force which comes from the solution to the equation of motion for a sliding block on a plane (see Hynes-Griffin and Franklin 1984). The term α was computed from Equation 12 (Hynes-Griffin and Franklin 1984):

$$\alpha = \frac{\cos (\beta - \theta - \phi)}{\cos \phi} \quad (7)$$

where

β = direction of the resultant shear force and displacement, and the inclination of the plane

θ = direction of the acceleration, measured from the horizontal

ϕ = friction angle between the block and the plane

The term β was assigned a value of 25° based on the average direction of the resultant shearing resistance of critical circles from the UTEXAS2 calculation; θ was set to zero since the applied accelerations are horizontal; and ϕ was set to 43° which is the effective friction angle of the embankment gravels. The fundamental period of the embankment used in this calculation was 0.855 sec. Permanent displacements were determined for each of the potential failure masses shown in Figures 77 and 78.

128. The Makdisi-Seed computations are summarized in Tables 18 and 19. Table 18 shows the results for the set of failure masses upstream of dam centerline and Table 19 shows the results for the set which involve materials

downstream of the dam's centerline. The displacements computed for each set are also presented in Figure 81. The computed maximum displacement in the upstream shell set of potential failure masses was about 0.42 ft for slip surfaces tangent to elevation 366 ft. The computed maximum displacement for the deeper circle was about 0.19 ft, also at elevation 366 ft. In all cases, at corresponding tangent elevations, the displacements for the upstream shell circle are greater than those for the deeper circle involving material downstream of the centerline. Thus, the Makdisi-Seed computations for both sets of potential upstream slip circles indicate that the Newmark-type displacements may be approximately 0.5 ft or less.

Sarma-Ambraseys method

129. The Sarma-Ambraseys technique was the second method used to compute the permanent displacements along potential slip surfaces. This technique uses the results of a Newmark sliding block analysis, yield accelerations, and the dynamic response analysis for estimating displacements (Hynes-Griffin 1979). The yield accelerations used in this analysis are the same as those used in the Makdisi-Seed method. The yield accelerations, k_y , are given in Figures 77 through 78 for upstream shell circles and the deeper circles crossing the centerline.

130. Figure 82 shows Newmark sliding block displacements computed for various values of N/A for Accelerograms A and B. The term N/A is the ratio of yield acceleration, k_y , to acceleration of the sliding mass, k_{max} . The curves for each accelerogram were obtained by computing the displacements for various values of N/A by numerical integration of the relative equations of motion. The displacement curves are computed for a magnification factor of one. In this analysis the curve for Accelerogram A was used since it gives higher displacements for all values of N/A .

131. Displacements were computed for the same slip surface locations in the embankment as for the Makdisi-Seed method for both upstream shell circles and the deeper circles. The displacements were computed in the following way. The maximum earthquake-induced acceleration of the sliding mass, A , was set equal to k_{max} determined in the Makdisi-Seed method. The yield accelerations, N , are equal to k_y . The ratio of N/A was then computed. Figure 82 was entered from the abscissa at approximate values of N/A and displacements for a magnification factor of one were determined using the curve for Accelerogram A. The magnification ratio was calculated by dividing

A (or k_{\max}) by 0.35 g which is the peak base ground motion acceleration. The chart displacements were multiplied by the magnification factor and by α to determine the field permanent displacements along the surfaces investigated. A value of 1.3 was computed for α as discussed in the previous section. Tables 20 and 21 summarize the calculations in tabular form for both the upstream shell and deeper circles. The displacements for both cases are plotted in Figure 83. The displacements computed for the upstream shell circles are somewhat greater than those computed for the deeper circles at corresponding tangent elevations. The Sarma-Ambraseys method indicates that the maximum potential displacement is about 0.05 ft and will occur in the upstream shell for a slip circle tangent to elevation 442 and elevation 366 ft. These displacements are smaller by almost a factor of 10 than those of Makdisi-Seed method discussed earlier where the computed maximum displacement in the shell was about 0.5 ft.

Stability Evaluation

132. The results of the dynamic response analysis and liquefaction potential evaluation of the idealized section of the Wing Dams indicate that residual excess pore pressures of about 15 to 25 percent will develop in the upstream shell. No significant excess pore pressures are expected in the core or downstream shell. The post-earthquake safety factor against sliding was computed to be 1.54. The permanent displacement analyses of the idealized Wing Dam section indicate that Newmark-type displacements will be less than 0.5 ft along potential sliding surfaces confined to the upstream of the dam centerline. Potential displacements will be even smaller for deeper failure surfaces which involve materials dam downstream of the centerline.

133. Based on the above analyses it is concluded that the Wing Dams will perform satisfactorily during the design earthquake. The magnitude of permanent displacements will be less than 0.5 ft and will probably be confined to the upstream shell. This amount of displacement should be tolerable as it involves virtually no loss of freeboard. No further study or remedial measures are recommended for the Wing Dams.

PART IX: SUMMARY AND CONCLUSIONS

134. This report documented the study of the seismic stability evaluation of the Right and Left Wing Dams at the Folsom Dam and Reservoir Project, located on the American River about 20 miles northeast of the city of Sacramento, California. In the review of the site geology and the seismic hazard assessment, it was concluded that no active faults are present immediately beneath any of the man-made water retaining structures at the site. The most severe earthquake shaking was determined to come from the East Branch of the Bear Mountains fault zone, which is considered capable of producing a maximum magnitude earthquake of $M = 6.5$. The shortest distance between the fault zone and the Folsom Project is 8 miles to Mormon Island Auxiliary Dam and 9.5 miles to the Concrete Gravity Dam. The design ground motions for the site are $a_{\max} = 0.35 \text{ g}$, $V_{\max} = 20 \text{ cm/sec}$ and duration ($\geq 0.05 \text{ g}$) = 16 sec.

135. The seismic stability evaluation of Right and Left Wing Dams consisted of a review of construction records, field and laboratory investigations, static and dynamic stress analyses, liquefaction potential evaluation, and post-earthquake slope stability analyses. The analyses of the idealized section included evaluation of liquefaction potential, assessment of post-earthquake slope stability, and Newmark-type permanent displacement analyses. The field-performance based liquefaction evaluation procedures developed by Professor H. B. Seed and his colleagues at the University of California, Berkeley, were used to estimate the cyclic strengths of the embankment and foundation materials from in situ tests, mainly the Becker Hammer and SPT soundings. Relative cyclic strengths and pore pressure generation behavior were determined from laboratory tests documented in Report 4 of this series. The cyclic strengths were compared with the earthquake induced cyclic stresses computed with FLUSH to determine safety factors against liquefaction and to estimate the residual excess pore pressures developed due to shaking. Post-earthquake slope stability calculations and Newmark-type permanent displacement analyses were then performed with the earthquake-induced residual excess pore pressure field. Two types of permanent displacement analyses were employed to estimate the magnitude of displacement. These were the Makdisi-Seed and the Sarma-Ambrayseys techniques.

136. The results of the dynamic response analysis and liquefaction potential evaluation of the idealized section of the Wing Dams indicate that

residual excess pore pressures of about 15 to 25 percent will develop in the upstream shell. No significant excess pore pressures are expected in the core or downstream shell. The post-earthquake safety factor against sliding was computed to be 1.54. The permanent displacement analyses of the idealized Wing Dam section indicate that Newmark-type displacements will be less than 0.5 ft along potential sliding surfaces confined to exist upstream of the dam centerline. Potential displacements will be even smaller for deeper failure surfaces which are contained downstream of the centerline.

137. Based on the above analyses it is concluded that the Wing Dams will perform satisfactorily during the design earthquake. The magnitude of permanent displacements will be less than 0.5 ft and will probably be confined to the upstream shell. This amount of displacement should be tolerable as it involves virtually no loss of freeboard. No further study or remedial measures are recommended for the Wing Dams.

REFERENCES

- Ballard, R. F., Jr. 1964. "Determination of Soil Shear Moduli at Depths by In Situ Vibratory Techniques," Miscellaneous Paper No. 4-691, US Army Engineer Waterways Experiment Station, Vicksburg, MS.
- Bolt, B. A. and Seed, H. B. 1983. "Accelerogram Selection Report for Folsom Dam Project, California." Contract Report DACW 05-83-Q-0205, US Army Engineer District, Sacramento, CA.
- Duncan, J. M., Seed, R. B., Wong, W. S. and Ozawa, Y. 1984. "FEADAM84: A Computer Program for Finite Element Analysis of Dams," Research Report No. SU/GT/84-03. Stanford University, Stanford, CA.
- Edris, E. V. and Wright, S. G. 1987. "User's Guide: UTEXAS2 Scope-Stability Package, Vol 1," Instruction Report GL-87-1, US Army Engineer Waterways Experiment Station, Vicksburg, MS.
- Hynes-Griffin, M. E. 1979. "Dynamic Analyses of Earth Embankments for Richard B. Russell Dam and Lake Project," Final report prepared for US Army Engineer District, Savannah, GA.
- Hynes-Griffin, M. E. and Franklin, A. G. 1984. "Rationalizing the Seismic Coefficient," Miscellaneous Paper GL-84-13, US Army Engineer Waterways Experiment Station, Vicksburg, MS.
- Kiersch, G. A., and Treasher, R. C. 1955. "Investigations, Areal and Engineering Geology - Folsom Dam Project, Central California," Economic Geology, Vol 50, No. 3, pp 271-310.
- Llopis, J. L. 1983 (Jul). "Preliminary Results of an In-Situ Seismic Investigation of Folsom Dam, California." Draft Letter Report to US Army Engineer District (CESPK-ED-F), Sacramento, California, from US Army Engineer Waterways Experiment station (CEWES-GH-I), Vicksburg, MS.
- Llopis, J. L. 1984 (Sep). "Preliminary Results of In Situ Surface Vibratory Tests of Folsom Dam, California." Letter Report to Commander, US Army Engineer District (CESPK-ED-F), Sacramento, California, from US Army Engineer Waterways Experiment Station (CEWES-GH-I), Vicksburg, MS.
- Lysmer, J., Udaka, T., Tsai, C. F., and Seed, H. B. 1973. "FLUSH: A Computer Program for Approximate 3-D Analysis of Soil-Structure Interaction Problems." Report No. EERC 75-30. Earthquake Engineering Research Center, University of California, Berkeley, CA.
- Makdisi, F., and Seed, H. B. 1979. "Simplified Procedure for Estimating Dam and Embankment Deformations," Journal of the Geotechnical Engineering Division, American Society of Civil Engineers, Vol 104, No. GT7, pp 849-867.
- Newmark, N. M. 1965. "Effects of Earthquakes on Dams and Embankments," Geotechnique, Vol 15, No. 2, pp 139-160.
- Sarma, S. K. 1979. "Response and Stability of Earth Dams During Strong Earthquakes." Miscellaneous Paper GL-79-13, US Army Engineer Waterways Experiment Station, CE, Vicksburg, MS.

Schnabel, P. B., Lysmer, J., and Seed, H. B. 1972. "SHAKE, A Computer Program for Earthquake Response Analysis of Horizontally Layered Sites," Report No. EERC 72-12, Earthquake Engineering Research Center, College of Engineering, University of California, Berkeley, CA.

Seed, H. B. 1979. "19th Rankine Lecture: Considerations in the Earthquake Resistant Design of Earth and Rockfill Dams," Geotechnique, Vol 29, No. 3, pp 215-263.

_____. 1983. "Earthquake-Resistant Design of Earth Dams." Presented at the American Society of Civil Engineers Spring Convention, May 1983, Philadelphia, PA.

Seed, H. B., and DeAlba, P. 1986. "Use of SPT and CPT Tests for Evaluating the Liquefaction Resistance of Sands," Proceedings, American Society of Civil Engineers Specialty Conference In Situ, special publication No. 6, Blacksburg, VA.

Seed, H. B., and Idriss, I. M., 1970. "Soil Moduli and Damping Factors for Dynamic Response Analyses." Report No. EERC 70-10. Earthquake Engineering Research Center, University of California, Berkeley, CA.

Seed, H. B., Idriss, I. M., and Arango, I. 1983. "Evaluation of Liquefaction Potential Using Field Performance Data," Journal of the Geotechnical Engineering Division, American Society of Civil Engineers, Vol 109, No. GT3, pp 458-482.

Seed, H. B. and Peacock, W. H. 1971. "Test Procedures for Measuring Soil Liquefaction Characteristics," Journal of the Soil Mechanics and Foundations Division, American Society of Civil Engineers, Vol 97, No. SM8. pp 1099-1119.

Seed, H. B., Tokimatsu, K., Harder, L. F., and Chung, R. M. 1984. "The Influence of SPT Procedures in Soil Liquefaction Resistance Evaluations," UCB/EERC Report No. 84/15, University of California, Berkeley, CA.

Seed, H. B., Wong, R. T., Idriss, I. M., and Tokimatsu, K. 1984. "Moduli and Damping Factors for Dynamic Analyses of Cohesionless Soils." Report No. EERC 84-14. Earthquake Engineering Research Center, University of California, Berkeley, CA.

Tierra Engineering Consultants, Inc. 1983. "Geologic and Seismologic Investigations of the Folsom, California Area." Contract Report DACW 05-82-C-0042, US Army Engineer District, Sacramento, CA.

US Army Engineer District, Sacramento. 1953. "Foundation Report, American River, California, Mormon Island Auxiliary Dam, Folsom Project." Sacramento, CA.

US Army Engineer Laboratory, South Pacific Division. 1986. "Report of Soil tests, Folsom Dam Laboratory Program," Sausalito, CA.

Table 1
Estimated Seismic Characteristics of Capable Faults (1)
(after Tierra Engineering Consultants, Inc. 1983)

<u>Name of Fault Zone</u>	<u>Minimum Distance To Site</u>	<u>Type of Faulting</u>	<u>Maximum Earthquake Magnitude (2)</u>	<u>Approximate Slip Rate (3)</u>	<u>Most Recent Displacement Known (4)</u>
San Andreas	102	Strike-slip	8	1-2 cm/yr	Historic
Hayward	85	Strike-slip	7	0.5 cm/yr	Historic
Calaveras	77	Strike-slip	7	0.25 cm/yr	Historic
Genoa Jack Valley	70+	Normal-slip	7.25	0.01-0.02	Holocene
West Walker River	85	Normal-slip	7.25	0.01	Historic
Melones	16.5	Normal-slip	6.5	0.0006-0.0001	Pleistocene ±100,000
East Branch Bear Mountains	8.0	Normal-slip	6.5 (5)	0.0006-0.0001	Pleistocene ±100,000

(1) Capable fault, under criteria defined by Tierra Engineering Consultants, Inc. (1983), is one that exhibited displacement at or near the ground surface within the past 35,000 years, recurrent movement within the past 500,000 years, exhibits creep movement, and/or exhibits aligned macro ($M \geq 3.5$) seismicity determined from instruments.

(2) Maximum earthquake estimate on rupture length of continuous strands, type of faulting, fault displacement, historic earthquakes, seismic moment, experience and judgement.

(3) Slip rates estimated from historic, geomorphic, or geologic evidence.

(4) Late Pleistocene displacement may be as old as 500,000 years ago or as young as 10,000 years ago.

(5) Hypothetical value (acceptance based on USBR Auburn Dam studies).

Table 2
Materials and Borrow Areas for Wing Dams

<u>Zone</u>	<u>Material</u>	<u>Use in Dams</u>	<u>Borrow Areas</u>
A	Rockfill (10-30 percent minus No. 4)	RWD shell	Stockpiles 1, 2, 3, and 4 (American River channel excavation)
B	Alluvial gravel dredge tailings	RWD transition	Stockpile 7 Borrow Area No. 7 Borrow Area No. 8
C	Decomposed granite (SM)	RWD core	Stockpile 6 Borrow Area No. 2
E	Dredge tailings	LWD shell	Borrow Area No. 5 (Blue Ravine)
F	Dredge tailings (processed minus 2 in.)	LWD filter	Borrow Area No. 5
G	Decomposed granite (SM)	LWD core	Borrow Area No. 1

Note: RWD = Right Wing Dam.
LWD = Left Wing Dam.

Table 3
Compaction Equipment and Effort Specified for
Wing Dam Zoned Fill

<u>Zone</u>	<u>Use in Dams</u>	<u>Equipment</u>	<u>Number of Passes or Coverages</u>	<u>Maximum Lift Thickness (in.)</u>
A	RWD shell	D-8 Cat. tractor	1 ^(C)	48 (Changed to 12 ft)
B	RWD transition	D-8 Cat. tractor	1 ^(C)	24
C	RWD core	Sheepsfoot roller Pneumatic-tired roller	12 ^(P) 6 ^(P)	12 18
E	LWD shell	D-8 Cat. tractor	1 ^(C)	24
F	LWD filter	D-8 Cat. tractor	1 ^(C)	12
G	LWD core	Sheepsfoot roller Pneumatic-tired roller	12 ^(P) 6 ^(P)	12 18

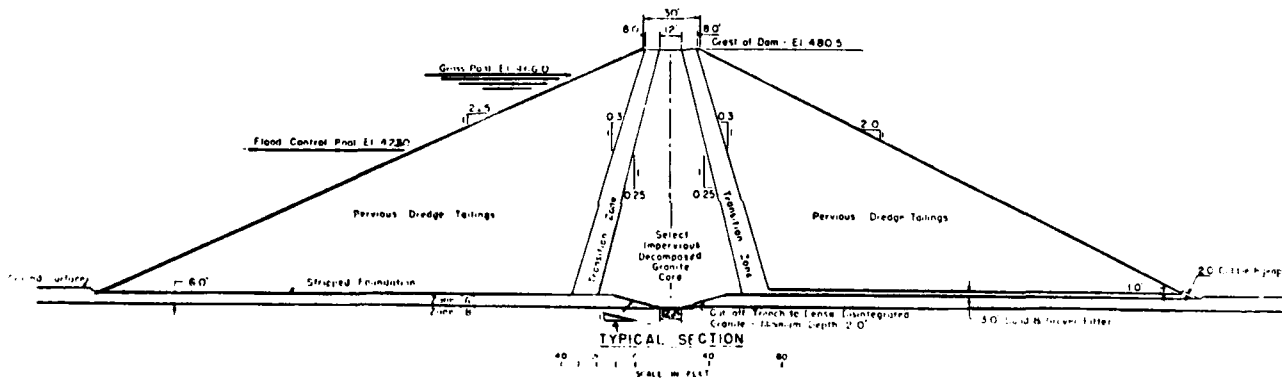
Note: (C) = Number of complete coverages, estimated to correspond to 3 or 4 passes.
(P) = Number of passes.
RWD = Right Wing Dam.
LWD = Left Wing Dam.

Table 4

Material Properties Used in Initial Design of Wing Dams

SOIL CHARACTERISTICS				
MATERIAL	IMPERVIOUS CORE	DREDGE TAILINGS	FOUNDATION	
			ZONE "A"	ZONE "B"
Dry Wt. lbs./cu.ft.	123.4 *	125.0	108.0	141.0
Moist Wt. lbs./cu.ft.	134.0	133.0	117.1	149.7
Saturated Wt. lbs./cu.ft.	140.0	143.8	130.4	151.2
Buoyed Wt.	77.6	81.4	68.0	88.8
Tangent ϕ	0.70	0.84	0.60	1.00
Cohesion lbs/sq.ft.	0.0	0.0	0.0	0.0
Permeability ft./day	0.5		10.0	7.0

* At 55% Modified A.A.S.H.O. Density



SUMMARY OF STABILITY ANALYSES				
SLOPE	CONDITION	FORCE	METHOD	MIN. F. S.
UPSTREAM	Reservoir Empty, Slope 1 on 2.25	Gravity	Infinite Slope	1.89
	Submerged Slope, Slope 1 on 2.25	Gravity	Infinite Slope	1.89
	Water Surface Elev. 427.0	Gravity	Circular Arc	1.54
	Water Surface Elev. 466.0	Gravity	Circular Arc	1.59
	Reservoir Empty, Slope 1 on 2.25	Gravity & 0.05 Earthquake	Infinite Slope	1.66
	Submerged Slope, Slope 1 on 2.25	Gravity & 0.05 Earthquake	Infinite Slope	1.51
	Water Surface Elev. 427.0	Gravity & 0.05 Earthquake	Circular Arc	1.26
	Water Surface Elev. 466.0	Gravity & 0.05 Earthquake	Circular Arc	1.26
DOWNSTREAM	Reservoir Empty, Slope 1 on 2	Gravity	Infinite Slope	1.68
	Water Surface Elev. 466.0	Gravity	Circular Arc	1.51
	Reservoir Empty, Slope 1 on 2	Gravity & 0.05 Earthquake	Infinite Slope	1.49
	Water Surface Elev. 466.0	Gravity & 0.05 Earthquake	Circular Arc	1.33

Table 5
In Situ Densities Measured in 4-ft Diameter Water Ring Density
Tests in Downstream Slope of Right Wing Dam
(Test Pits 1, 2, and 3)

<u>Test No.</u>	<u>Test Pit</u>	<u>Depth (ft)</u>	<u>In Situ Moist Density (pcf)</u>	<u>In Situ Dry Density (pcf)</u>	<u>Mean Grain Size, D₅₀ (mm)</u>	<u>Fines Content (% passing No. 200 Sieve)</u>
1	1	2.5	126.0	124.6	38	1
2	1	2.5	126.8	125.4	33	1
3	1	5.0	137.7	135.2	30	3
4	1	5.0	130.3	122.0	21	2
5	1	7.5	128.5	124.1	21	5
6	1	7.5	134.9	132.5	18	4
7	1	11.0	137.8	135.0	23	3
8	2	2.5	140.6	139.4	23	4
9	2	2.5	146.7	144.0	20	5
10	2	5.5	145.9	141.5	19	4
11	2	5.5	140.1	140.6	19	4
12	3	2.5	139.6	134.2	15	8
13	3	2.5	139.6	127.8	13	6
14	3	6.0	151.1	147.0	20	2
15	3	6.0	152.9	147.6	20	2
16	3	8.5	144.0	138.1	9	6
17	3	8.5	152.1	147.9	20	3
18	3	10.5	<u>145.6</u>	<u>142.7</u>	<u>25</u>	<u>4</u>
Avg			140.0	136.1	22	4

Table 6

In Situ Densities Measured in 4-ft Diameter Water Ring Density
Tests in Downstream Slope of the Left Wing Dam (Test Pit 4)

<u>Test No.</u>	<u>Depth (ft)</u>	<u>In situ Moist Density (pcf)</u>	<u>In situ Dry Density (pcf)</u>	<u>Mean Grain Size D₅₀ (mm)</u>	<u>Fines Content (% passing No. 200 Sieve)</u>
19	2.5	127.2	124.9	32	4
20	2.5	133.9	130.6	32	4
21	5.5	137.8	129.7	18	6
22	5.5	134.5	131.7	20	7
23	8.5	136.6	131.7	24	5
24	8.5	143.8	138.7	18	4
25	11.0	140.6	136.0	27	3
26	11.0	138.8	133.4	22	4
27	13.0	145.7	136.1	18	3
28	13.0	137.2	131.2	27	8
29	15.0	136.9	131.8	34	5
30	15.0	142.3	136.7	24	7
31	17.0	129.4	125.0	29	2
32	17.0	134.4	130.9	24	6
33	20.0	145.0	138.3	17	8
34	20.0	<u>146.9</u>	<u>138.6</u>	<u>17</u>	<u>8</u>
Avg		138.2	132.8	24	6

Table 7

Materials and Borrow Areas for Mormon Island Auxiliary Dam

<u>Zone</u>	<u>Material</u>	<u>Use in Dam</u>	<u>Borrow Areas</u>
1	Dredge tailings	Shell	Borrow Area No. 5 (Blue Ravine)
2	Dredge tailings (processed minus 2 in.)	Filter	Borrow Area No. 5
3	Decomposed granite	Core/filter	Borrow Area No. 1
4	Alluvium and slope wash (SC, CL, GC)	Central core	Borrow Area No. 6

Table 8
In Situ Densities of Embankment Gravel Measured in 4-ft Diameter
Water Ring Density Tests in Downstream Slope of Mormon Island
Auxiliary Dam

<u>Test No.</u>	<u>Depth (ft)</u>	<u>In situ Moist Density (pcf)</u>	<u>In situ Dry Density (pcf)</u>	<u>Mean Grain Size D₅₀ (mm)</u>	<u>Fines Content (% passing No. 200 Sieve)</u>
1	2	140.8	130.4	28	3
2	5	148.2	143.3	29	5
3	5	143.1	138.7	31	6
4	7.5	143.5	140.2	38	6
5	7.5	147.1	142.9	38	3
6	9	154.2	148.7	38	5
7	9	151.9	142.1	25	6
8	14	148.7	145.7	28	7
9	14	151.9	146.1	38	6
10	15.5	134.0	124.2	28	5
11	15.5	128.7	121.3	30	5
12	17	146.1	141.3	36	3
13	17	135.5	128.3	41	4
14	19	136.4	132.3	45	4
15	19	150.7	146.3	48	4
16	3	<u>138.4</u>	<u>131.7</u>	<u>27</u>	<u>4</u>
Avg		143.7	137.7	34	5

Table 9
Compaction Equipment and Effort Specified
for Gravel Zone Fill

<u>Zone</u>	<u>Use in Dams</u>	<u>Equipment</u>	<u>Number of Coverages*</u>	<u>Maximum Lift Thickness (in.)</u>
A	RWD shell	D-8 Cat. tractor	1 1	24 12 ft
1	MID shell	D-8 Cat. tractor	1	24
B	RWD transition	D-8 Cat. tractor	1	24
E	LWD shell	D-8 Cat. tractor	1	24
2	MID filter	D-8 Cat. tractor	1	12
F	LWD filter	D-8 Cat. tractor	1	12

* One complete coverage is estimated to correspond to 3 or 4 passes of the compaction equipment.

Table 10
Summary of Geophysical and Relative Density Results

Approx. Depth Interval (ft)	Dam	Shear Wave Velocity (fps)	K _{2max}	Test Pit D _R (percent)
0-10	MID	825	106	71
	RWD	850	112	63
	LWD	900	126	60
20-60	MID	1,200	115	--
	RWD	1,050	90	--
	LWD	1,200	115	--

Note:
$$K_{2max} = \frac{v_s^2 \times \rho}{1,000 \times \sigma'_m{}^{1/2}}$$

where

v_s = measured shear wave velocity in feet per second

ρ = mass density, $\frac{\text{lb-sec}^2}{\text{ft}}$

σ'_m = effective mean normal pressure, pounds per square foot

Table 11

Location Information for Becker Hammer Soundings Performed on the
Downstream Slope of the Right Wing Dam During the 1988

Field Investigations

<u>Sounding</u>	<u>Station (ft)</u>	<u>Centerline Offset (ft)</u>	<u>Top of Hole Elevation (ft)</u>	<u>Depth (ft)</u>
BH 14-88	278+00	51	466.9	50
BH 15-88	274+00	80	451.6	56
BH 16-88	272+00	95	444.1	39
BH 17-88	270+00	113	435.1	34

Table 12
Equivalent $(N_1)_{60}$ Blowcount Statistics Obtained from the
Becker Hammer Penetration Tests Performed in Zone A
of the Downstream Shell of the Right Wing Dam

<u>Sounding</u>	<u>Depth Range For Zone A (ft)</u>	<u>Number of Samples</u>	<u>$(N_1)_{60}$ Statistics</u>	
			<u>Mean (blows/ft)</u>	<u>Standard Deviation (blows/ft)</u>
BH 14-88	--	--	--	--
BH 15-88	6-11	6	30.3	6.8
BH 16-88	6-15	10	29.6	13.4
BH 17-88	6-18	13	11.4	5.8

Notes: $(N_1)_{60}$ values at depths of 5 ft or less or at elevations below Elevation 360 were excluded from the analysis.
The computation of $(N_1)_{60}$ is discussed in Appendix A.

Table 13
Equivalent $(N_1)_{60}$ Blowcount Statistics Obtained from the
Becker Hammer Penetration Tests Performed in Zone B
of the Downstream Shell of the Right Wing Dam

<u>Sounding</u>	<u>Depth Range For Zone A (ft)</u>	<u>Number of Samples</u>	<u>$(N_1)_{60}$ Statistics</u>	
			<u>Mean (blows/ft)</u>	<u>Standard Deviation (blows/ft)</u>
BH 14-88	12-32	25	36.5	18.4
BH 15-88	16-41	30	35.2	12.8
BH 16-88	19-35	20	39.5	10.7
BH 17-88	19-25	9	22.8	7.4
Global statistics:		84	35.3	13.4

Table 14

Location Information for Becker Hammer Soundings Performed on the
Downstream Slope of the Left Wing Dam

<u>Sounding</u>	<u>Station (ft)</u>	<u>Centerline Offset (ft)</u>	<u>Top of Hole Elevation (ft)</u>	<u>Depth (ft)</u>
BH 18-88	304+39	129	424.1	72
BH 19-89	304+74	129	424.5	64

Table 15
Equivalent $(N_1)_{60}$ Blowcount Statistics Obtained from
Becker Hammer Penetration Tests Performed in Zone E
of the Downstream Shell of the Left Wing Dam

<u>Sounding</u>	<u>Depth Range For Zone A (ft)</u>	<u>Number of Samples</u>	<u>$(N_1)_{60}$ Statistics</u>	
			<u>Mean (blows/ft)</u>	<u>Standard Deviation (blows/ft)</u>
BH 18-88	6-63	58	22.4	10.0
BH 19-89	6-63	<u>59</u>	<u>22.5</u>	<u>10.2</u>
Global statistics:		117	22.4	10.1

Notes: $(N_1)_{60}$ values at depths of 5 ft or less or at elevations below Elevation 360 were excluded from the analysis.
The computation of $(N_1)_{60}$ is discussed in Appendix A.

Table 16
Hyperbolic Parameters Input to FEADAM for Static Analysis of Wing Dams

Material Location	Effective Unit Weight (pcf)	Young's Modulus		Young's Modulus Exponent N	Failure Ratio R_f	Bulk Modulus K_b	Bulk Modulus Exponent M	Effective Cohesion Intercept c (ksf)	Effective Friction Angle ϕ (°)	Change in ϕ Per Log Cycle Change in Confining Stress $\Delta\phi$	Static Stress Ratio K_o
		Loading K (ksf)	Unloading K_{ur} (ksf)								
Saturated shell	90	1,900	1,900	.39	.9	1,287	.33	0	43	0	0.5
Dry shell	139	1,900	1,900	.39	.9	1,267	.33	0	43	0	0.5
Saturated core	79.4	1,175	1,175	.15	.69	979	.43	0	37	0	0.43
Dry core	136	1,175	1,175	.15	.69	979	.43	0	37	0	0.43
Rock	150	10,000	10,000	1.0	.9	10,000	1.0	5	50	0	0.5

Table 17
Unit Weights and Shear Strength Parameters Used In
Post-Earthquake Stability Calculations

<u>Material Type</u>	<u>Unit Weight (pcf)</u>	<u>Cohesion c (psf)</u>	<u>Effective Friction Angle ϕ' (degrees)</u>
Embankment gravels:			
Moist	146	0	43
Submerged	152	0	43
Core - Decomposed			
Granite:			
Moist	136	0	31
Submerged	142	0	31
Foundation bedrock			
Weathered granite:	150	1,000	35

Note: Shear strengths (c and $\tan \phi'$) for core and the undredged alluvium were reduced by a factor of 20 percent.

Table 18

Summary of Makdisi-Seed Permanent Displacement Calculations for Potential Slip Surfaces
Contained Upstream of Centerline*

Y/H (percent)	Coordinates of Center		Radius of Circular Surface R (ft)	\ddot{U}_{max} at Crest (g)	k_y (g)	$\frac{k_{max}}{\ddot{U}_{max}}$	k_{max} (g)	$\frac{k_y}{k_{max}}$	$\frac{U/k_{max}}{g \times T_0}$	U (ft)	$U \times \alpha$ (ft)	
	X (ft)	Y (ft)										
20.00	857.00	732.00	290.00	.54	.23	.88	.48	.48	.02	.30	1.30	.39
40.00	740.00	800.00	402.00	.54	.17	.70	.30	.45	.03	.29	1.30	.38
60.00	662.00	824.00	458.00	.54	.11	.52	.28	.39	.04	.32	1.30	.42
80.00	547.00	969.00	641.00	.54	.10	.41	.22	.47	.02	.15	1.30	.19
100.00	496.00	923.00	633.00	.54	.11	.31	.18	.57	.01	.07	1.30	.09

Notes: $T_0 = 0.855$ sec.
 $\ddot{U}_{max} = 0.54$ g at crest.
 M = 6.5.
 Record B.

Table 19

Summary of Makdisi-Seed Permanent Displacement Calculations for Potential Slip Surfaces
That Involve Materials Downstream of Centerline*

Y/H (percent)	Coordinates of Center		Radius of Circular Surface R (ft)	\ddot{u}_{max} at Crest (g)	k_y (g)	$\frac{k_{max}}{\ddot{u}_{max}}$	k_{max} (g)	$\frac{k_y}{k_{max}}$	$\frac{U/k_{max}}{g \times T_o} \times$	U (ft)	$\frac{U \times \alpha}{\alpha}$	U \times α (ft)
	X (ft)	Y (ft)										
20.00	807.00	732.00	290.00	.54	.20	.88	.48	.59	.01	.16	1.30	.20
40.00	700.00	1,117.00	720.00	.54	.20	.70	.38	.52	.02	.20	1.30	.26
60.00	705.00	865.00	499.00	.54	.15	.52	.28	.52	.02	.15	1.30	.19
80.00	600.00	1,040.00	705.00	.54	.13	.41	.22	.61	.01	.06	1.30	.08
100.00	530.00	1,050.00	760.00	.54	.15	.34	.10	.79	.00	.01	1.30	.01

Notes: $T_o = 0.855$ sec.
 $\ddot{u}_{max} = 0.54$ g at crest.
 $M = 6.5$.
 Record B.

Table 20

Summary of Sarma-Ambrayseys Permanent Displacement
Calculations for Potential Slip Surfaces That
are Contained Upstream of Centerline*

<u>Y/H</u> <u>(percent)</u>	<u>a_{max}</u> <u>(rock,</u> <u>g)</u>	<u>A</u> <u>(K_{max},</u> <u>g)</u>	<u>N</u> <u>(K_y)</u>	<u>N/A</u>	<u>U</u> <u>(cm)</u>	<u>A/a</u>	<u>U ×</u> <u>(A/a)</u> <u>(cm)</u>	<u>α</u>	<u>U ×</u> <u>(A/a)</u> <u>× α</u> <u>(cm)</u>	<u>U ×</u> <u>(A/a)</u> <u>× α</u> <u>(ft)</u>
20.00	.35	.48	.23	.47	.80	1.37	1.10	1.30	1.43	.05
40.00	.35	.38	.17	.45	.93	1.09	1.01	1.30	1.31	.04
60.00	.35	.28	.11	.39	1.40	.80	1.12	1.30	1.46	.05
80.00	.35	.22	.10	.47	.80	.63	.50	1.30	.65	.02
100.00	.35	.18	.11	.58	.39	.51	.20	1.30	.26	.01

Notes: $T_o = 0.855$ sec.
 $\ddot{U}_{max} = 0.54$ g at crest.
 $M = 6.5$.
 Record A.

Table 21

Summary of Sarma-Ambrayseys Permanent Displacement Calculations for
Potential Slip Surfaces That Involve Materials Downstream
of Centerline*

Y/H (percent)	a_{\max} (rock, g)	A (K_{\max} , g)	N (K_y)	N/A	U (cm)	A/a	U × (A/a) (cm)	α	U × (A/a) × α (cm)	U × (A/a) × α (ft)
20.00	.35	.48	.28	.59	.37	1.37	.51	1.30	.66	.02
40.00	.35	.38	.20	.52	.50	1.09	.54	1.30	.70	.02
60.00	.35	.28	.15	.52	.50	.80	.40	1.30	.51	.02
80.00	.35	.22	.13	.61	.30	.63	.19	1.30	.25	.01
100.00	.35	.10	.15	.81	.11	.51	.05	1.30	.07	.00

Notes: $T = 0.855$ sec.
 $\ddot{u}_{\max}^o = 0.54$ g at crest.
 $M = 6.5$.
 Record A.

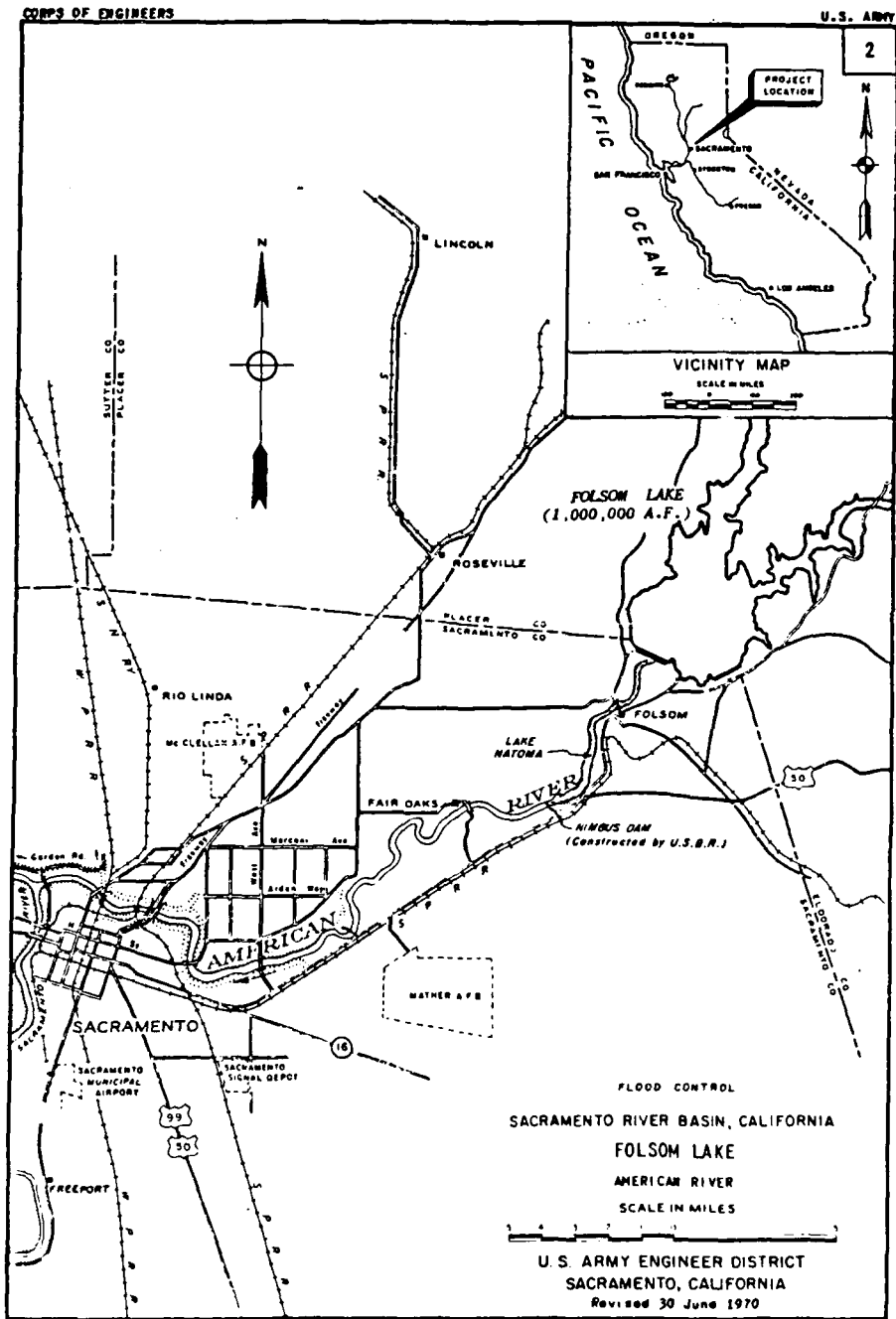


Figure 1. Location of Folsom Dam and Reservoir Project

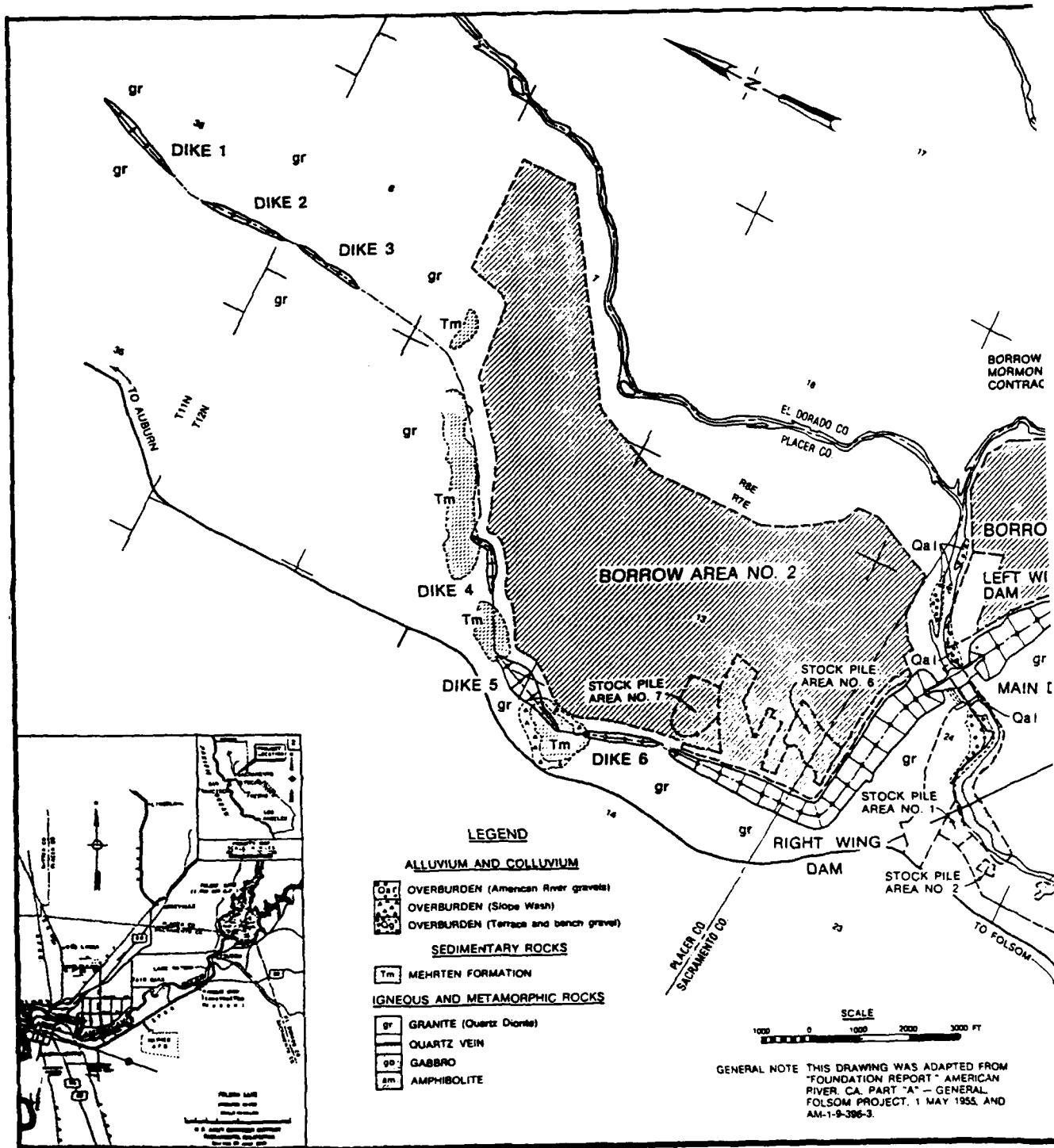
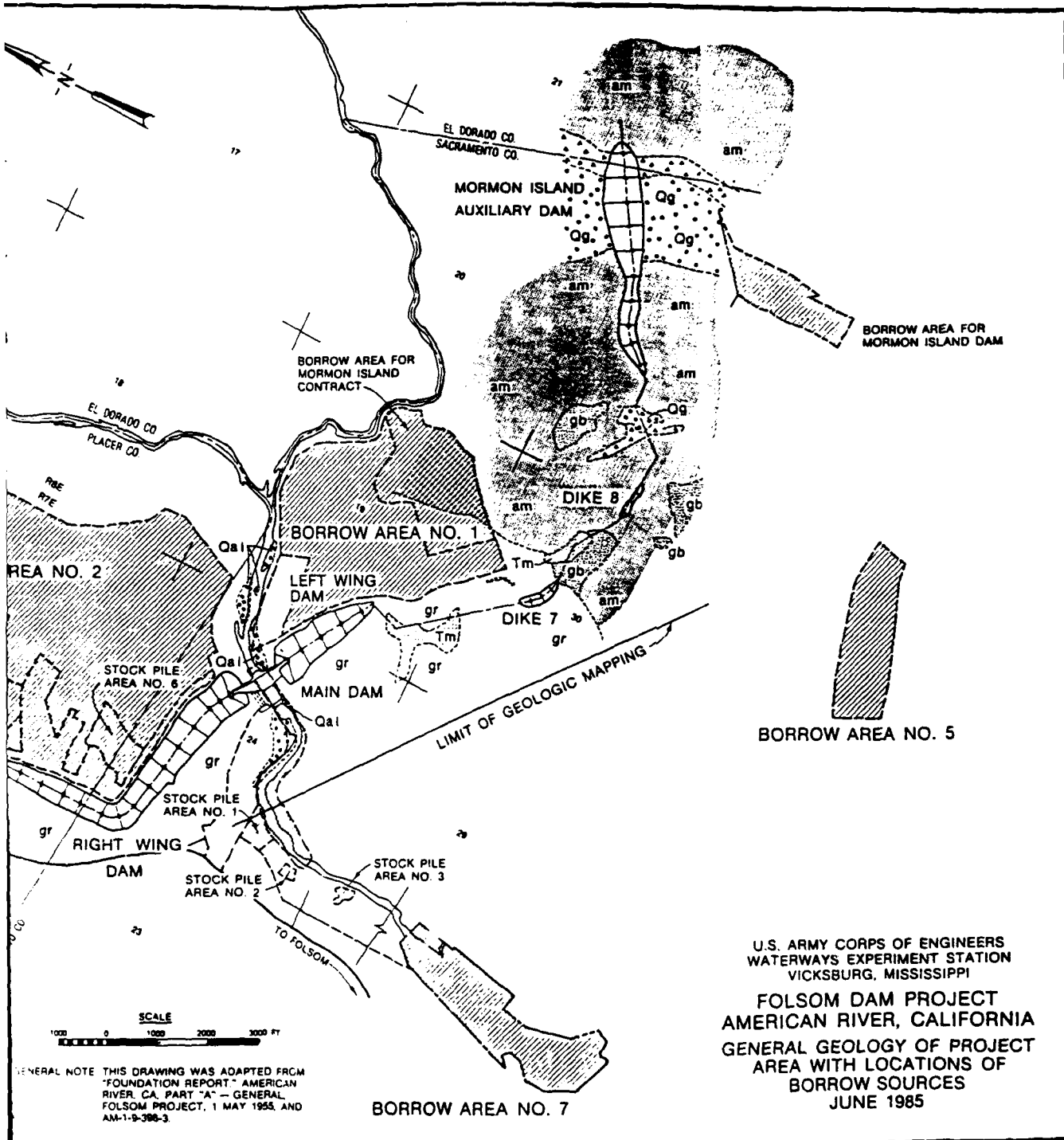


Figure 2. Plan of man-made retaining structures

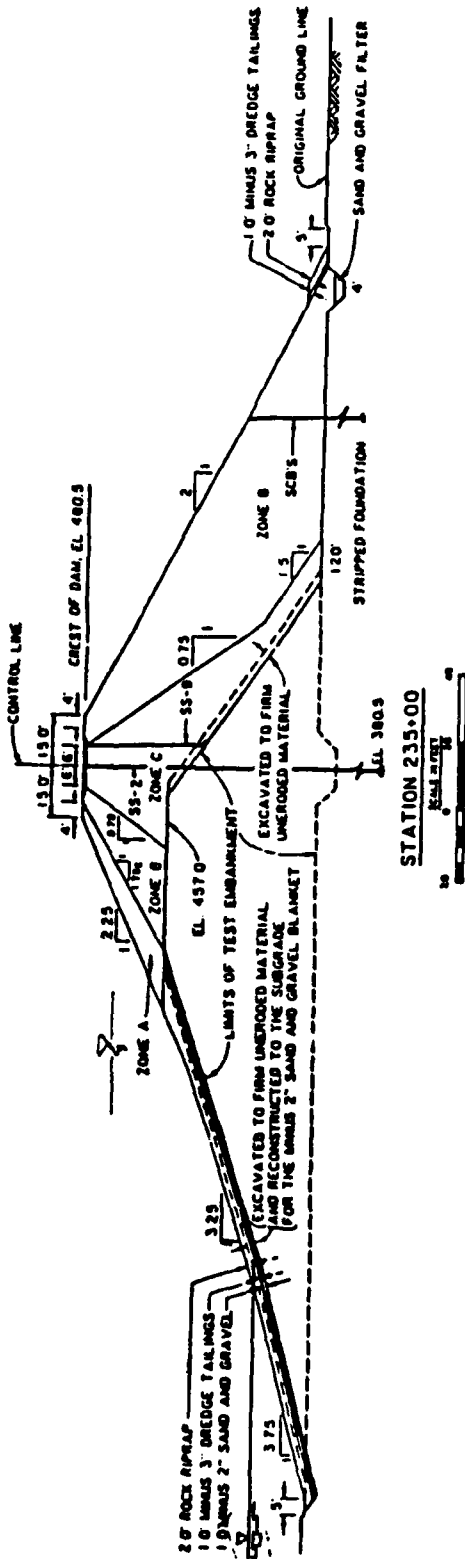


GENERAL NOTE THIS DRAWING WAS ADAPTED FROM
 "FOUNDATION REPORT" AMERICAN
 RIVER, CALIF. PART "A" - GENERAL
 FOLSOM PROJECT, 1 MAY 1955, AND
 AM-1-9-368-3.

U.S. ARMY CORPS OF ENGINEERS
 WATERWAYS EXPERIMENT STATION
 VICKSBURG, MISSISSIPPI
 FOLSOM DAM PROJECT
 AMERICAN RIVER, CALIFORNIA
 GENERAL GEOLOGY OF PROJECT
 AREA WITH LOCATIONS OF
 BORROW SOURCES
 JUNE 1985

man-made retaining structures at Folsom Dam Project

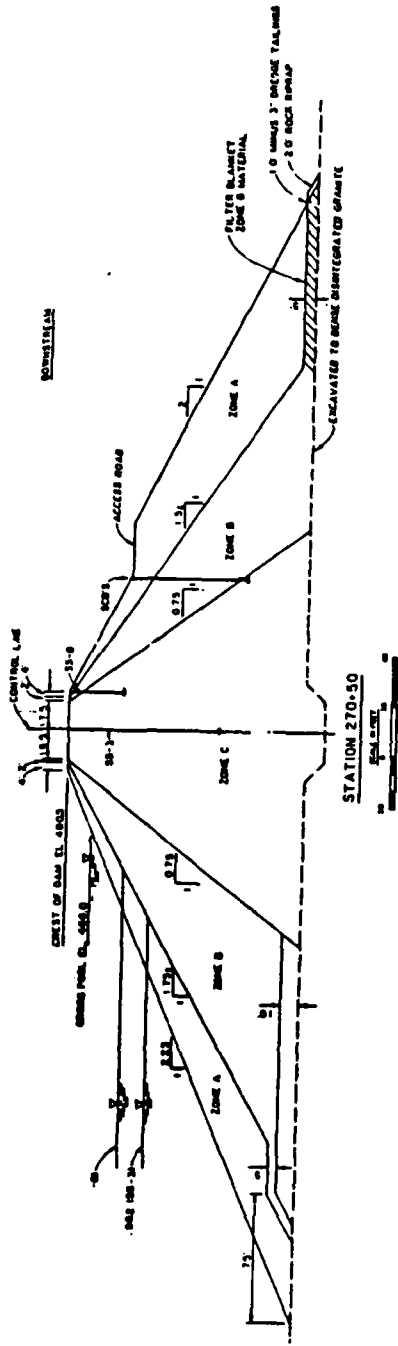
2



Material Descriptions

- Zone A - Rock From the American river channel
- Zone B - Unprocessed sand, gravel, and cobbles from American river channel excavation
- Zone C - Decomposed granite from Borrow Area No. 2 and suitable fine-grained river channel excavation

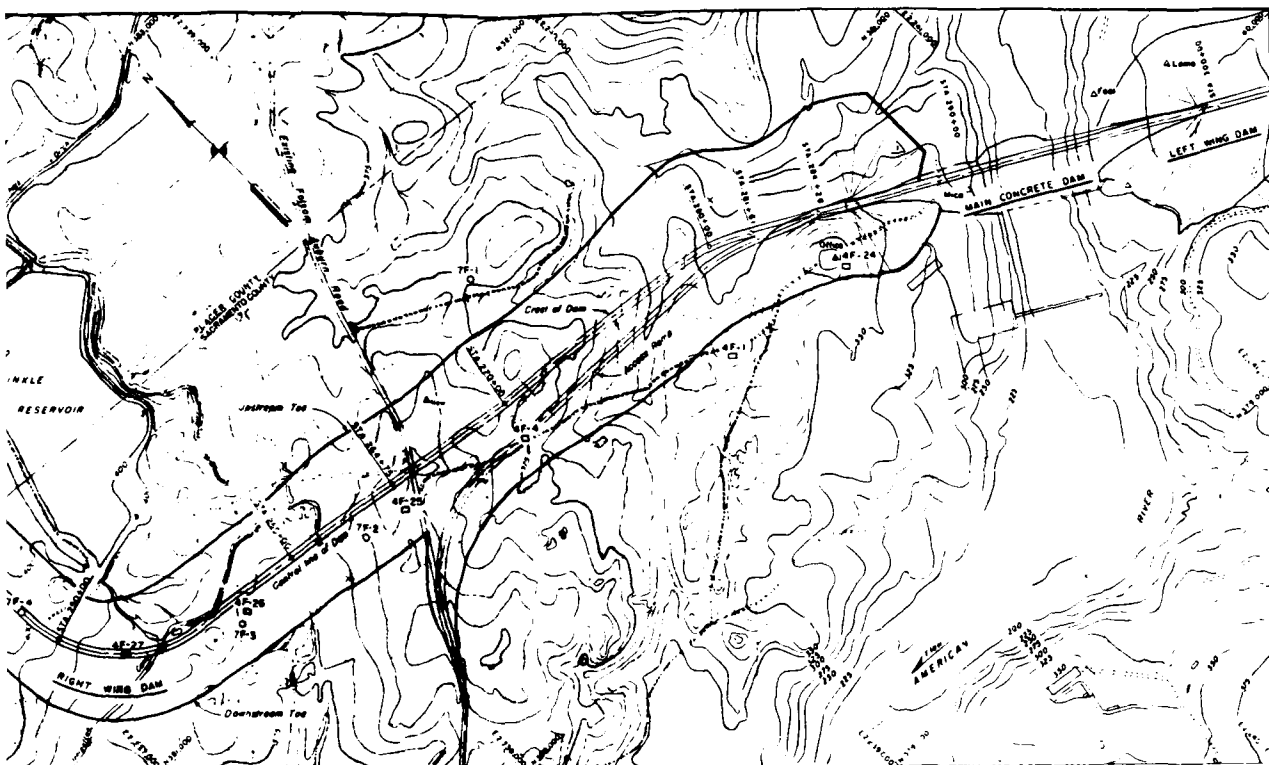
Figure 4. Section of Right Wing Dam at Station 235+00



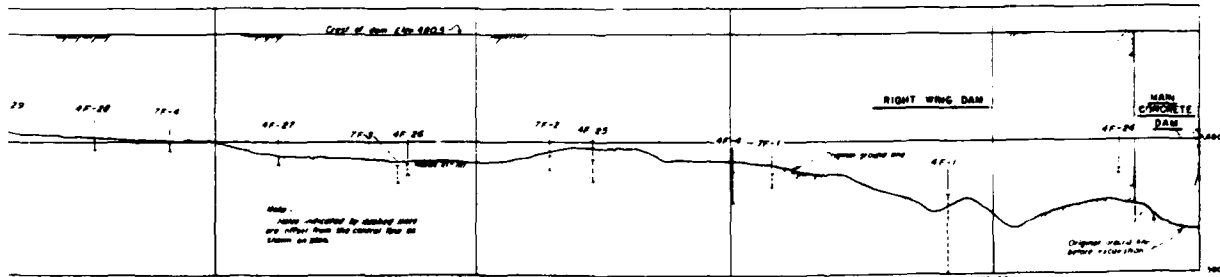
Material Descriptions

- Zone A - Rock From the American river channel
- Zone B - Unprocessed sand, gravel, and cobbles from American river channel excavation
- Zone C - Decomposed granite from Borrow Area No. 2 and suitable fine-grained river channel excavation

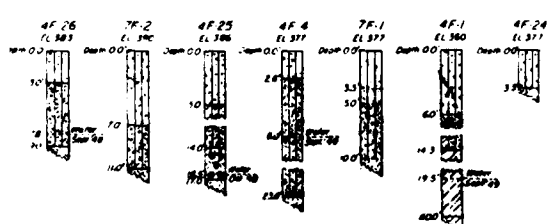
Figure 5a. Section of Right Wing Dam through Station 270+50



PLAN
SCALE 4" = 100'



PROFILE ON CONTROL LINE
SCALE AS SHOWN



- NOTES**
1. Elevation is Sea Level Datum of 1929.
 2. Elevations shown on logs are ground surface elevations.
 3. Laboratory classifications shown for all materials according to the Corps of Engineers' Standard Soil Classification. The term "gravel" applies to gravel sizes larger than the No. 10 sieve.
 4. All foundation material indicated by logs herein is decomposed granite weathered in place, except where noted otherwise in a note.
 5. All 4F holes are open pits.
 6. All 7F holes were drilled by a falling drill rig using a 7" diameter rotary core drill.
 7. Typical subsurface sections are shown on sheets No. 400/2, 400/3 and 400/4.
 8. Elevation topography taken prior to the December 1956 floods.
 9. This drawing was issued from as-constructed sheet No. 400/2.2 File No. 20-1-1-600.

INTEGRATED WATER BASK DEVELOPMENT CALIFORNIA
FOLSOM RESERVOIR PROJECT
AMERICAN RIVER
FOLSOM DAM
FOUNDATION EXPLORATION
RIGHT WING DAM
PLAN, PROFILE AND LOGS

400/2.2

Figure 5b

2

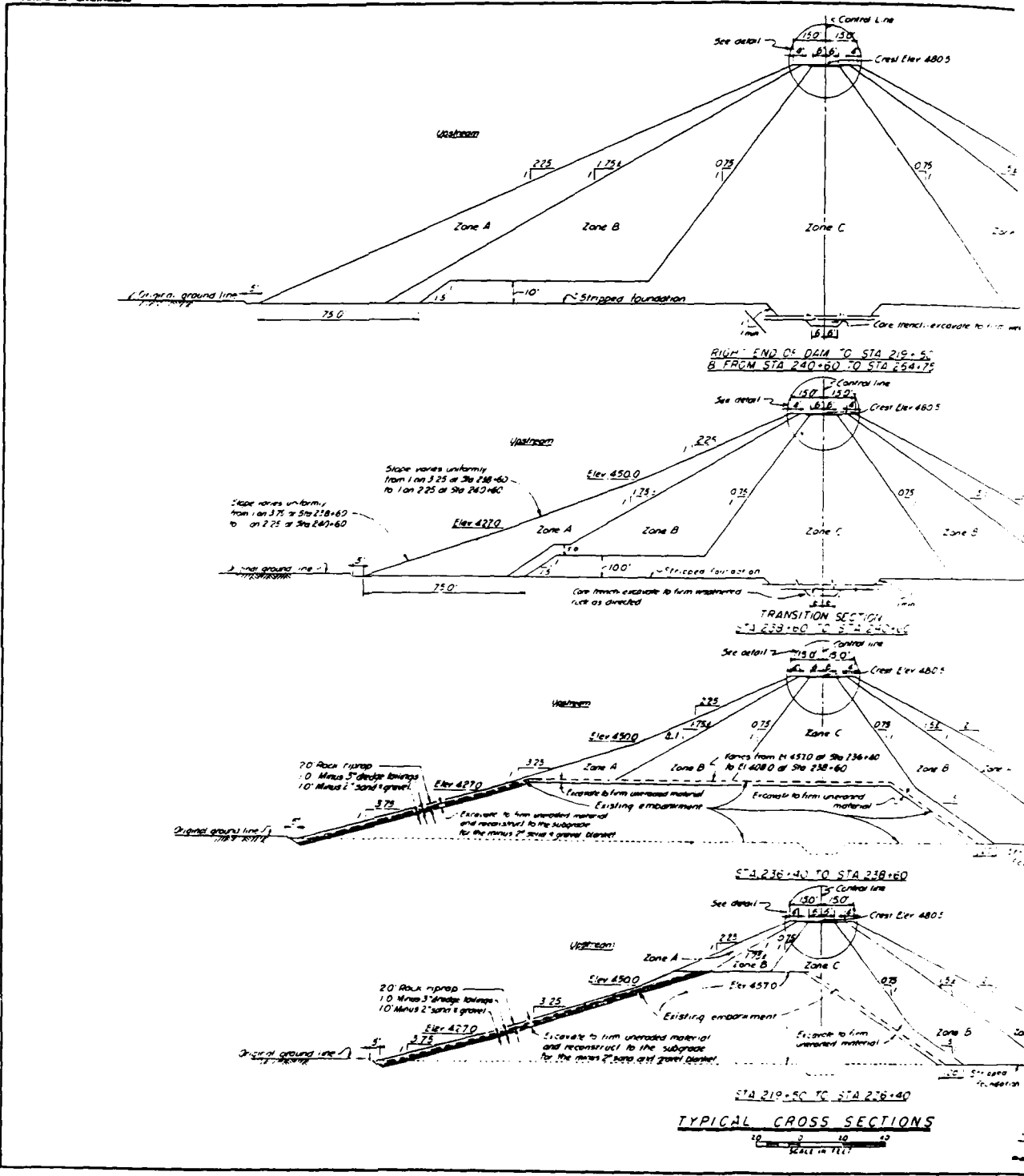


Figure 5c

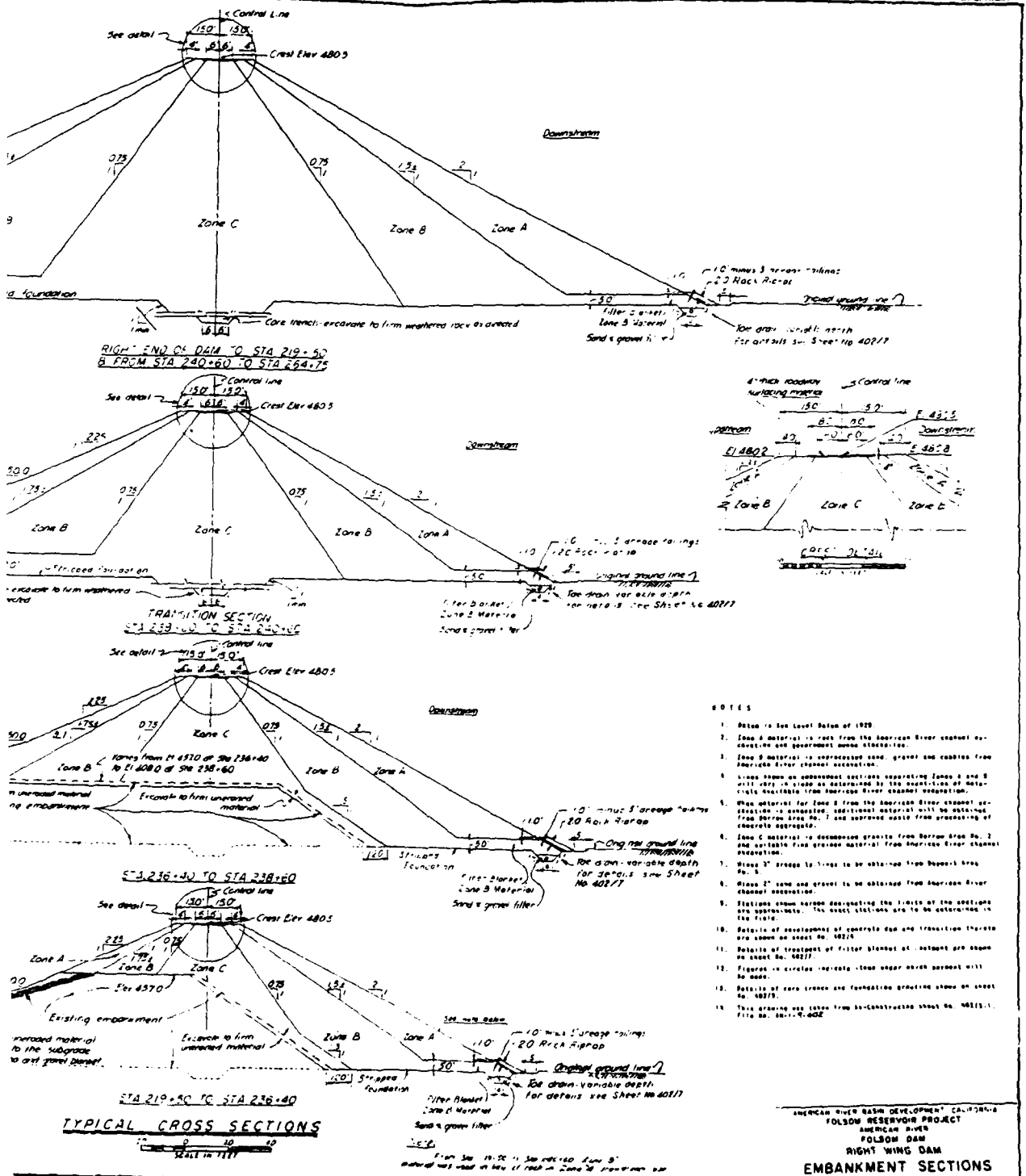
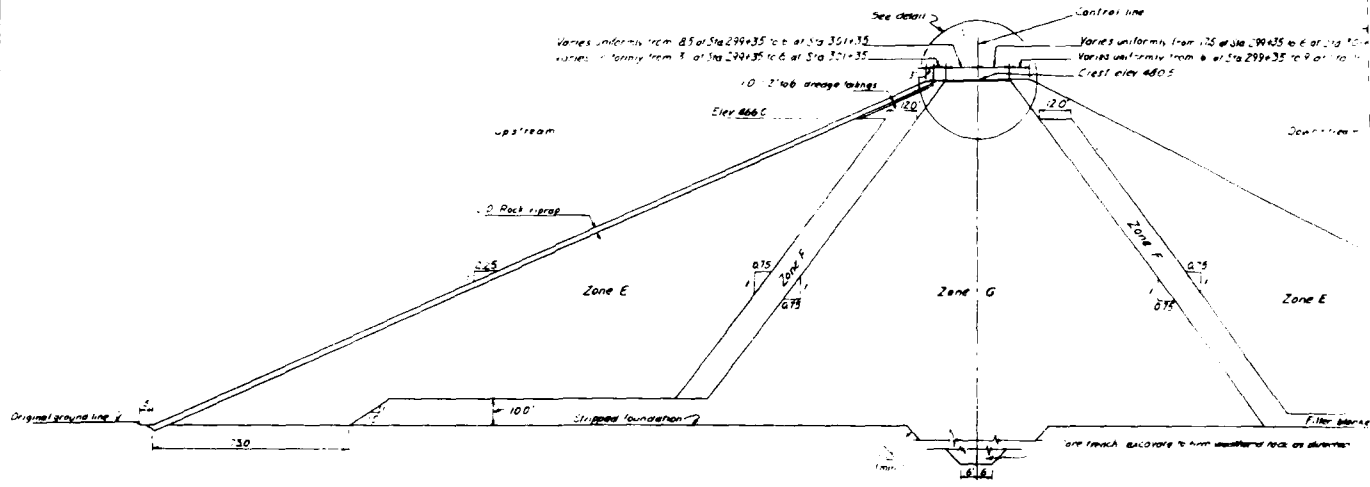
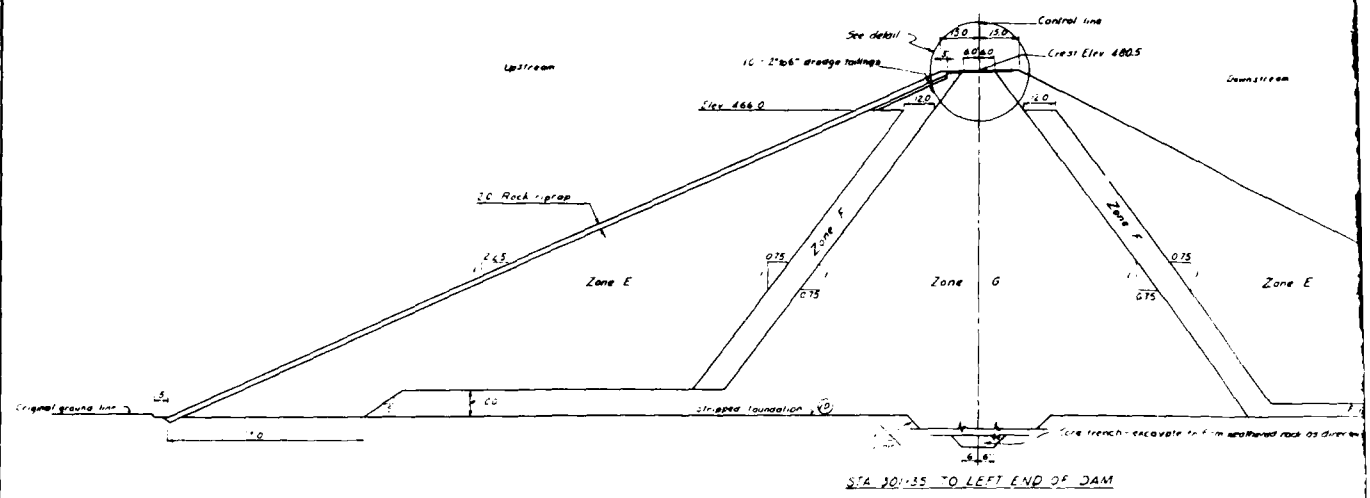
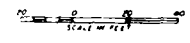


Figure 5c

2



STA 299+35 TO STA 301+35
TYPICAL CROSS SECTIONS



- NOTES
1. Refer to the level datum of 100.
 2. Zone E material to be processed in Station Area No. 5.
 3. Zone F material to be placed in Station Area No. 5.
 4. Zone G material to be processed in Station Area No. 5.
 5. Zone H material to be processed in Station Area No. 5.
 6. Each zone to be 480 feet from the crest in sheet No. 180-3.
 7. Date of development of concrete sheet in sheet No. 102-8.
 8. Date of treatment of concrete in sheet No. 102-8.
 9. Refer to detail No. 102-8.
 10. Date of core trench and founded to 102-8.
 11. A 2' dia trench to be excavated to 102-8.

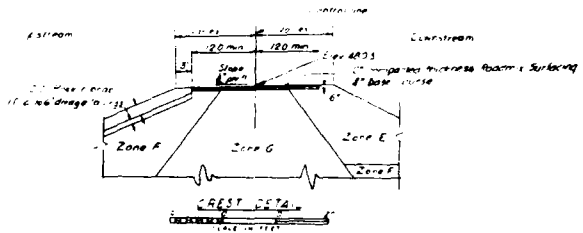
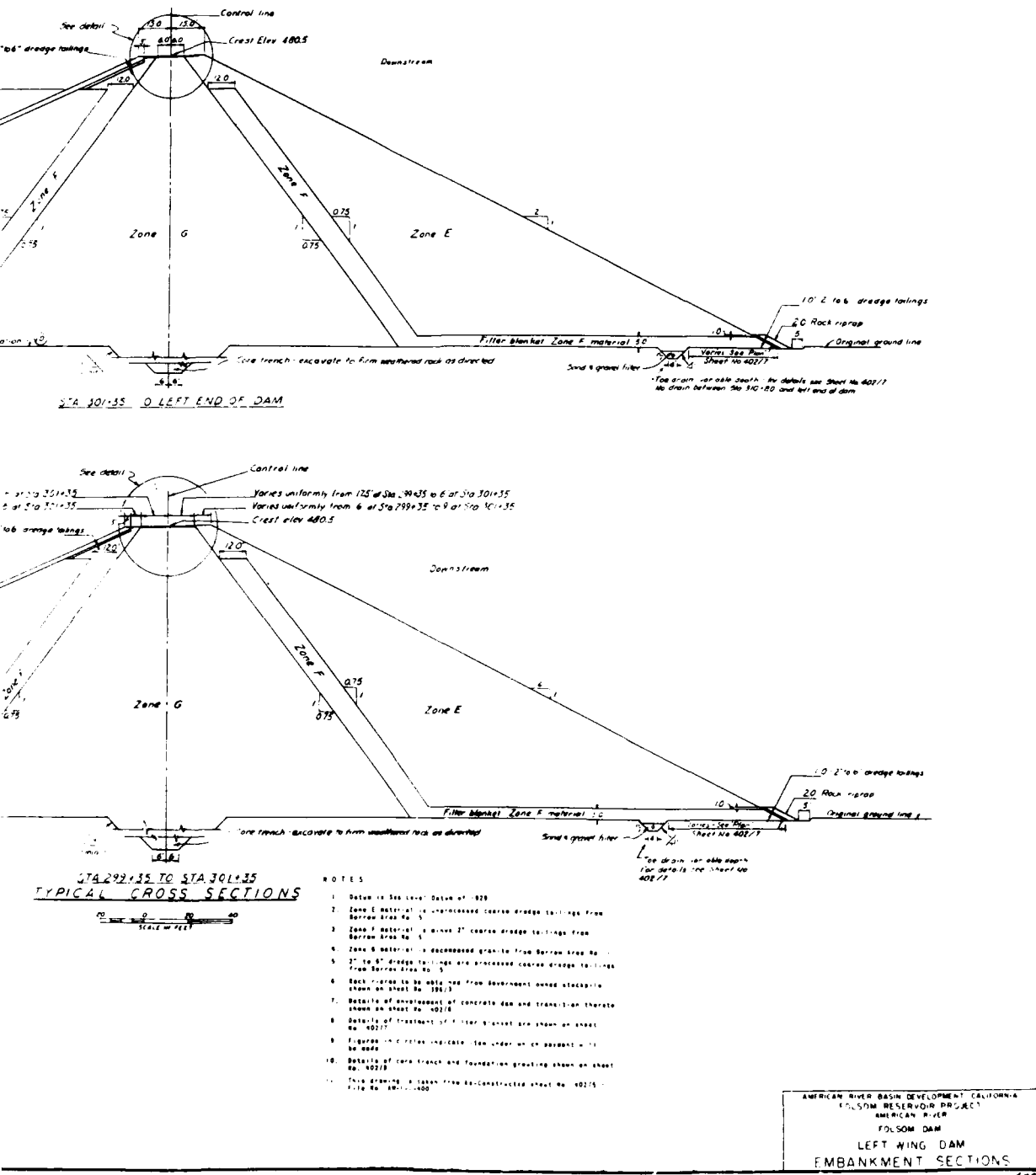
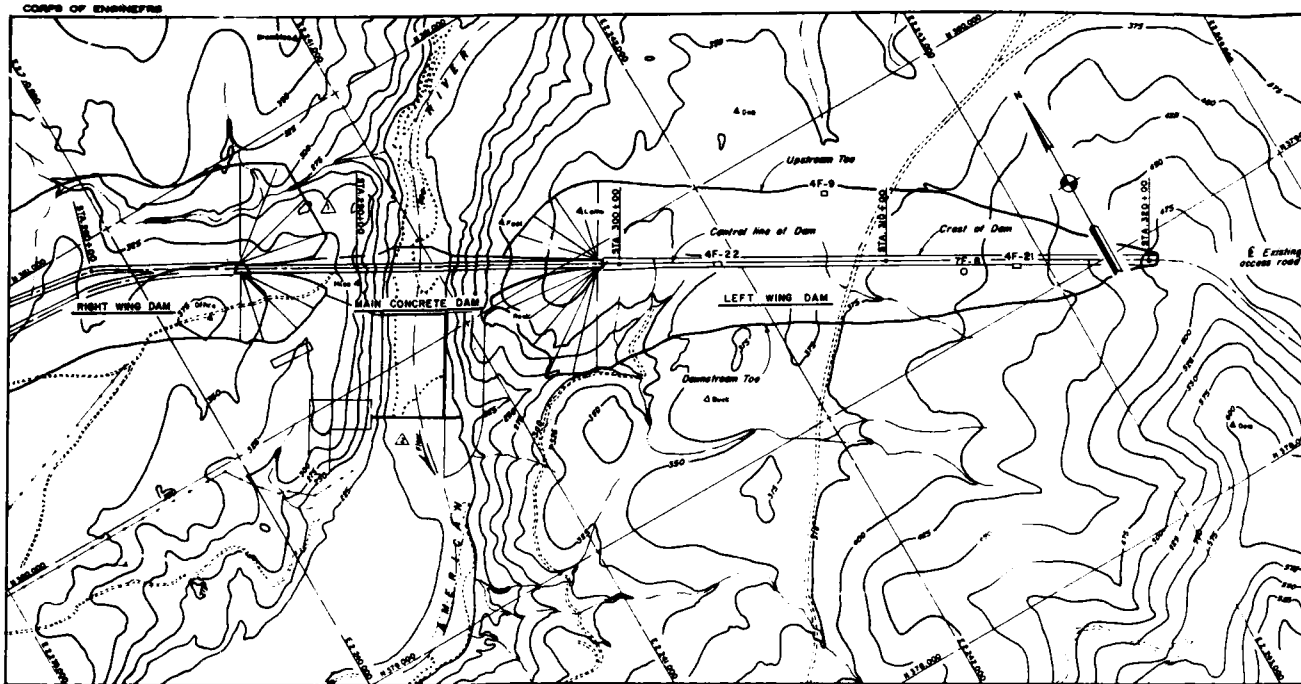


Figure 6b

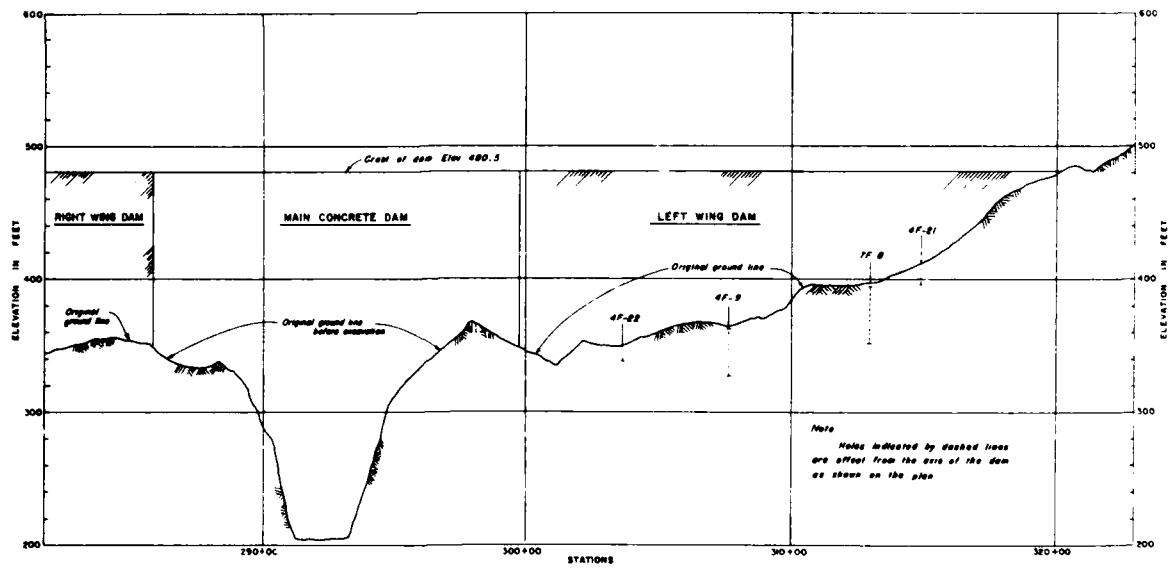


- NOTES
1. Datum is Sea Level Datum of 1929
 2. Zone E material is unprocessed coarse dredge tailings from Borrow Area No. 5
 3. Zone F material is mixed 2" coarse dredge tailings from Borrow Area No. 5
 4. Zone B material is decomposed gravel from Borrow Area No. 5
 5. 2" to 6" dredge tailings are processed coarse dredge tailings from Borrow Area No. 5
 6. Rock riprap to be able use from Government owned stockpile shown on sheet No. 402/3
 7. Details of envelopment of concrete dam and transition structure shown on sheet No. 402/4
 8. Details of treatment of filter blanket are shown on sheet No. 402/7
 9. Figures in circles indicate (see under an on adjacent sheet) to be used
 10. Details of core trench and foundation grouting shown on sheet No. 402/3
 11. This drawing is taken from Reconstructed sheet No. 402/5 - Title No. 100-1-400

Figure 6b



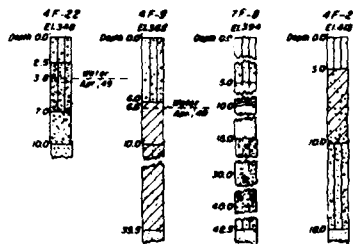
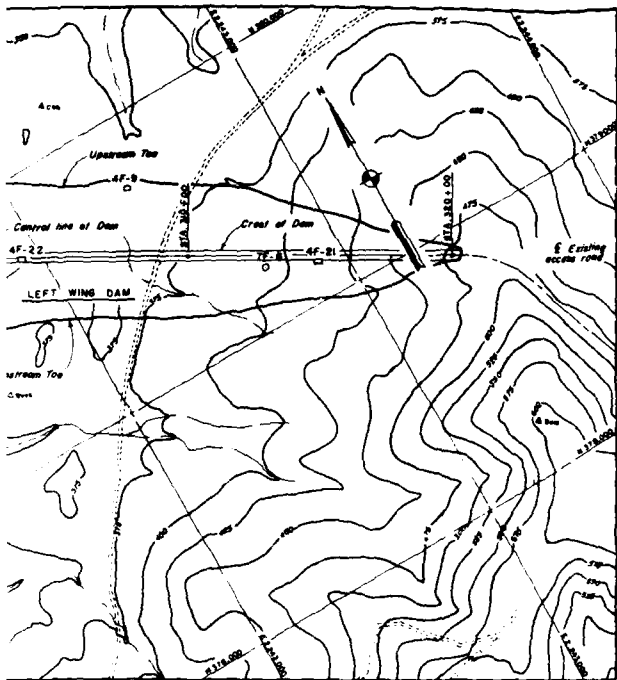
PLAN
SCALE IN FEET



PROFILE ON CONTROL LINE
SCALE AS SHOWN

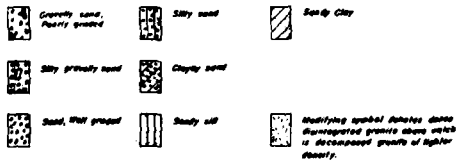
Figure 6c

1



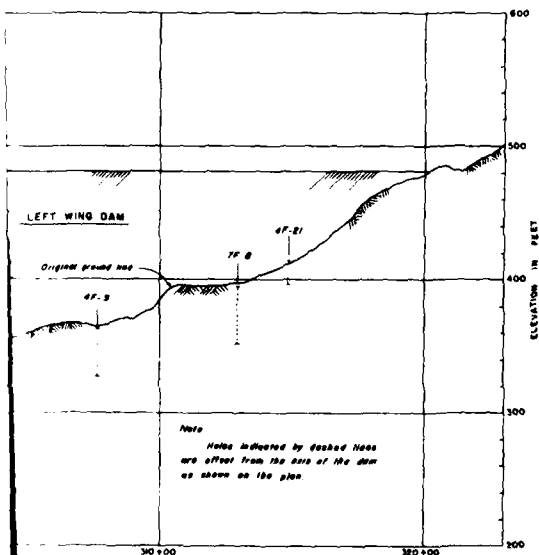
LOGS OF HOLES
SCALE AS SHOWN

LEGEND



NOTES:

1. Datum is Sea Level Datum of 1929.
2. Elevations shown on logs are ground surface elevations.
3. Laboratory classifications shown for all materials according to the Corps of Engineers' Uniform Soil Classification. The term "gravel" applies to grain sizes larger than the No. 10 sieve.
4. All foundation material indicated by log symbol is decomposed granite weathered in place.
5. All of holes are open pits.
6. All FF holes were drilled by a falling drill rig using a 7" diameter rotary core drill.
7. Typical subsoil sections are shown on sheets No. 60276 and 60278.
8. Additional logs of concrete dam foundation exploration are shown on sheets No. 60275 to 29.
9. Diversed temporarily taken prior to the November 1950 floods.
10. This drawing was taken from As-Constructed sheet No. 60276-2, File No. 6011-1-100.



AMERICAN RIVER BASIN DEVELOPMENT, CALIFORNIA
FOLSOM RESERVOIR PROJECT
AMERICAN RIVER
FOLSOM DAM
FOUNDATION EXPLORATION
LEFT WING DAM
PLAN, PROFILE AND LOGS

400/3.2

Figure 6c

2

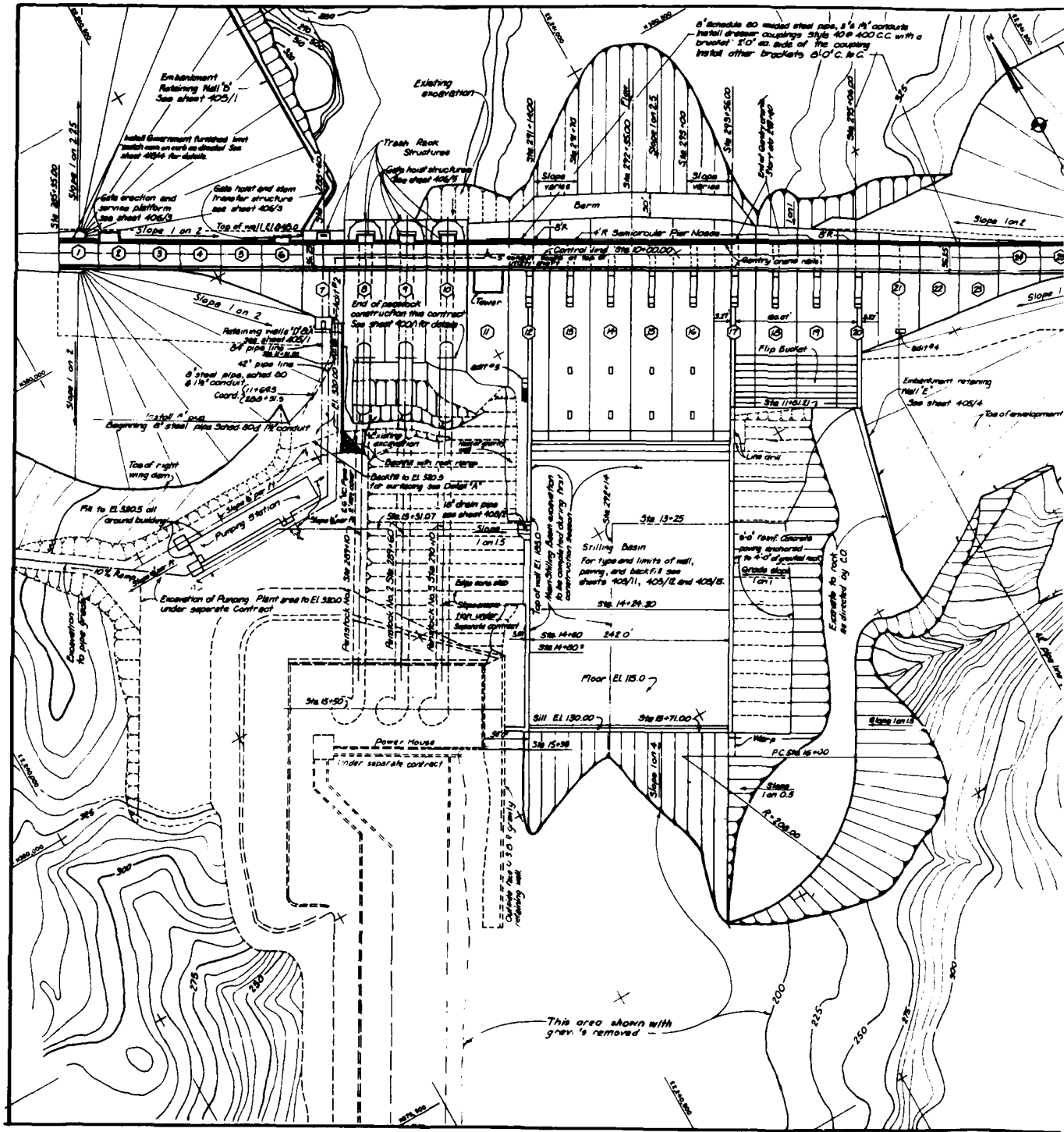


Figure 7. Plan of Concrete Gravity Dam

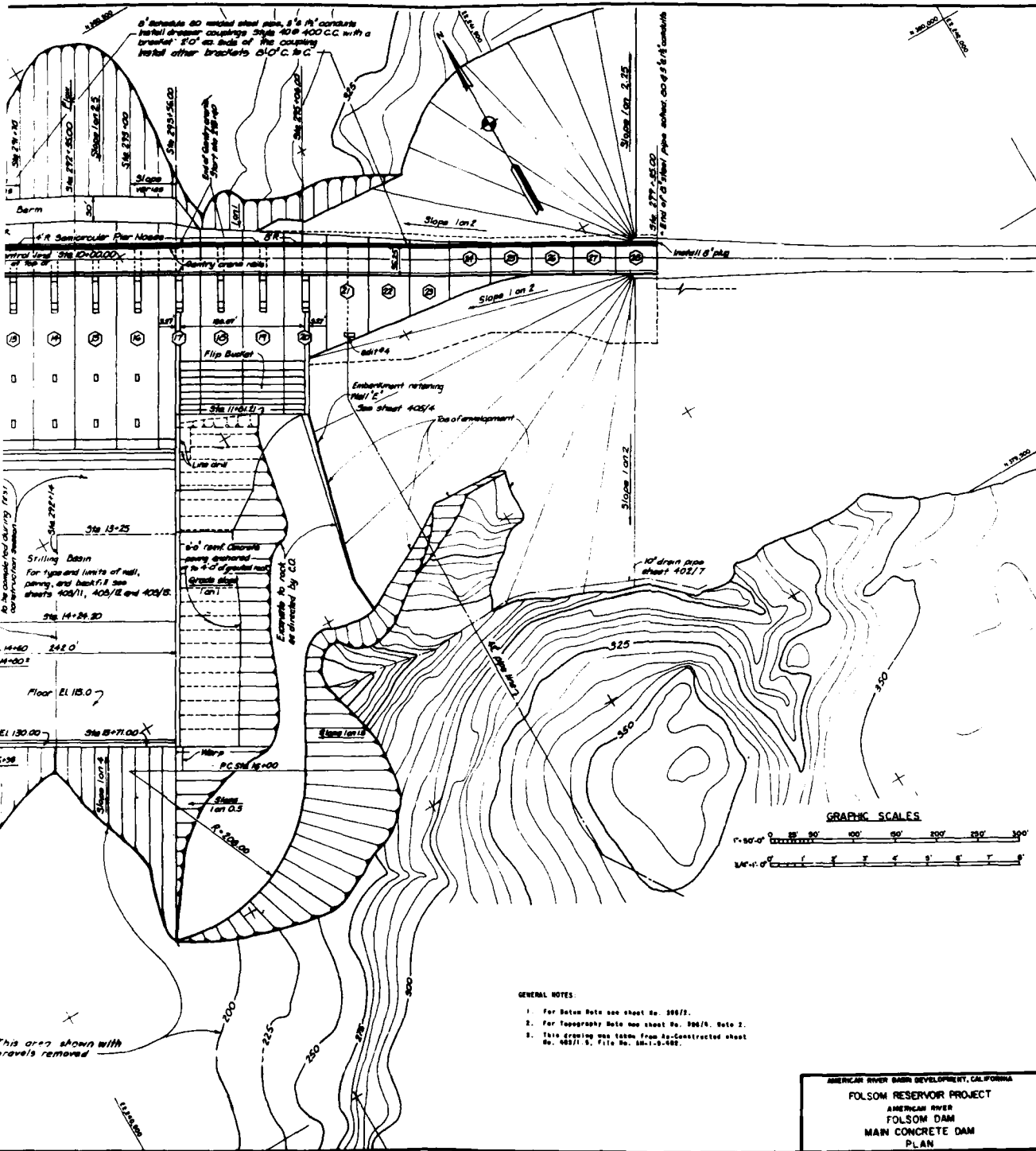


Figure 7. Plan of Concrete Gravity Dam

1

2

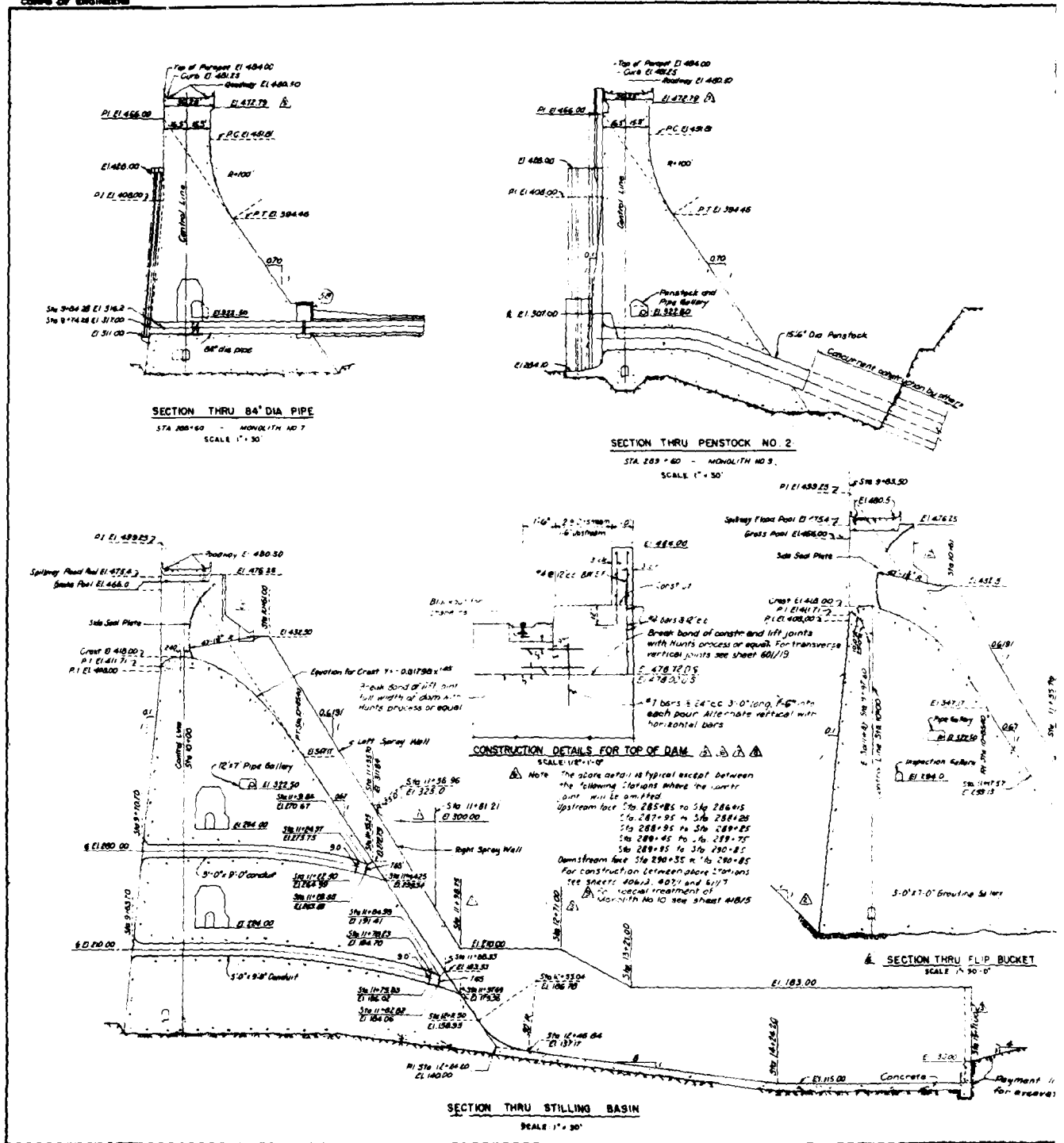
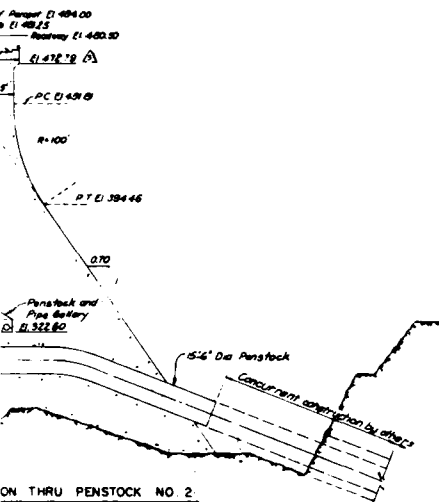
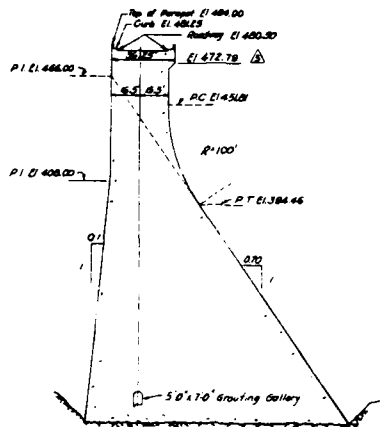


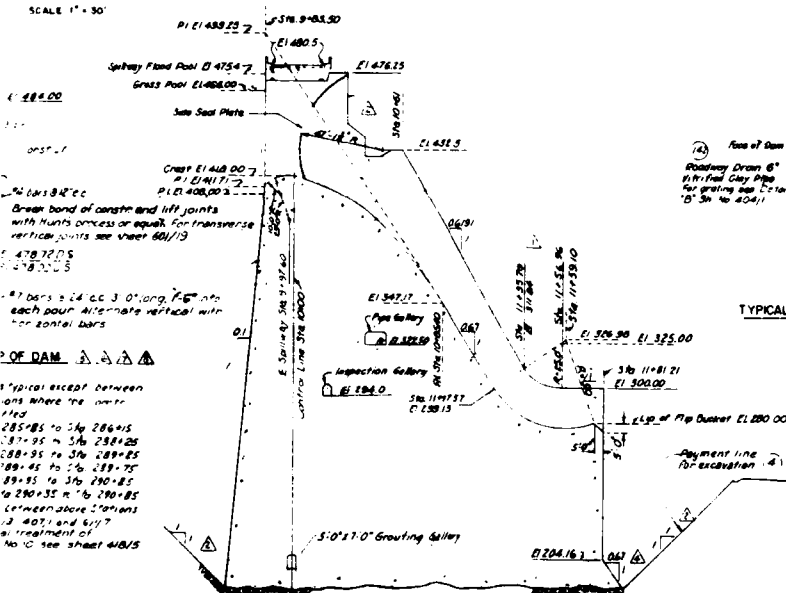
Figure 9. Typical sections of Concrete Gravity



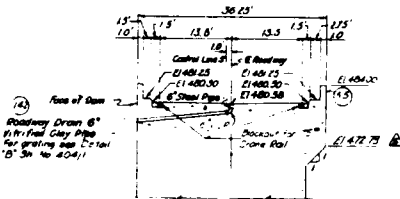
SECTION THRU PENSTOCK NO. 2
 289'-60" - MONOLITH NO. 5
 SCALE 1" = 30'



TYPICAL NON-OVERFLOW SECTION
 378'-28'-10" - MONOLITH NO. 22
 SCALE 1" = 30'

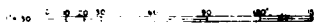


SECTION THRU FLIP BUCKET
 SCALE 1" = 30'-0"



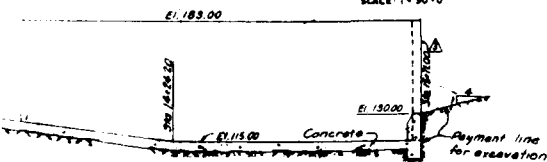
TYPICAL DETAIL AT TOP OF NON-OVERFLOW SECTION
 SCALE 1" = 10'

GRAPHIC SCALES



GENERAL NOTES

1. Figures in circles indicate times under which payment will be made.
2. Payment for all concrete shown on this sheet will be made at contract unit price, less unless otherwise noted.
3. Payment for cement for all concrete shown on this sheet will be made at contract unit price, less.
4. This drawing is taken from As-Constructed sheet No. 40313 B, File No. 40-119-405.



AMERICAN RIVER BASIN DEVELOPMENT CALIFORNIA
 FOLSOM RESERVOIR PROJECT
 AMERICAN RIVER
FOLSOM DAM
 MAIN CONCRETE DAM
 TYPICAL SECTIONS

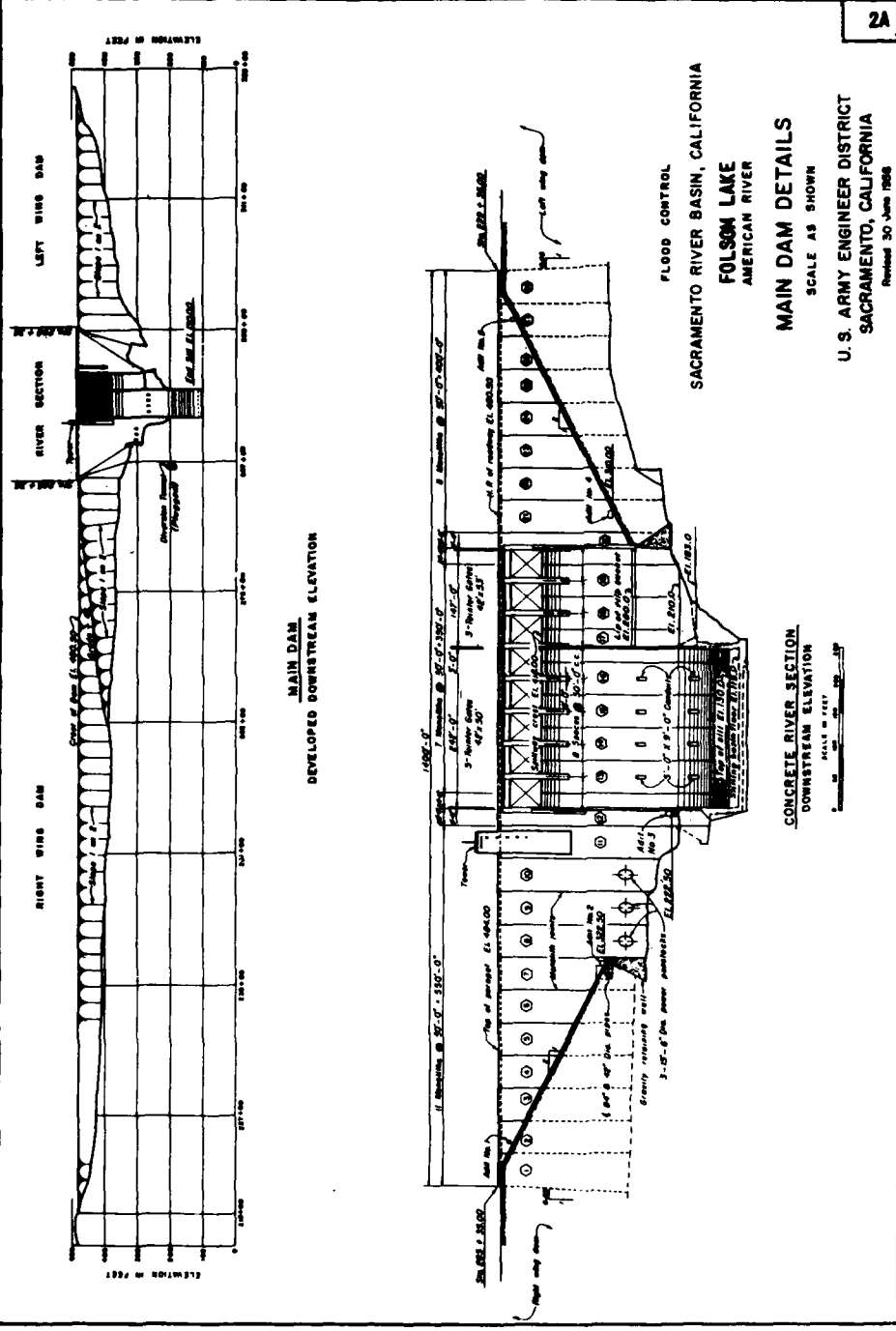


Figure 10. Developed downstream elevation of Wing Dams and Concrete Gravity Dam

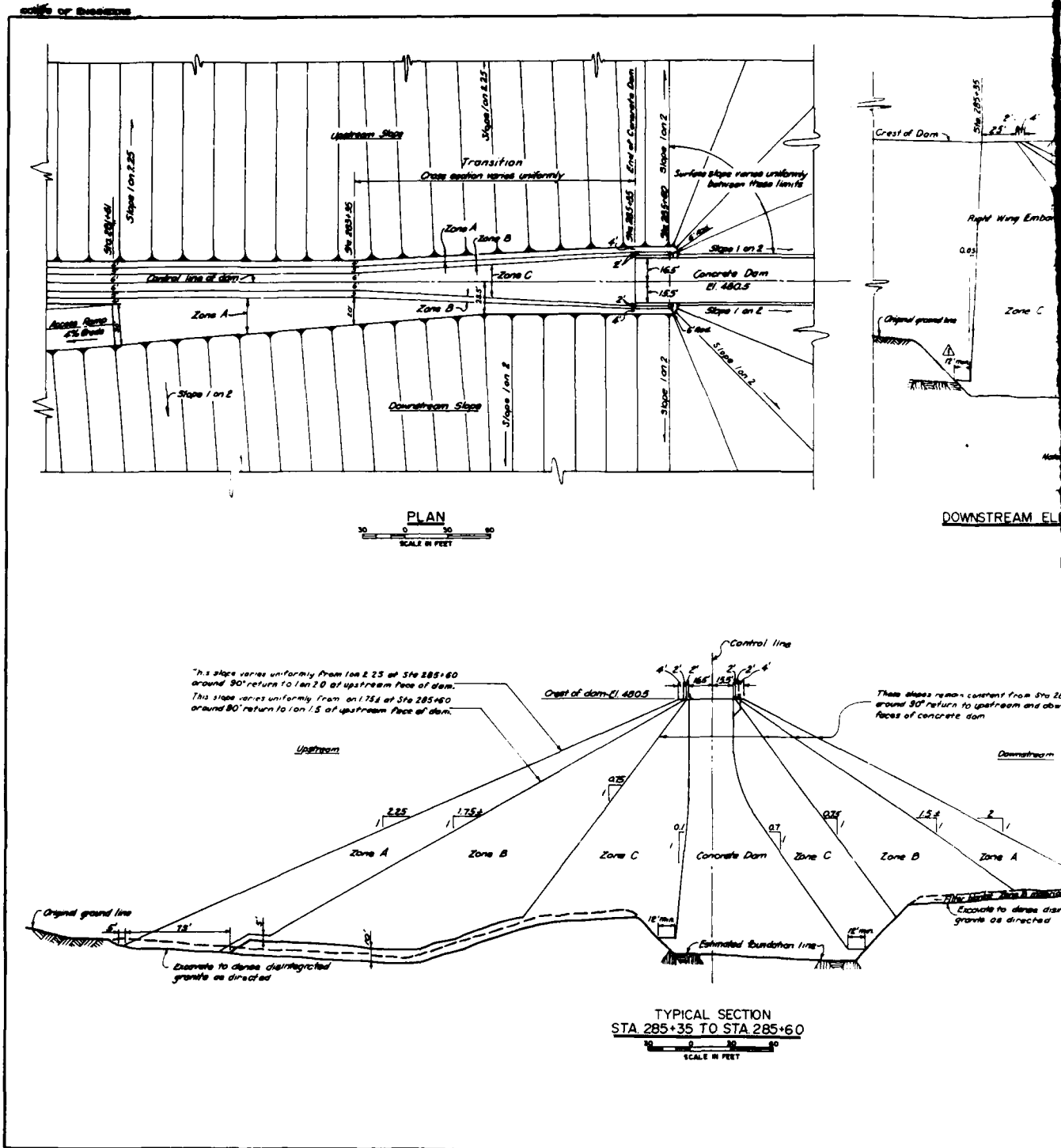
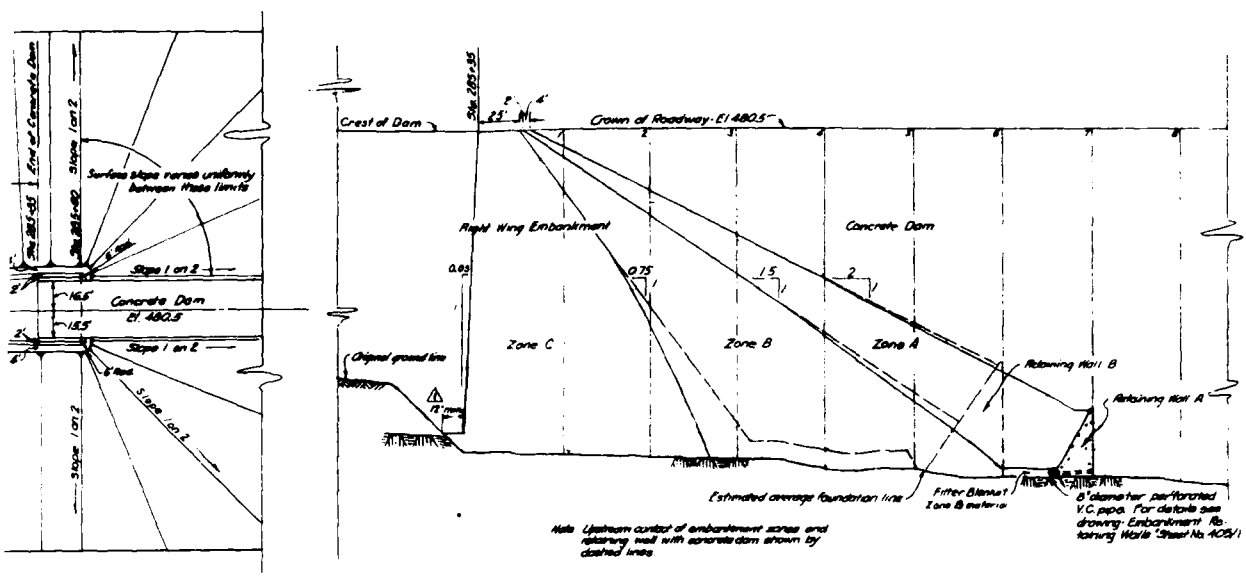
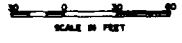


Figure 11. Plan and sections of Right Wing Dam interface

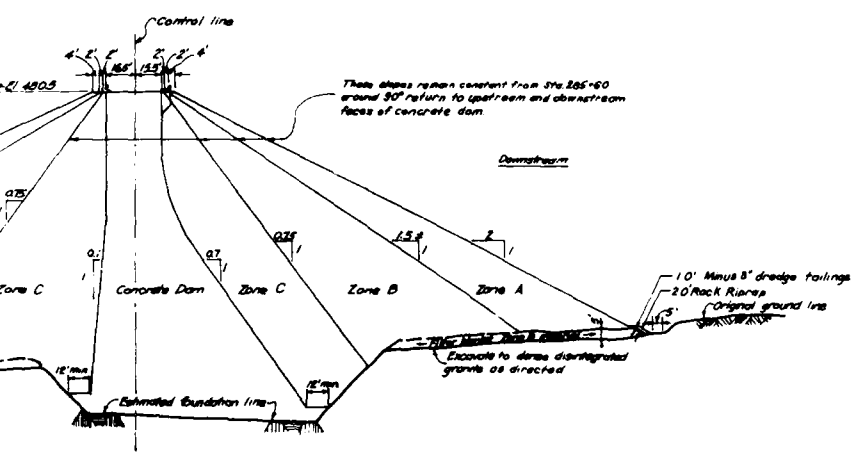


DOWNSTREAM ELEVATION OF EMBANKMENT ENVELOPMENT CONTACT



NOTES

1. Datum is Sea Level Datum of 1929.
2. Zone A material is rock from the American River channel excavation and government owned stockpile.
3. Zone B material is unprocessed sand and gravel from the American River channel excavation.
4. Lines shown on abutment sections separating Zones A & B will vary in slope as determined by the quantities of material available from American River channel excavation.
5. When material for Zone B from the American River channel excavation is exhausted, additional material will be obtained from Barron Area No. 7 and approved waste from processing of concrete aggregate.
6. Zone C material is decomposed granite from Barron Area No. 3 and suitable fine grained material from American River channel excavation.
7. Rock riprap to be obtained from government owned stockpile shown on sheet No. 402/3.
8. Minus 8" dredge tailings to be obtained from Deposit Area No. 6.
9. For typical sections between Sta. 281+1 to Sta. 283+5 and Sta. 285+05 to Sta. 285+95, see sheet No. 402/2.
10. Figures in circles indicate loads under which payment will be made.
11. This drawing is taken from as-constructed sheet No. 402/1, File No. 28-11-4-402.



**TYPICAL SECTION
STA 285+35 TO STA 285+60**



AMERICAN RIVER BASIN DEVELOPMENT, CALIFORNIA
FOLSOM RESERVOIR PROJECT
 AMERICAN RIVER
FOLSOM DAM
RIGHT WING DAM
ENVELOPMENT OF CONCRETE DAM

and sections of Right Wing Dam interface area

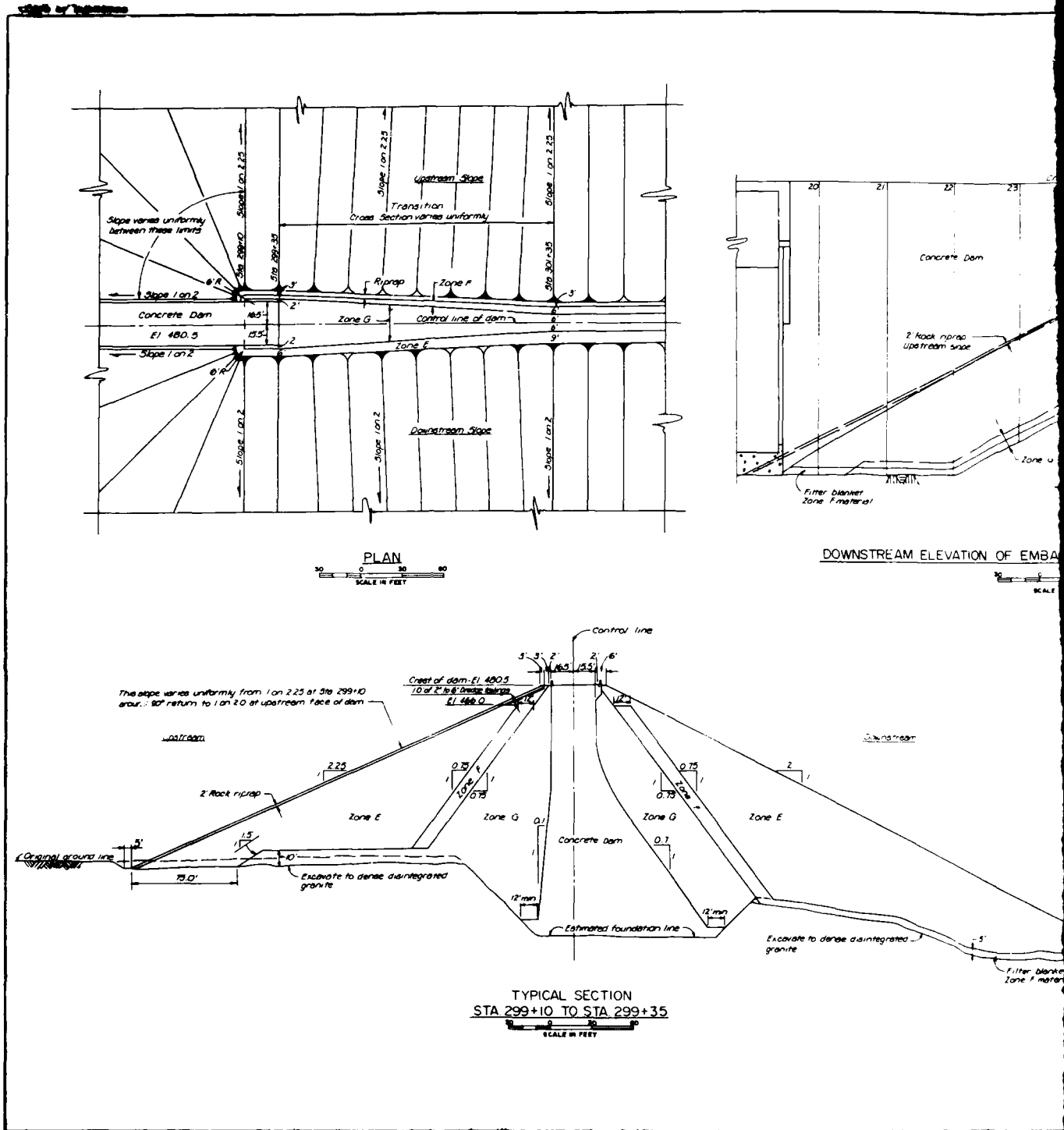


Figure 12. Plan and sections of Left Wing Dam interface

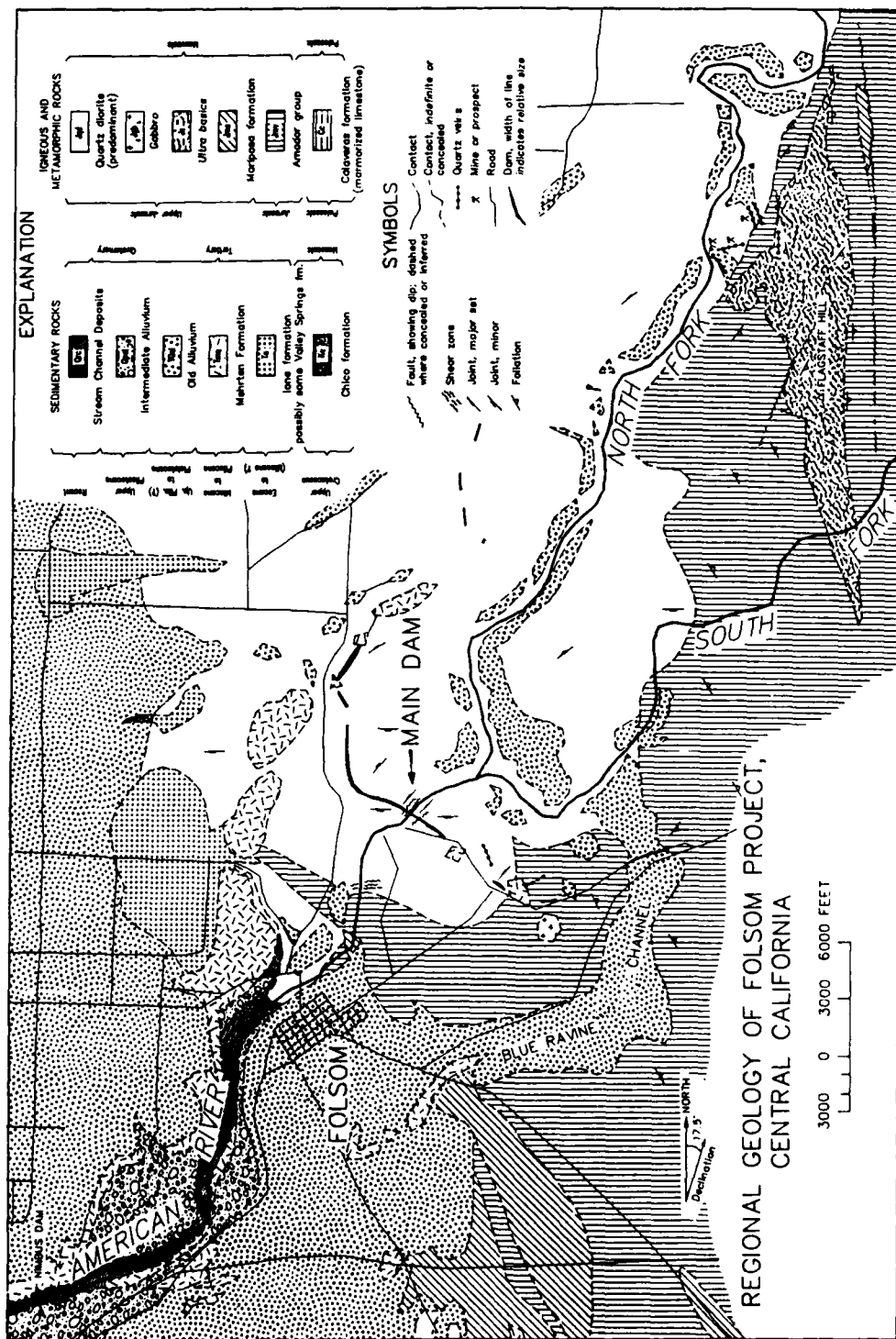


Figure 13. Geologic map, parts of the Folsom and Auburn Quadrangles

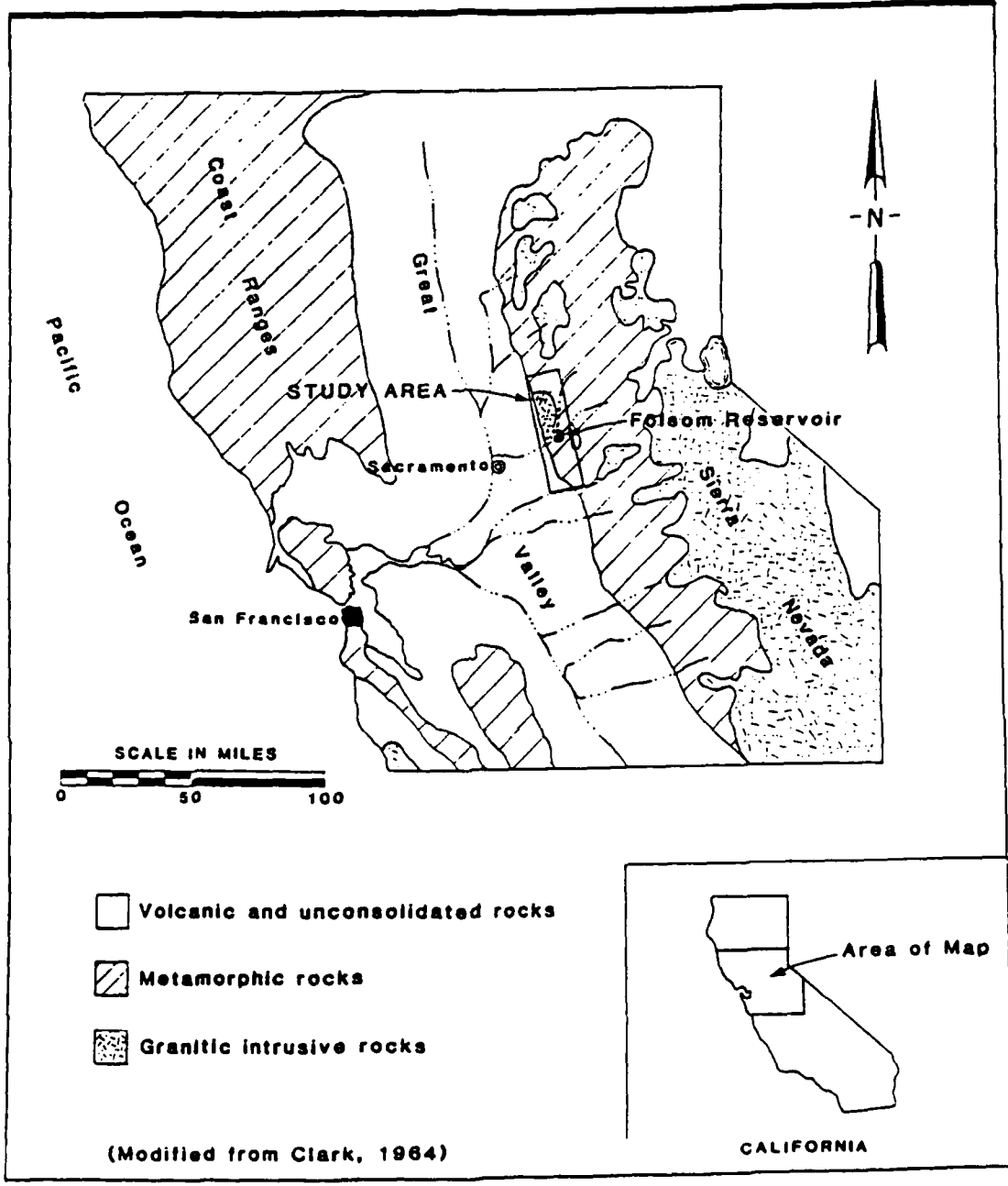


Figure 14. Regional geologic map (after Tierra Engineering Consultants 1983)

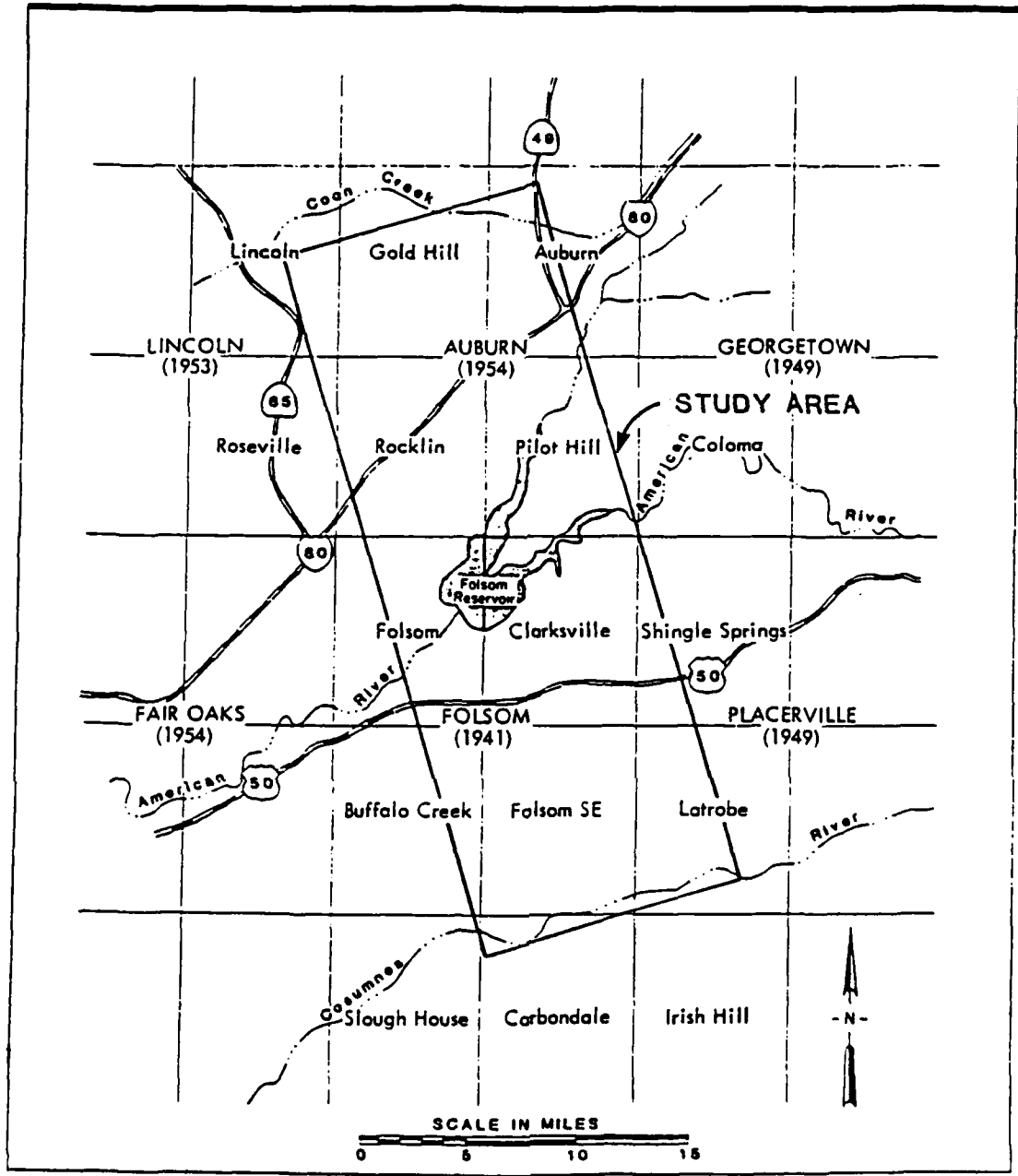


Figure 15. Identification of study area (from USGS 7.5 and 15 ft topographic maps, after Tierra Engineering Consultants 1983)

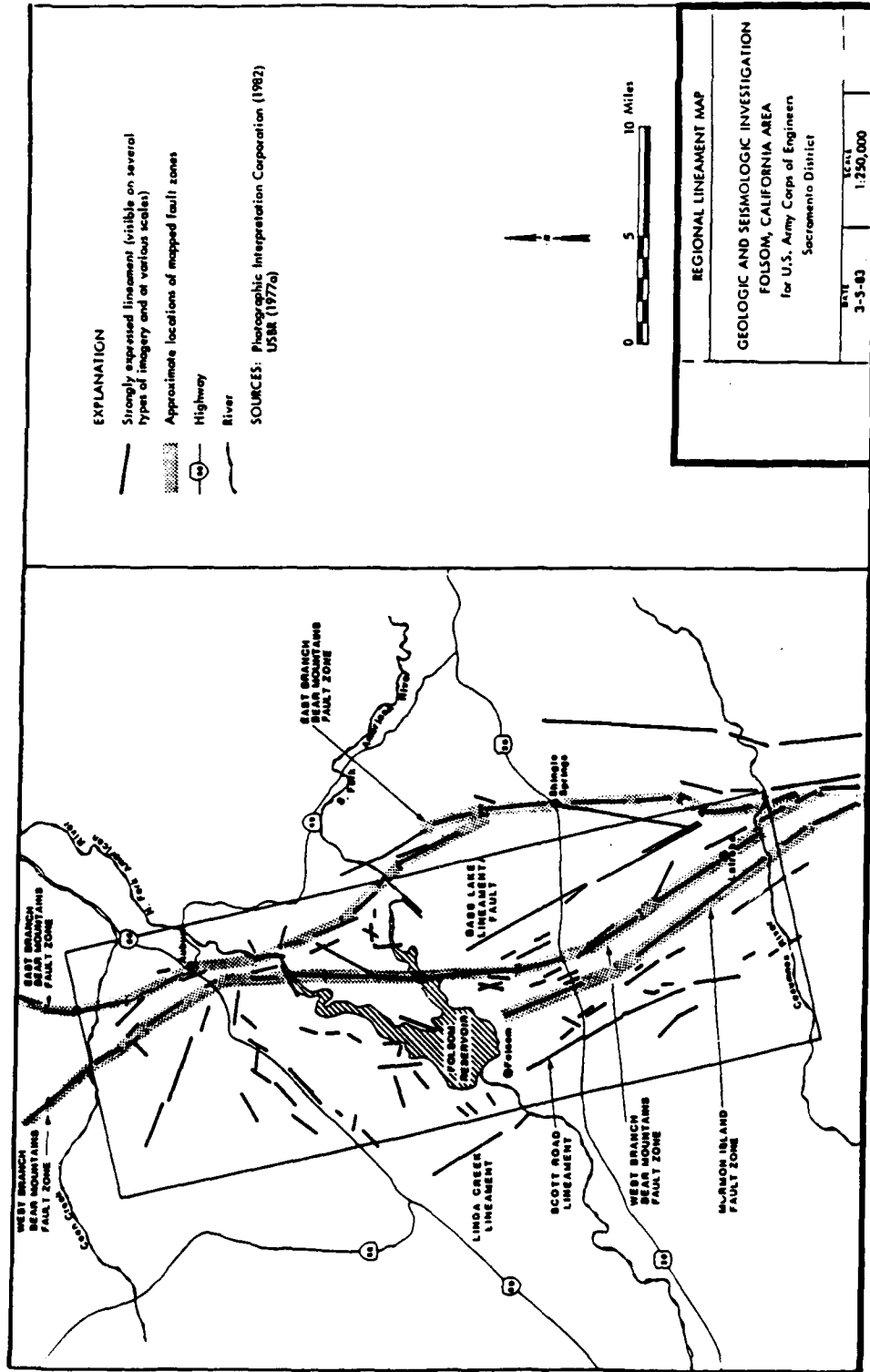
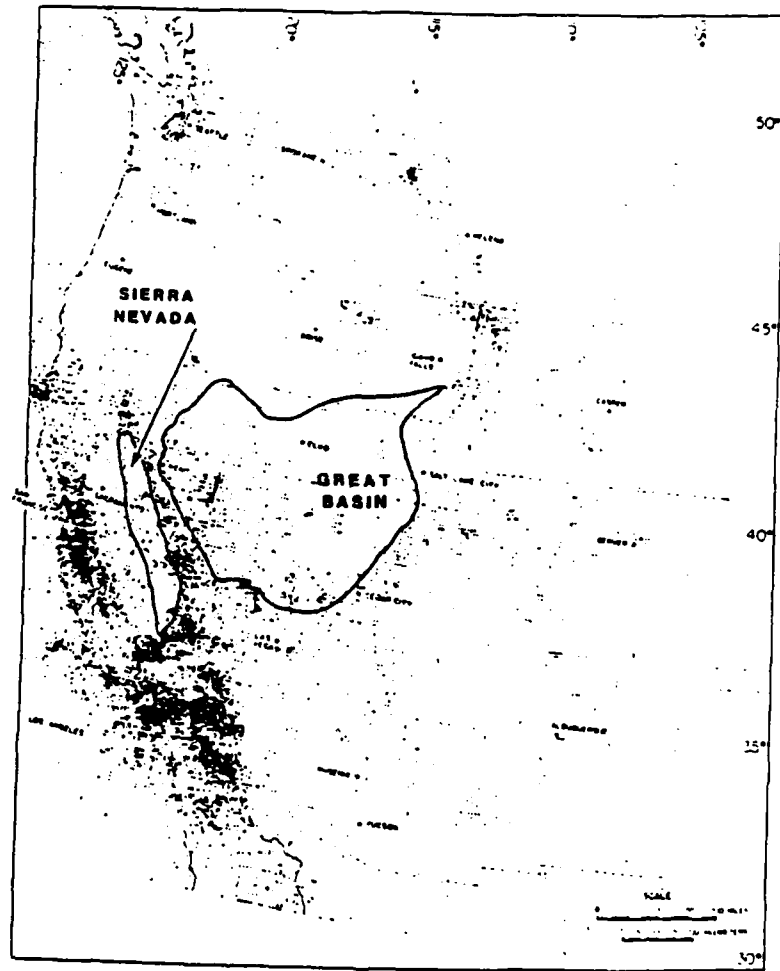


Figure 17. Regional lineament map (after Tierra Engineering Consultants 1983)



SOURCE: Adapted from Smith, 1978

Figure 18. Epicenter Map of Western United States (after Tierra Engineering Consultants 1983)

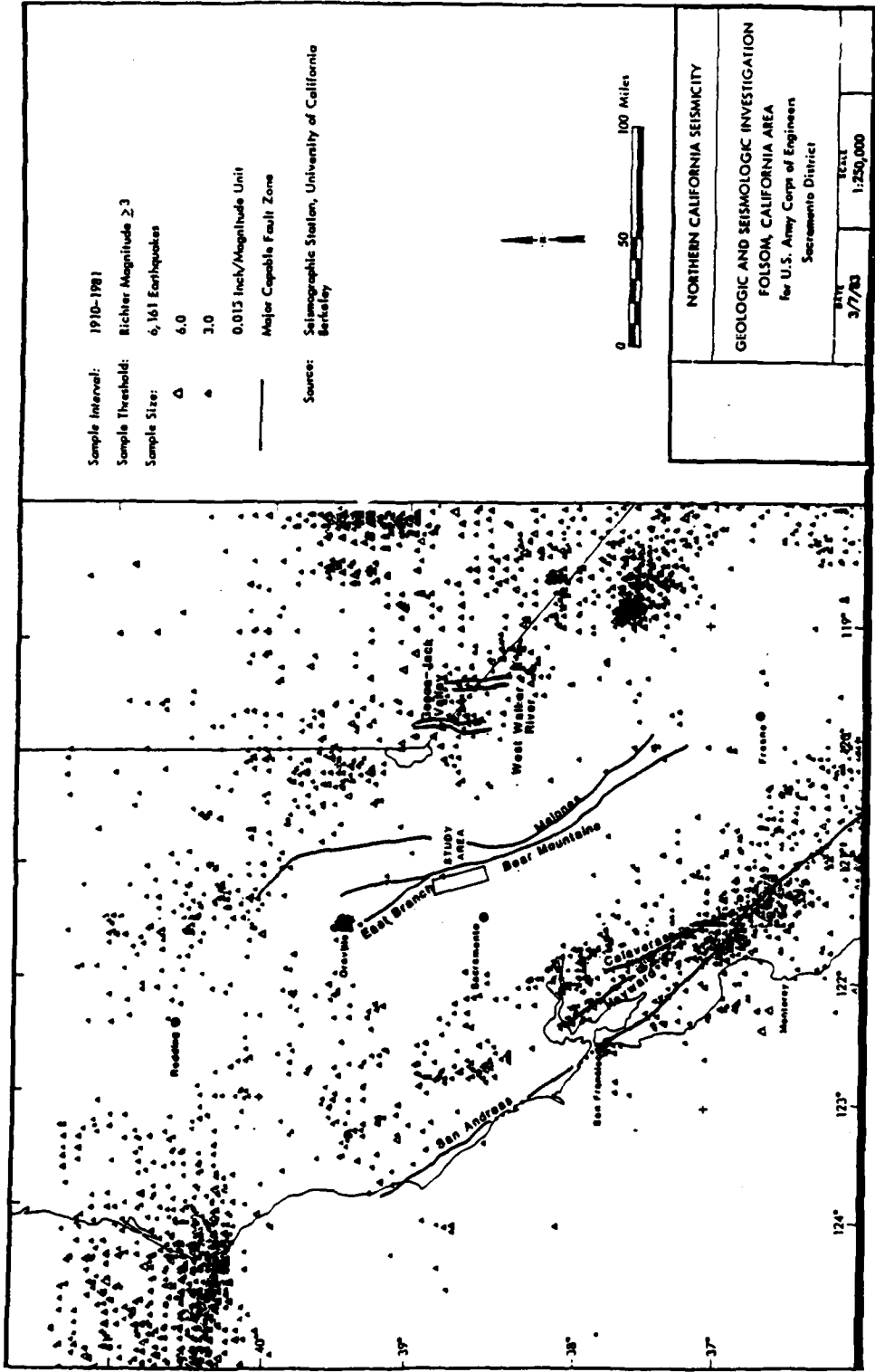
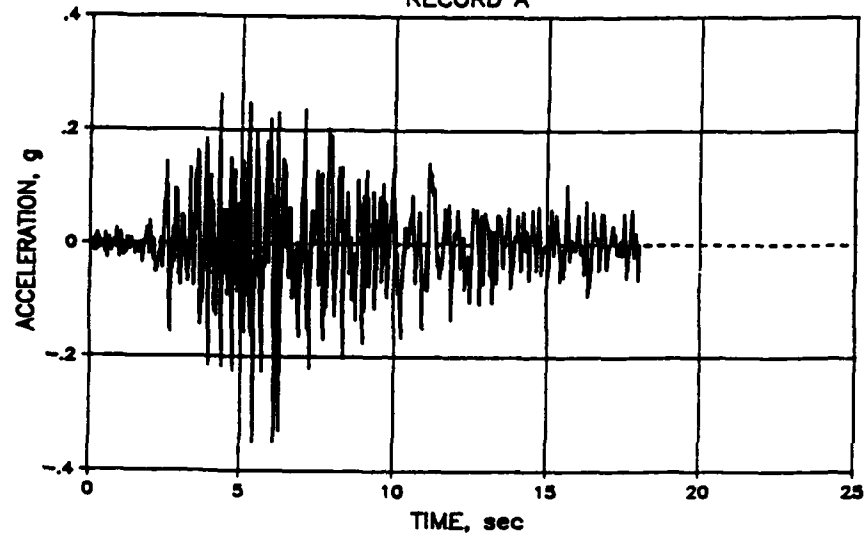


Figure 19. Seismicity map for Northern California (after Tierra Engineering Consultants 1983)

FOLSOM DAM PROJECT
RECORD A



RECORD B

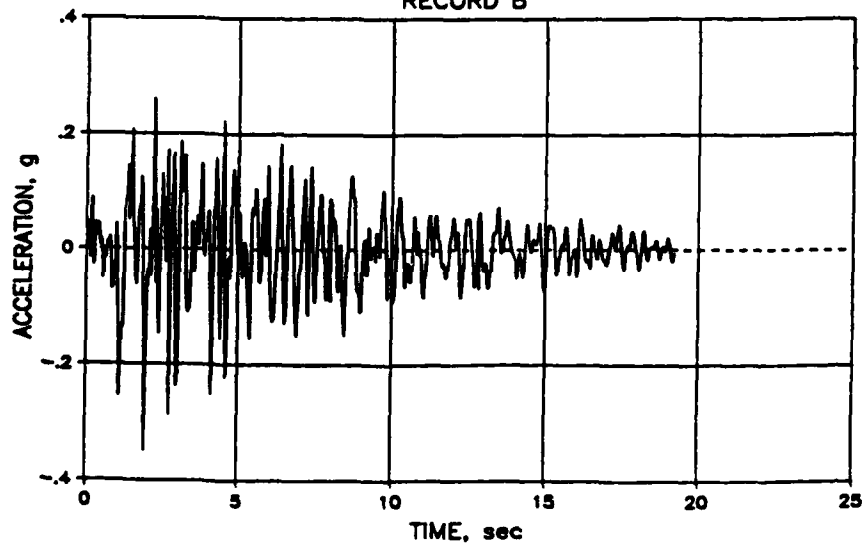


Figure 20. Acceleration histories used in the analysis

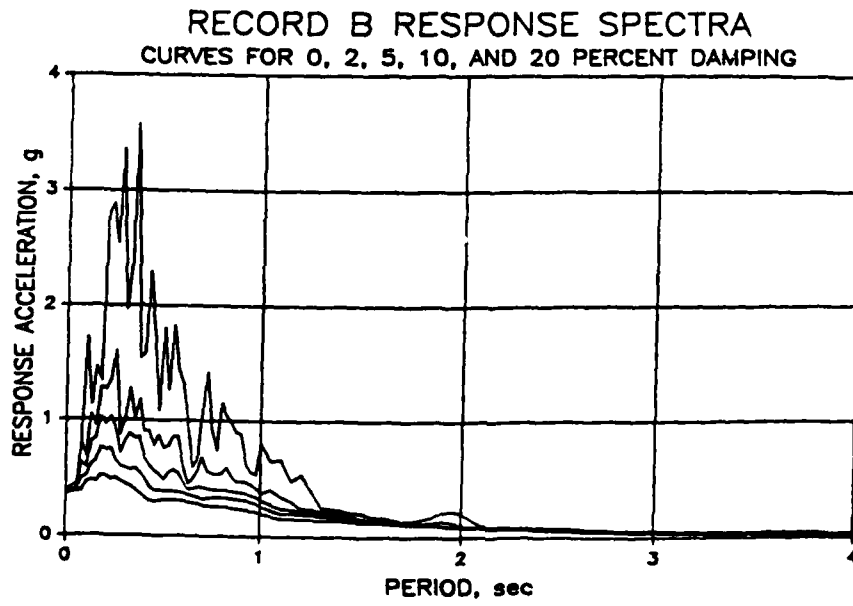
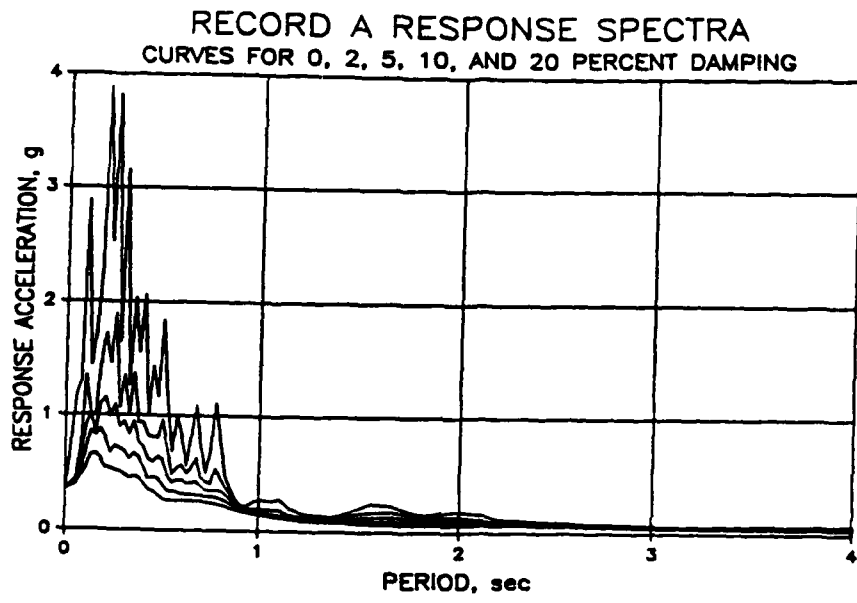


Figure 21. Response spectra of Records A and B

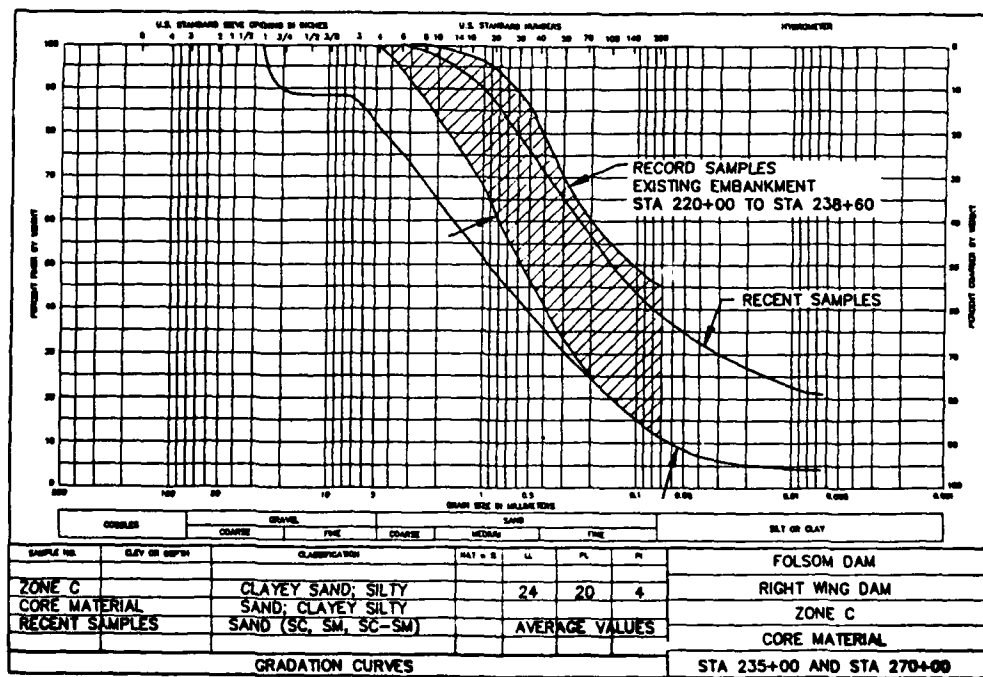
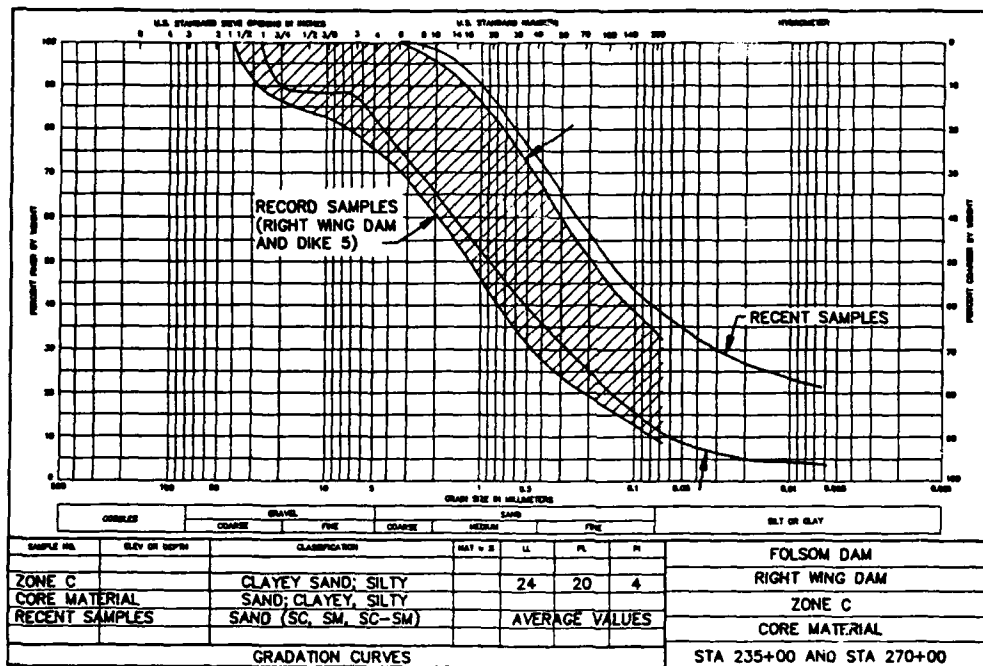


Figure 22. Grain size distribution for materials of Zone C and existing dam in Right Wing Dam (from construction records)

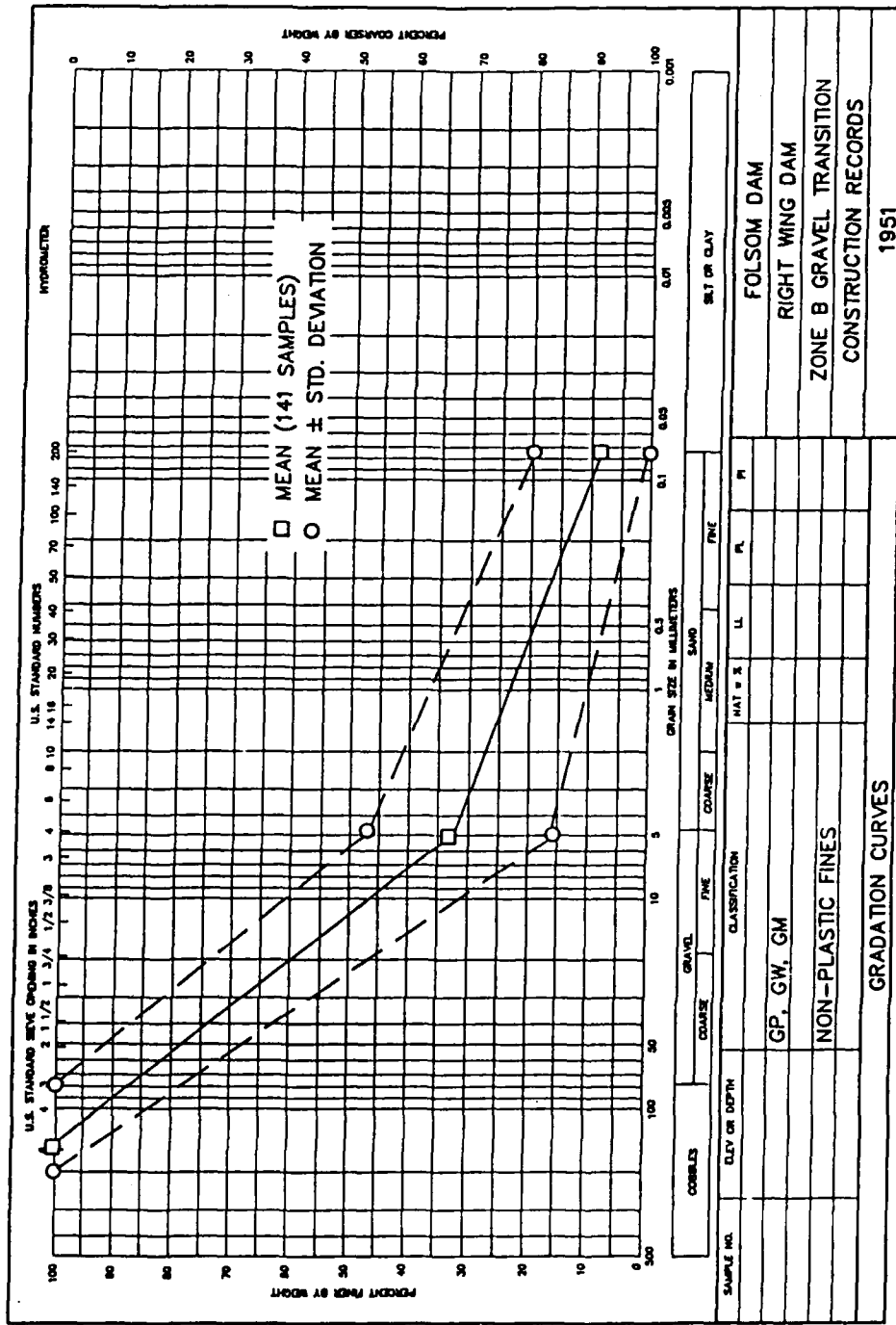
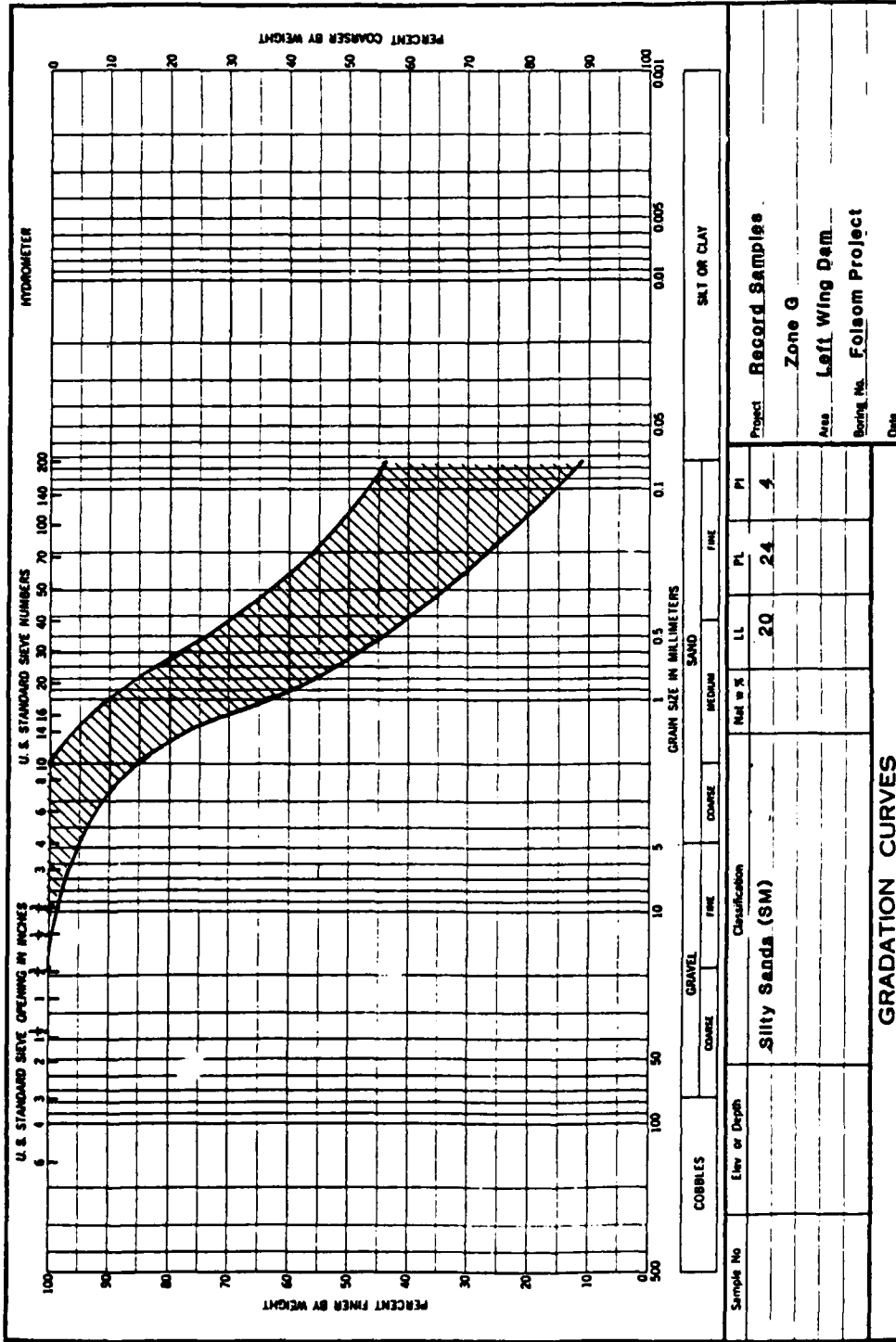
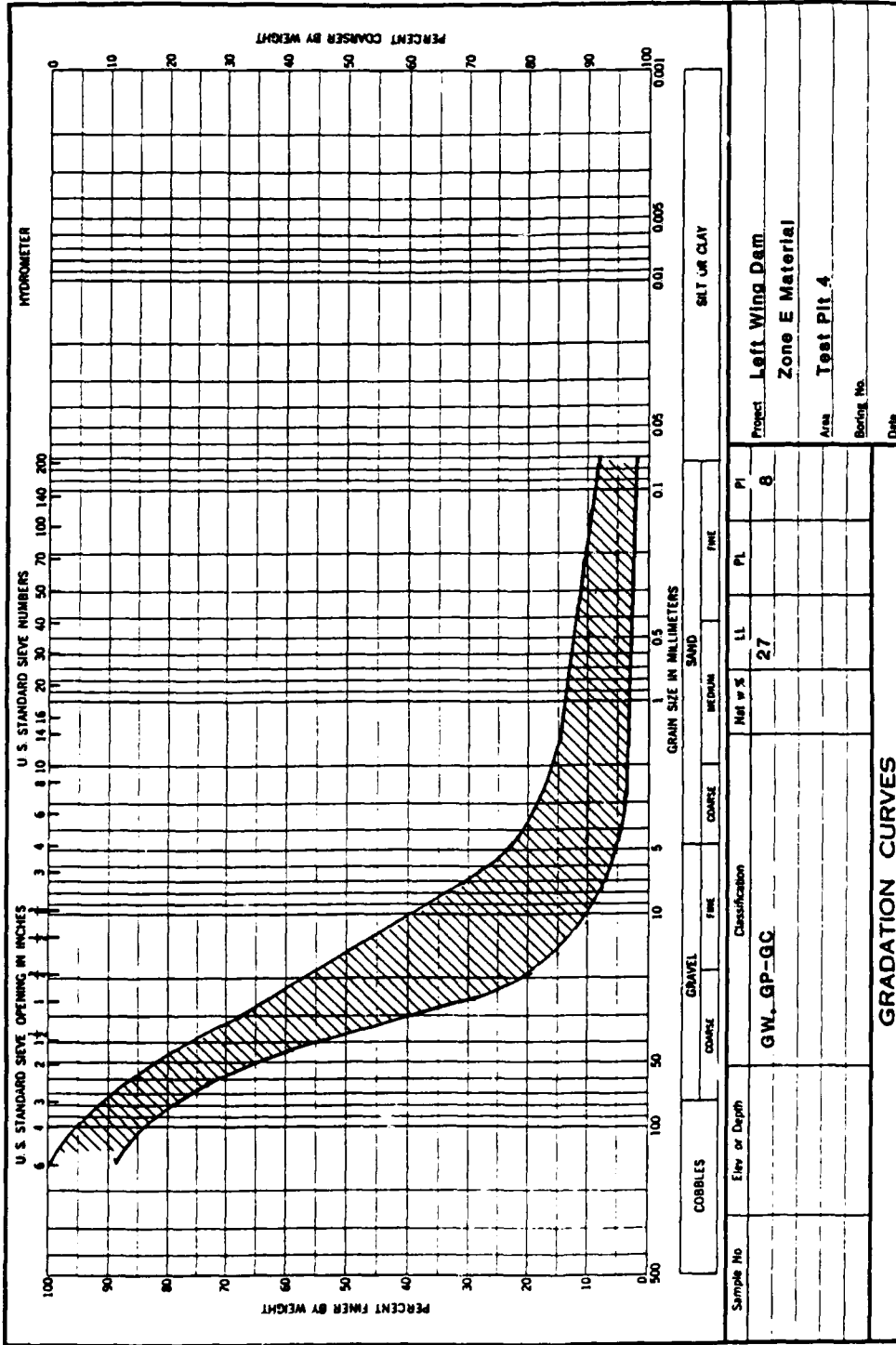


Figure 23. Gratation of Zone B gravel transition in Right Wing Dam from construction records (1951)



ENG FORM 2087
 1 MAY 63

Figure 24. Range of gradations observed in record samples from Zone G, core of Left Wing Dam



ENG FORM 1 MAY 63 2087

Figure 25. Gradations observed in Test Pit 4 in downstream shell of Left Wing Dam, Zone E

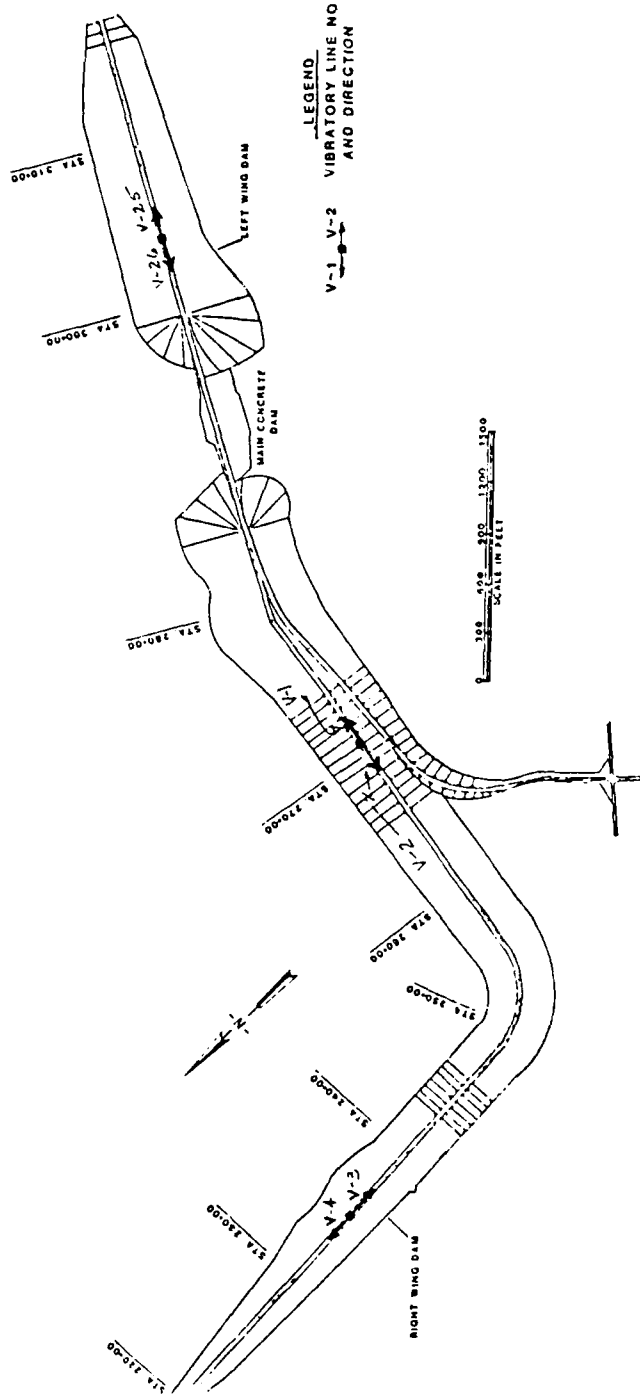


Figure 26. Locations of Rayleigh wave tests performed on crest at Left and Right Wing Dams

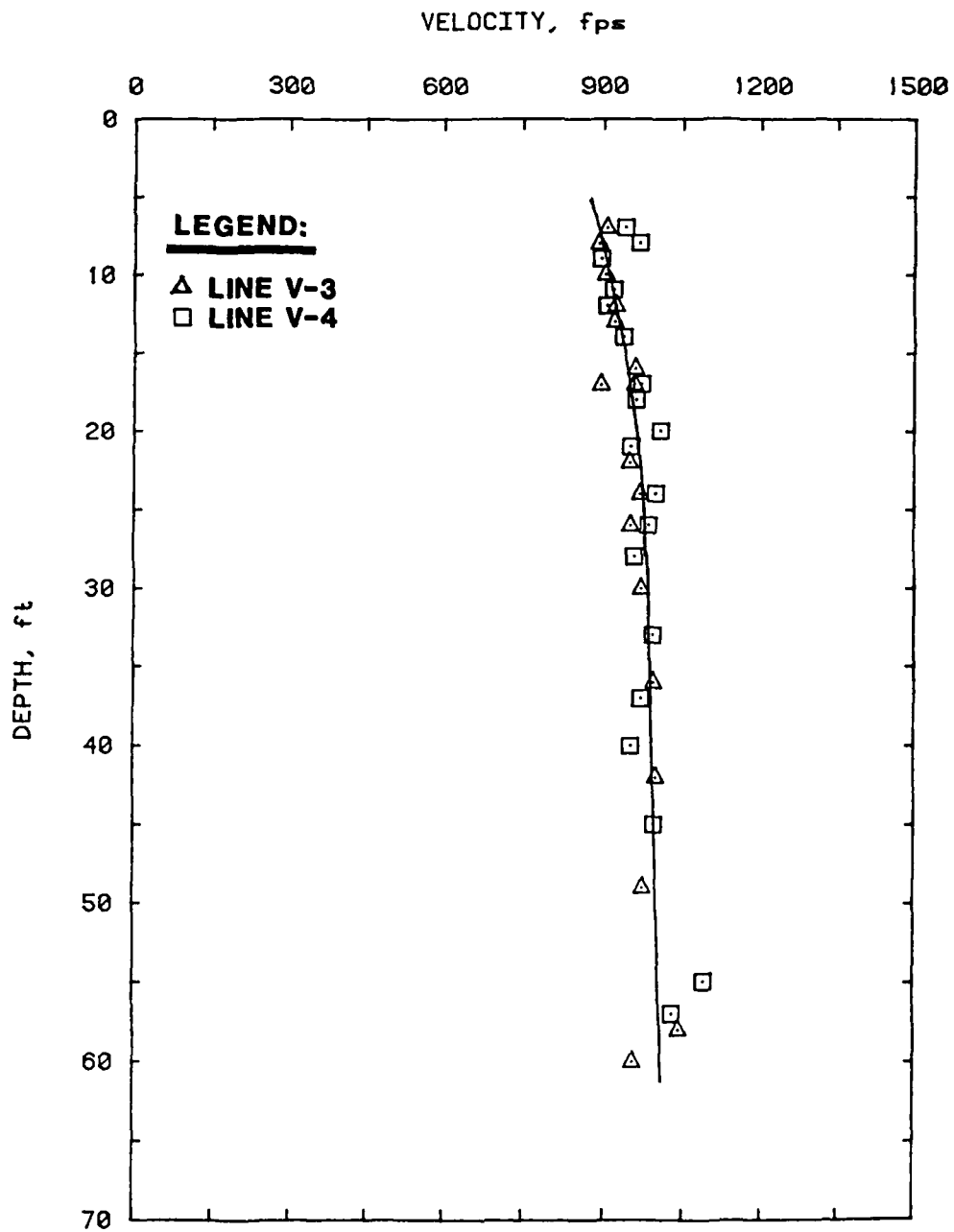


Figure 27. Rayleigh wave velocity versus depth for surface vibratory lines V-3 and V-4 at Station 235 of Right Wing Dam

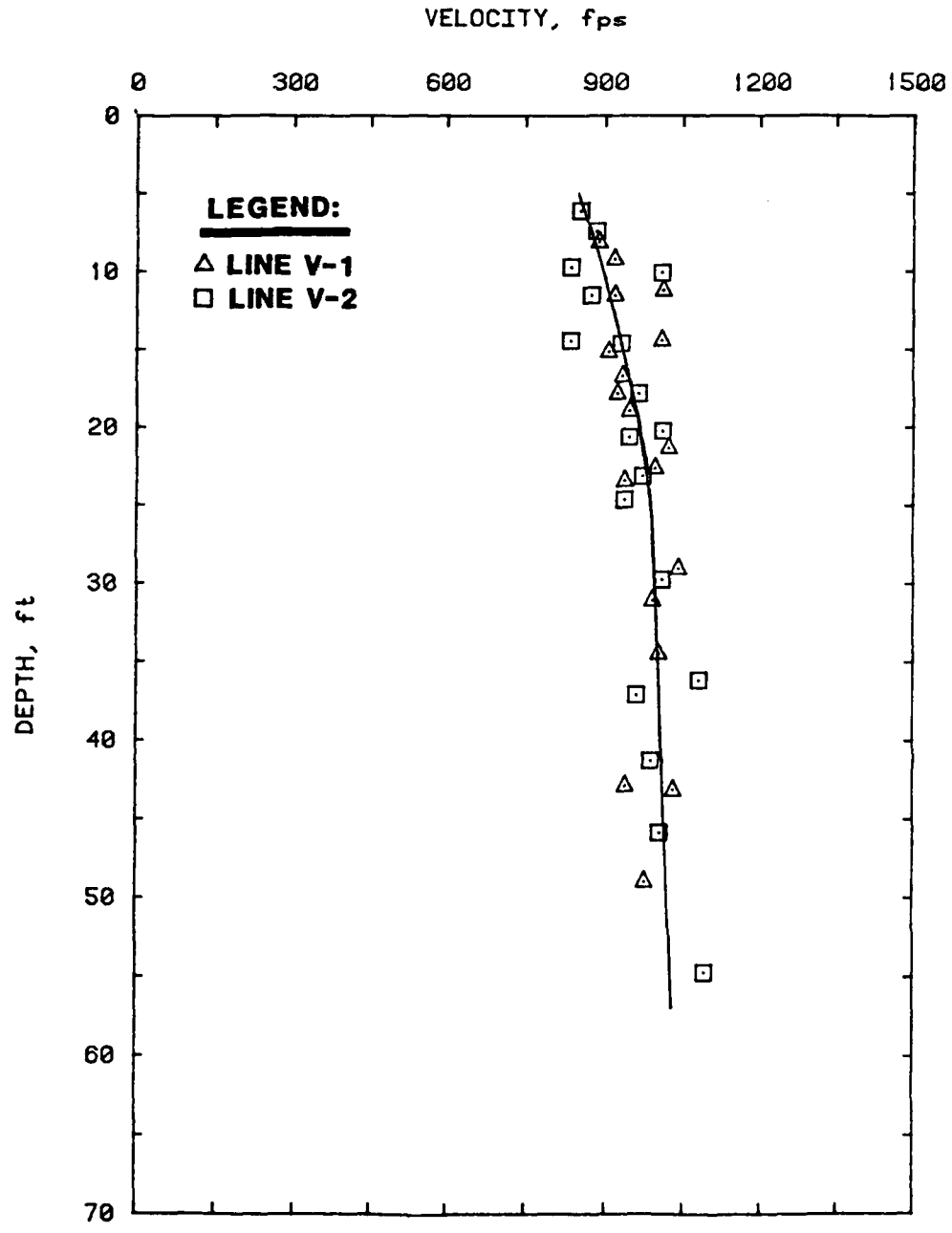
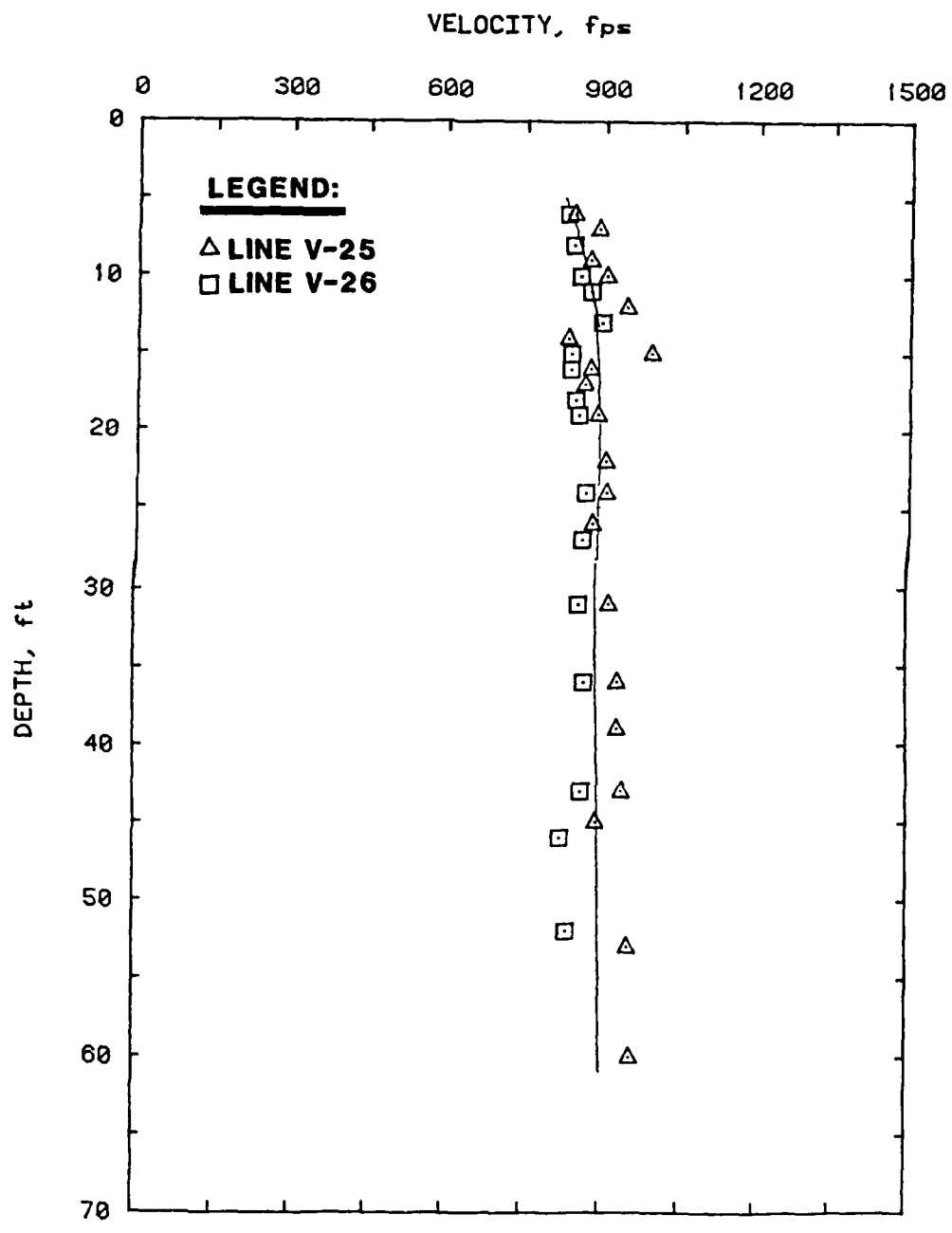


Figure 28. Rayleigh wave velocity versus depth for surface vibratory lines V-1 and V-2 at Station 270 of Right Wing Dam



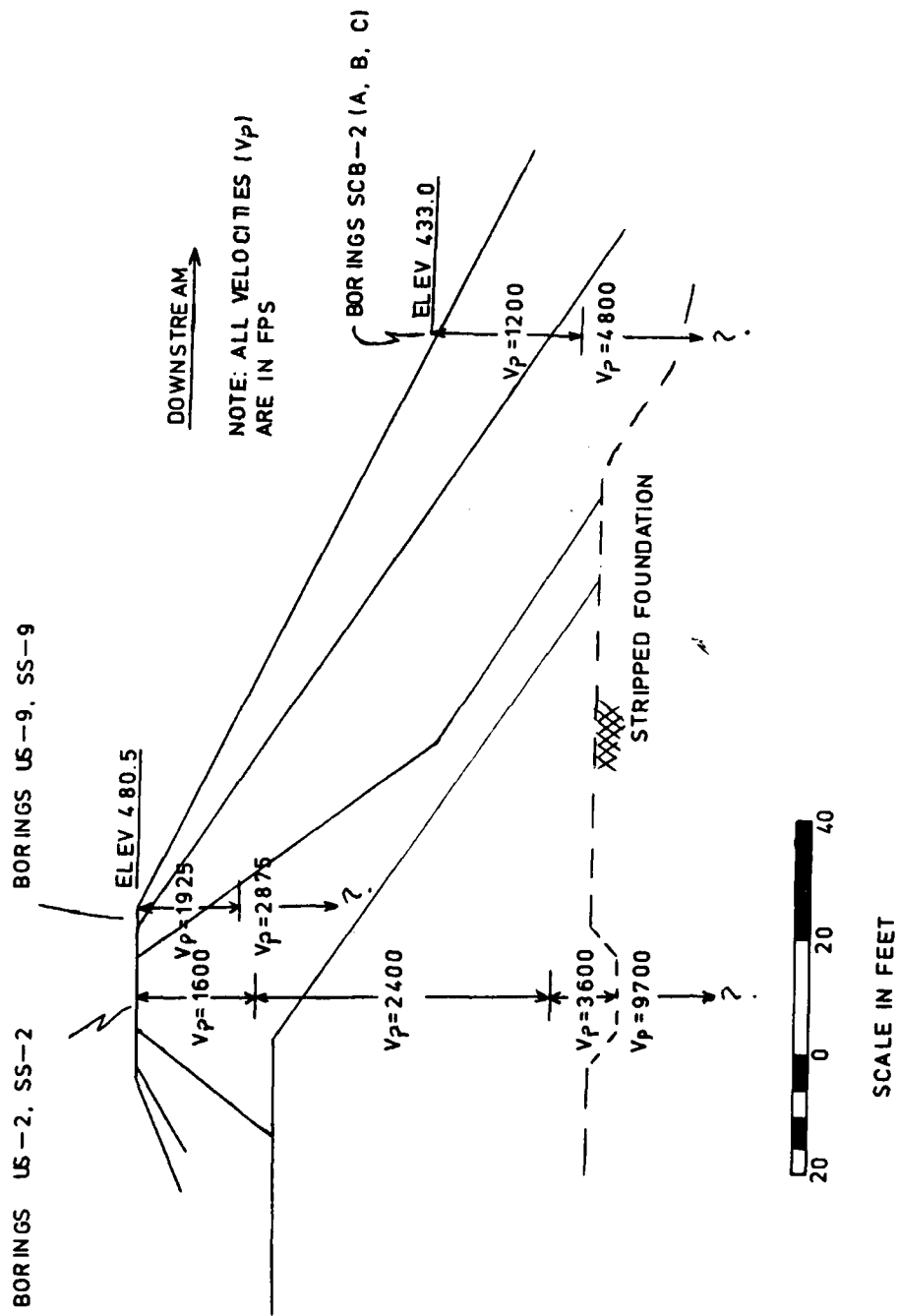


Figure 30. P-wave velocity zones interpreted from crosshole tests performed at Station 235 of the Right Wing Dam

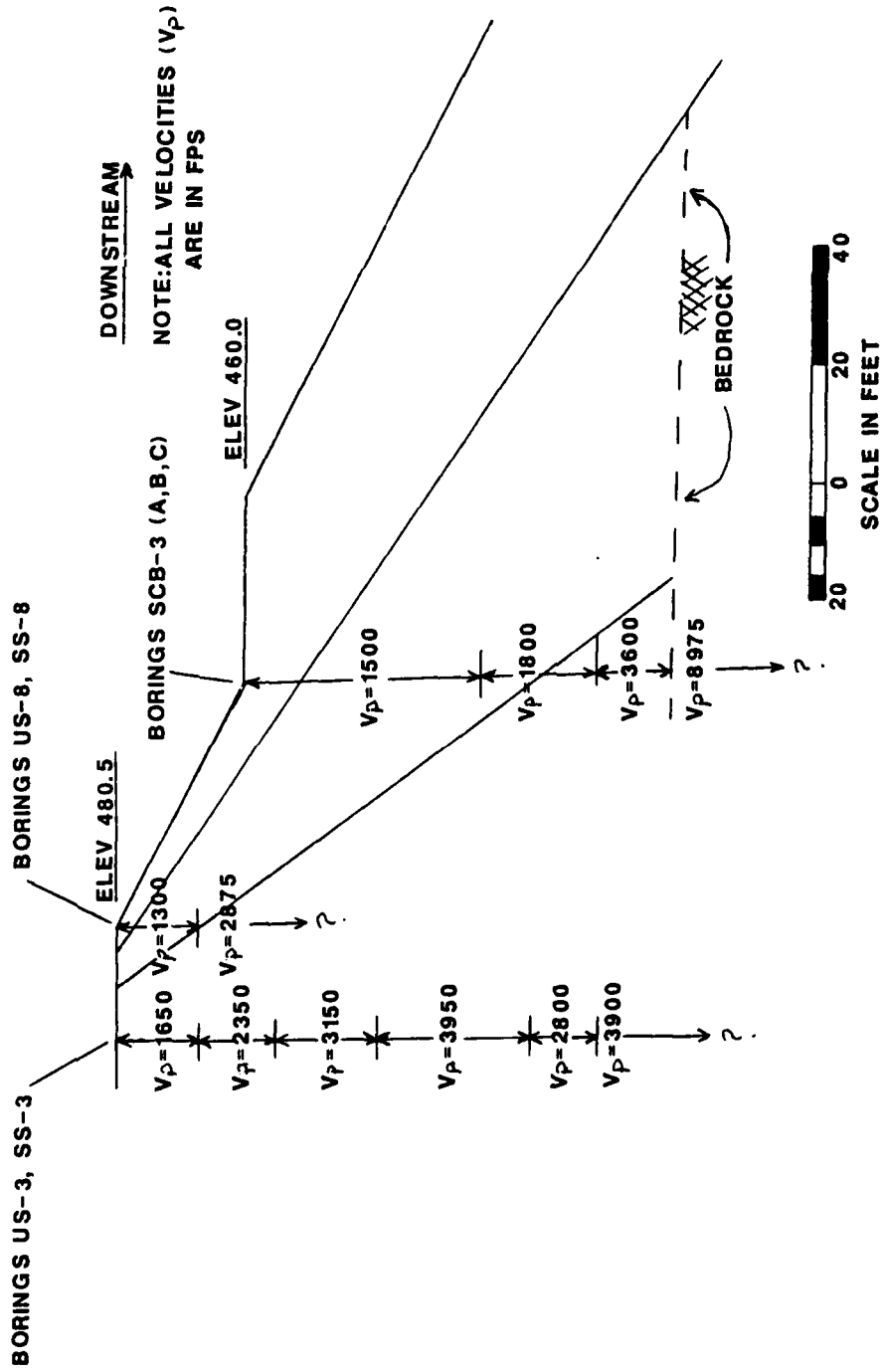


Figure 31. P-wave velocity zones interpreted from crosshole tests performed at Station 269 of the Right Wing Dam

NOTE: ALL VELOCITIES (V_p)
ARE IN FPS

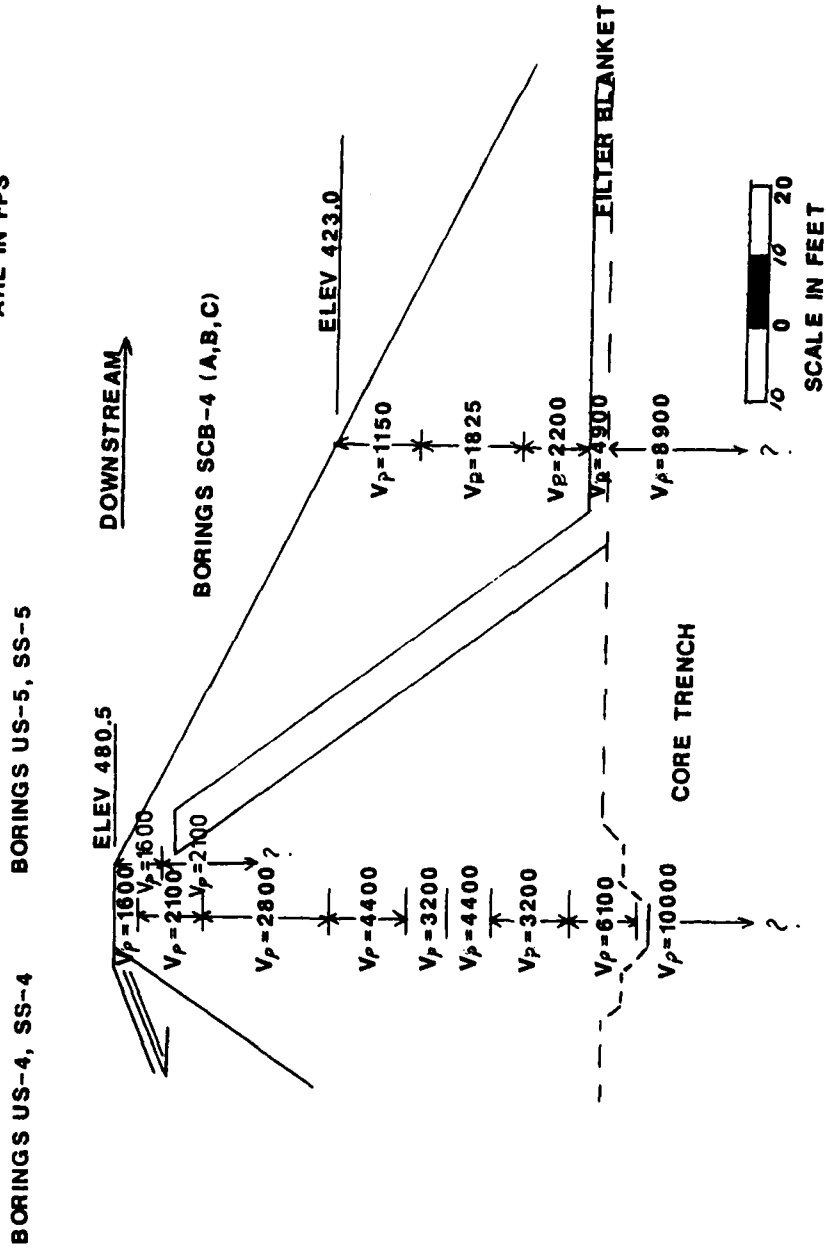


Figure 32. P-wave velocity zones interpreted from crosshole tests performed at Station 303 of the Left Wing Dam

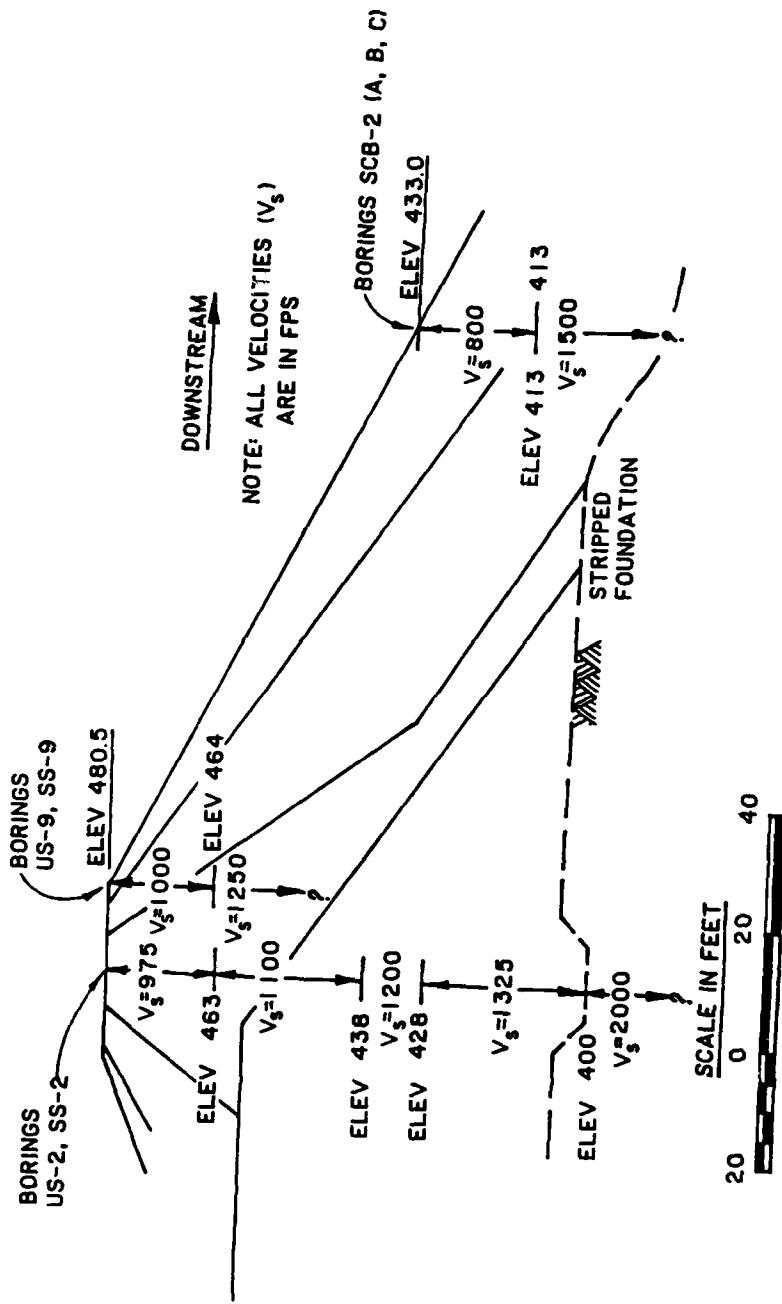


Figure 33. S-wave velocity zones interpreted from crosshole tests performed at Station 235 of the Right Wing Dam

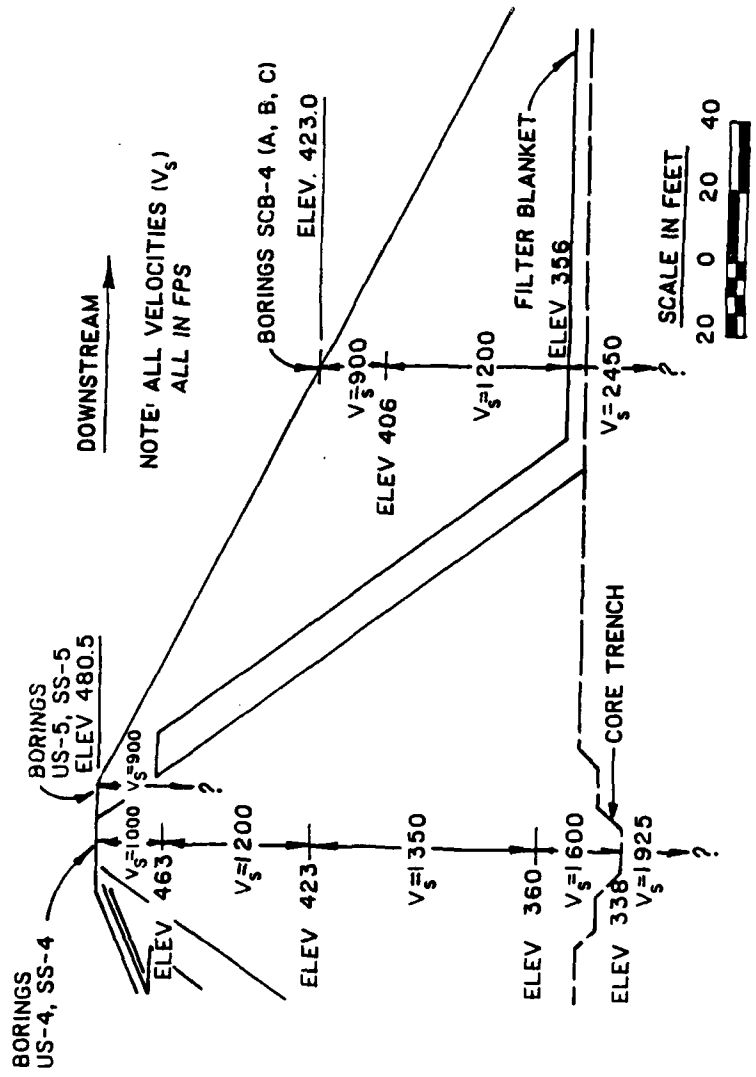


Figure 35. S-wave velocity zones interpreted from crosshole tests performed at Station 303 of the Left Wing Dam

DYNAMIC MATERIAL PROPERTIES INPUT TO FLUSH

DENSITIES (pcf):

- SHELL (SUB) - 162
- SHELL (DRY) - 139
- CORE (SUB) - 142
- ROCK - 150

NOTE: ALL VELOCITIES ARE IN f/s

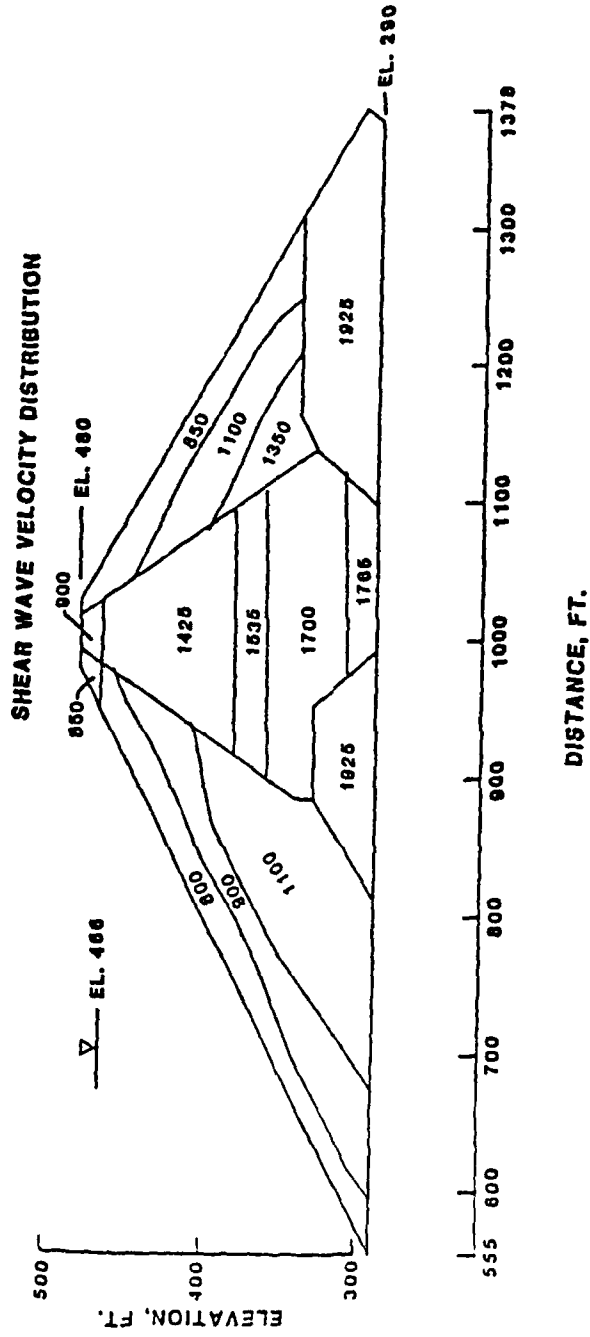


Figure 36. S-wave velocity zones used in dynamic analysis

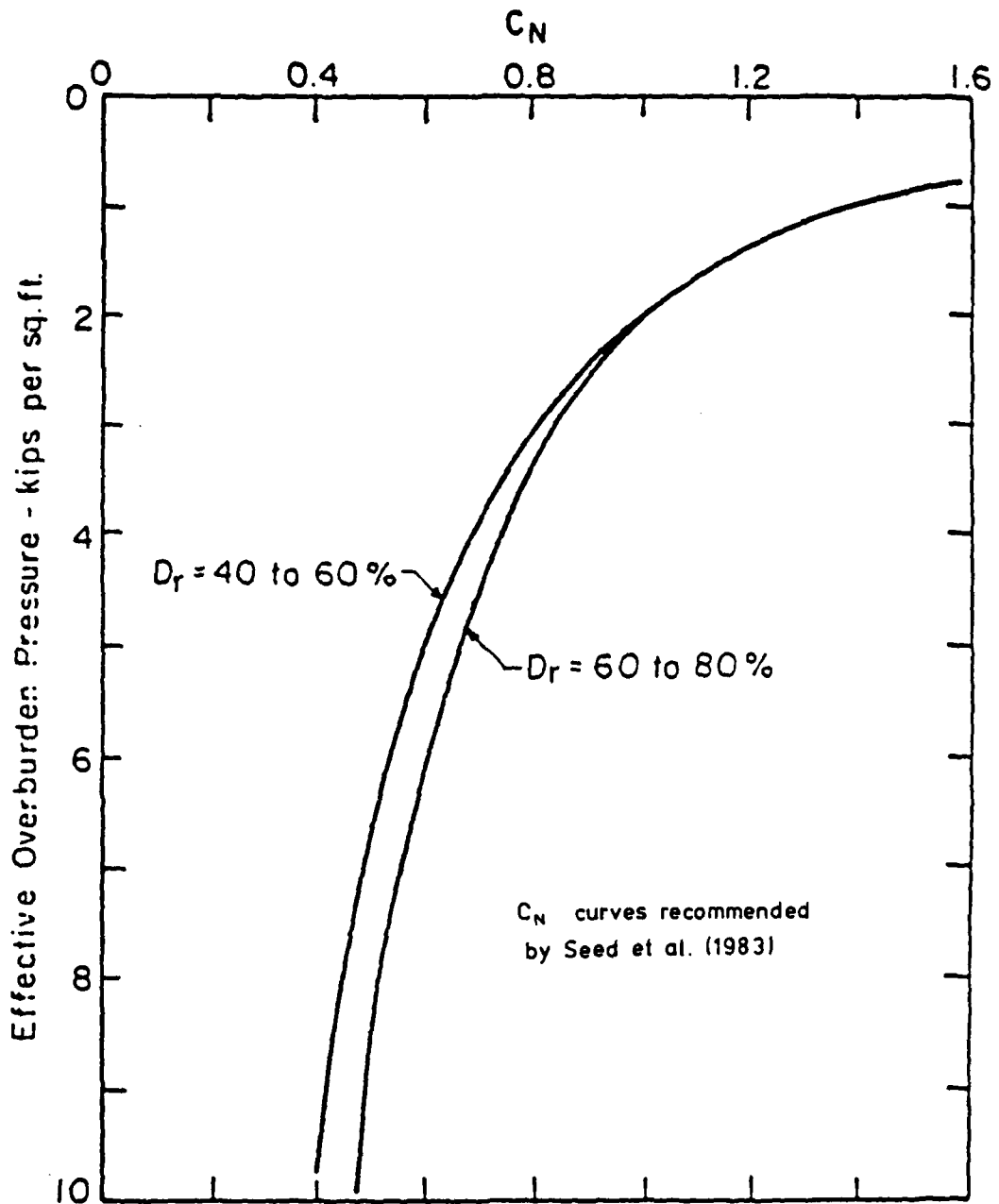


Figure 37. C_n versus vertical effective stress

BORING SS-2

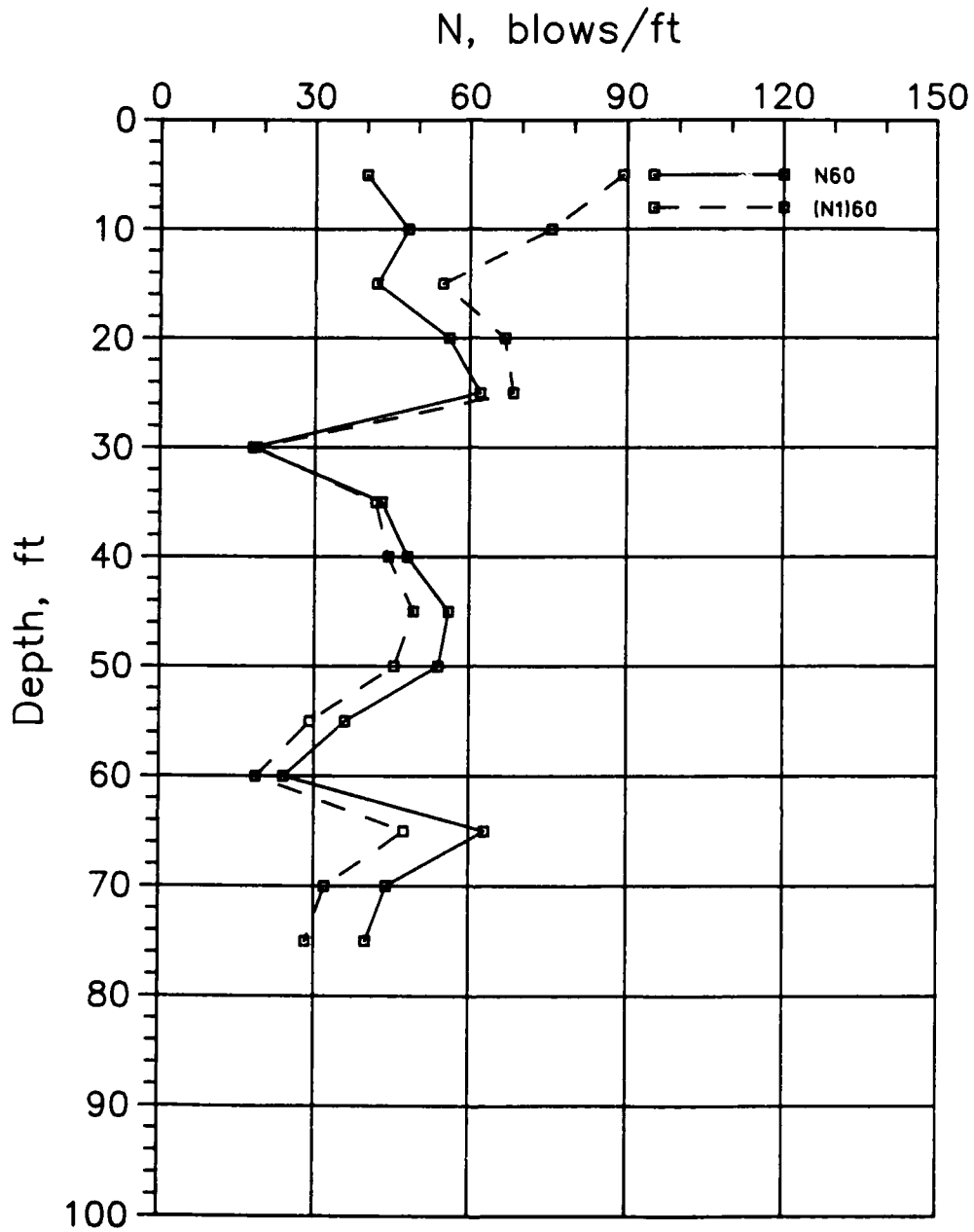


Figure 38. Standard penetration test results for Boring SS-2 at Station 235 of the Right Wing Dam

BORING SS-8

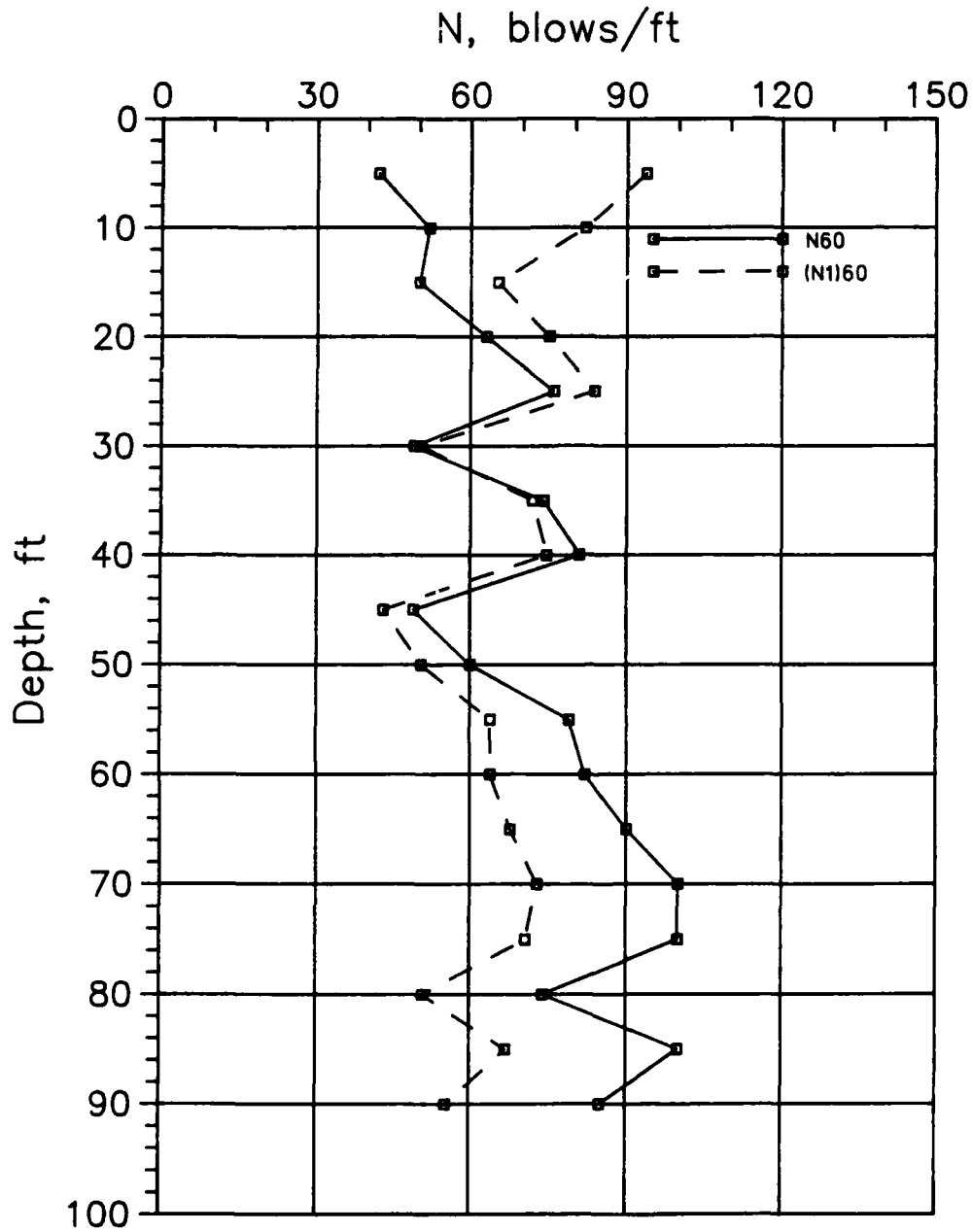


Figure 39. Standard penetration test results for Boring SS-8 at Station 270 of the Right Wing Dam

BORING SS-4

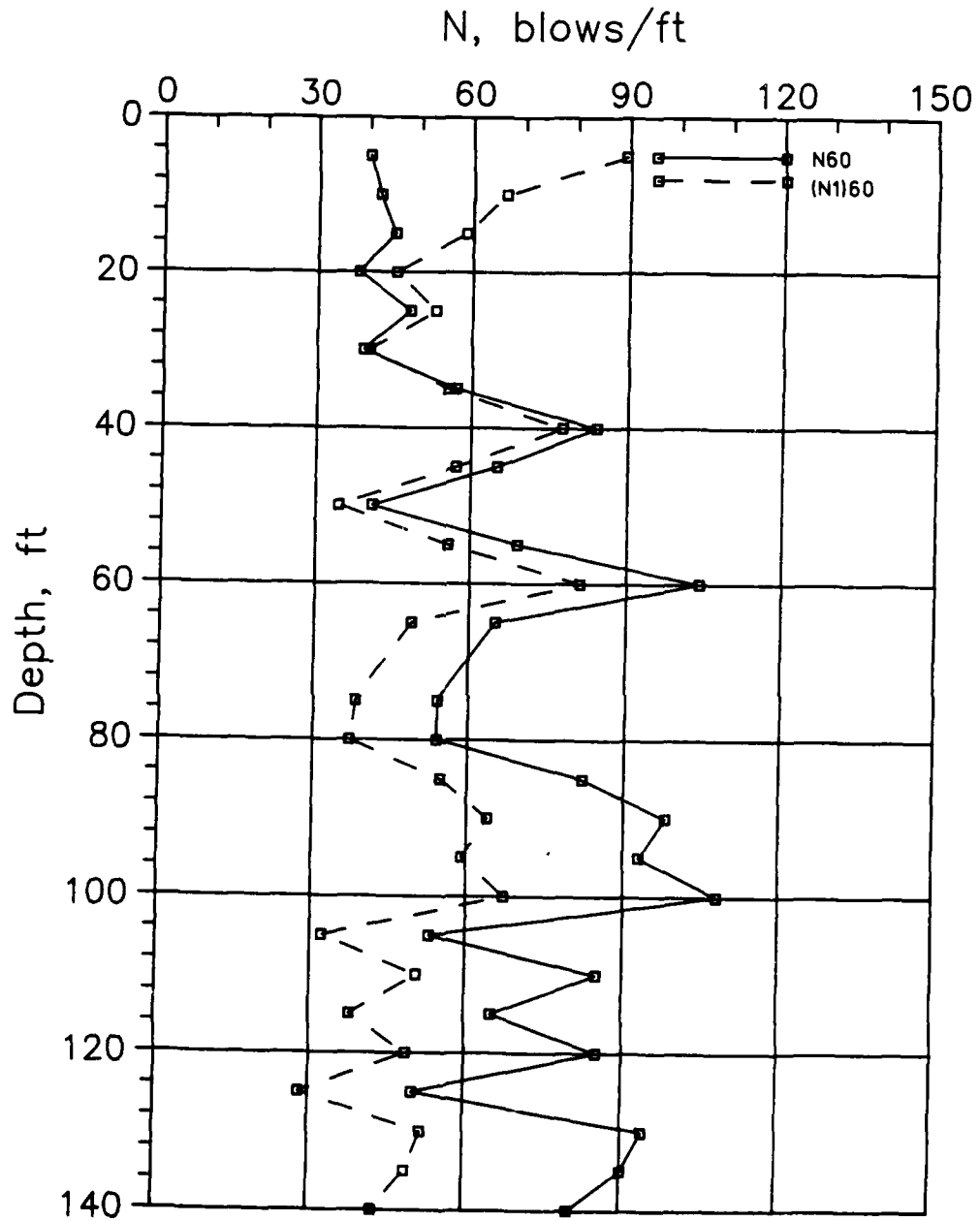


Figure 40. Standard penetration test results for Boring SS-4 at Station 303 of the Left Wing Dam

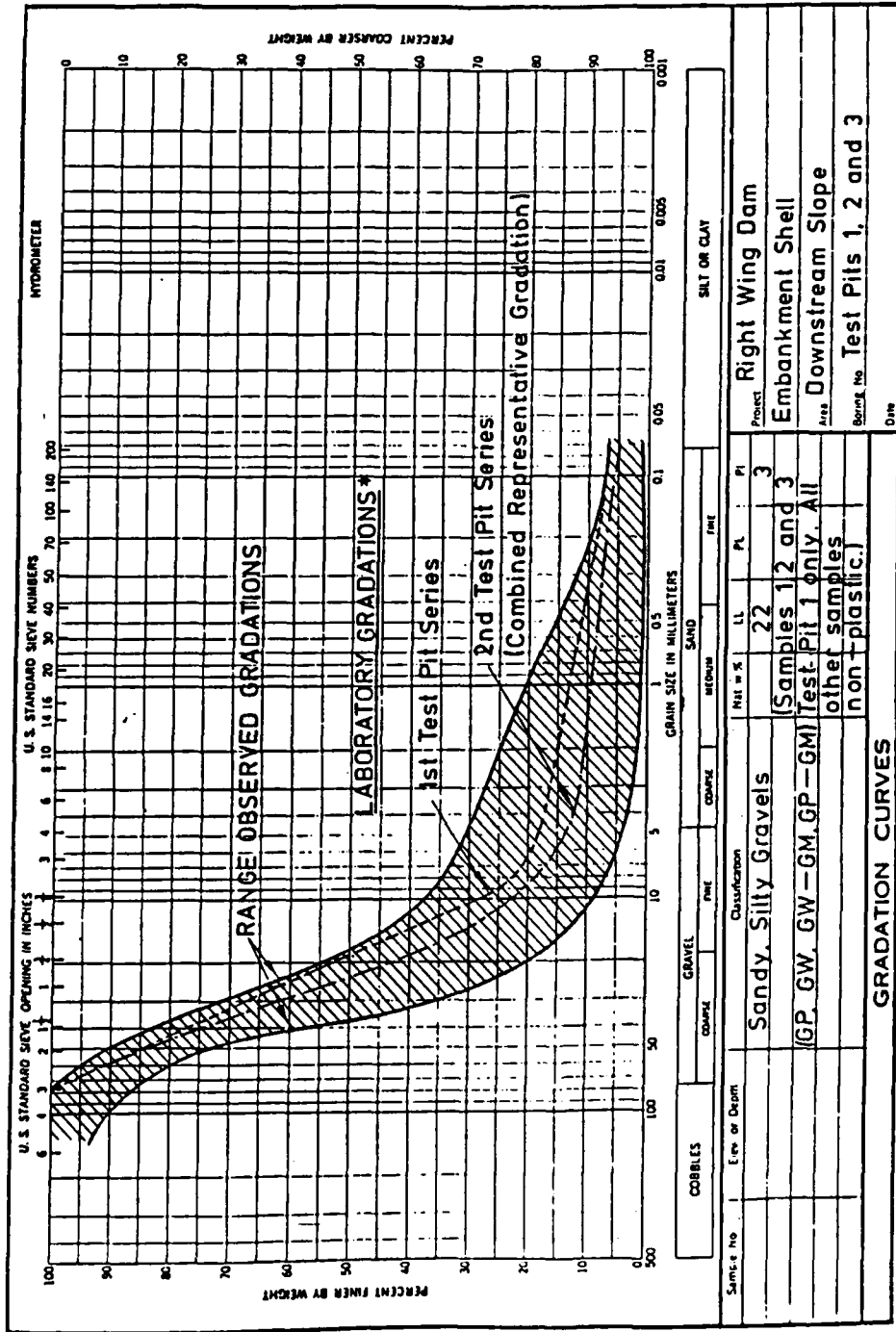


Figure 41. Range of observed gradations from the three test pits at the Right Wing Dam

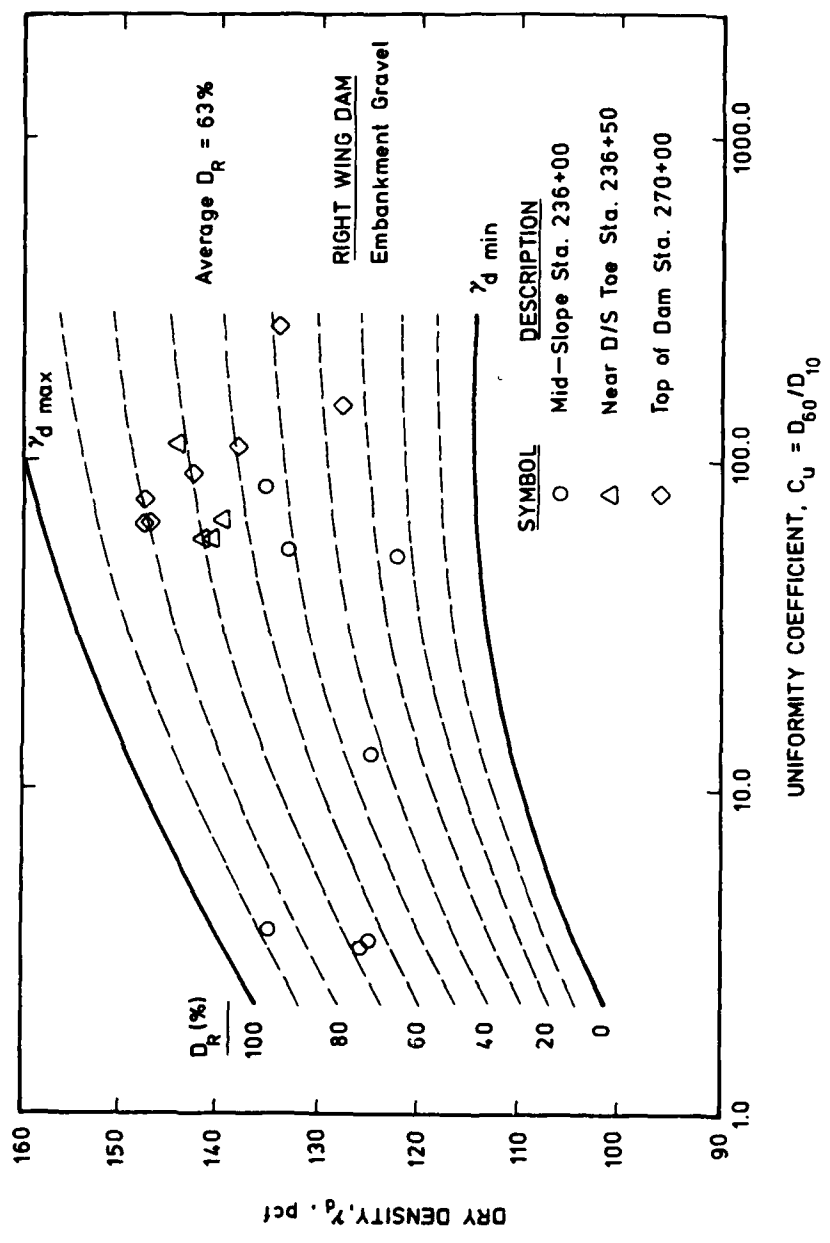


Figure 43. Relative density of Right Wing Dam embankment gravels as function of uniformity coefficient and dry density

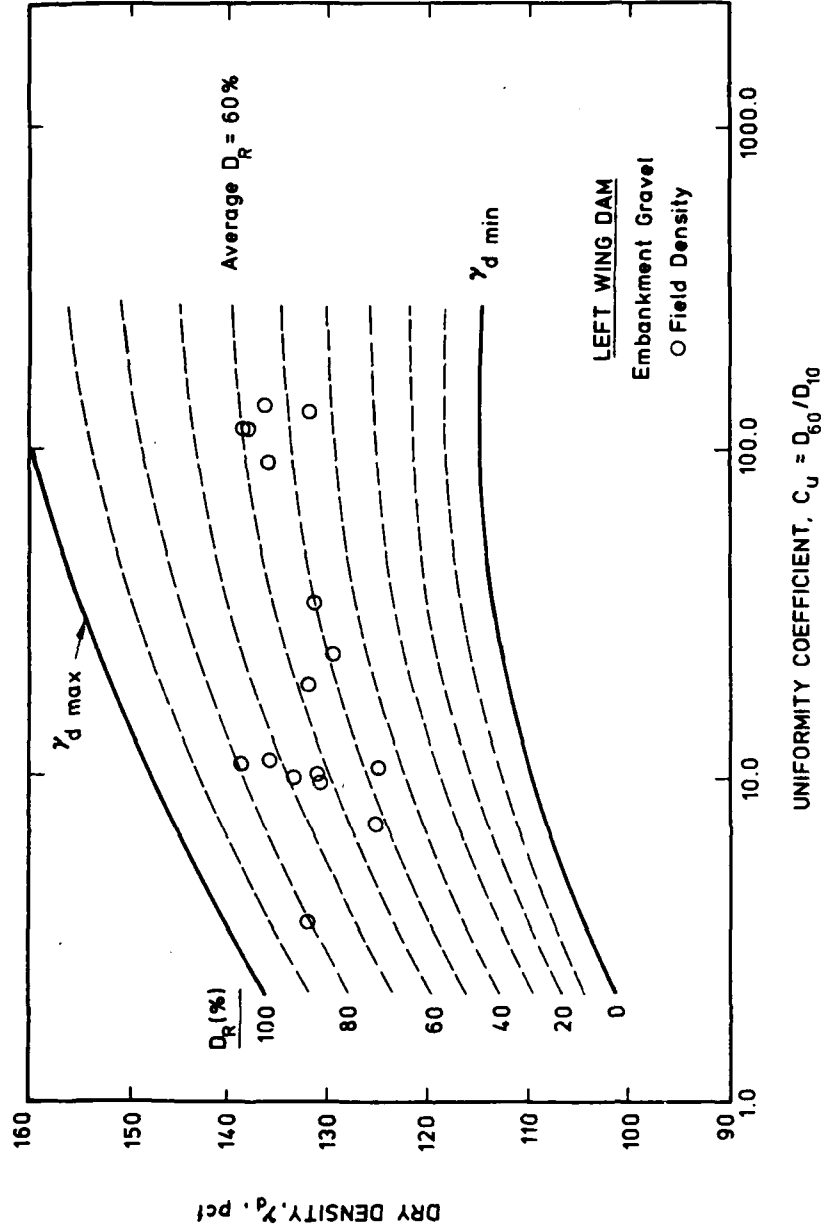


Figure 44. Relative density of Left Wing Dam embankment gravels as function of uniformity coefficient and dry density

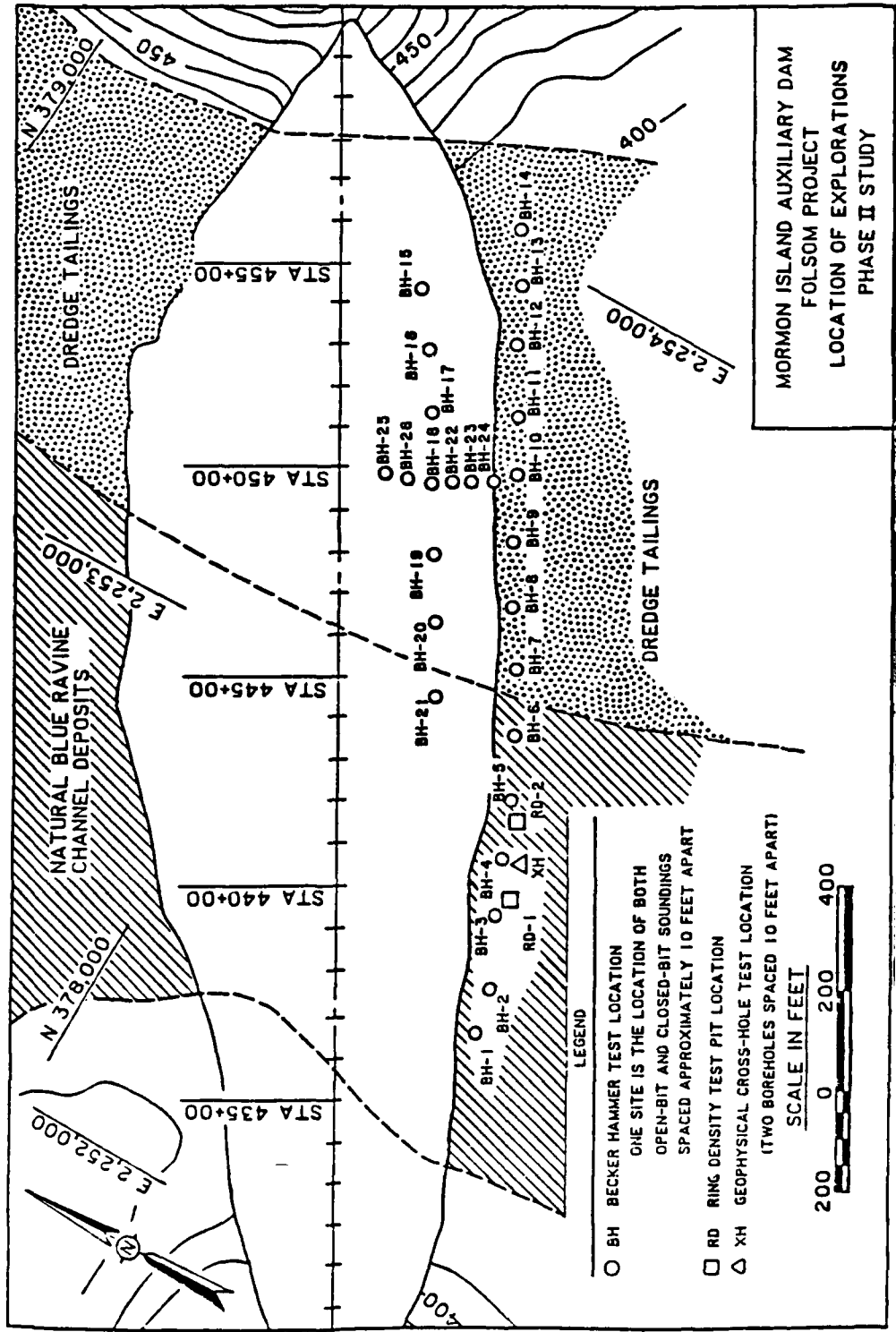


Figure 45a. Location of Phase II Field Explorations at Mormon Island Auxiliary Dam

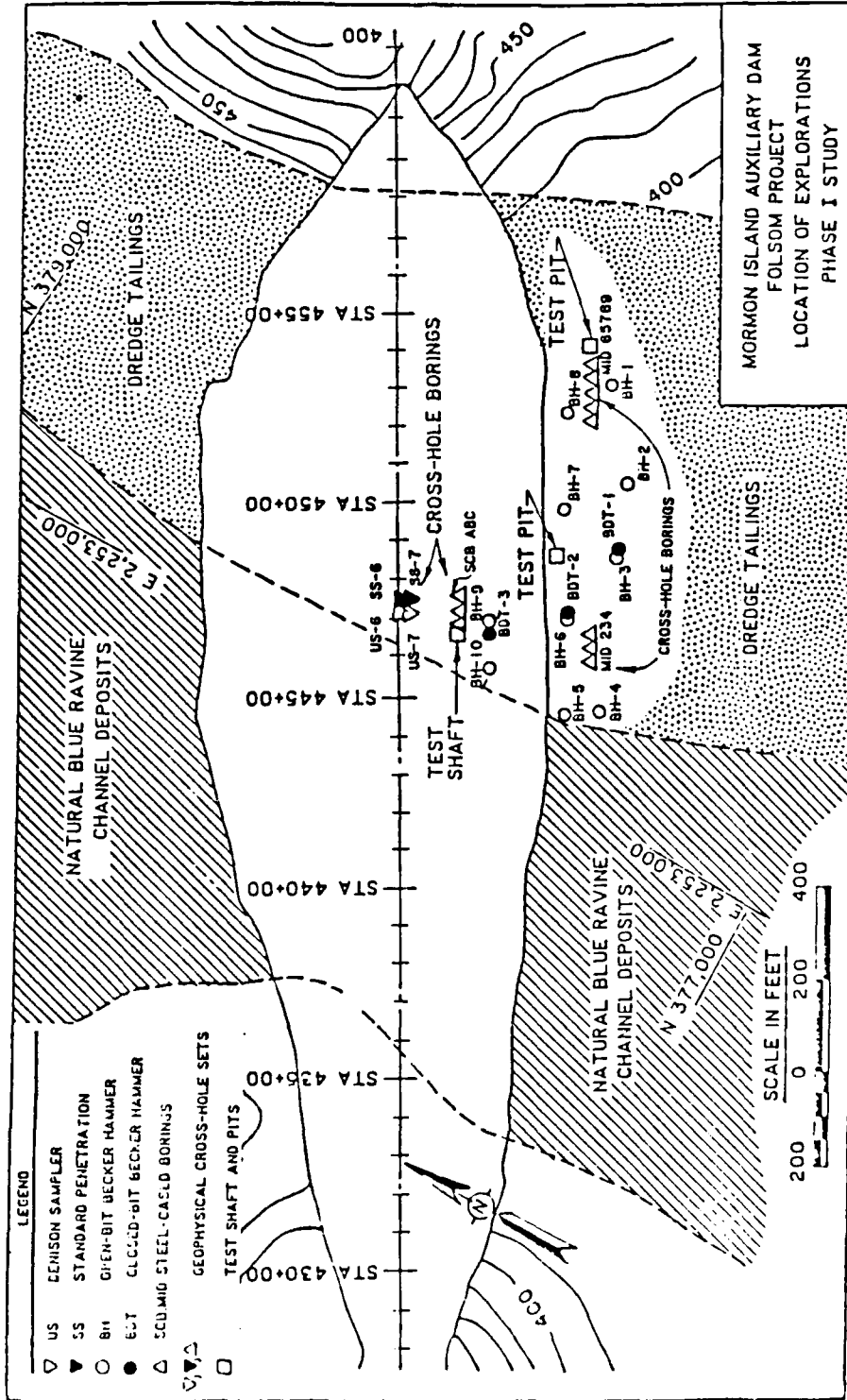
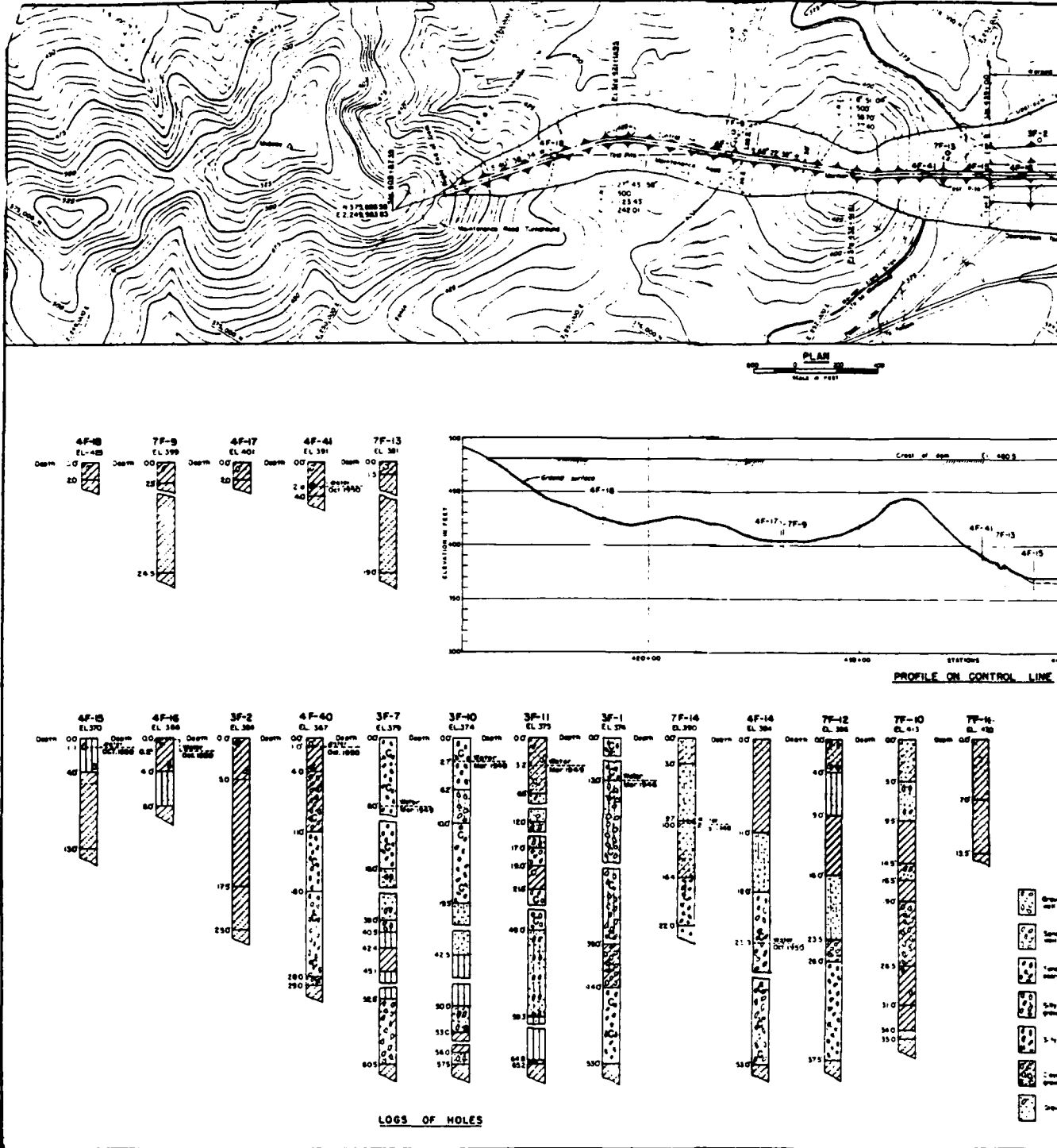
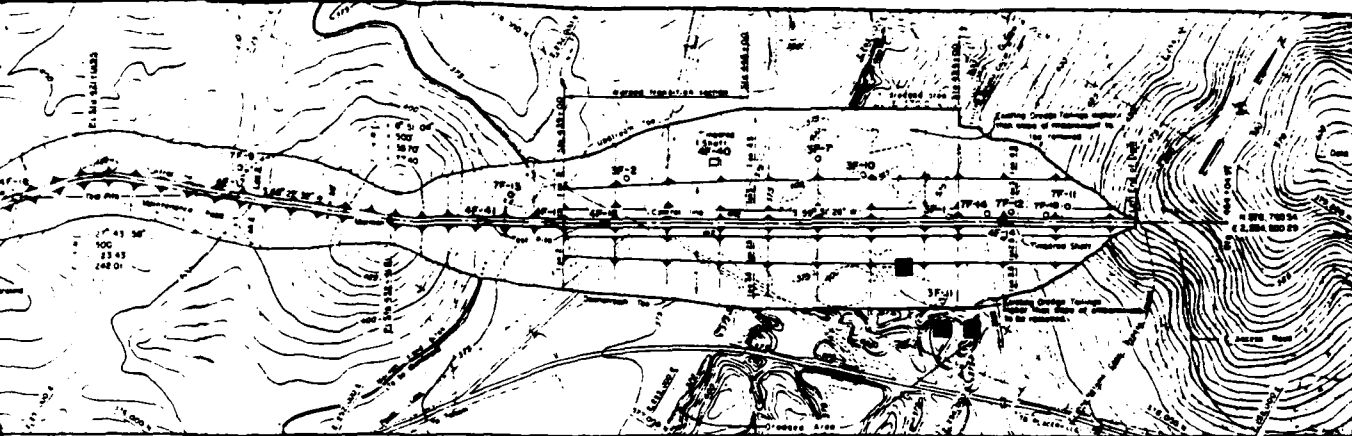
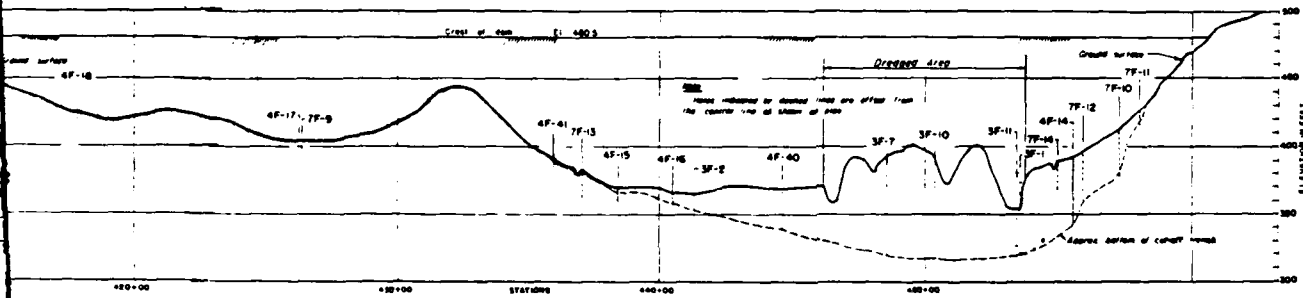


Figure 45b. Plan view of field investigations at Mormon Island Auxiliary Dam

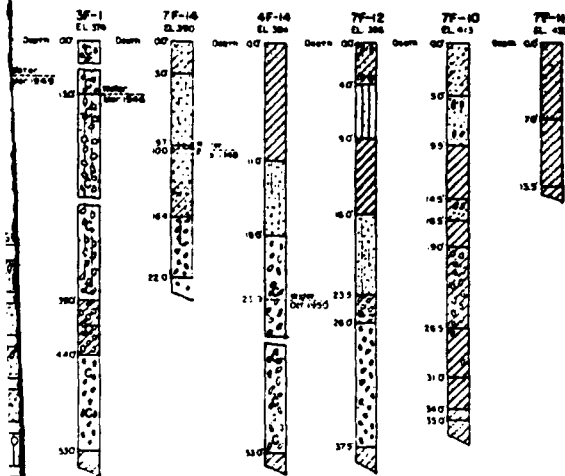




PLAN
SCALE 1" = 100'



PROFILE ON CONTROL LINE



LEGEND

Gravel and cobbles	Silty gravel and sand	Stronger clay
Sandy gravel and coarse sand	Silty sand	Weaker sandy clay
Sandy gravel, coarse sand	Clean gravel and sand	Sandy clay
Silt and gravel	Coarse sand	Lean clay
Silt and sand	Gravels and silty sand	Fat clay
Fine sandy gravel	Sandy silt	Heavy sandy silt/clay
Silty sand	Cobbles	

NOTES

- 1 Datum is Sea Level Datum of 1929.
- 2 Elevations shown on logs are ground surface elevations.
- 3 Laboratory classification shown for all materials, according to the Corps of Engineers' Uniform Soil Classification, except those shown in logs of holes 3F-1, 3F-2, 7F-13 and 7F-14, which are field classifications.
- 4 Holes 3F-1 and 3F-2 were drilled with a 12" churn drill. Holes 3F-7, 3F-10 and 3F-11 were drilled with a 10" churn drill. Samples were taken with a power auger and push tube sampler, where possible.
- 5 All 4F holes are open pits or shafts.
- 6 All 7F holes were drilled with a Failing drill rig using a 7" diameter rotary core drill.
- 7 Typical embankment sections shown on Sheet No 357/7.
- 8 Limit of contractor's work areas including waste areas are shown on drawing Sheet No 357/2.
- 9 Slopes of warped transition vary uniformly from Station 439+00 to 448+00.
- 10 The term gravel, under the classification system used for this drawing, applies to grain sizes larger than the No. 10 sieve.
- 11 The term cobbles includes material from 3" to 18" in size and the presence of some is indicated by the letter "C" in the logs.
- 12 This drawing was taken from As-Constructed sheet no 357/3, File No AM-1-9-357.

AMERICAN RIVER BASIN DEVELOPMENT - CALIFORNIA
FOLSOM RESERVOIR PROJECT
AMERICAN RIVER
MORMON ISLAND AUXILIARY DAM
FOUNDATION EXPLORATION
PLAN, PROFILE AND LOGS OF HOLES

Plan and axial section of Mormon Island Auxiliary Dam

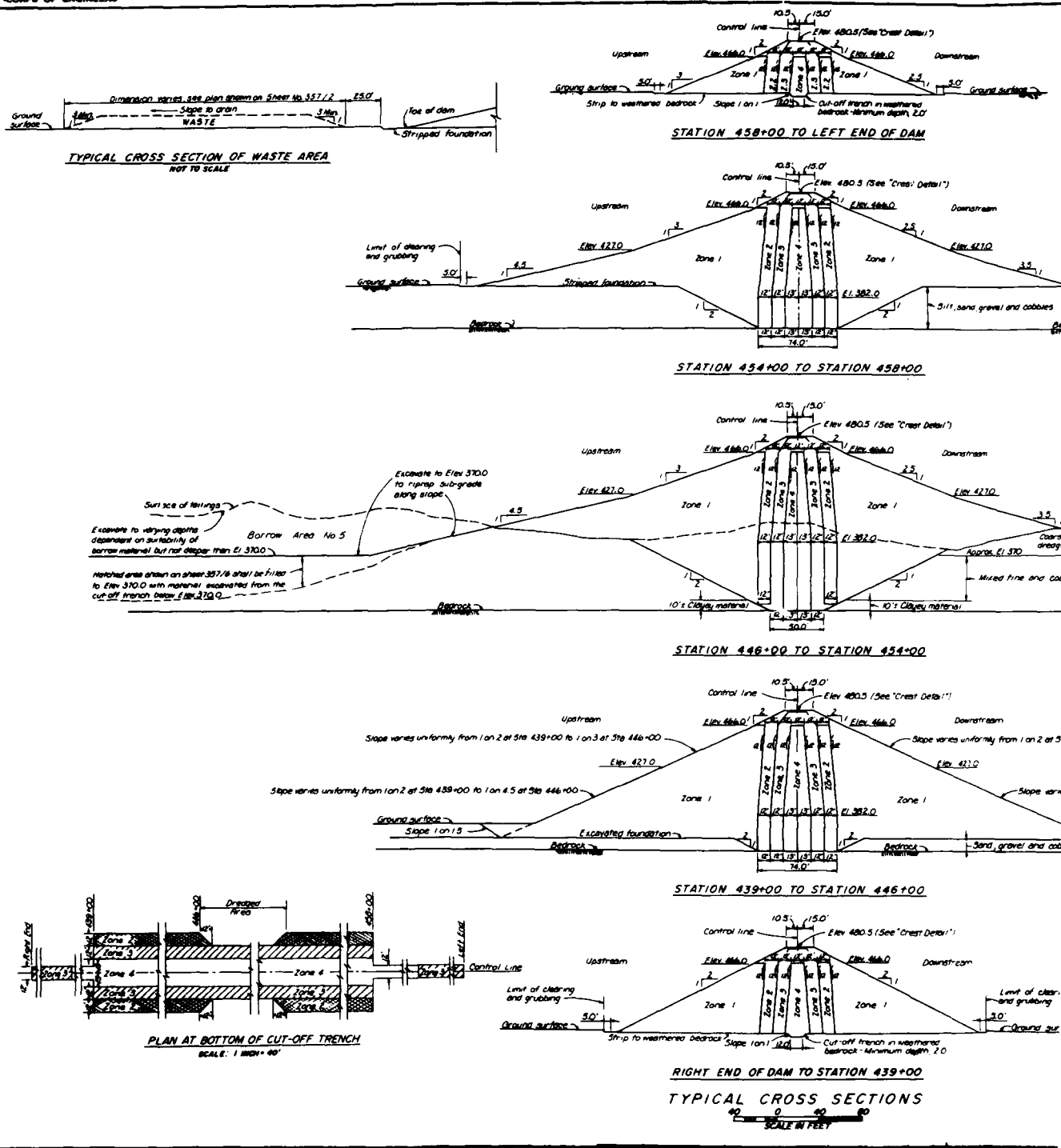
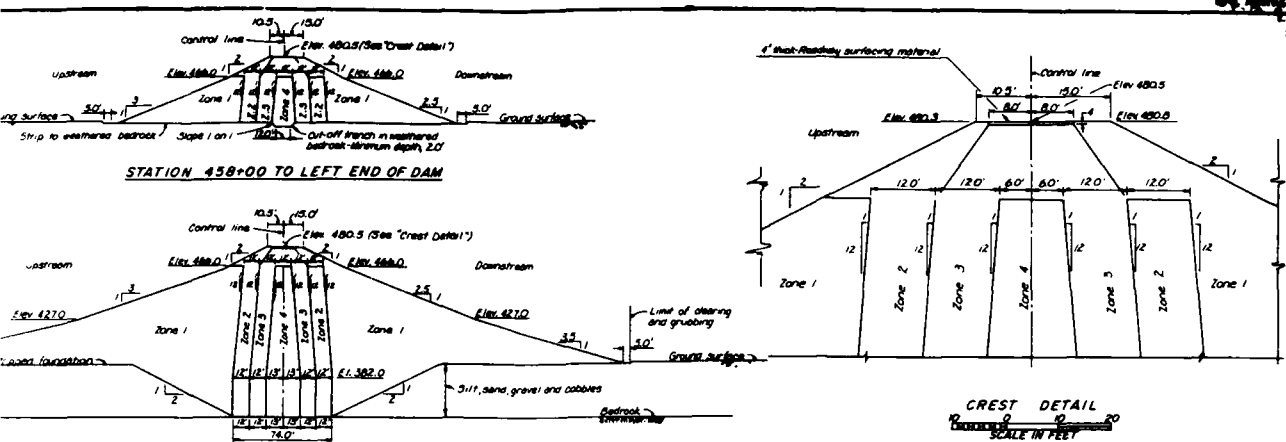


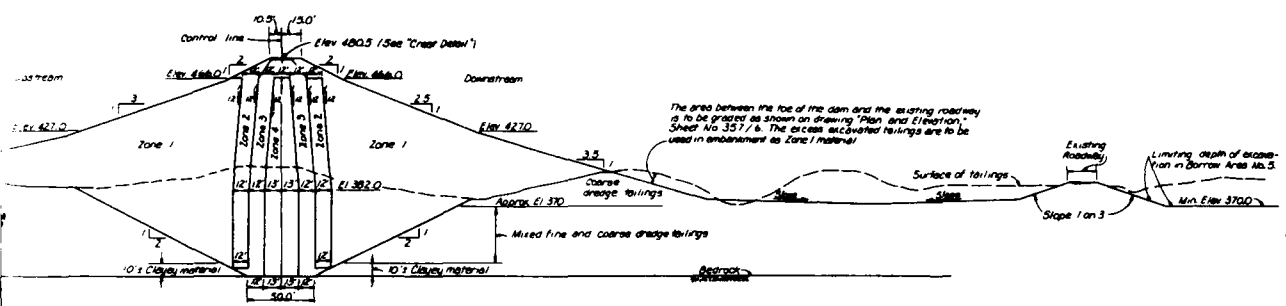
Figure 46. Cross-sectional views of Mormon Island Aux



STATION 458+00 TO LEFT END OF DAM

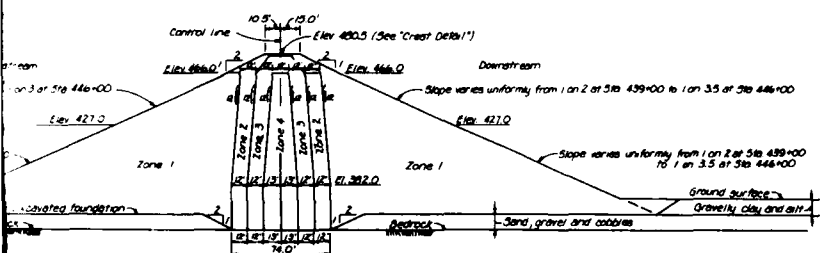
STATION 454+00 TO STATION 458+00

CREST DETAIL
SCALE IN FEET

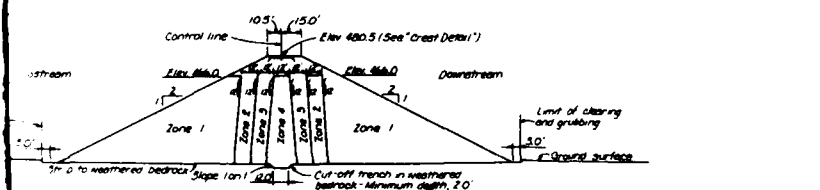


STATION 446+00 TO STATION 454+00

- NOTES:
1. Datum is Sea Level Datum of 1929.
 2. Zone 1 material to be unprocessed dredge tailings from Borrow Area No. 5 above the approximate elevation of 378.0.
 3. Zone 2 material to be the finest 2" portion of dredge tailings from Borrow Area No. 5 above the approximate elevation of 370.0.
 4. Zone 3 material is decomposed granite from Borrow Area No. 1.
 5. Zone 4 material to be obtained from Borrow Area No. 4.
 6. Stations shown herein designating the limits of the sections are approximate. The exact stations are to be determined in the field after the foundation and cut-off trench excavation have been completed.
 7. Figures in circles indicate items under which payment will be made.
 8. Foundation Grant Certificate limits under this contract No. 321-098 to Sta. 429+00. Breaching from Sta. 422+00 to right end of dam to be done by others.
 9. This drawing was taken from As-Constructed sheet No. 35717-2, Title No. 681-1-1-557.



STATION 439+00 TO STATION 446+00



RIGHT END OF DAM TO STATION 439+00

TYPICAL CROSS SECTIONS
SCALE IN FEET

AMERICAN RIVER BASIN DEVELOPMENT, CALIFORNIA
FOLSOM RESERVOIR PROJECT
AMERICAN RIVER
MORMON ISLAND AUXILIARY DAM
EMBANKMENT SECTIONS

95772

Cross-sectional views of Mormon Island Auxiliary Dam

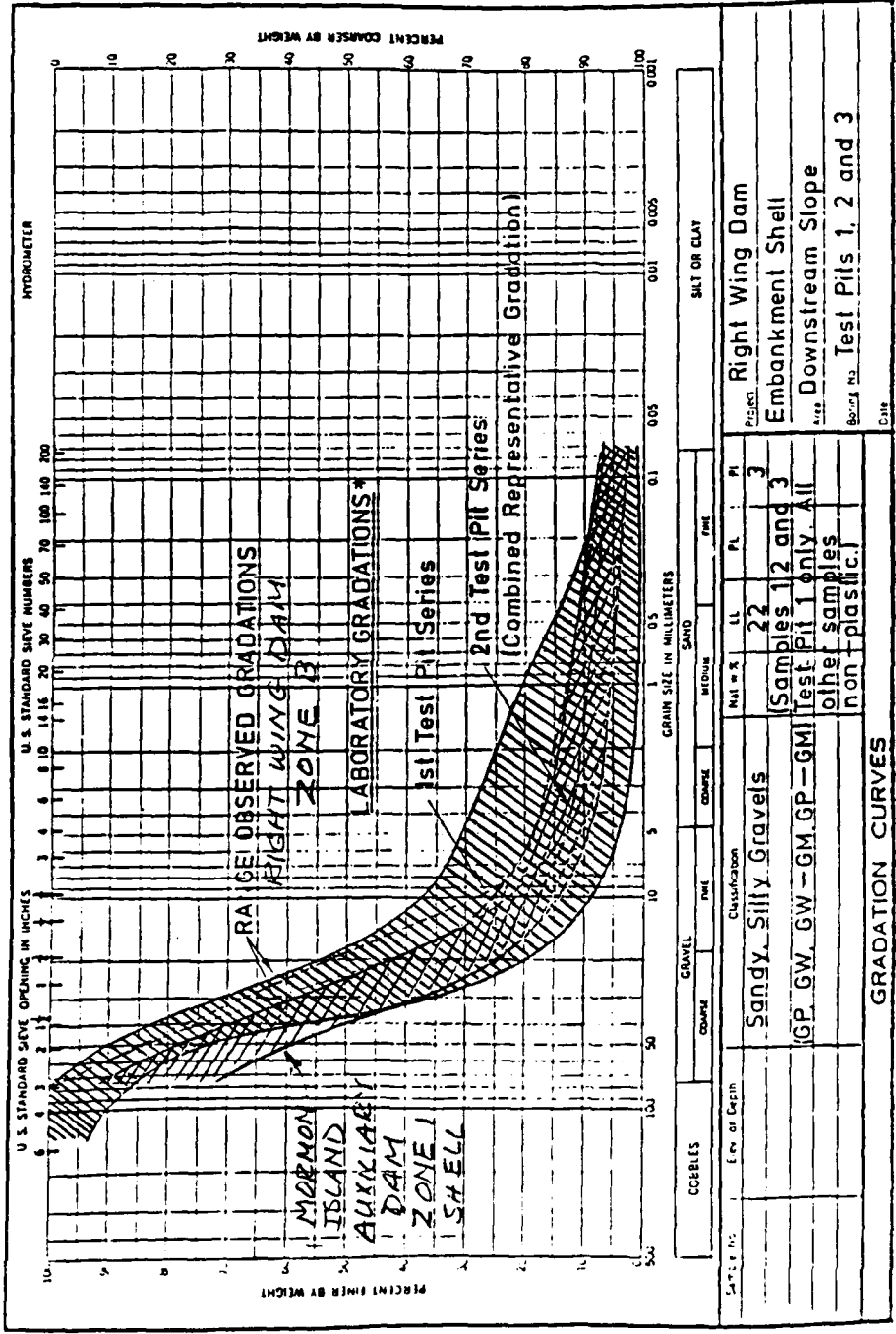


Figure 47. Comparison of gradations of Mormon Island gravels with Right Wing Dam gravels

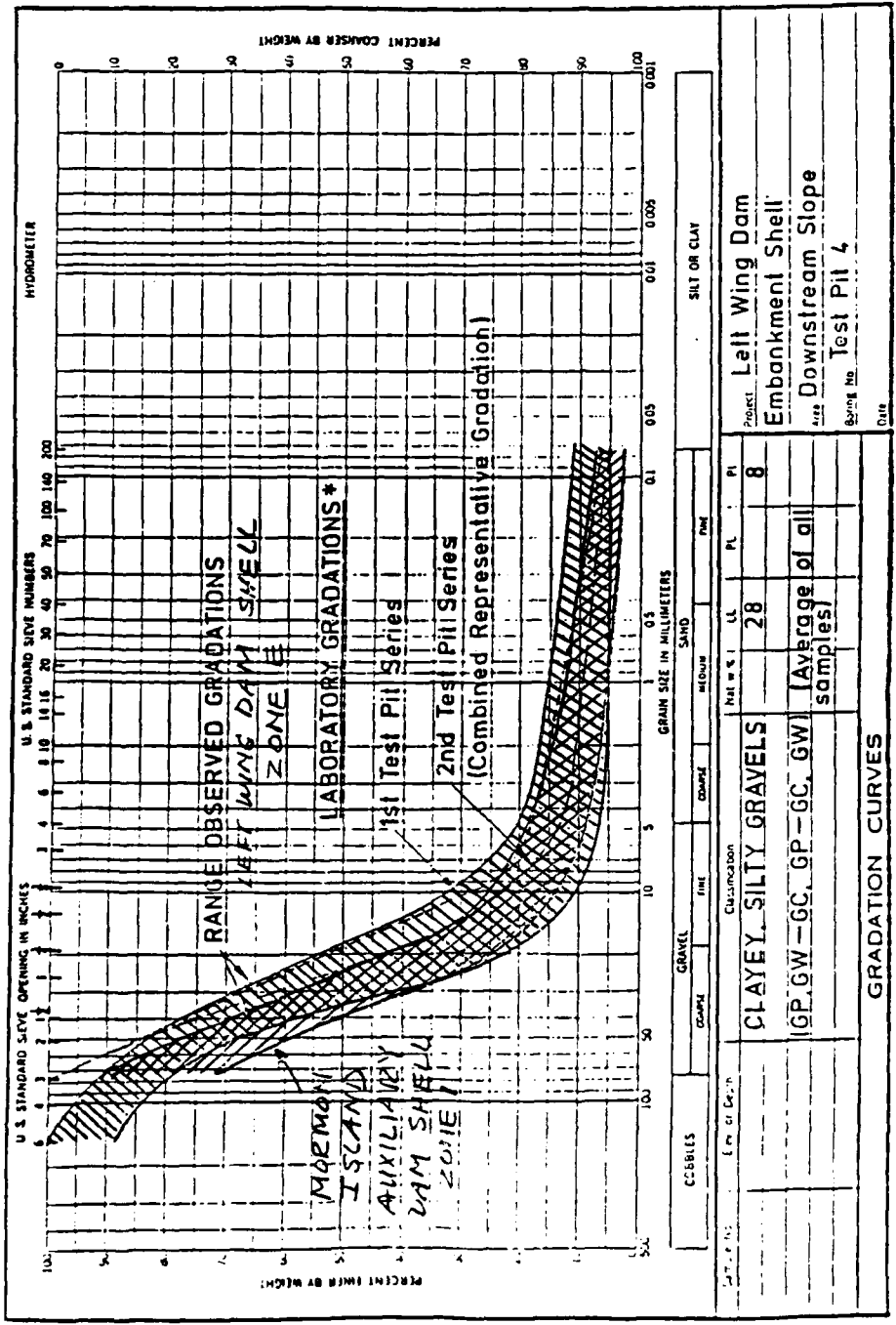


Figure 48. Comparison of gradations of Mormon Island gravels with Left Wing Dam gravels

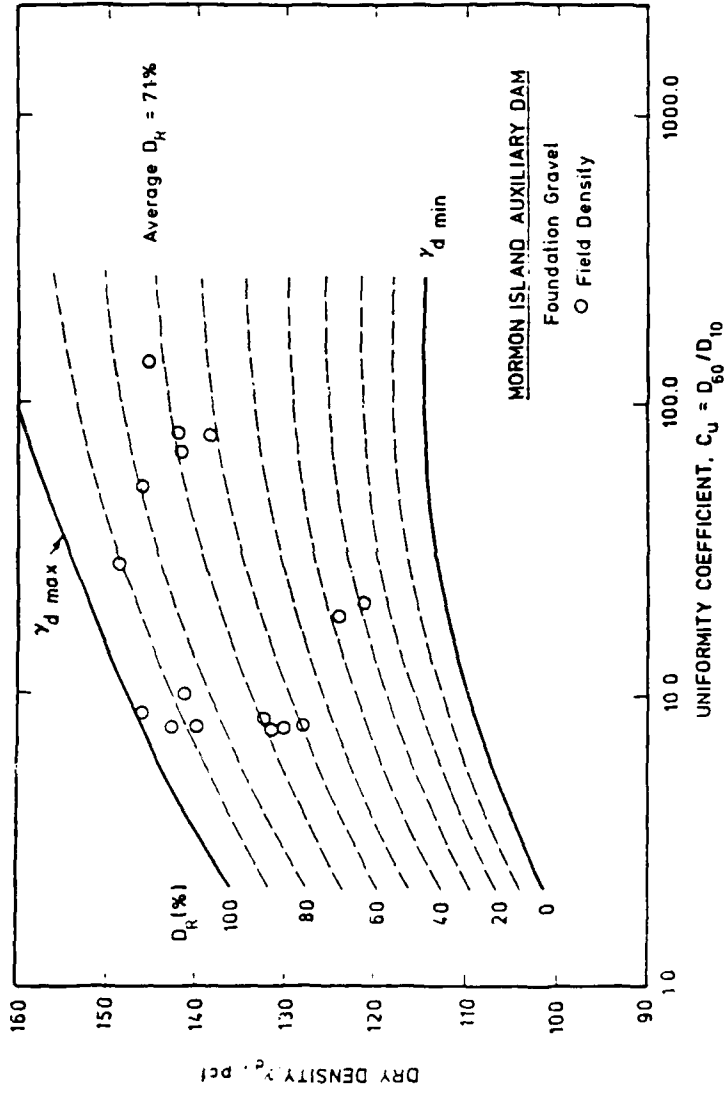


Figure 49. Range of observed gradations from the test shaft at Mormon Island Auxiliary Dam

EMBANKMENT N1(60)'s --(GRAVEL CURVE)

MID - BPT15 THRU BPT21 , 25 & 26

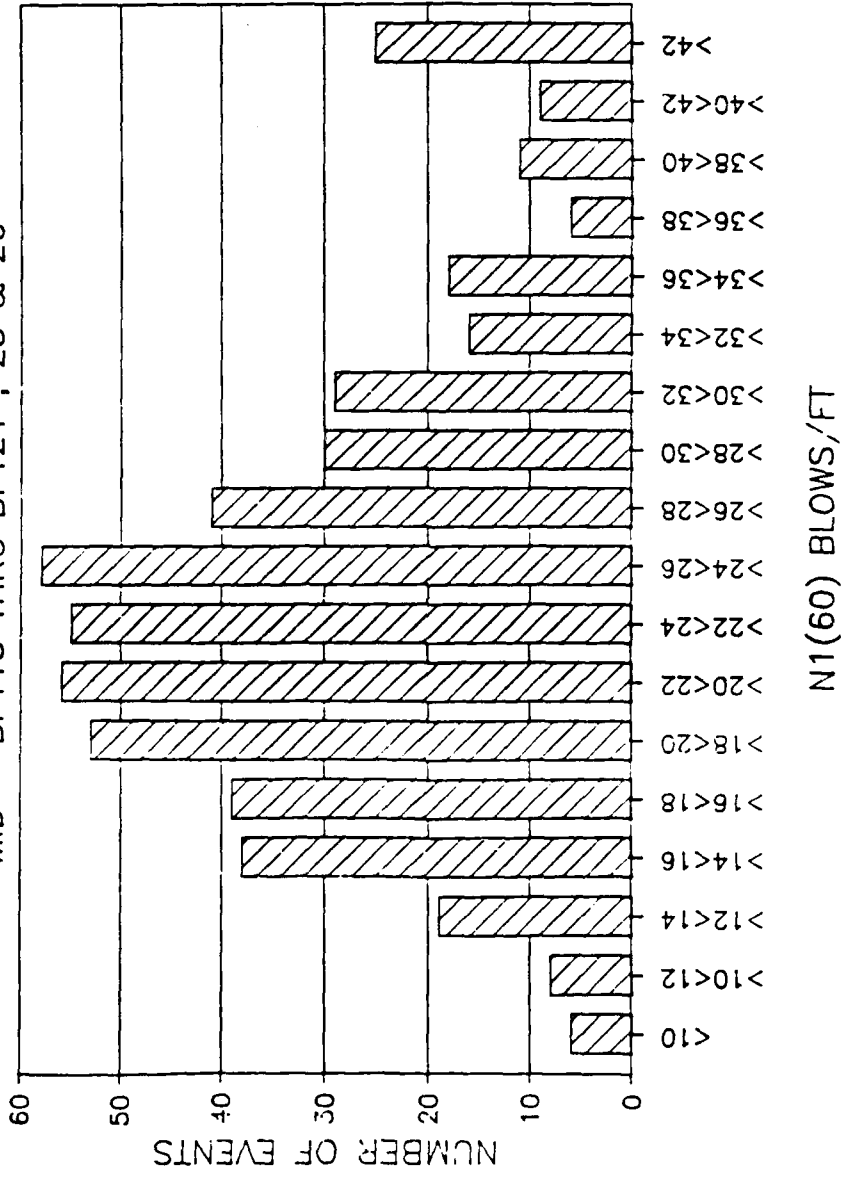


Figure 50. Statistical distribution of equivalent (N1)60 blowcounts obtained in Becker Hammer Penetration Tests during the 1987 field investigations performed at Mormon Island Auxiliary Dam

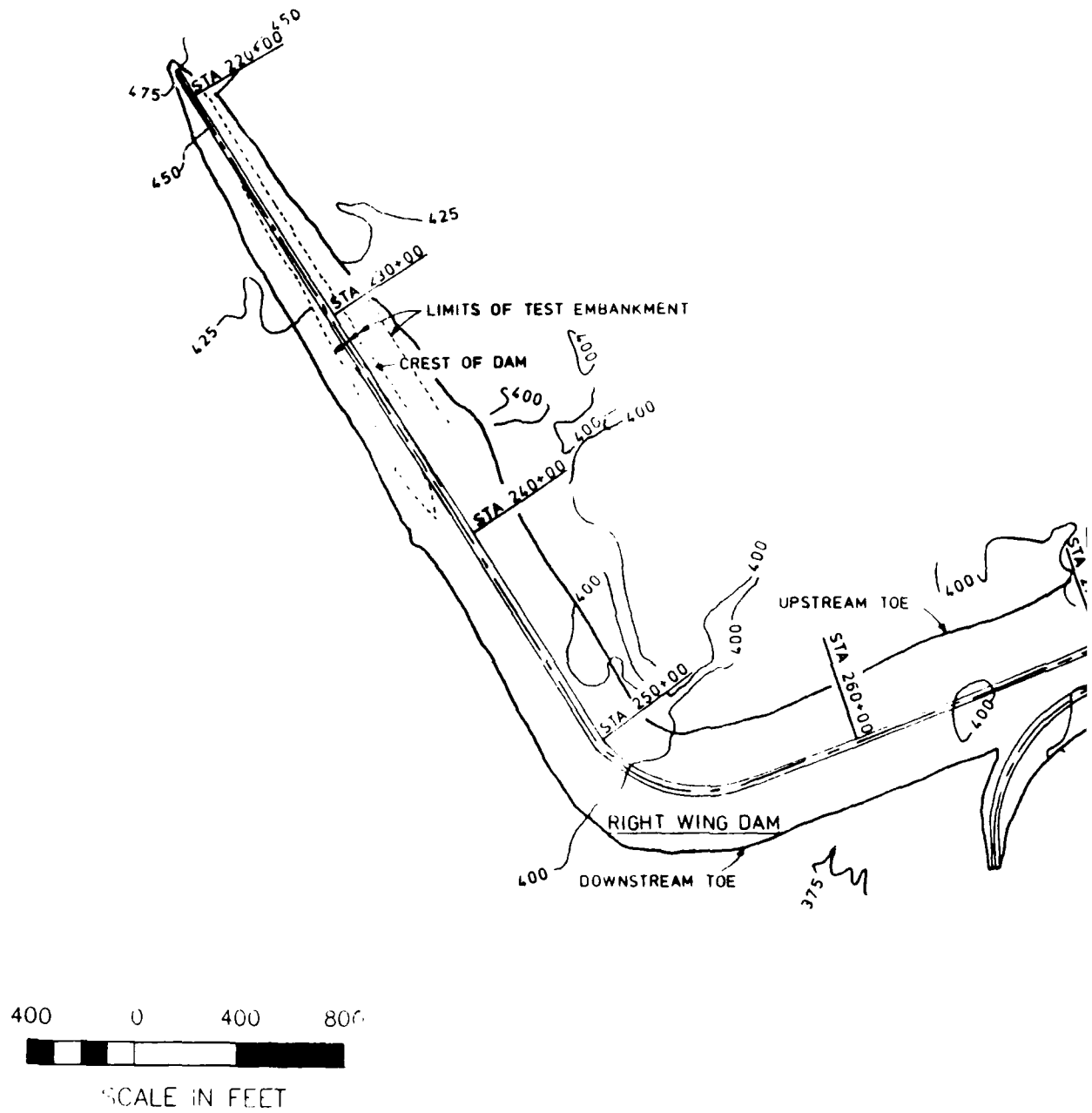
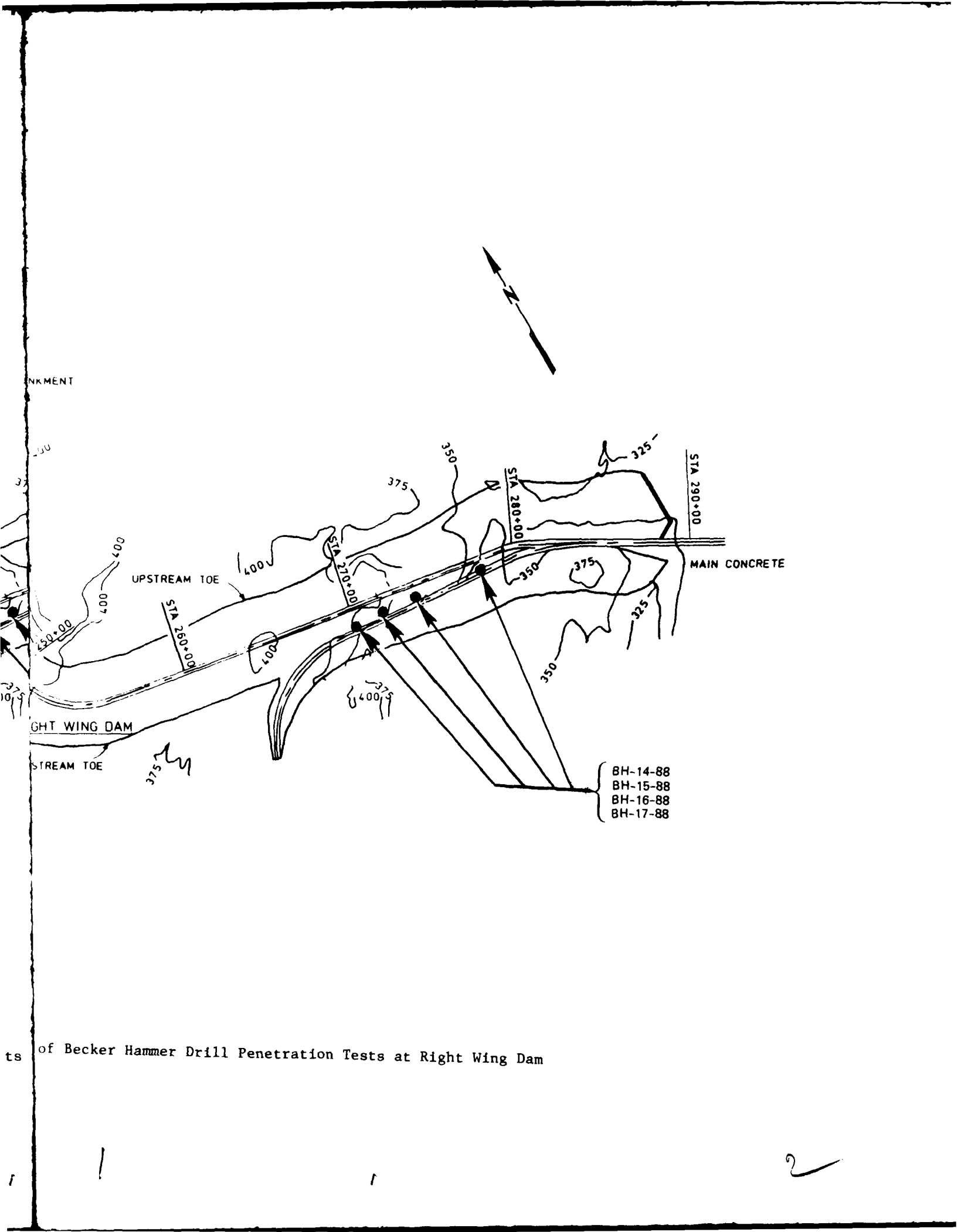
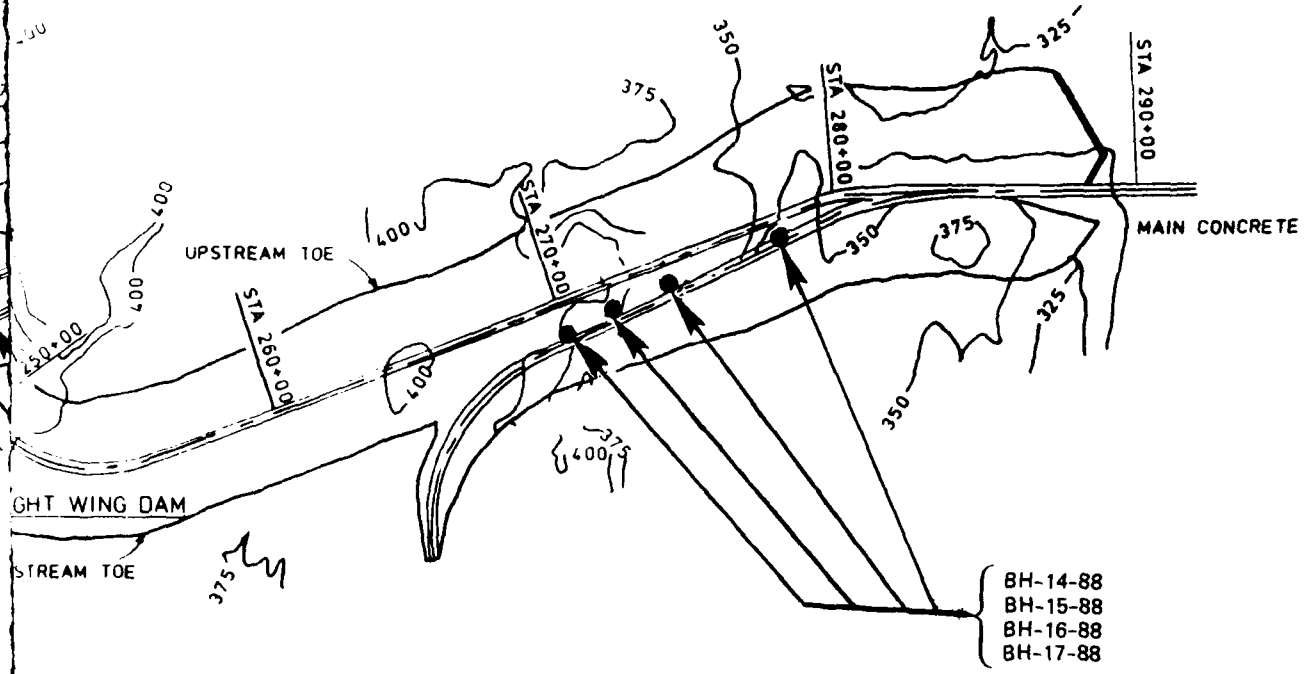


Figure 51. Locations of Becker Hammer Drill Penetration



EMENT



ts of Becker Hammer Drill Penetration Tests at Right Wing Dam

2

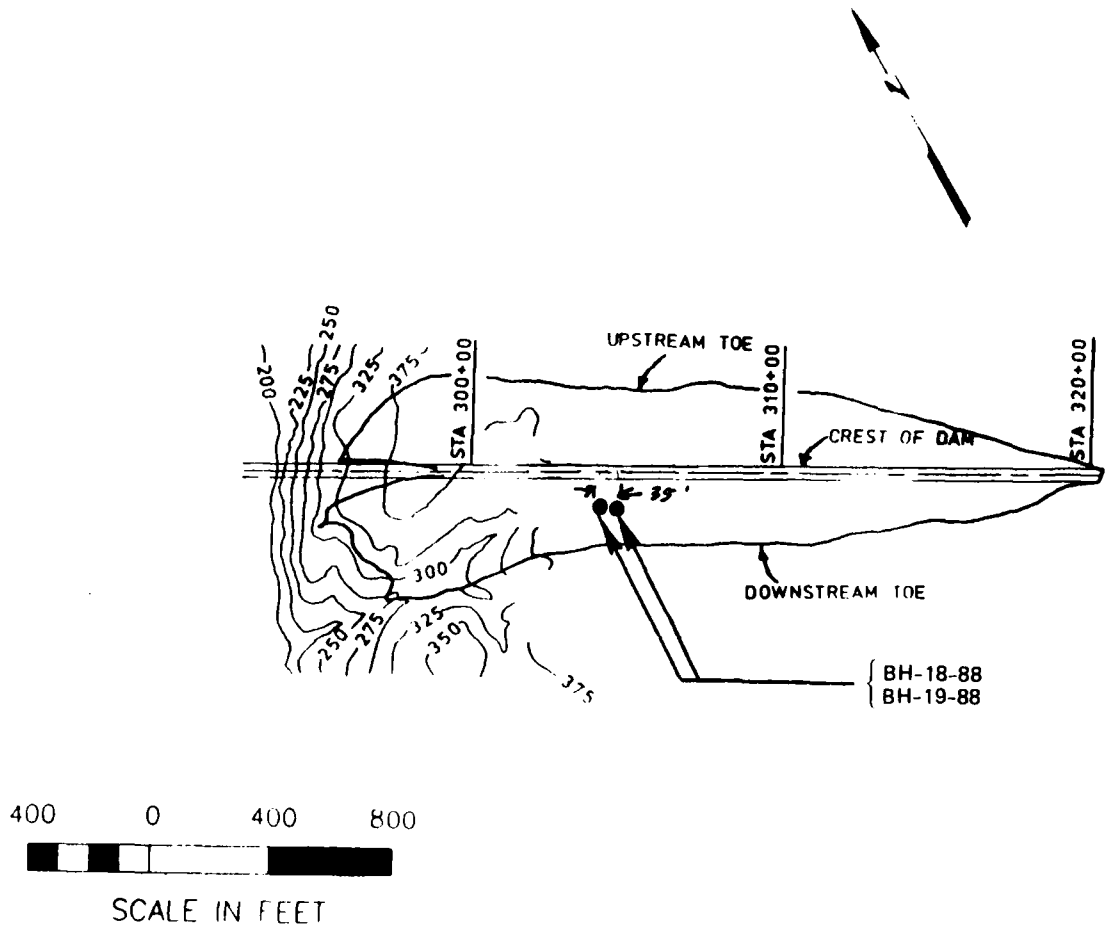


Figure 52. Locations of Becker Hammer Drill Penetration Tests at Left Wing Dam

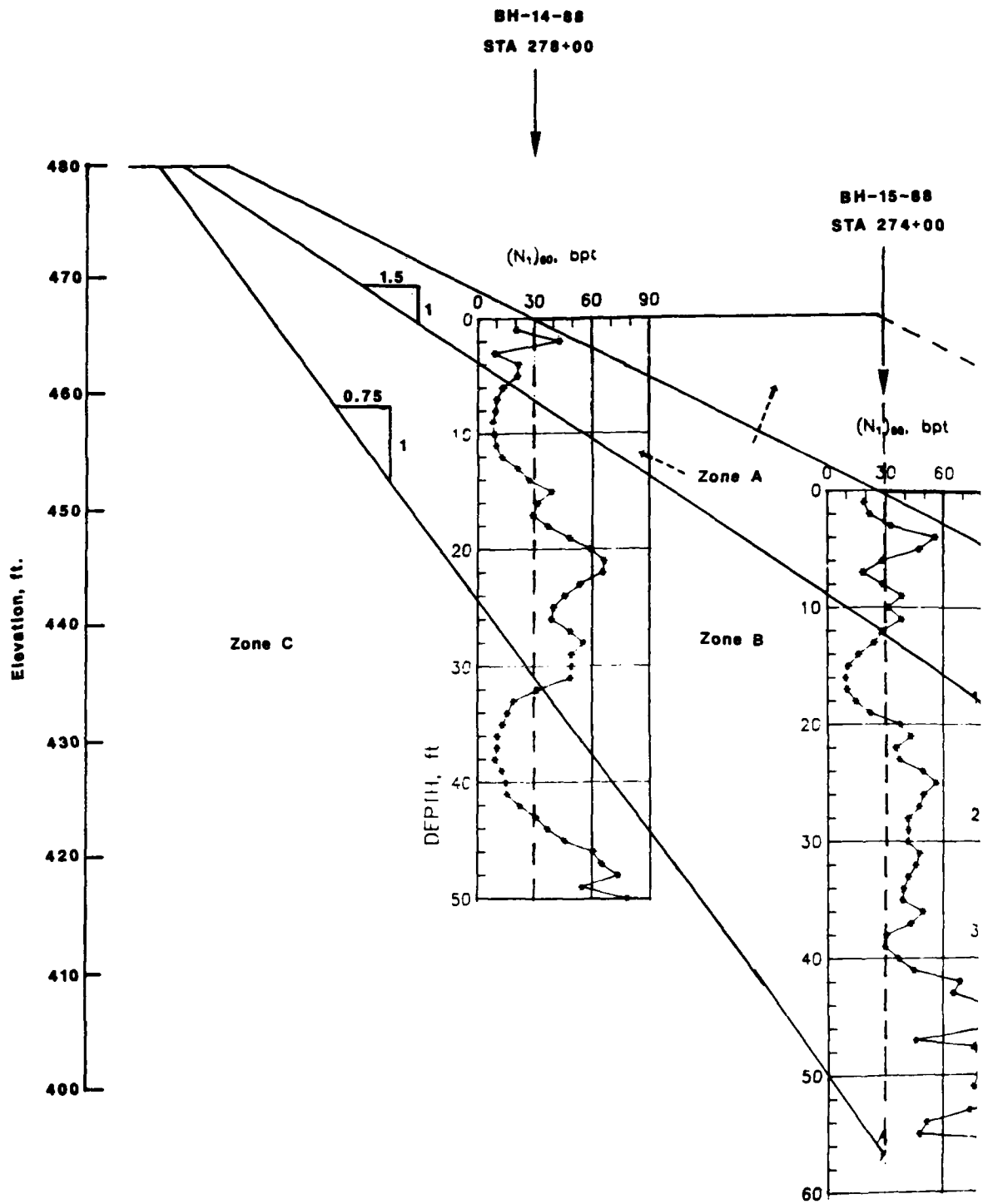
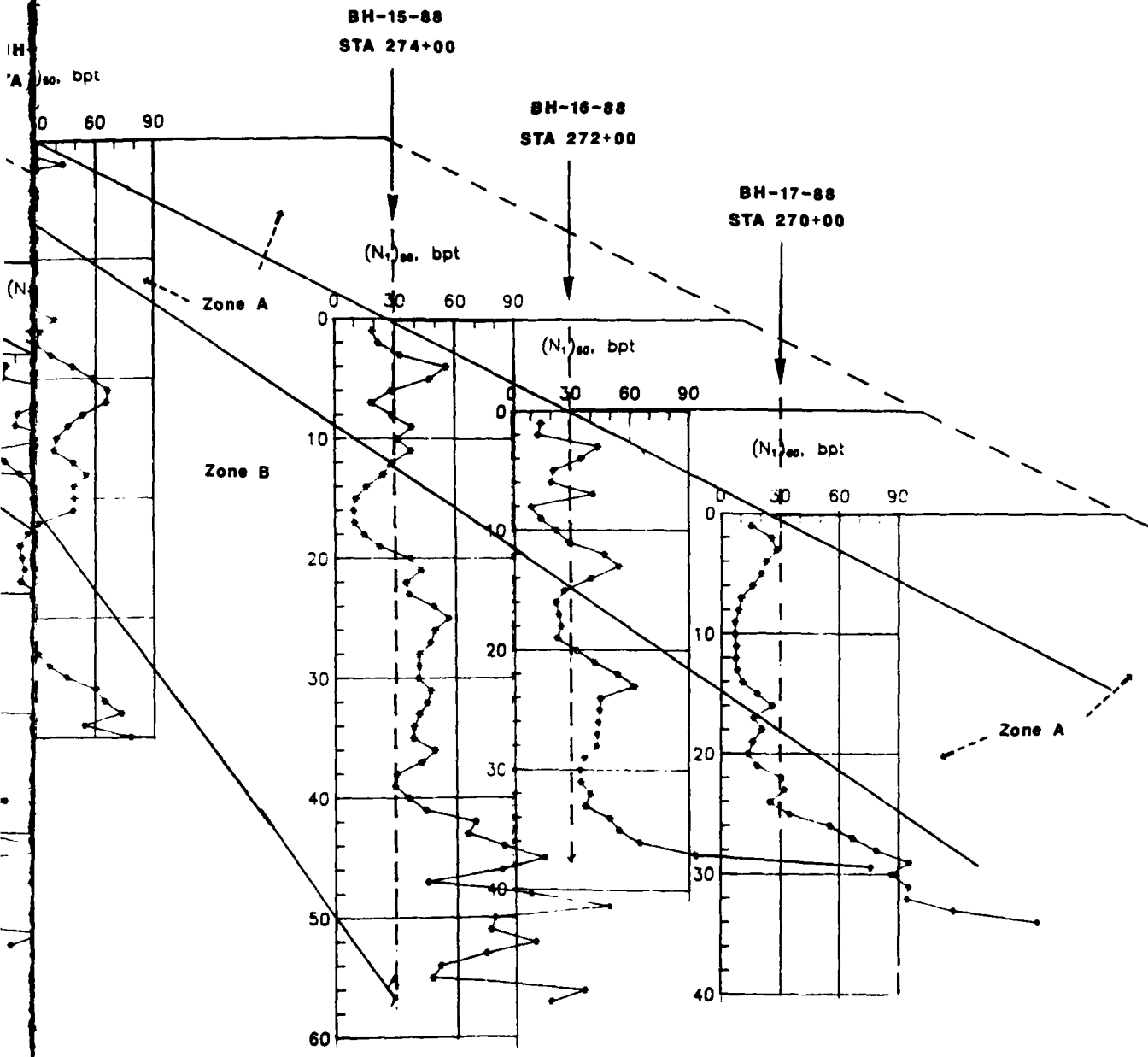


Figure 53. Equivalent SPT $(N_1)_{60}$ blowcounts and Drill Penetration Tests performed in

14-88
78+00



Equivalent SPT $(N_1)_{60}$ blowcounts obtained from Becker Hammer Drill Penetration Tests performed in the Right Wing Dam

1

2

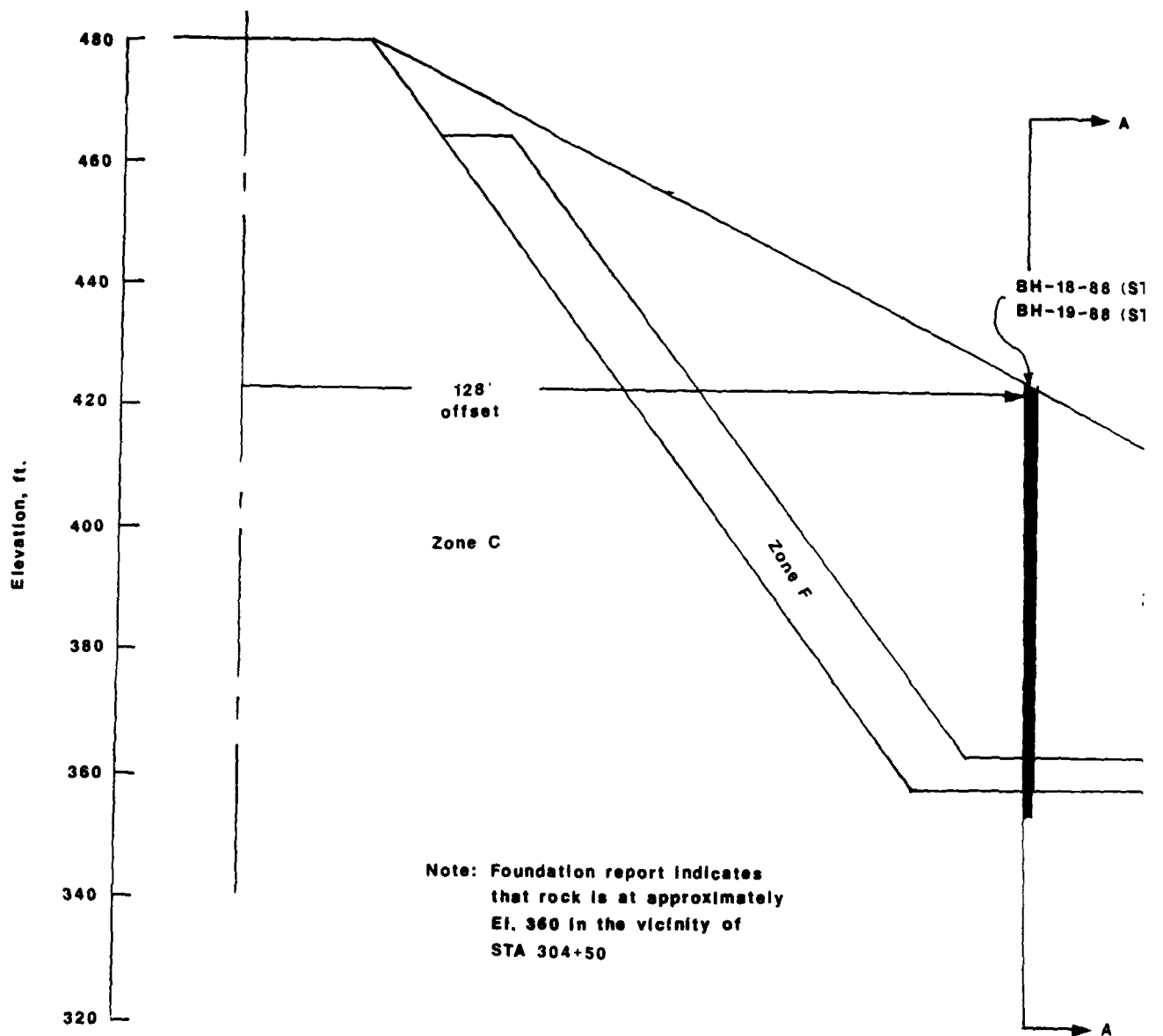
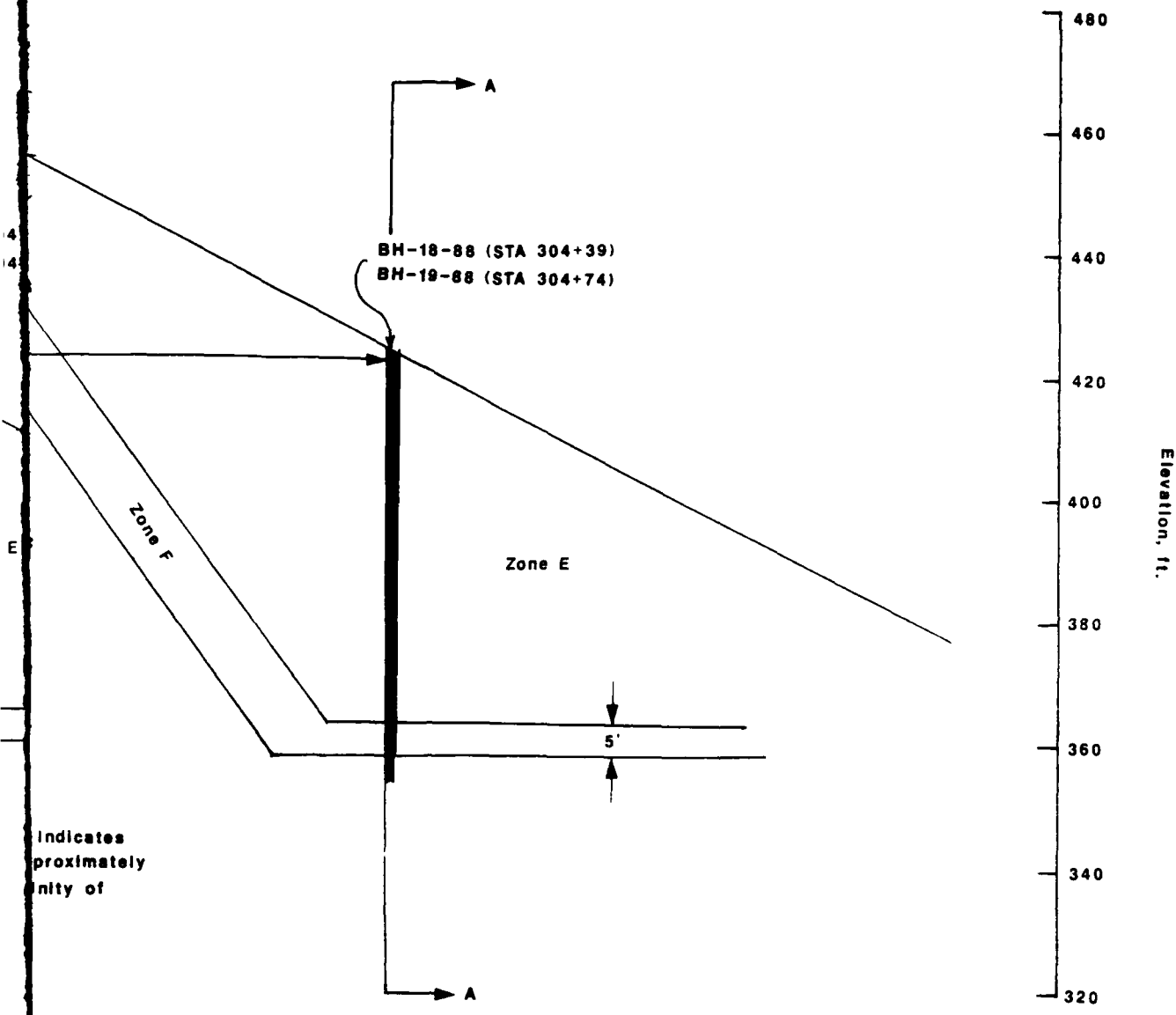


Figure 54. Transverse cross-sectional view of the dow of the Left Wing Dam in the vicinity of Station



reverse cross-sectional view of the downstream portion
Wing Dam in the vicinity of Station 304+50

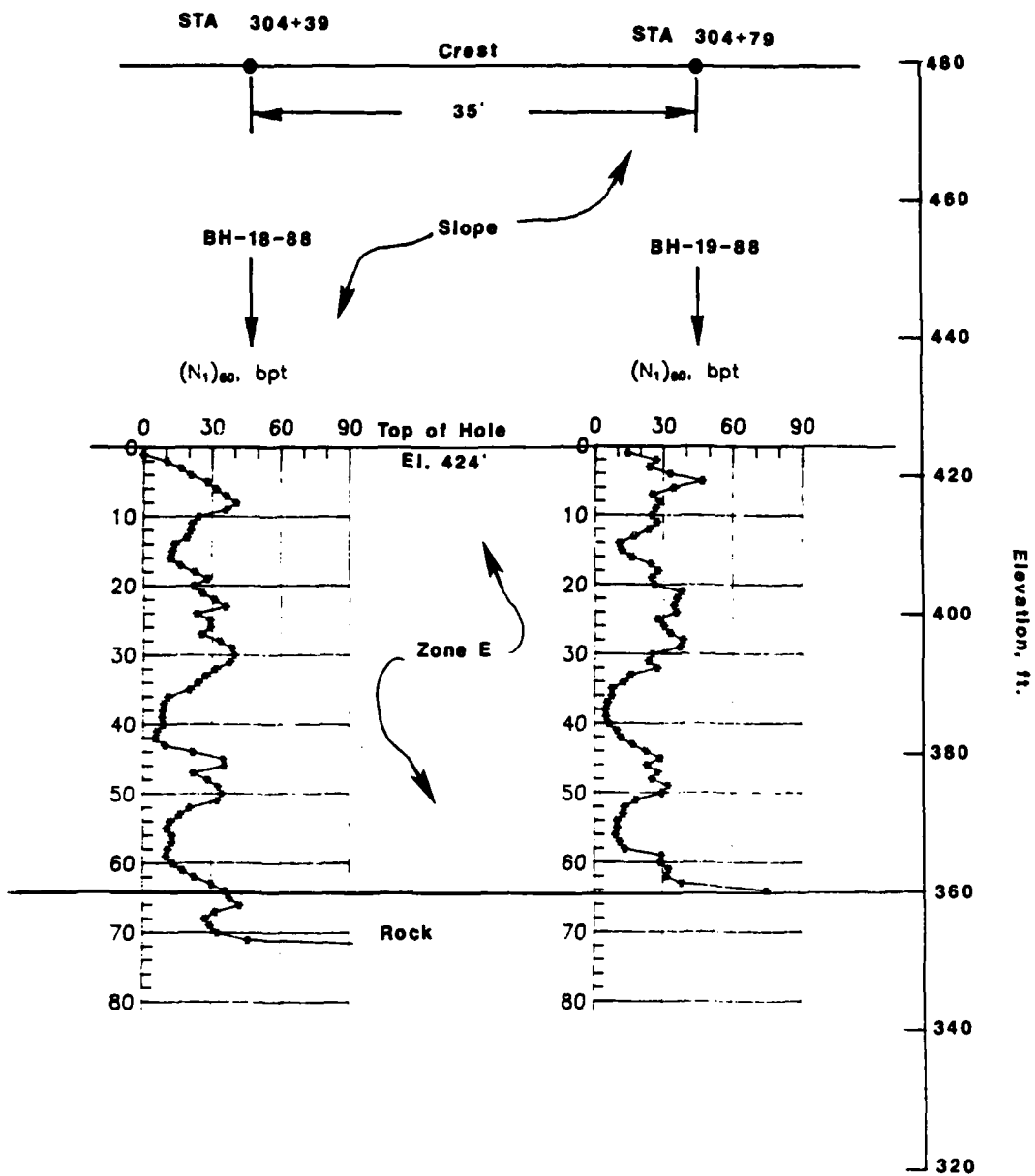


Figure 55. Equivalent SPT (N_1)₆₀ blowcounts obtained from Becker Hammer Drill Penetration Tests performed in the Left Wing Dam

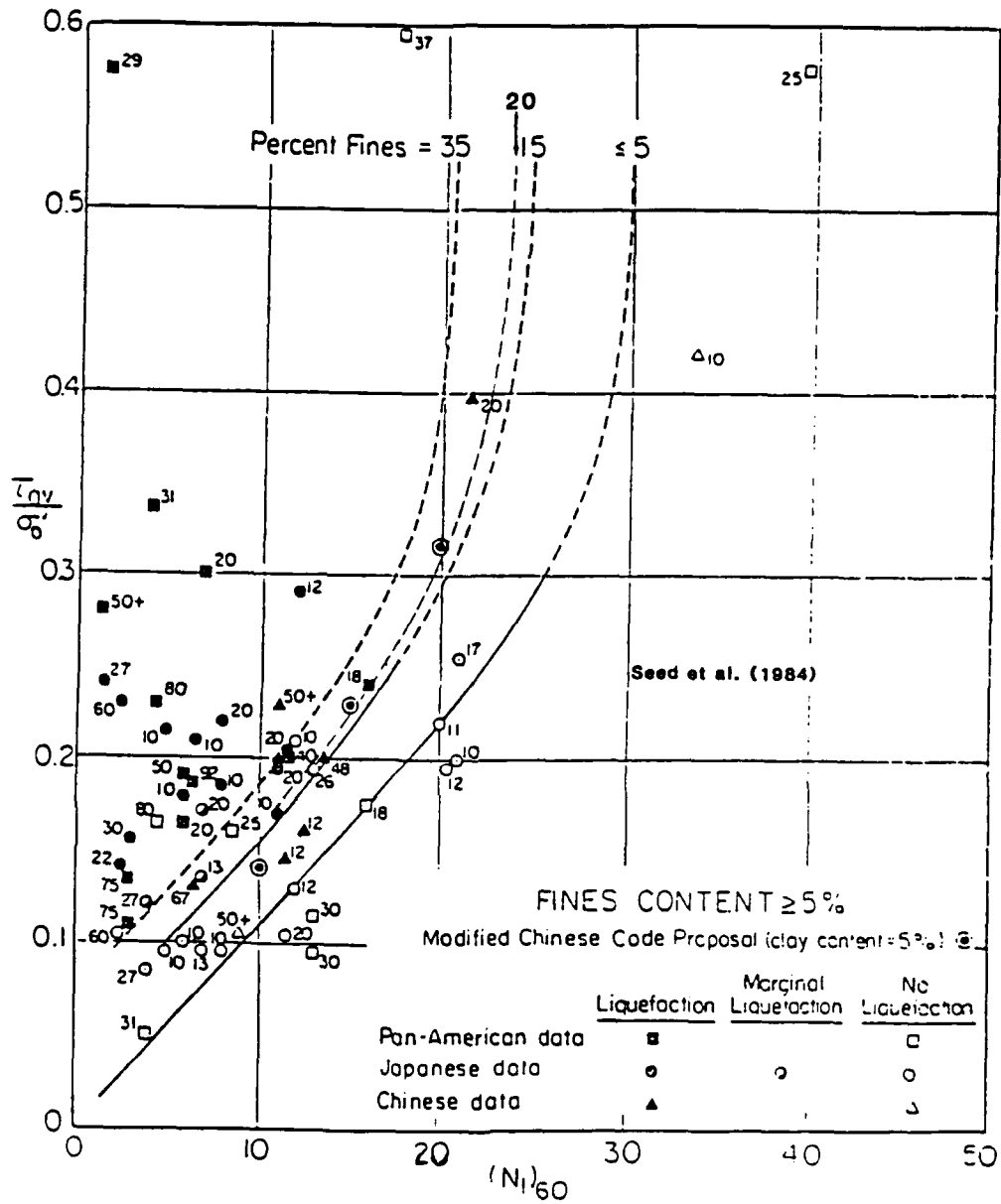
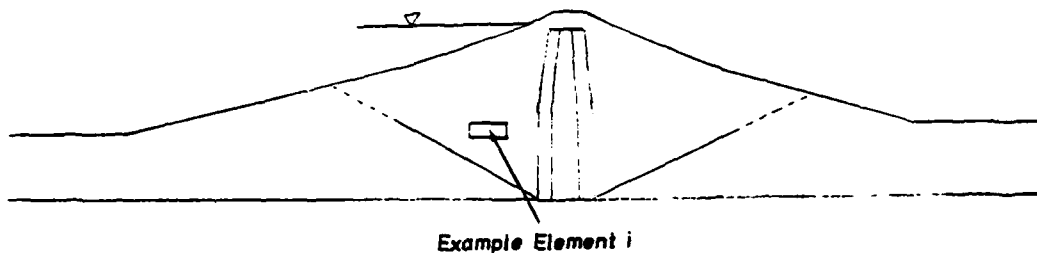


Figure 56. Relationship between stress ratio causing liquefaction and $(N_1)_{60}$ values for silty sands for $M = 7\frac{1}{2}$ earthquakes (from Seed, Tokimatsu, Harder, and Chung 1984)

Determination of Appropriate Cyclic Strength for Example Element

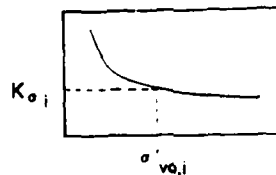


1. Analysis of Becker Penetration Test results and application of Seed's empirical procedure shows:

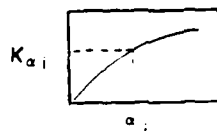
$$(N_1)_{60} = 23 \quad \text{for embankment gravel}$$

$$\left(\frac{\tau_{CAVE}}{\sigma'_{vo}} \right) \approx 0.35 \quad \text{for } M_L = 6.5, \sigma'_{vo} = 1 \text{ tsf, and } \alpha = 0$$

2. Static FEM yields $\sigma'_{vo,i}$ and α_i for element i .
3. K_{σ_i} is determined from chart with $\sigma'_{vo,i}$:



4. K_{α_i} is determined from chart with α_i :



5. Cyclic strength, τ_{α_i} , for element i is:

$$\tau_{\alpha_i} \left(\frac{\tau_{CAVE}}{\sigma'_{vo}} \right)_{\substack{\alpha=1 \\ \alpha=0}} = \left(\frac{\tau_{CAVE}}{\sigma'_{vo}} \right)_{\alpha=0} \times K_{\sigma_i} \times K_{\alpha_i} \times \sigma'_{vo,i}$$

$$= (0.35) \times K_{\sigma_i} \times K_{\alpha_i} \times \sigma'_{vo,i}$$

Figure 57. Schematic representation of procedure for calculating the appropriate cyclic strength for elements in idealized embankment section

ADJUSTMENT FACTOR

K_{σ} versus Vertical Effective Stress

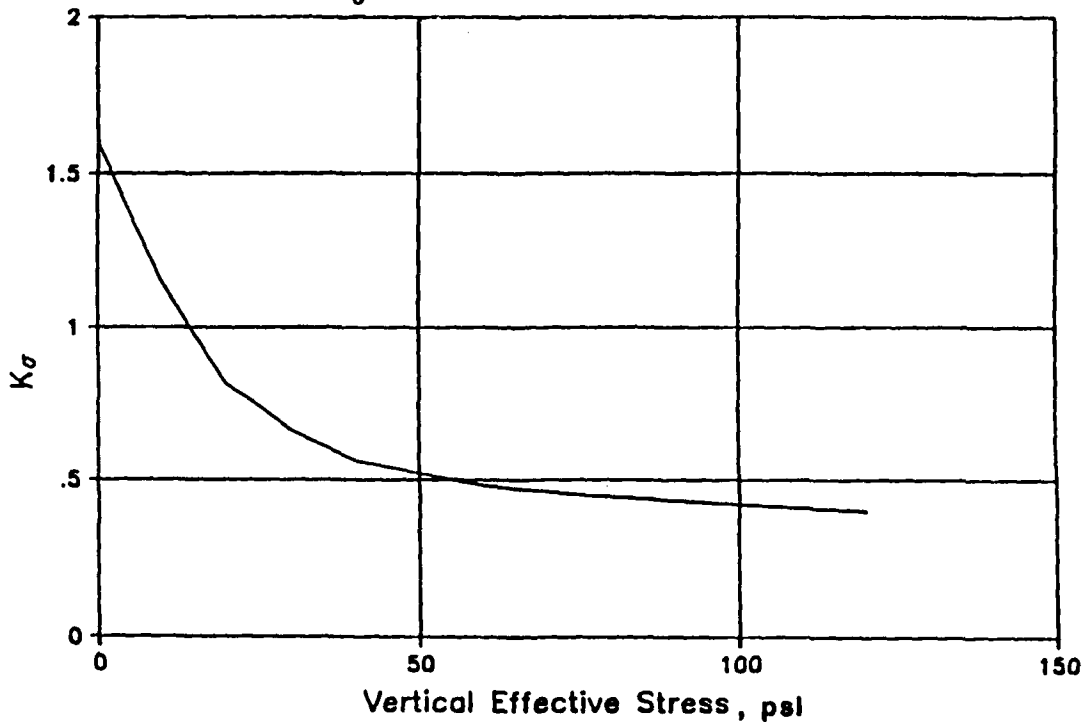


Figure 58. Adjustment factor, K_{σ} , for change in cyclic stress ratio required to cause $R_u = 100$ percent with change in effective normal stress, determined from laboratory tests on Folsom gravels

ADJUSTMENT FACTOR

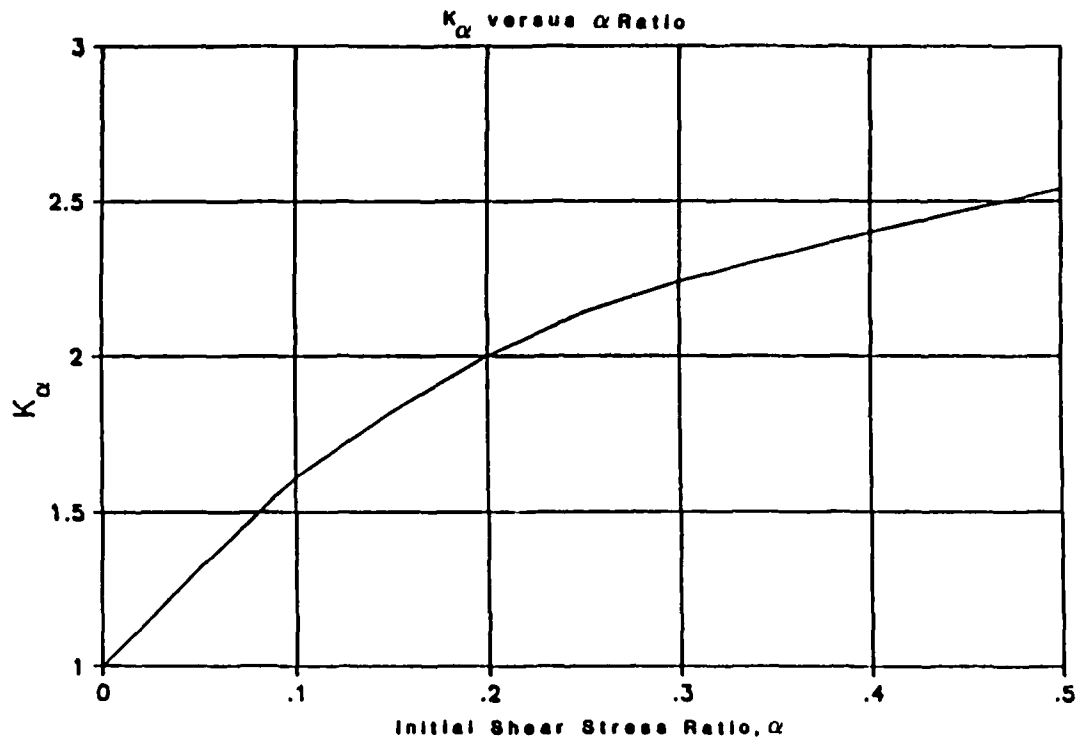


Figure 59. Adjustment factor, K_α for change in cyclic stress ratio required to cause $R_U = 100$ percent with change in initial shear stress ratio, α , determined from laboratory tests on Folsom gravels

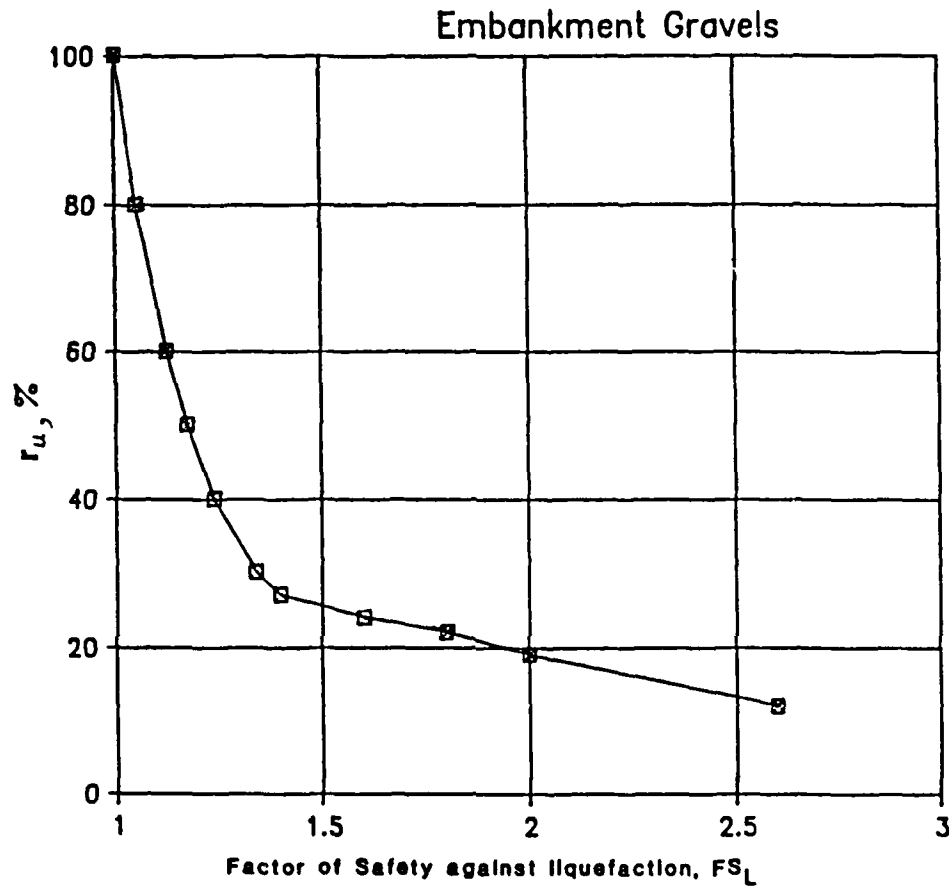
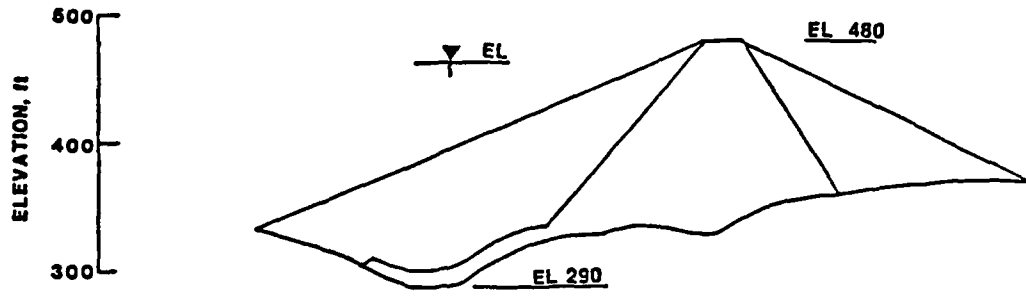
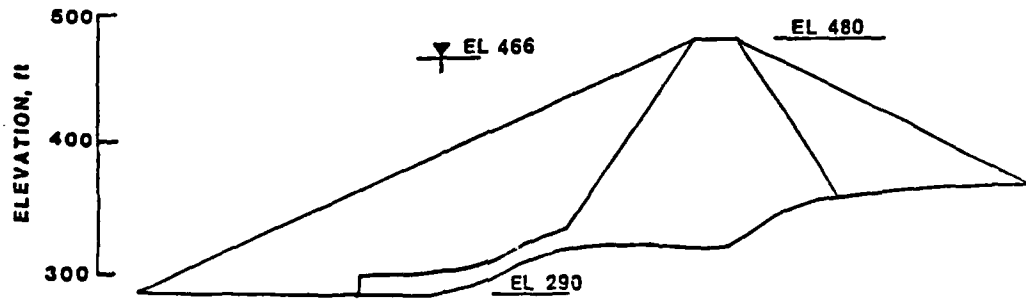


Figure 60. Residual excess pore pressure ratio, r_u , and corresponding values of factors of safety against liquefaction, FS_L , estimated from laboratory tests on Folsom gravels



ACTUAL SECTION -



LOCALIZED ANALYSIS SECTION - STA - 283 + 00

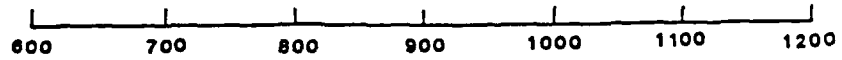


Figure 61. Cross section views of Right Wing Dam, Station 283

FINITE ELEMENT MESH FOR RIGHT WING DAM -

325 ELEMENTS
343 NODAL POINTS

NOTE: ALL ELEMENTS BELOW HEAVY LINE ARE SUBMERGED.

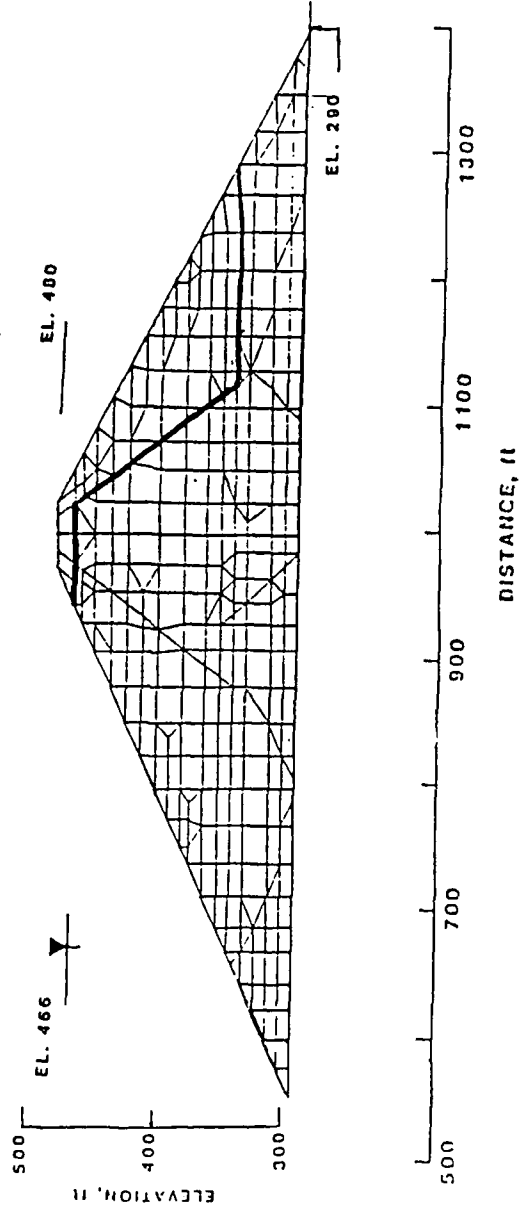


Figure 62. Finite element mesh of representative cross-section for Wing Dams

STRESSES ARE IN ksi

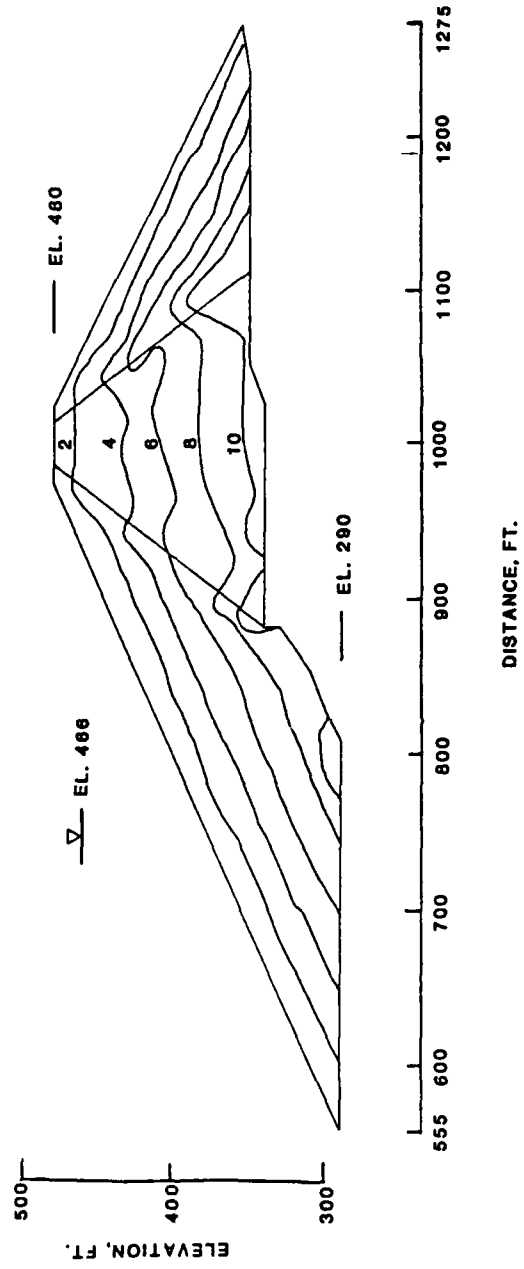


Figure 63. Vertical effective contours for Wing Dam analysis section

RIGHT WING DAM -- HORIZONTAL EFFECTIVE STRESSES COMPUTED BY FEADAM

STRESSES ARE IN ksi

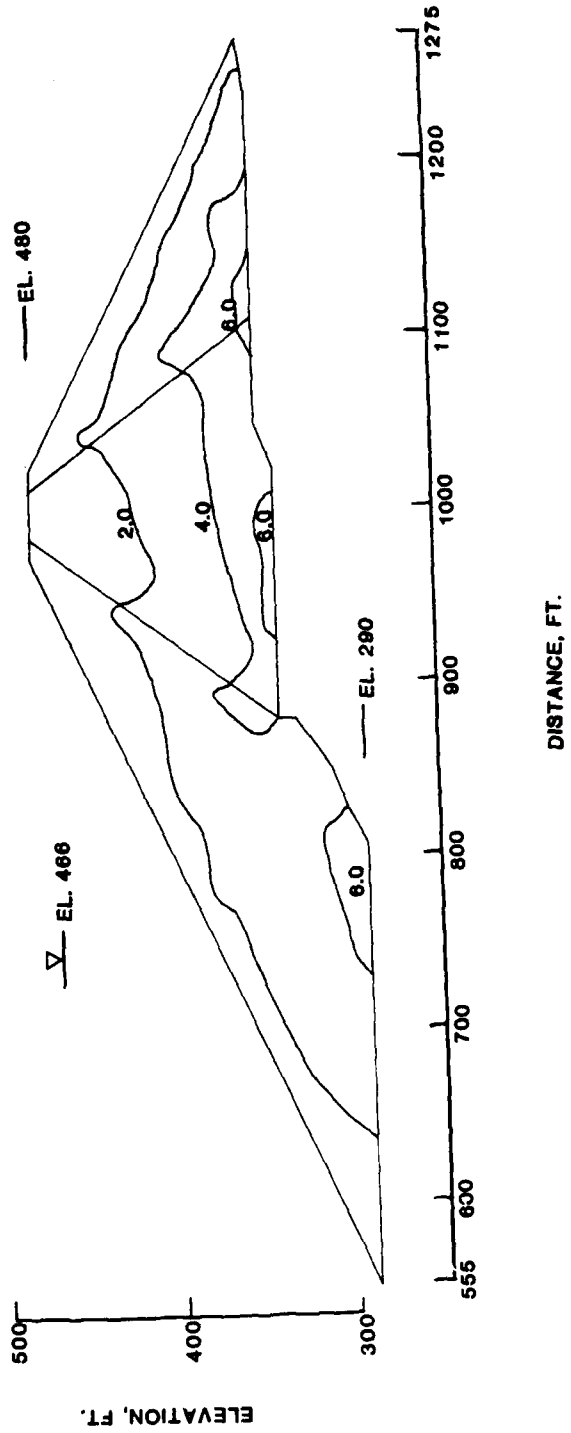


Figure 64. Contours of horizontal effective stress

STRESSES ARE IN Ksf

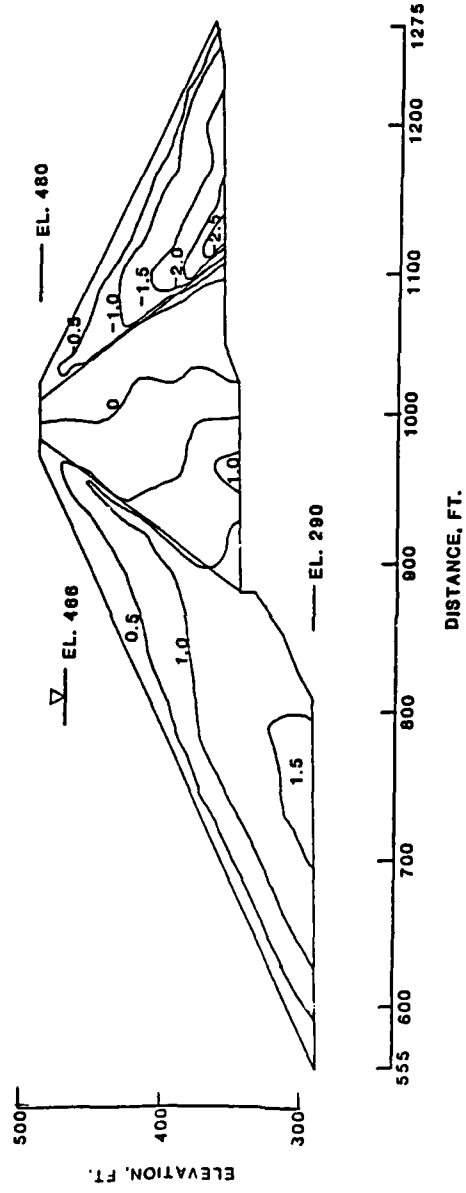


Figure 65. Contours of initial static shear stresses on horizontal planes for Wing Dam analysis section

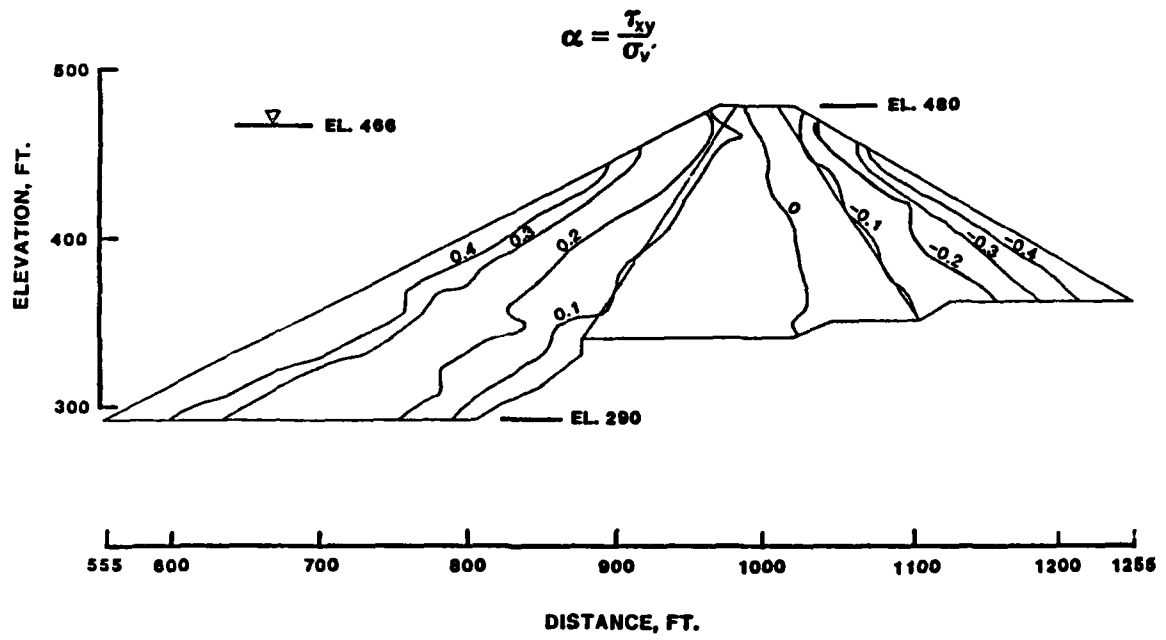


Figure 66. Contours of initial shear stress ratio, α , for Wing Dam analysis section

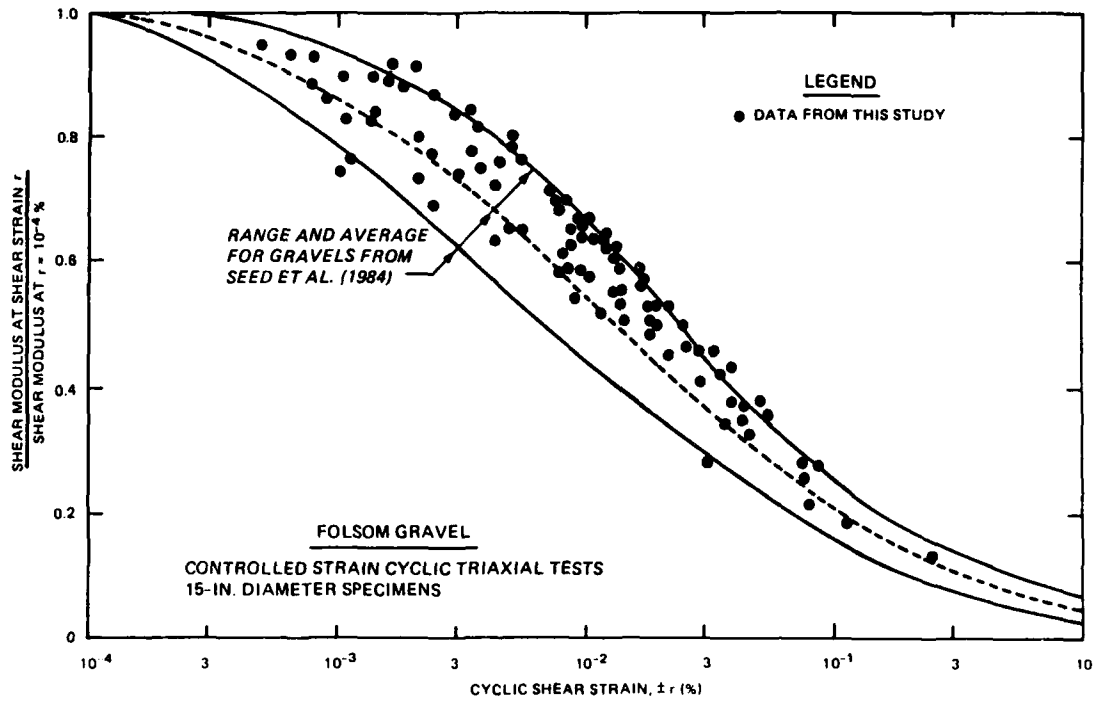
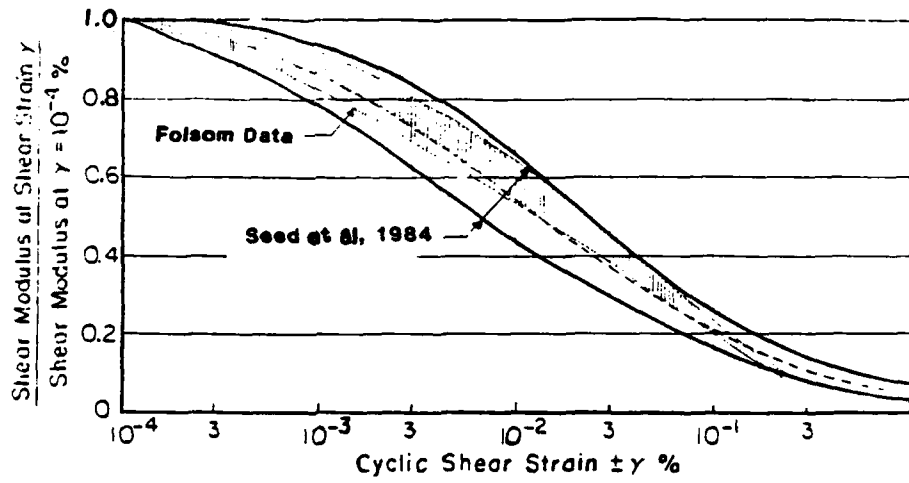
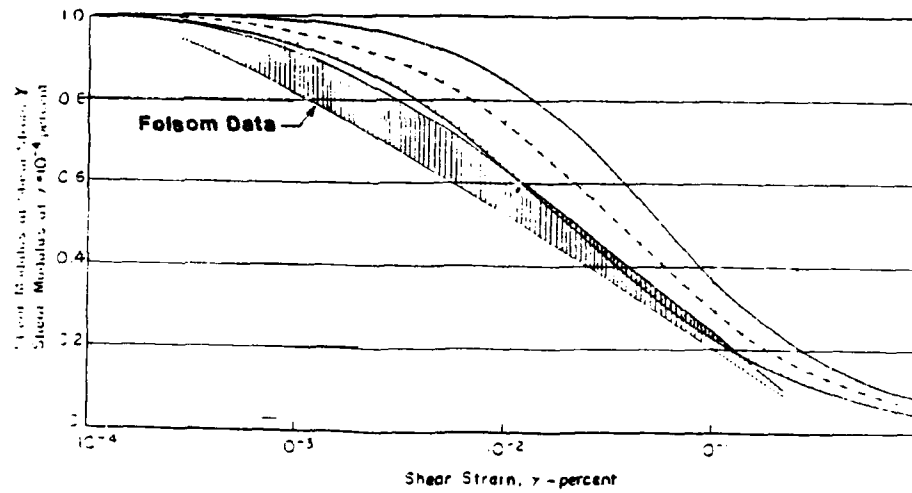


Figure 67. Variation of shear modulus with shear strain for Folsom gravel estimated from extrapolated values of K_2 at $\gamma = 10^{-4}$ percent



a. Variation of shear modulus with shear strain for gravelly soils



b. Variation of shear modulus with shear strain for sands
(after Seed and Idriss 1970)

Figure 68. Comparison of shear modulus degradation curves from Seed et al. (1984) and Seed et al. (1970) with laboratory test data on Folsom gravels

RIGHT WING DAM -- DYNAMIC SHEAR STRESSES COMPUTED BY FLUSH

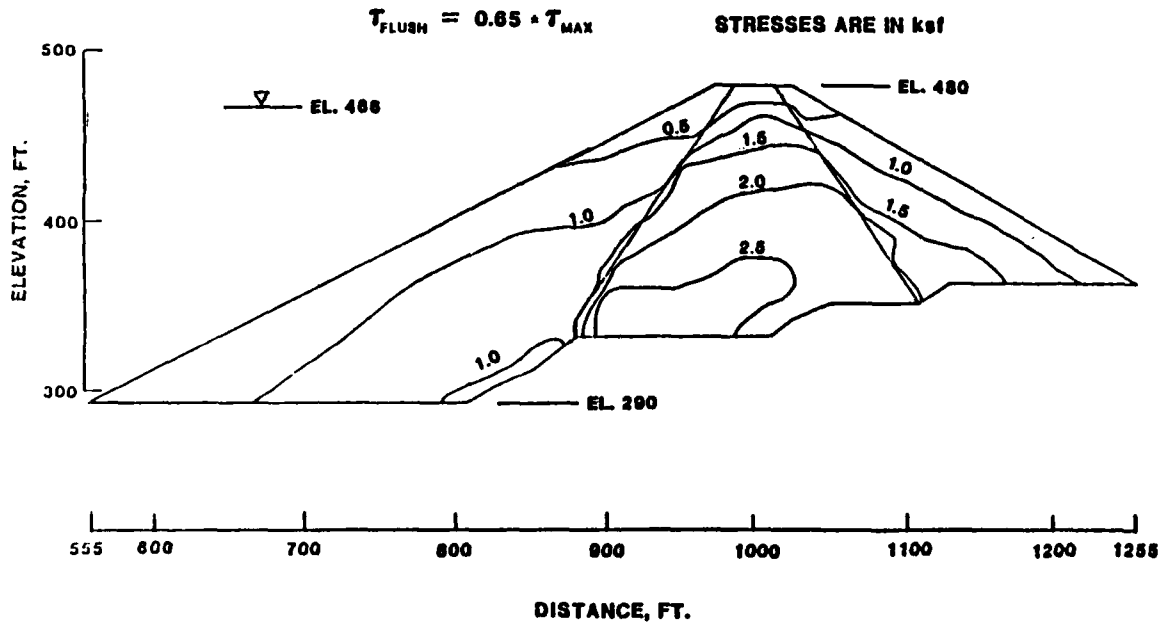


Figure 69. Average earthquake-induced shear stresses, τ_{FLUSH} , computed by FLUSH with Accelerogram B in Wing Dam analysis section

ACCELERATIONS COMPUTED WITH FLUSH

ACCELERATIONS ARE IN g's

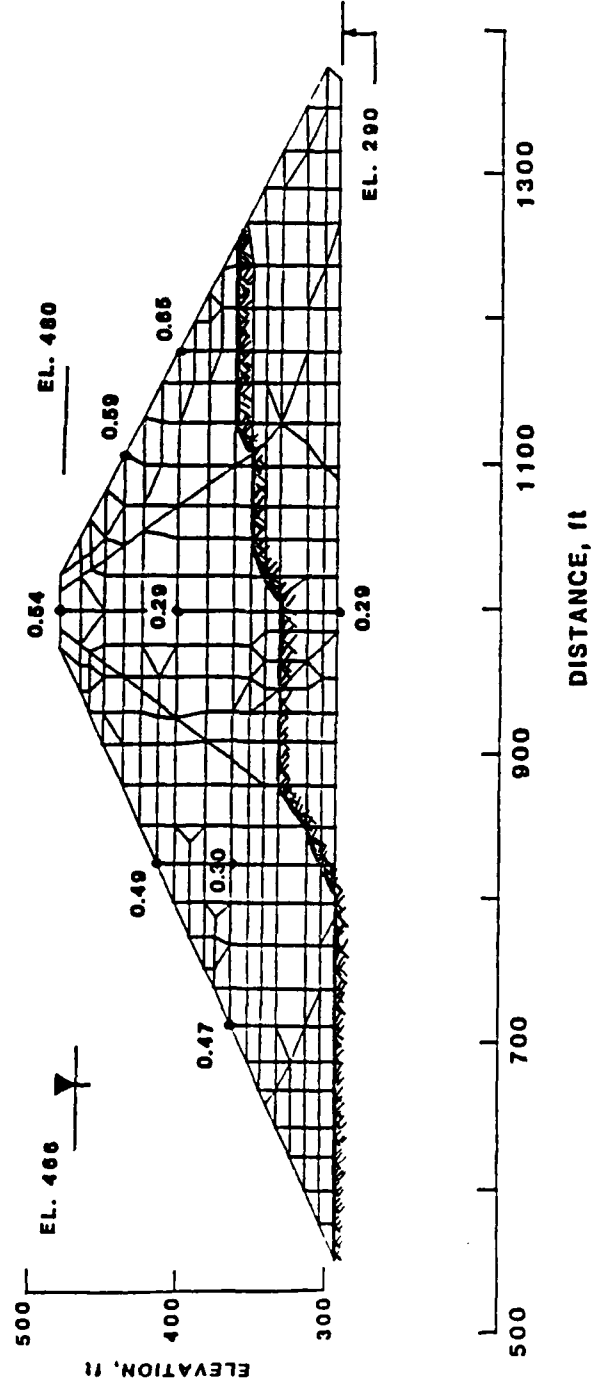


Figure 70. Peak accelerations computed by FLUSH with Accelerogram B in Wing Dam analysis section

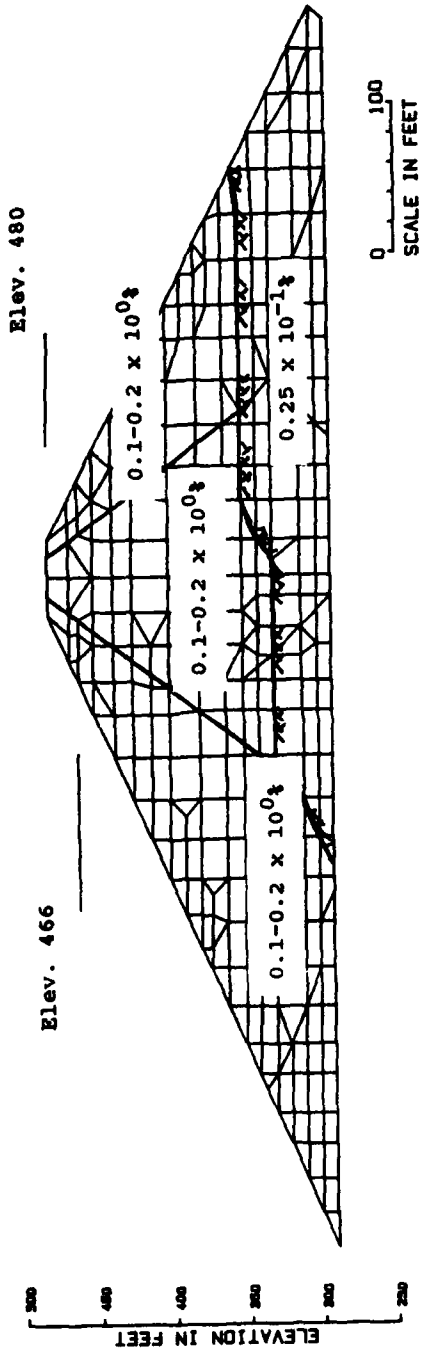


Figure 71. Earthquake induced shear strains

FOURIER AMPLIFICATION FUNCTION

FOR FLUSH NODAL PT. 155 - CREST AT C. L.

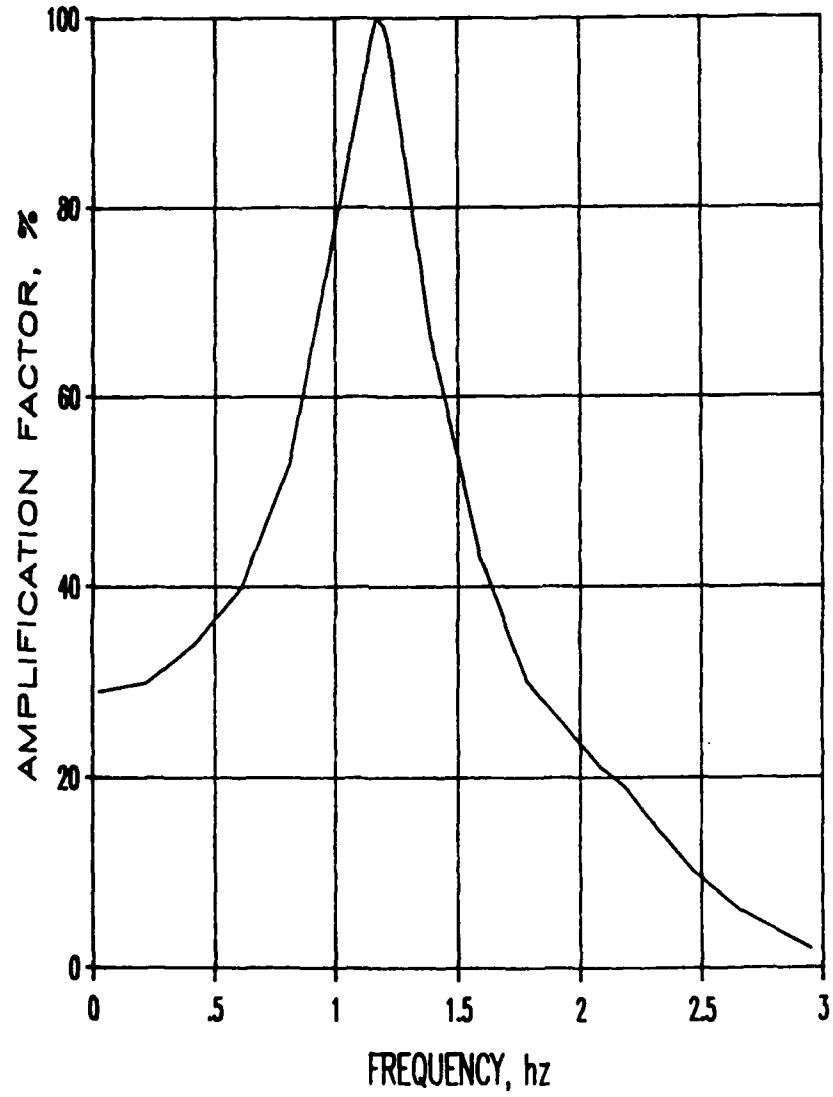


Figure 72. Fourier Amplification Function for node at crest elevation on CL

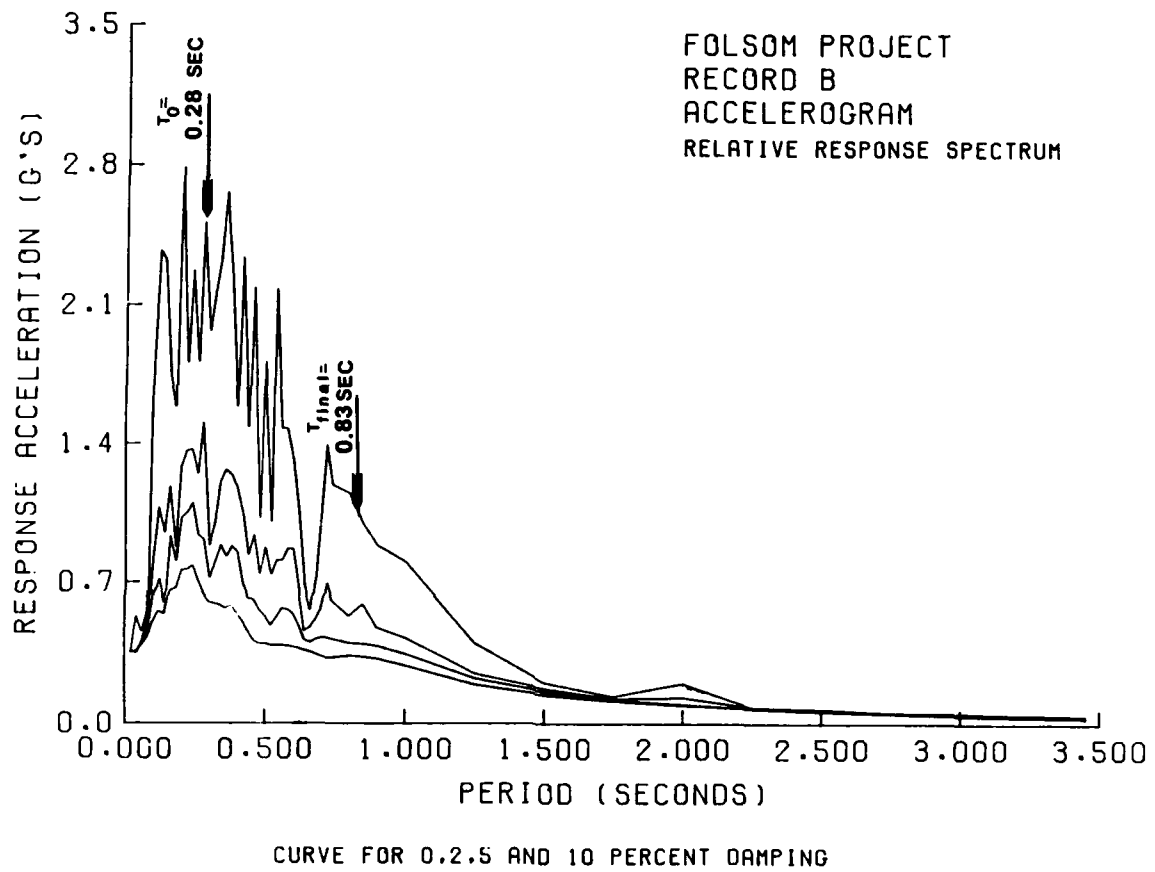


Figure 73. Initial and post-earthquake fundamental periods for Wind Dam analysis section compared with Accelerogram B response spectra

FOLSOM PROJECT - RIGHT WING DAM

CROSS SECTION FOR ROCK FOUNDATION

STA 285+00

CONTOURS OF FACTOR OF SAFETY AGAINST LIQUEFACTION

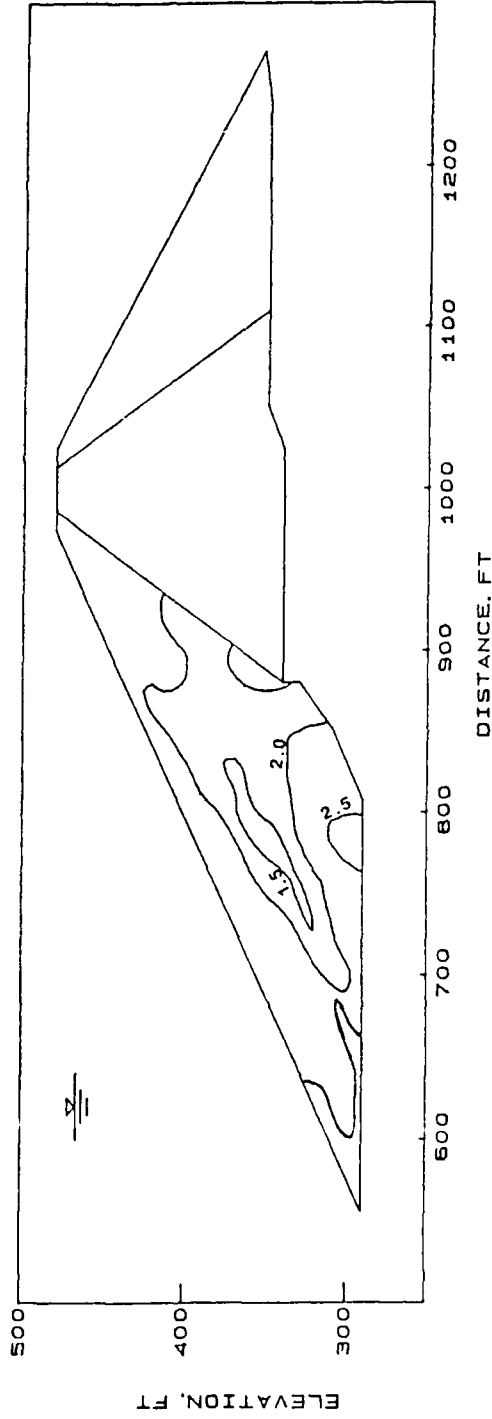


Figure 74. Contours of safety factor against liquefaction for idealized section of Right Wing Dam Station 285+00

FOLSOM PROJECT - RIGHT WING DAM

CROSS SECTION FOR ROCK FOUNDATION

STA 285+00

CONTOURS OF EXCESS PORE PRESSURE

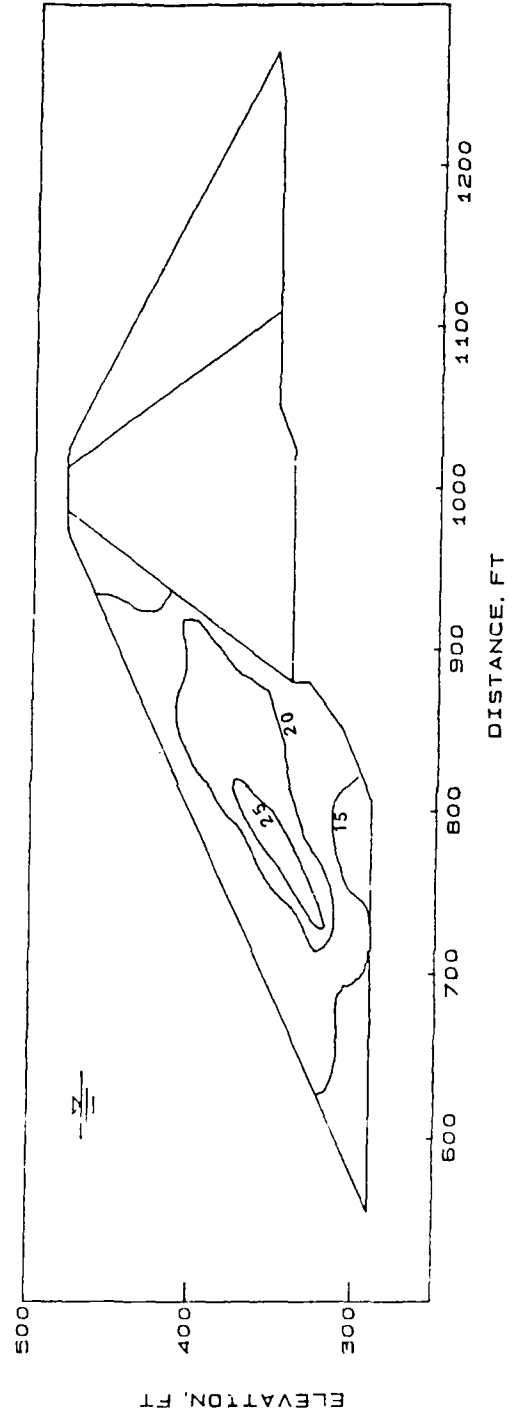


Figure 75. Contours of excess pore pressure ratio, R_u , in percent for idealized section of Right Wing Dam Station 285+00

POST-EARTHQUAKE STABILITY ANALYSIS

FOLSOM - RIGHT WING DAM STA. 285+00

FACTOR OF SAFETY AGAINST SLOPE FAILURE I

PRE-EARTHQUAKE = 2.20
POST-EARTHQUAKE = 1.54

KEY I

CRITICAL CIRCLE *****
R_uX CONTOURS _____

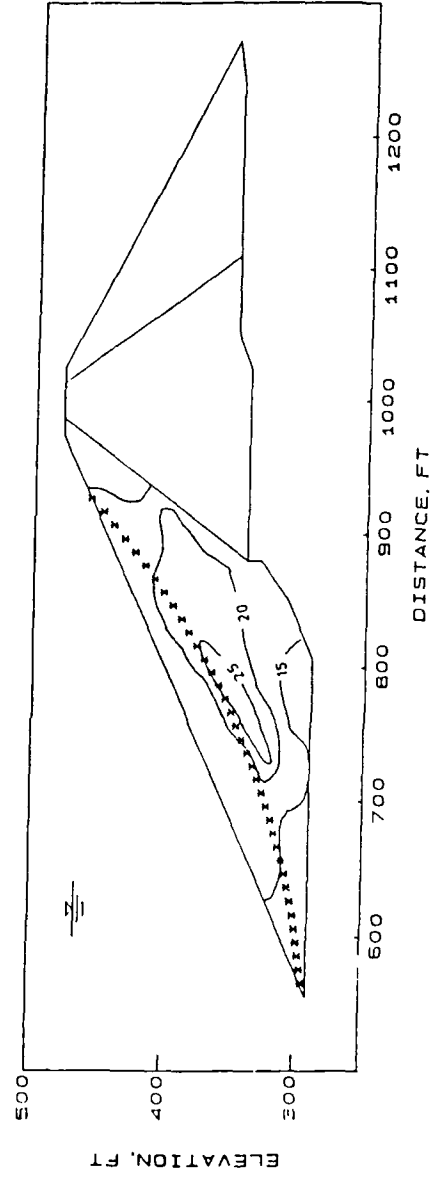


Figure 76. Safety factor against sliding and critical circle in post earthquake stability analysis

POST-EARTHQUAKE PERMANENT DISPLACEMENT ANALYSIS

FOLSOM - RIGHT WING DAM STA. 285+00

YIELD ACCELERATION SEISMIC COEFFICIENT (KY)

CASE I FAILURE CIRCLES CONFINED TO EXIT UPSTREAM OF CENTERLINE

KEY I

FAILURE CIRCLES *****
RUX CONTOURS _____

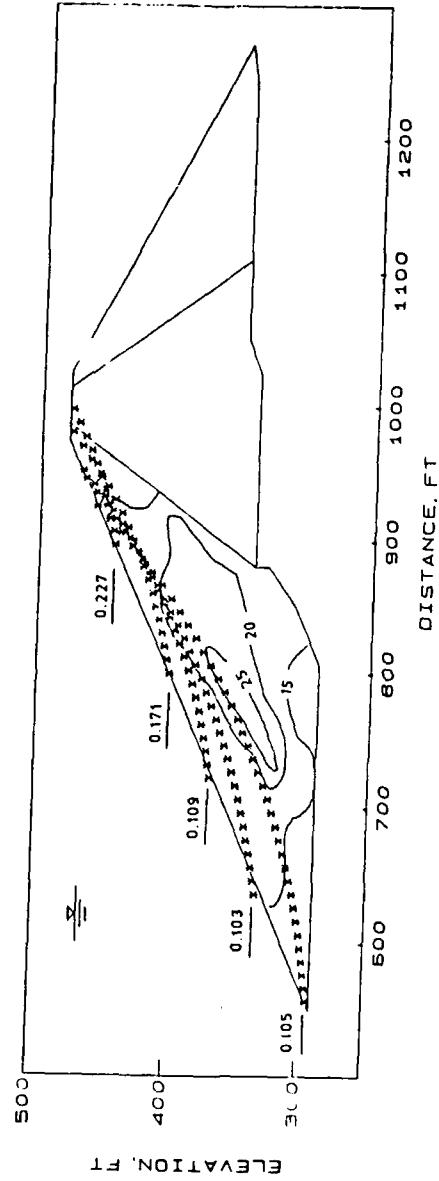


Figure 77. Yield accelerations for critical slip circles involving only materials upstream of centerline

ELEVATION vs YIELD ACCELERATION

RIGHT WING DAM STA. 285+00

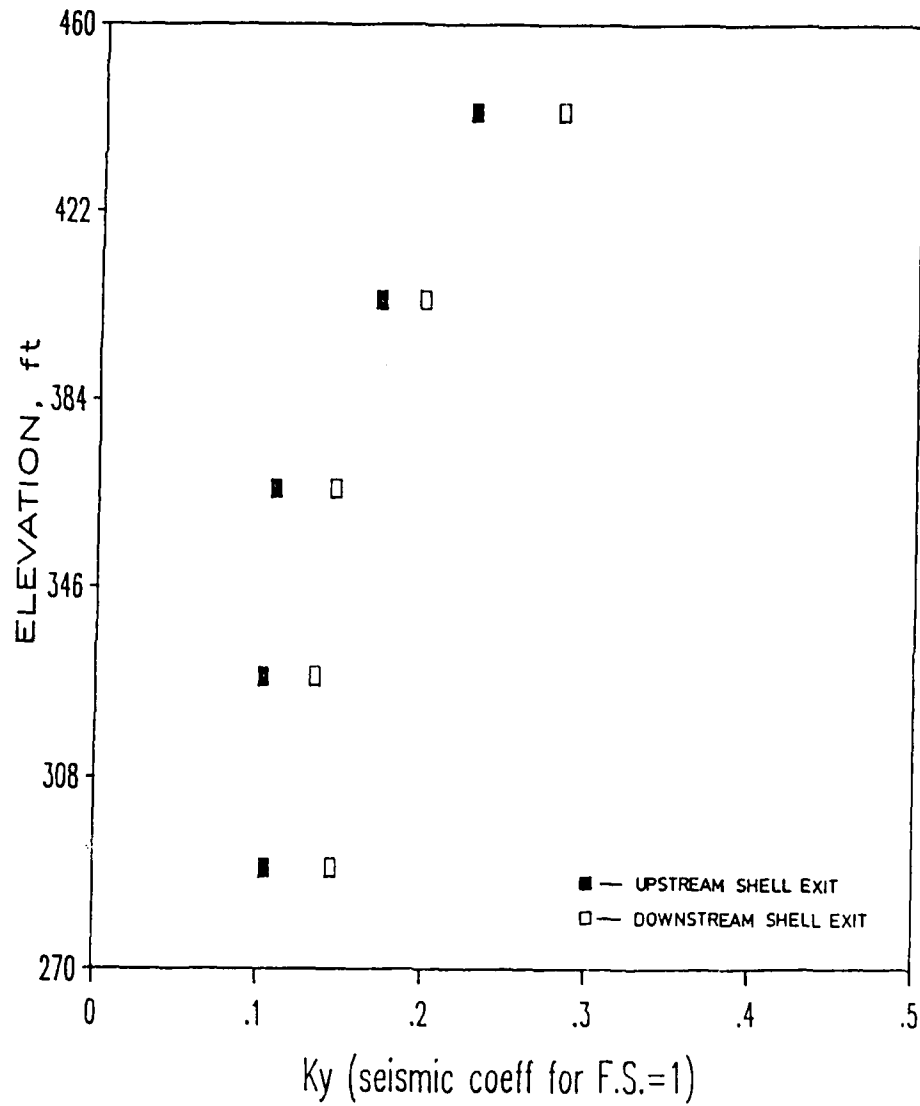


Figure 79. Yield accelerations versus depth for Right Wing Dam

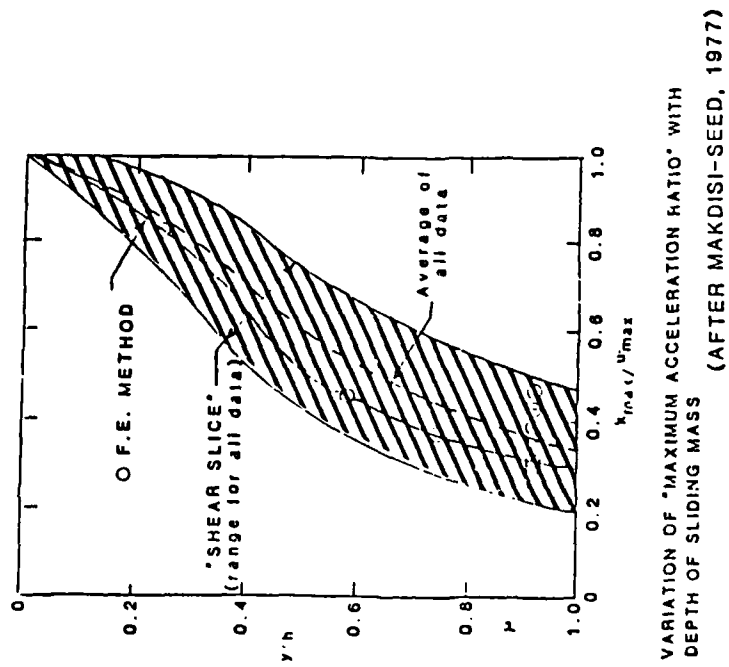
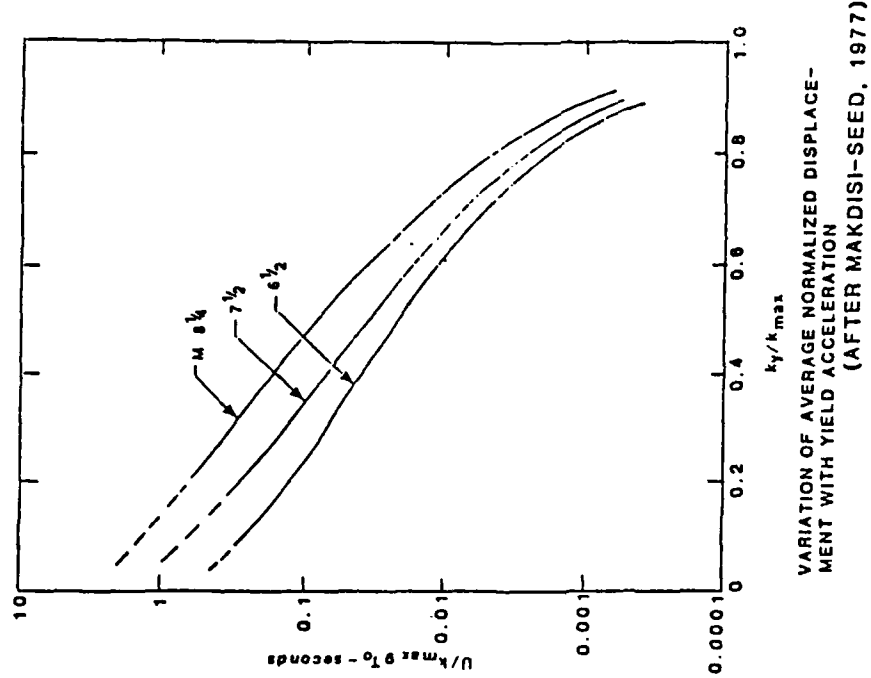


Figure 80. Normalized charts for computing permanent displacement using the Makdisi-Seed technique

DISPLACEMENT vs ELEVATION

MAKDISI-SEED METHOD, RECORD B

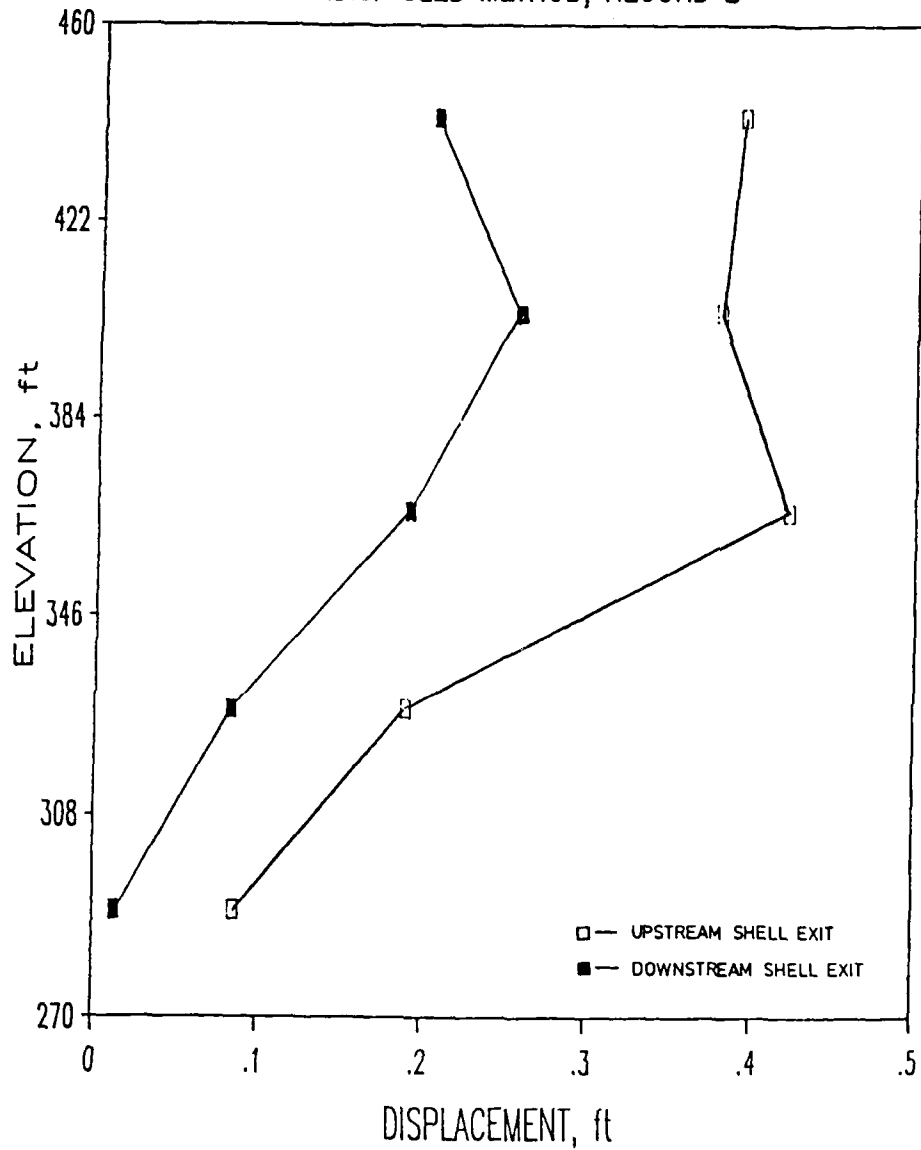
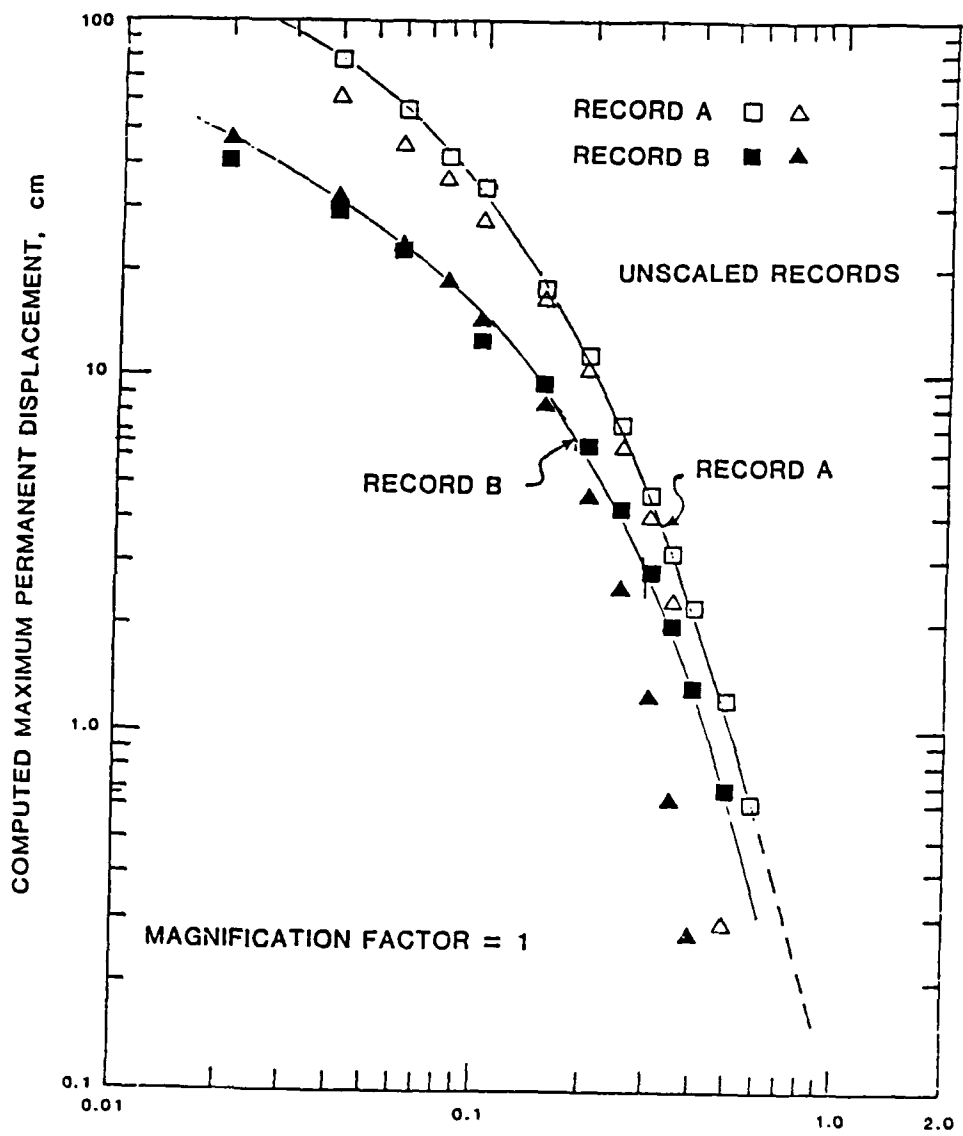


Figure 81. Permanent displacements computed for the idealized Right Wing Dam, Station 285+00



$$\frac{N}{A} = \frac{\text{MAXIMUM EARTHQUAKE COEFFICIENT}}{\text{MAXIMUM EARTHQUAKE ACCELERATION}}$$

Figure 82. Results of Newmark Sliding Block Analysis computed displacements for Accelerograms A and B

DISPLACEMENT vs ELEVATION

SARMA METHOD, RECORD B

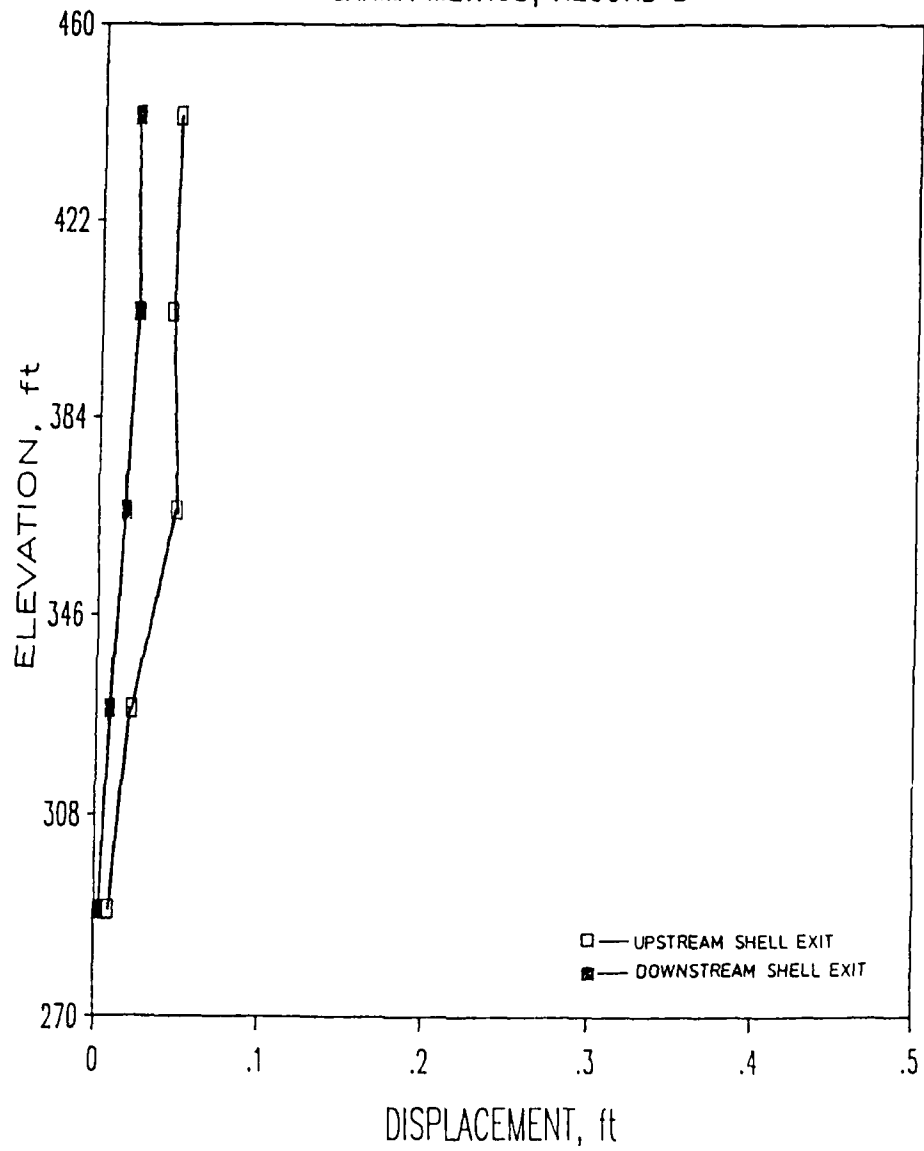


Figure 83. Permanent displacements computed for the idealized Right Wing Dam, Station 285+00

APPENDIX A

EVALUATION OF BECKER PENETRATION TESTS PERFORMED IN 1988
AT RIGHT AND LEFT WING DAMS

EVALUATION OF BECKER PENETRATION TESTS PERFORMED IN 1988
RIGHT AND LEFT WING DAMS

General

1. As discussed in the main text, a limited program of closed bit Becker Hammer tests were performed in the downstream shells of the Right and Left Wing Dams at the Folsom Project. Data was collected to validate that the penetration resistances of the embankment gravels in the Wing Dams were approximately equal to or greater than those of the similar embankment gravels present at the Mormon Island Auxiliary Dam. This confirmation was necessary because the cyclic strength used in the dynamic analysis of the Wing Dams was determined from the penetration resistance of the embankment gravels of Mormon Island Auxiliary Dam.

2. The tests were performed between 12 October and 25 October by Becker Drills of Commerce City, Colorado. The drilling was accomplished using a truck mounted B-180 Link-Belt pile driver. The soundings were made using an 8-tooth crowd-out bit with a 6-5/8 in. O.D. casing. All tests were performed without a blower or a supercharger.

Data Reduction Procedures

3. In the field, Becker blowcounts, N_B , and bounce chamber pressure readings were recorded over 1 ft intervals for each sounding. Each N_B blowcount was converted to an equivalent SPT N_{60} (energy corrected) blowcount and $(N_1)_{60}$ (overburden corrected) blowcount. A schematic of this process is presented in Figure A1.

4. The energy corrections are based on the results of Dr. Les Harder's research on the Becker Hammer Drill (Harder and Seed 1986). The conversion of field Becker blowcounts into equivalent SPT blowcounts depends upon the combustion conditions (throttle settings, temperature, and altitude) of the diesel powered drill rig and the type of equipment used (type of bit, size of casing, and drill rig). The Becker blowcounts, N_B , were first corrected to equivalent blowcounts for a constant calibrated combustion condition using the chart in Figure A2. The notation for these converted Becker blowcounts is N_{BC} . This is accomplished by plotting a point for N_B and the bounce

pressure reading on the chart. The abscissa of the intersection of the blowcount correction curve passing through the point and the constant combustion curve adopted for calibration is the value of the N_{BC} blowcount. However, it was necessary to multiply the N_{BC} values obtained from the chart by a factor of 1.5 to account for the difference between the energy levels of the B-180 drill rig from which the data was obtained and the AP-1000 drill rig upon which the chart is based.

5. The chart in Figure A3 was used to convert the N_{BC} blowcounts to their equivalent Standard Penetration Test (SPT) N_{60} blowcounts. The equivalent N_{60} blowcount was determined from the ordinate value of the curve after entering the chart at the appropriate value for N_{BC} .

6. The overburden correction to convert equivalent SPT N_{60} was made using the following formula:

$$(N_1)_{60} = C_n \times N_{60} \quad (1)$$

where

N_{60} = SPT blowcount at energy level of 60 percent of the maximum theoretical level

$(N_1)_{60}$ = SPT blowcount at energy level of 60 percent and overburden pressure of 1 tsf

C_n = overburden correction factor which is dependent upon the vertical effective stress

7. The C_n curves used in this study are shown in Figure A4. This figure shows the curves recommended by Seed (1983) (based on the work by Marcuson and Bieganousky 1978) to be used for sands with loose ($D_r = 40$ to 60 percent) to medium-dense ($D_r = 60$ to 80 percent) relative densities. The third curve is for gravels and is an extrapolation based on the relationships between mean grain size, C_n , and confining pressure from data reported by Marcuson and Bieganousky (1978). A discussion for the rationale behind this extrapolation is included in Report 8 of this series. In this study the gravel curve was used for all blowcounts in the Right and Left Wing Dams. It is noted that for a given vertical stress the use of the gravel curve will result in a smaller overburden correction than will the use of the sand curve which in turn will result in a higher value for $(N_1)_{60}$.

8. To determine the overburden corrected blowcount, the effective vertical confining stress must be computed for each location where a blowcount is

measured. For each location, an adjustment is made to the vertical effective stress computed in a two-dimensional, non-linear static finite element analysis to account for the fact that the overburden correction (C_n) charts were developed for level ground conditions rather than sloping ground. The vertical effective stresses were computed in the static finite element analysis which is described in Part V of this report. The equivalent vertical effective stress used in the selection of C_n , was determined from the following formula:

$$\sigma'_{vl} = 1.67 \times \sigma'_{ms} \quad (5)$$

where

σ'_{vl} = equivalent level ground vertical effective stress used to determine C_n

σ'_{ms} = effective mean stress under sloping ground determined in the static finite element analysis

Equation 5 was derived by equating the expressions for mean normal pressure for sloping ground, plane strain conditions and for level ground conditions and solving for the equivalent level ground vertical stress as shown in Figure A5. Equation 5 was developed using a Poisson's ratio of 0.3 and a K_0 of 0.4. The figure shows that the mean confining stress corresponding to the vertical effective stress in sloping ground is larger than that in level ground for the same depth below the surface.

Presentation of Data

9. Six Becker Hammer soundings designated BH 14-88 through BH 19-88 were performed at the Wing Dams. Four soundings, BH 14-88 through BH 17-88, were performed at the Right Wing Dam and two soundings, BH 18-88 and BH 19-88 were performed at the Left Wing Dam. The locations of these soundings are shown in the main text in the plan view of Figures 51 and 52. The blowcount data from each of these six soundings is presented in Figures A6 through A11. Each figure contains plots of N_B , N_{BC} , N_{60} , and $(N_1)_{60}$ versus depth. All data was reduced following the data reduction procedures outlined in the preceding paragraphs. A discussion of the analysis of this data is presented in the main text.

REFERENCES

Harder, L. F., and Seed, H. B. 1986. "Determination of Becker Penetration Resistance for Coarse-Grained Soils Using the Becker Hammer Drill," UCB/EERC Report No. 86/96, University of California, Berkeley, CA.

Seed, H. G., Idriss, I. M., and Arango, I. 1983. "Evaluation of Liquefaction Potential Using Field Performance Data," Journal of Geotechnical Engineering Division, American Society of Civil Engineers, Vol 97, No. SM8, pp 1099-1119.

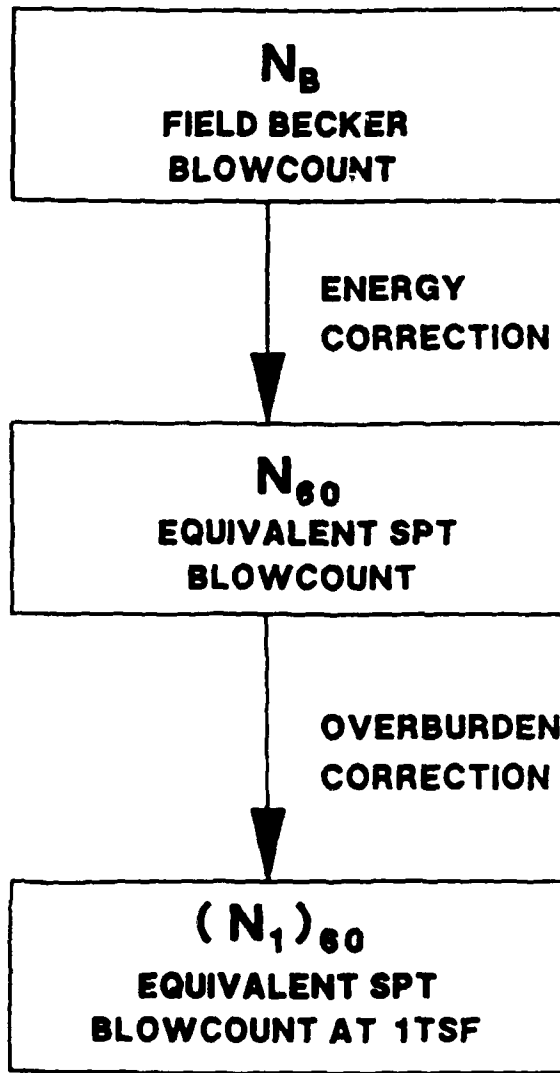
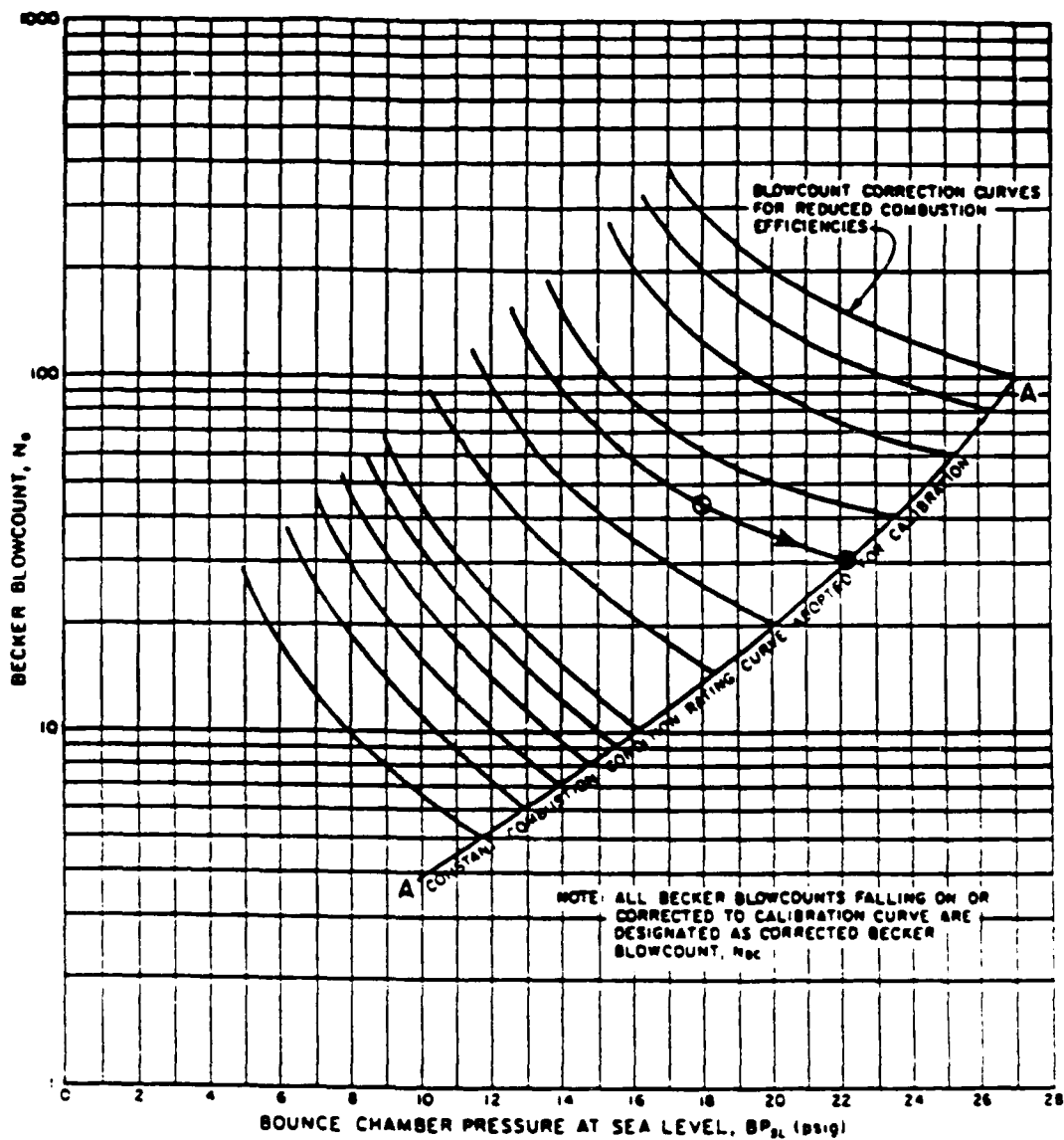


Figure A1. Schematic illustrating the conversion of N_B to equivalent SPT $(N_1)_{60}$ blowcounts



- EXAMPLE MEASURED BLOWCOUNT, N_b
- EXAMPLE CORRECTED BLOWCOUNT, N_{bc}

Figure A2. Correction curves adopted to correct Becker blowcounts to constant combustion curves adopted for calibration (Harder and Seed 1986)

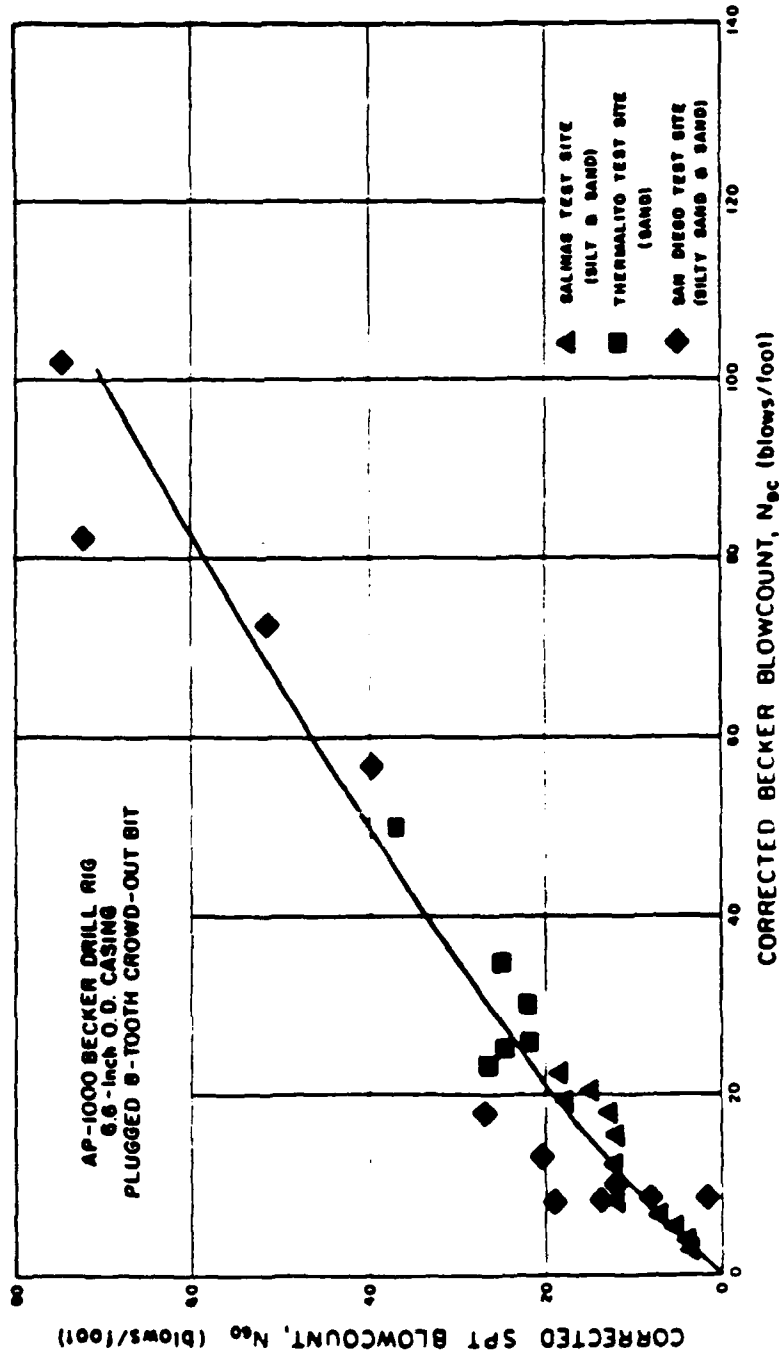


Figure A3. Correlation between corrected Becker and SPT blowcounts (Harder and Seed 1986)

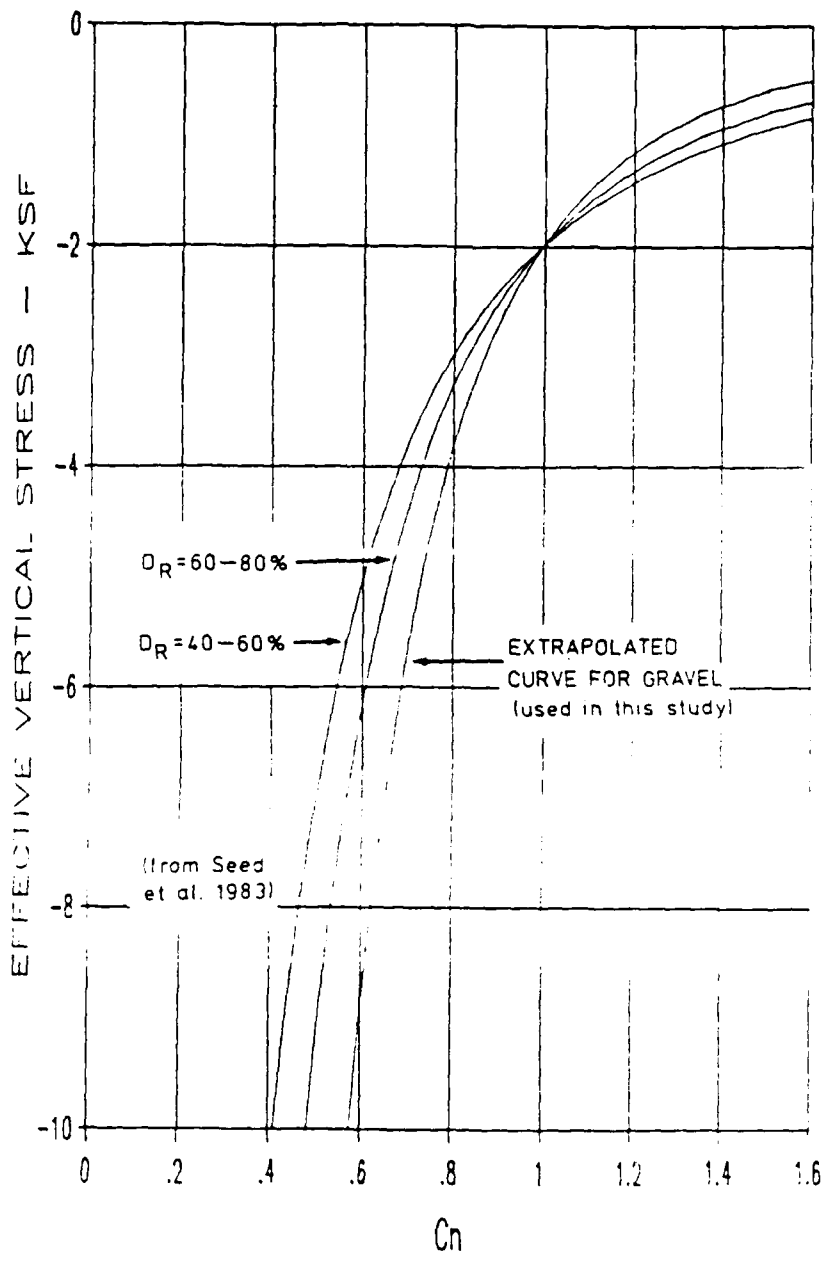
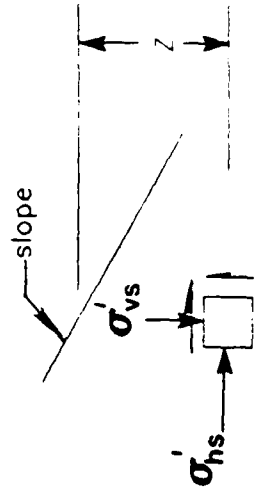
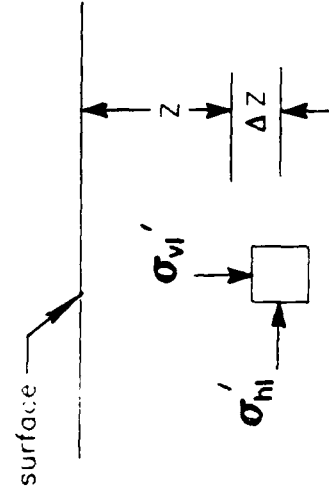


Figure A4. C_n curves used in the seismic stability evaluation of the Folsom Project

SLOPING GROUND



LEVEL GROUND



PLANE STRAIN

K₀ CONDITIONS

$$1) \sigma'_{ms} = (\sigma'_{vs} + \sigma'_{hs}) (1 + \nu) \frac{1}{3} \quad 2) \sigma'_{ml} = \frac{(\sigma'_{vl} + 2 K_0 \sigma'_{vl})}{3}$$

Equating 1) and 2) with $K_0 = 0.4$ and $\nu = 0.3$ yields:

$$\sigma'_{vl} = 1.67 \times \sigma'_{ms}$$

Figure A5. Formula used to compute the equivalent level ground vertical effective stress

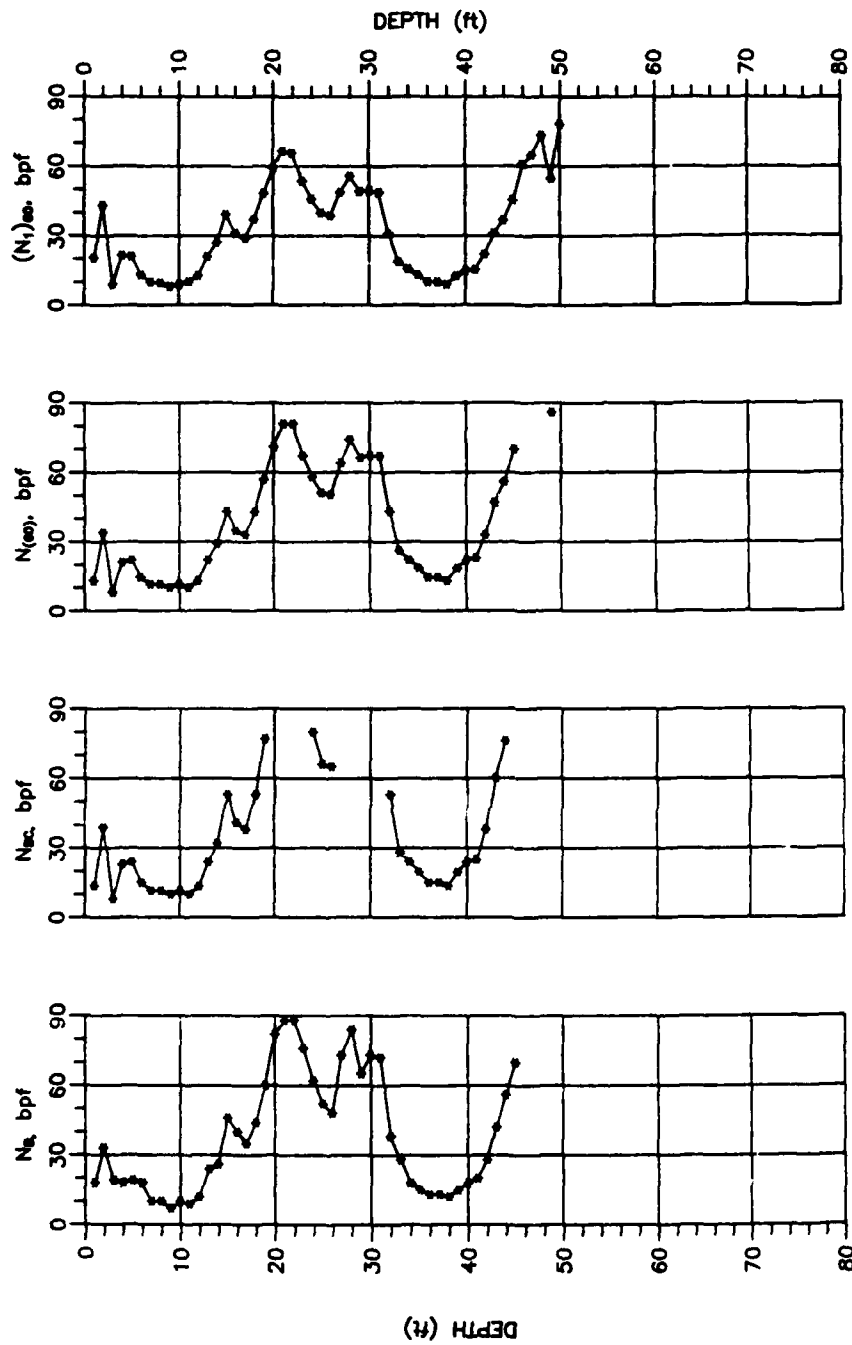


Figure A6. Becker Hammer Drill Penetration Test data from BH-14-88

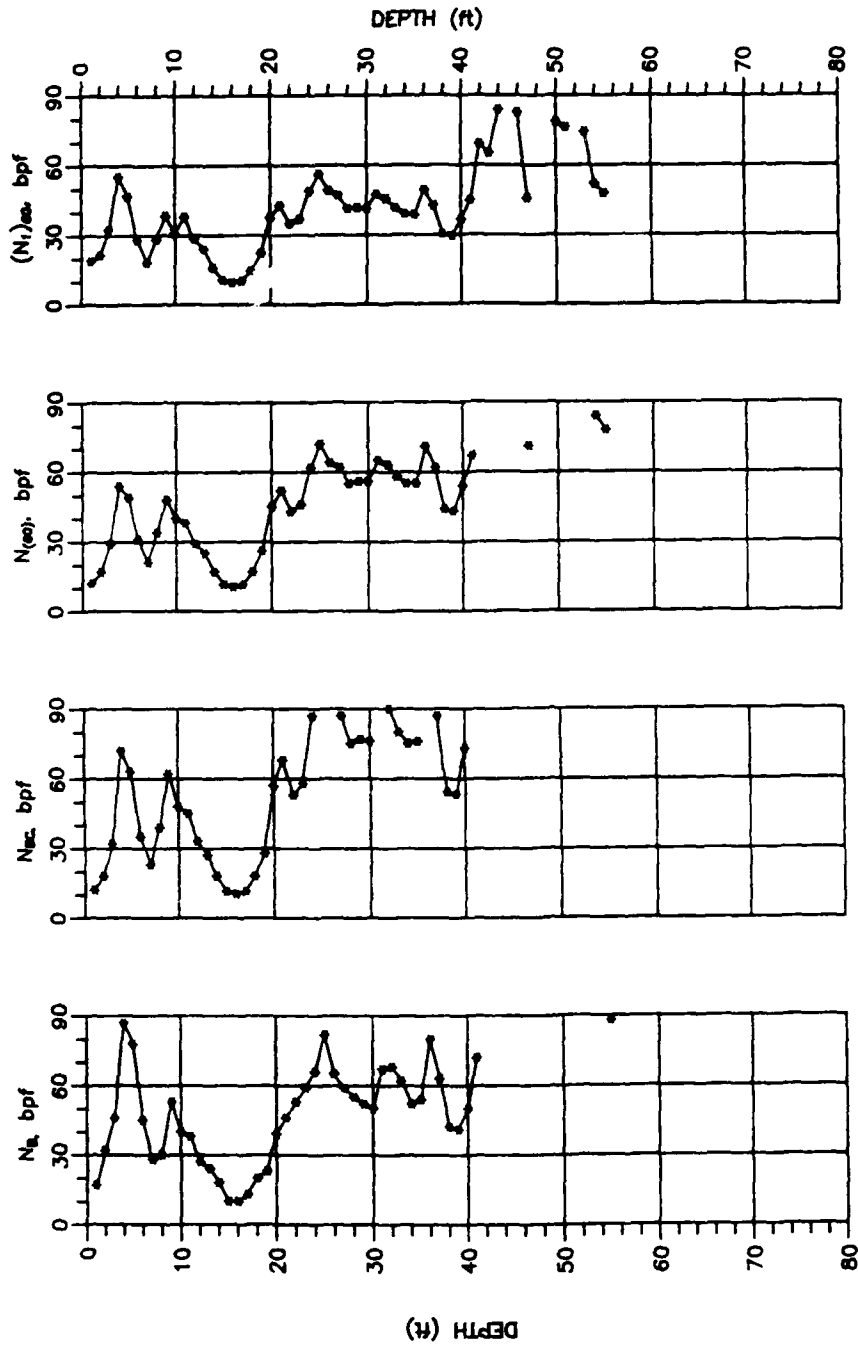


Figure A7. Becker Hammer Drill Penetration Test data from BH-15-88

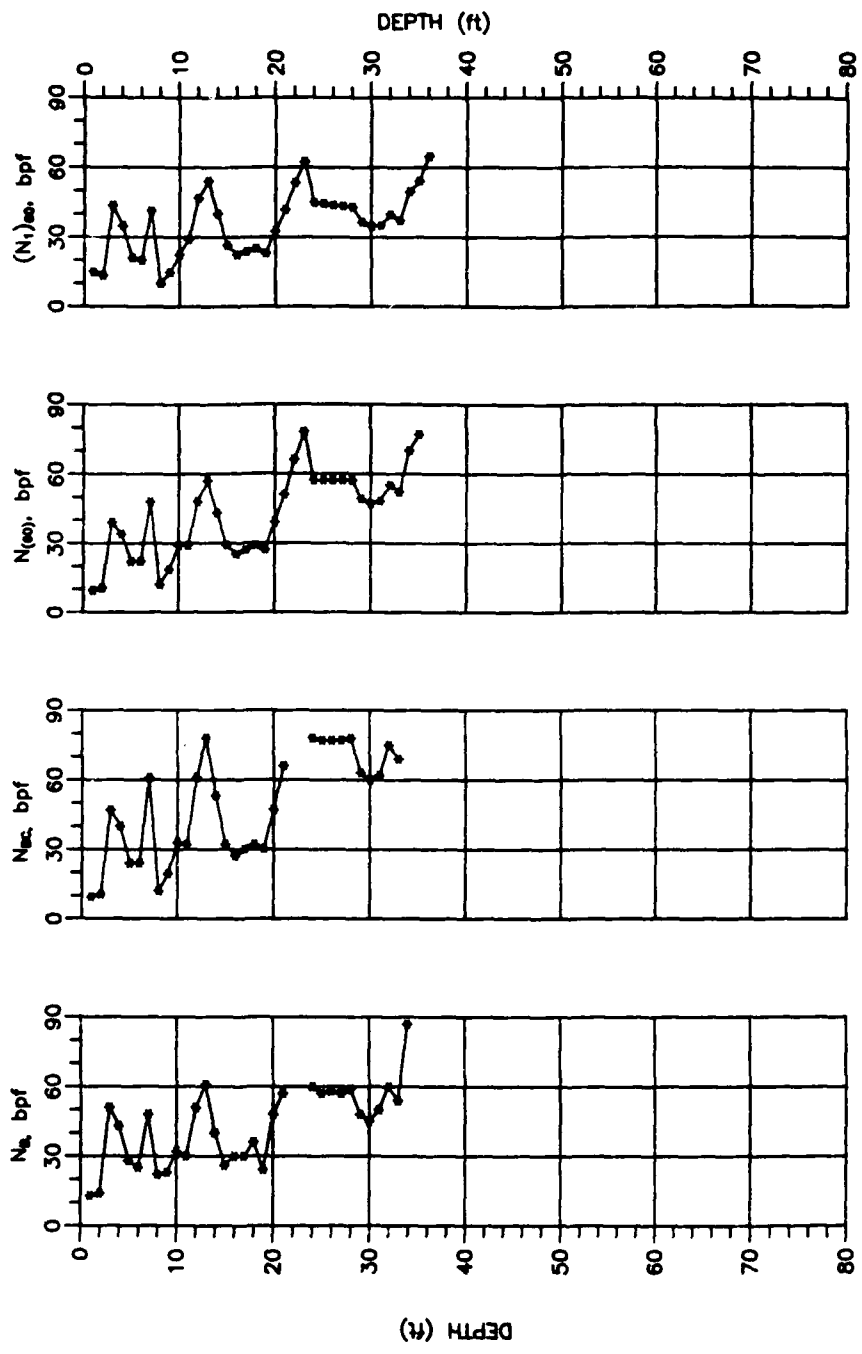


Figure A8. Becker Hammer Drill Penetration Test data from BH-16-88

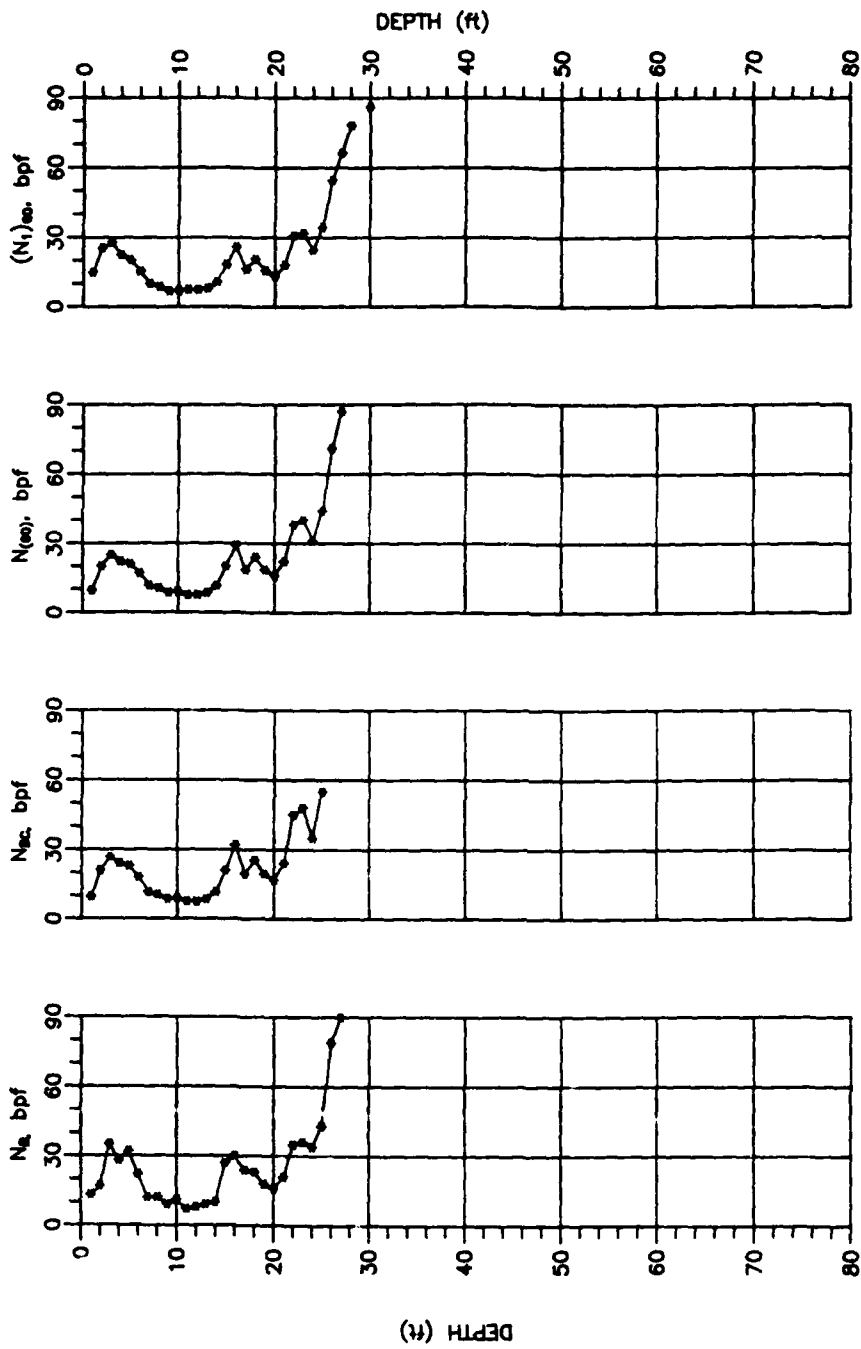


Figure A9. Becker Hammer Drill Penetration Test data from BH-17-88

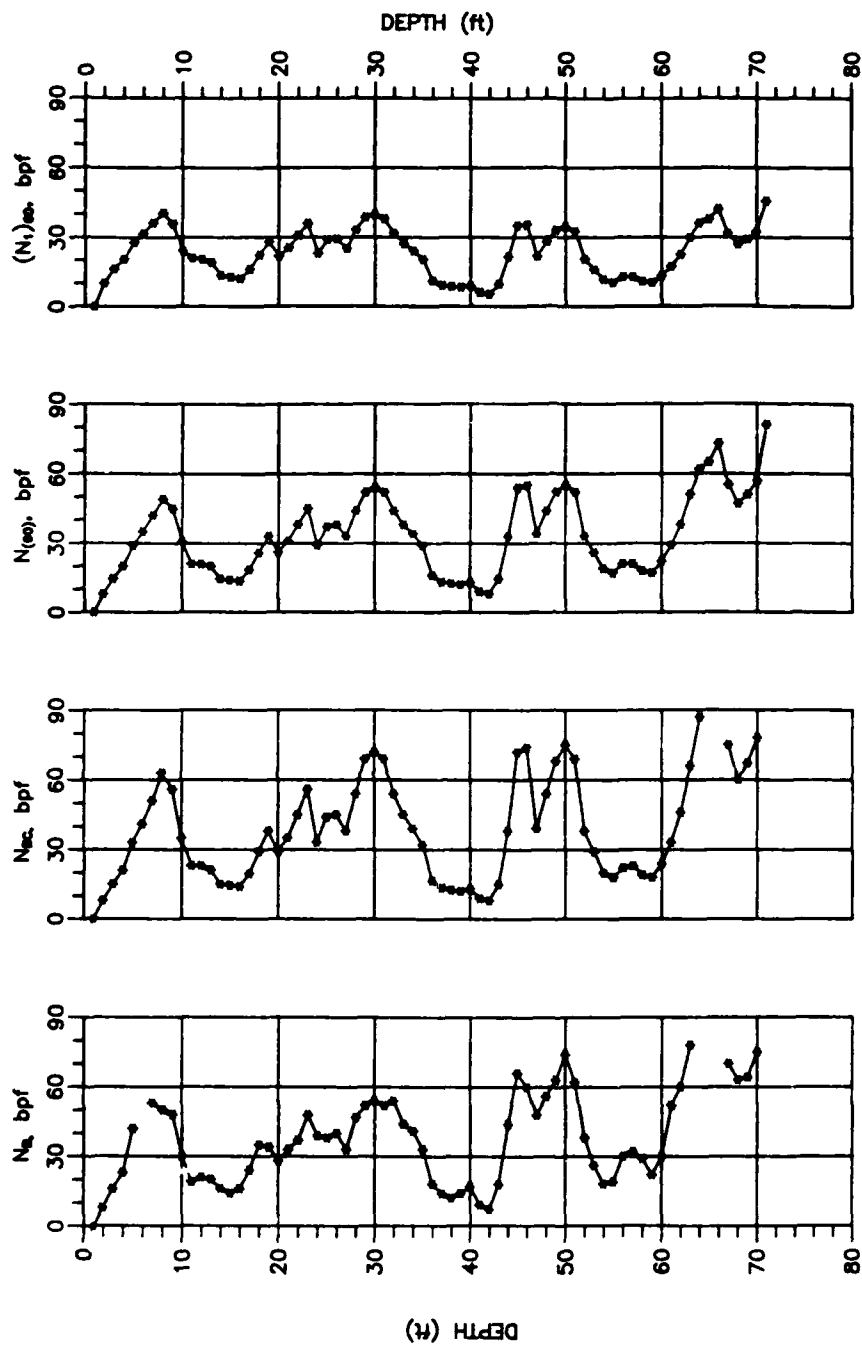


Figure A10. Becker Hammer Drill Penetration Test data from BH-18-88

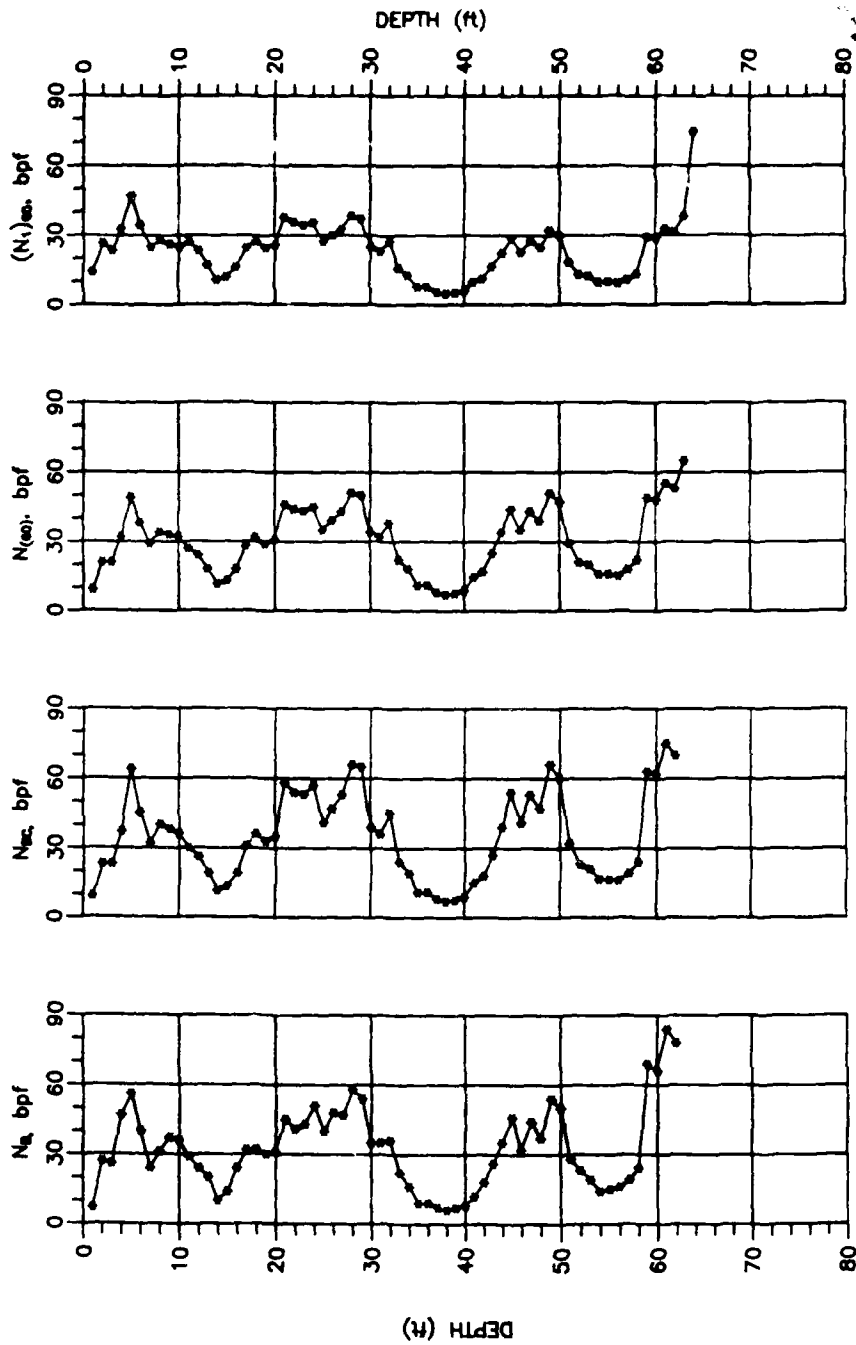


Figure A11. Becker Hammer Drill Penetration Test data from BH-19-88